UNIVERSITY OF SOUTHAMPTON

FACULTY OF ENGINEERING, SCIENCE & MATHEMATICS

Institute of Sound and Vibration Research

USE OF A TWIN-INVERTED PULSE SONAR (TWIPS) TO DISCERN BETWEEN SOLID OBJECTS AND BUBBLES

by

Daniel Clark Finfer

Thesis for the degree of Doctor of Philosophy

July 2009

Abstract

UNIVERSITY OF SOUTHAMPTON
ABSTRACT
FACULTY OF ENGINEERING, SCIENCE & MATHEMATICS
INSTITUTE OF SOUND AND VIBRATION RESEARCH
Doctor of Philosophy
USE OF A TWIN-INVERTED PULSE SONAR (TWIPS) TO DISCERN BETWEEN SOLID OBJECTS AND BUBBLES
by Daniel Clark Finfer

This thesis shows how a twin-inverted pulse sonar (TWIPS) can take advantage of nonlinear bubble dynamics to suppress undesirable bubble clutter in sonar systems. This sonar requires the production of two high-amplitude pulses in short succession, the second of which must be 180° out of phase with the first. It will be shown that the echoes from these excitations can be combined to selectively suppress between even- and odd- harmonic energy. After a simulation is used to prove the TWIPS concept, an experiment will be described wherein this method was tested in a controlled environment on a replicated oceanic bubble cloud. The novel bubble-cloud generating machine will be described in detail. The results from a TWIPS sea-trial will then be used to show that the method works not only in controlled environments, but also in the open water. Finally, a review will explore newly-discovered links between the echolocation abilities of acoustically-active, coastally restricted cetaceans and TWIPS. That review will show using pre-existing data that some coastal dolphin species seem capable of generating pulse-pairs wherein the second pulse is 180° out of phase with the first.

Table of Contents

List of symbols and abbreviations

Symbols

a	arbitrary constant
A	cross-sectional area
A	generic species
$b(t)$	time-varying variable
bw	a property as defined in bubbly water
B	generic species
B	bulk modulus
c	acoustic damping
c_A	speed of sound in air
c_o	speed of sound
c_w	speed of sound in water
C_d	drag coefficient
d_{detect}	distance of a detected object from the receiver
D	source directivity
D_1	decision: true
D_0	decision: false
DI	directivity index
e	≈2.71828183...
e	echo
$E(\theta,\varphi)$	three-dimensional directivity pattern of an array
$E_e(\theta)$	two-dimensional directivity pattern of an element within an array
f	frequency
f'	Doppler-shifted frequency
f_{op}	operating frequency for a detection system
f_{pr}	pulse repetition frequency
f_{res}	resonance frequency
F	force
F_b	force of buoyancy
F_d	force of drag
g	function
G	roughness parameter (only where referencing the experiment of Medwin [1])
h	height of surface undulations, per Rayleigh roughness parameter
H_1	Hypothesis: True
H_0	Hypothesis: False
H_{sol}	Henry's constant for an aqueous solution
I_{ax}	intensity along a given axis
I_I	incident intensity
I_{ref}	reference intensity
I_t	transmitted intensity
k	wavenumber, ω/c_o
k_a	wavenumber in air

k_1	a stiffness
L	primary dimension of an object
L_{REF}	reference length, taken to be 1 m after Clay and Medwin [2]. Pierce notes that some earlier literature uses a reference length of 1 yard [3].
m	integer
m_1	a mass
n_1	system output in presence of target
n_0	system output in absence of target
N	square root of the number of elements in a square, planar array (*i.e.* in an N x N array)
p	pressure inside the bubble
$p_{i,e}$	pressure inside the bubble when undisturbed
p_o	hydrostatic liquid pressure outside bubble
p_v	vapour pressure within a bubble
p_∞	pressure in the water at some distance far enough away from the bubble to be undisturbed by local acoustic pressure fluctuation
p_o	equilibrium pressure
p_1	an acoustic pulse
p_{ref}	a reference pressure
P	an acoustic pressure
P_A	magnitude of an oscillating wave
P_+	sum of two halves of a pulse pair
P_-	difference of two halves of a pulse pair
P_{comb}	driving pressure consisting of the sum of two coherent signals of different frequency
P_{rev}	reverberation pressure
$\mathbf{P_i}$	incident pressure
$\mathbf{P_r}$	reflected pressure
$\mathbf{P_t}$	transmitted pressure
P_α	driving pressure of frequency α
P_β	driving pressure of frequency β
q	quality factor
Q	probability of a particular decision
r	distance from the centre of the bubble
R	bubble radius
$\dot{R}$	first derivative, bubble radius
$\ddot{R}$	second derivative, bubble radius
Re	Reynold's number
R_I	intensity reflection coefficient
R_Π	power reflection coefficient
$\mathbf{R}$	pressure reflection coefficient
s	array element spacing
s_0	a power series coefficient
s_1	a power series coefficient
s_2	a power series coefficient
s_3	a power series coefficient
s_4	a power series coefficient

List of Symbols and Abbreviations

$s[n]$	ensemble of random variables
t	time
t'	integration time
T_I	intensity transmission coefficient
T_Π	power transmission coefficient
T_{15}	reverberation time as linearly extrapolated from time-averaged decay after 15 ms
$\mathbf{T}$	pressure transmission coefficient
T1	TWIPS1
T2a	TWIPS2b
T2b	TWIPS2a
TS	target strength
$\vec{u}$	velocity vector
υ	system output
V_{air}	volume of air
V_{detect}	velocity of detected object
V_s	velocity estimate
V_b	velocity of a bubble along the axis extending between the observer and the bubble
V_{st}	velocity according to Stoke's law
V_t	terminal velocity of a rising bubble
V_{water}	volume of water
$\mathbb{V}$	volume of bubble
w	a property as defined in bubble-free water
x	a coordinate
x_s	source position in x-coordinate
$x_{\mathbf{A}}$	mole fraction of species **A**
x^+	the value of x as approached from the positive end of the number line
x^-	the value of x as approached from the negative end of the number line
$\mathbb{Y}$	general response of an oscillator
y	a coordinate
y_s	source position in y-coordinate
z	depth
γ	ratio of specific heats
β	damping factor
λ	wavelength
κ	polytropic index
ν	kinematic fluid viscosity
θ	angle
θ_a	horizontal angle in a 2-dimensional directivity pattern
θ_i	angle of incident energy
θ_r	angle of reflected energy
π	≈3.141593...
Π	function describing the frequency response of a forced oscillator
ς	root-mean-square wave height

List of Symbols and Abbreviations

σ	surface tension of a liquid
σ_{scat}	Scattering cross-section
σ_{back}	Back-scattering cross-section
ρ	density
ρ_a	density of air
ρ_w	density of water
σ_{back}	backscattering cross-section of a single bubble (m)
ζ	differential equation set substitution variable
ξ	differential equation set substitution variable
τ	TWIPS interpulse delay
τ_{detect}	echolocation delay
τ_{burst}	length of a tone-burst in a multi-pulse structure
τ_{delay}	length of delay between onset of successive tone-bursts in a multi-pulse structure
φ	phase
φ_a	vertical angle in the directivity pattern of a 2-dimensional array
ω	radial frequency (radian s^{-1})
ω_1	driving frequency
ω_2	one octave above driving frequency ($2\ \omega_1$)
ω_a	Lower limit: half-power bandwidth of an echolocation signal
ω_b	Upper limit: half-power bandwidth of an echolocation signal
ω_α	one of two driving frequencies in a combination frequency input
ω_β	one of two driving frequencies in a combination frequency input
ω_{damped}	oscillatory frequency of a damped system
ω_M	Minnaert resonance frequency (radian s^{-1})
ω_o	Natural frequency of undamped system
Ω	cross-sectional area onto which a sound is incident

Abbreviations

BFG	bubbly fluid generator
cf.	short for the latin *confer*, meaning "compare"
°C	degrees Celsius
et al.	*et alii*, meaning "and others"
°F	degrees Fahrenheit
GAO	General Accounting Office
HIFU	high intensity focused ultrasound
i.e.	*id est*, meaning "that is; in other words"
ISVR	Institute of Sound and Vibration Research, University of Southampton
lidar	lasar detection and ranging
log	logarithm base-ten;

n.b. log(y) = x is equivalent to $y = 10^x$

MCM	mine countermeasure
n.b.	*nota bene*, meaning "note carefully"
ND	non-dimensionalised
N	North
PC	personal computer
radar	radio detection and ranging
RIB	rigid-inflatable boat
RMS	root mean square
ROC	receiver-operating characteristic
SNR	Signal to noise ratio
sonar	sound navigation and ranging
SSGN	**S**hip **S**ubmersible, **G**uided missile, **N**uclear powered. This is the United States Navy hull classification symbol for a nuclear powered cruise missile submarine.
SW	shallow water
TVG	time varying gain
TWIPS	Twin inverted pulse sonar
VHF	Very high frequency
UAUA	Ultrasonics and Underwater Acoustics Research Team, ISVR
UAV	Unmanned aerial vehicle
UUV	unmanned underwater vehicle
UCA	ultrasound contrast agent
US	United States

List of symbols and abbreviations

Acknowledgements

בס"ד

The wide scope of the topics addressed within these pages (classical acoustics, nonlinear dynamics, marine biology, sonar design, *etc.*) is testament to the varied ways in which I been able to grow in the past four years. These growth demands would have been debilitating to me were it not for the attentions paid to me by several people, some of whom I would now like to acknowledge.

It has been rewarding and exciting to work as a student of Professor T G Leighton for the last several years. He has challenged me enormously, and encouraged me to develop my abilities in a wide range of research areas. The breadth of his knowledge is astounding. Furthermore, the way in which he works tirelessly to share this knowledge with his students should be a source of unending inspiration to all faculty within the Institute of Sound and Vibration Research, and the international community of science educators at large.

I am also thankful for having benefitted from Professor P R White's insight into this topic. His deep knowledge of sonar systems and theoretical knowledge of signal processing was enormously useful in preparing this dissertation. I have always looked forward to my meetings with him, not only because of his scientific wisdom, but also because of his kind demeanour and brilliant sense of humour.

Preliminary – Acknowledgements

I thank Professor J K Hammond for the counsel and guidance he offered me before his recent retirement. Further, I would like to recognise Dr J K Dix for his contributions of time and expertise to the TWIPS experiment. Mr G T Yim and Mr D G H Coles each contributed many days towards my experiment in the A B Wood Tank. To say that my experiment would not have been logistically feasible without the help of Mr Yim and Mr Coles is in no way an exaggeration. In studying TWIPS, I was fortunate to have the opportunity to assist in the supervision of two exceptional undergraduates who studied topics related to my own research: Mr E J Grover and Miss A M Liszczyk. Each of these students made critical contributions to the final output of this PhD. Additional contributors to the experiments reported within this dissertation include Dr G Robb, Mr M Cooling, Dr C Powles, and Ms A Mantouka. I would like to thank Prof J S Bolton, Prof P A Davies, Prof L G Mongeau, and Prof A Bayliss for setting me on to the track which eventually brought me to England.

Additional thanks are due to the generous academics who during the preparation of this topic invited me meet with them on their own campuses: Prof R Roy (Boston University), Prof P Wilson (University of Texas, Austin), Prof D Hamilton (University of Texas, Austin), and Prof M J Buckingham (Scripps Institution of Oceanography, San Diego).

I am indebted with gratitude to my parents for their support of me throughout my university studies. Finally, this document would never have come to fruition were it not for the simultaneous motivation and support of my beloved wife, Yehudit Elisheva.

1 Introduction

One of the greatest challenges facing operators in the littoral zone is the inability to distinguish solid objects from bubbles using sonar. This challenge impedes mine-hunting capabilities, swimmer detection, and the ability to differentiate hard surfaces from gassy entities in boat-wakes. This thesis dissertation describes a novel method by which it is possible to overcome the irregularities in acoustic propagation due to the presence of bubbles, so as to reveal the presence of solid objects in the water column. It will be seen that the developed method could indeed find application in areas as varied as ocean acoustics, biomedical ultrasound, lidar, and radar.

1.1 Sonar in littoral waters

The resolution of the Cold War and the onset of the Gulf conflict in 1991 marked a change in focus for naval strategists. In the 1970's and 80's, NATO and Soviet efforts had aimed to master deep-water acoustics and long-range propagation so as to dominate the deep-ocean basins of the world [4]. However, the unique challenges faced in the lead-up to the liberation of Kuwait exposed the fact that almost no naval countermeasures existed which were capable of handling the unique challenges presented by the shallow, turbulent, sandy, and bubbly waters encountered in the Persian Gulf. The desire to minimize system development overheads makes it advantageous for military contractors to adapt for coastal waters those technologies

which already exist (that is, systems which were initially intended for deep water). As a result, large craft which were designed to cope with the threat of other like-sized threats are now in the process of being re-engineered [5, 6]. An example of one such refit is shown below in Figure 1.1.

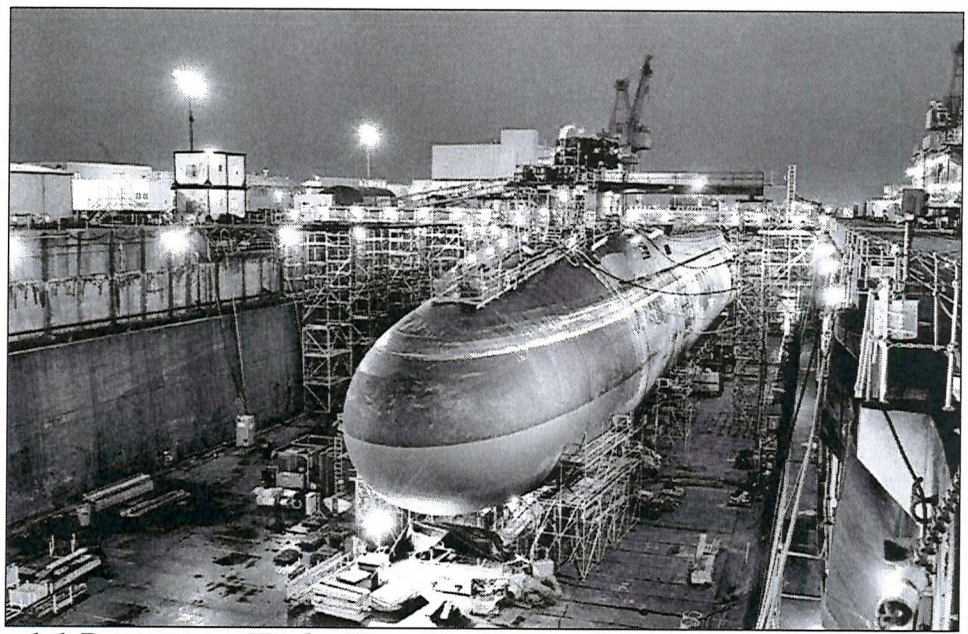

Figure 1.1 Bremerton, Wash. (Mar. 15, 2004) - Night falls at Puget Sound Naval Shipyard and Intermediate Maintenance Facility, Bremerton, Wash., as work continues on the strategic missile submarine USS Ohio (SSGN 726). Ohio is one of four Trident Submarines undergoing conversion to a new class of guided missile submarines. The SSGN conversion program takes Ohio-class ballistic missile submarines through an extensive overhaul that will improve their capability to support and launch up to 154 Tomahawk missiles. They will also provide the capability to carry other payloads, such as unmanned underwater vehicles (UUVs), unmanned aerial vehicles (UAVs) and Special Forces equipment. This new platform will also have the capability to carry and support more than 66 Navy SEALs (SEa, Air and Land) and insert them clandestinely into potential conflict areas. Caption and photo released by US Navy. Photo by Wendy Hallmark.

Emerging conflicts place high technology NATO assets directly opposed against, and within striking distance of shallow-water based, crude ordinance. During such 'sub-conventional' [7] combat engagements, critical and dangerous opposition targets may be dimensionally very small. Detection of such targets, when in the

water, is further complicated by the fact that, in acoustical terms, shallow water is fraught with difficulty. These difficulties arise as the result of several factors, including surface undulations [8], suspended sediment [9], ambient noise issues [10], and especially bubbles [11]. Since the end of Operation Desert Storm, researchers have made great strides towards understanding and predicting the acoustical effects of these physical artefacts. However, large uncertainties still reside within basic shallow water (SW) sonar propagation models. As SW reverberation is often the limiting factor in relation to the use of active sonar systems for target detection, localisation, and classification, SW reverberation has become a research area of "intense interest" [12]. In essence, the acoustical complexities of the littoral battle-space facilitate the successful realisation of objectives by relatively inexperienced enemies who may be equipped with only remedial systems.

The danger presented by underwater asymmetric warfare was highlighted during Operation Desert Storm (August 1990 - February 1991). The Desert Shield/Desert Storm summary report of US Naval operations prepared by the Chief of Naval Operations in March of 1991 explained how experience in the Gulf exposed hardware and intelligence shortcomings in mine countermeasures (MCM) operations [13]:

> Our Cold War focus on the Soviet threat fostered reliance on our overseas allies for mine countermeasures in forward areas.

> The MCM assets of our allies - - - on whom we have relied for MCM support in NATO contingencies for years - - proved their mettle in the Gulf, both in Operation EARNEST WILL (during the Iran-Iraq war) and DESERT STORM. Both operations highlighted the need for a robust, deployable U.S. Navy MCM capability. We are undertaking a comprehensive review of both our mine countermeasures strategy and the readiness of our forces to ensure our ability to conduct independent mine countermeasures operations when required.

Modern MCM solutions tend to favour autonomous detection platforms which are "mission reconfigurable"[1]. Reconfigurability is a feature which is hardly trivial, given the potential for physical variability of shallow water environments from one location to another [14], or even from day to day [15].

Many western military strategists are currently concerned with the potential for a conflict near the coast of China, and especially in the Strait of Taiwan (100 miles across at its widest point, with a maximum depth of only 70 m). According to The Economist for 4 August 2007 [16],

> "American global supremacy is not about to be challenged by

---

[1] Mission reconfigurability refers to the ease with which a system's hardware and software can be adapted to the needs of varying types of objectives (*eg.* from reconnaissance to mine-hunting or bottom-surveying).

> China's tinkering with [large, deep-water craft such as] aircraft-carriers. Even if China were to commission one—which analysts think unlikely before at least 2015—it would be useless in the most probable area of potential conflict between China and America, the Taiwan Strait". [16]

The 1996 Taiwan Strait crisis highlighted the fact that quick response by forces representing democratic power is essential to counter any efforts by the People's Republic of China to intimidate Taiwan militarily [17]. The speed of a safely advancing forward unit is ultimately determined by the speed of MCM operations, which is a "notoriously time-consuming task that can require meticulous operations by participating surface ships, submarines, and helicopters. The Navy's mine countermeasures (MCM) capabilities have been an area of concern in Congress and elsewhere for a number of years" [18].

It has been acknowledged that the US Navy "does not have a means for effectively breaching enemy sea mines in the surf zone [or] detecting and neutralizing enemy submarines in shallow water" [19]. Based on this analysis, the lessons learned during the Gulf crises, and the strategic concerns of Congress for future conflicts, it is clear that advancement of MCM capabilities for shallow waters is a relevant and worthwhile pursuit. Therefore, the goal of this thesis - to develop the first practicable solution for the detection of solid objects in surf zone-like conditions - is well justified.

1.2 Passive and active techniques

Acoustic detection and localisation methods fall into two categories: passive and active. Passive methods take advantage of energy introduced by the source. If sufficient multiple passive receivers are used and noise does not overwhelm the signal of interest, it is possible to estimate the location of the source in three-dimensions [20]. Active methods, however, require that some acoustic energy be deliberately introduced so that echolocation can be performed. Passive methods are especially desirable in situations where environmental sensitivity or covertness are required, but are difficult to implement in cases where background noise levels are high [21]. As argued above, one of the principal mission-types which is impeded by the presence of bubbles is mine detection. Most mines are entirely passive, and emit no significant acoustical energy of their own. A technique for finding mines in bubbly water or gassy sediment will therefore require some introduction of acoustical energy: an active technique.

This argument is further bolstered by the consideration of background noise levels which will likely be encountered during system application. Bubble clouds can be generated by either man-made or natural sources, examples of each respectively being ship propellers [22] and breaking waves [23]. As both of these sources are very noisy, a technique intended for use near bubble clouds must be able to compete with high background noise levels. To summarise this point,

since the solution sought here will be implemented to search for nearly-silent objects, and in environments with very high background noise levels, it seems advantageous to pursue an acoustically active system.

1.3 Attenuation: A limiting factor

Difficulties arise when studying sound propagation in bubbly water for two reasons – bubbles both scatter and attenuate the sound. In general terms, scattering is a source of problems in many systems which exploit wave propagation, regardless of the medium, frequency range, or radiation-type of interest. As a result, scattering suppression is a topic which has received a great deal of attention in the scientific literature. The goal here is argue that the apparent loss in acoustic information which results from wave scattering can, in some sense, be regained.

By contrast, attenuation is an irreversible process. If a source sends information to a receiver, but the useful information becomes overwhelmed by noise, then it is not logically viable to develop some algorithm which can reliably recover the now-missing data.

In concise terms, while scattering *may* be reversible, attenuation is intrinsically irreversible. This fact presents a practical limitation on how well targets in bubbly water can be detected, a subject which will be treated in more detail within the analysis presented in Chapter 2.

1.4 Solution inspirations

The suppression of acoustic bubble scattering was considered by Leighton in 2004 [24]. In that publication, he called the following two concepts to attention:

1) Scattering suppression is not altogether divorced from scattering enhancement. Both efforts require some prior knowledge of how the field will scatter – thus if some method exists to enhance scatter, it might be possible to reverse that method to suppress scatter. In fact, an entire facet of the field of medical ultrasonics, pulse inversion, is dedicated to the enhancement of bubble scatter.
2) The problem of detecting solid objects in bubbly water is not limited to human marine operations. Cetaceans are known to depend on active biosonar for at least some portion of their hunting and navigation activities. Perhaps marine mammals have evolved to cope with the difficulties presented by bubble scattering in a way that can be exploited by human beings.

This doctoral investigation was prompted by the synthesis of these two concepts, each of which will now be considered.

1.4.1 Biomedical contrast enhancement

Biomedical ultrasound is in principle very similar to an active sonar system [25]. Acoustic pulses are introduced into the body, and the temporal distribution of reflections corresponds to the physical arrangement of various reflecting bodies within the patient. Thus, to

be acoustically perceptible, an object must reflect sound. The degree to which a particular object reflects sound is dependent on the magnitude of impedance mismatch between that object and its surroundings. The acoustic mismatch between blood and body tissue is, practically speaking, very low. Thus, circulatory systems within the body are essentially acoustically non-reflective [26]. In many cases, however, it is desirable to highlight blood flow. To make it possible for blood-flow to appear in ultrasound scans, it is common to introduce "acoustical contrast agents" – engineered gas bubbles – which are highly acoustically mismatched with the surrounding blood, and so act as a flow-tracer (similar to the way in which paraffin is used in some wind-tunnels to highlight flow streaklines [27]). The acoustic visibility of contrast agents can be enhanced by causing the bubbles to pulsate in a nonlinear manner. One common way to exploit these nonlinear dynamics is by use of a pulse-inversion scheme [28, 29]. In simplistic terms, pulse inversion works in the following manner: Two pulses are emitted; a primary pulse, followed a short time later by phase-reversed version of that pulse. The scattered return from these two signals is then combined in a manner such that the non-linear components from the signal are enhanced, whilst signal components corresponding to linear scatter are suppressed. It will be seen that pulse-inversion is the inspiration for the solution implemented in this thesis. Biomedical ultrasound contrast agents and pulse inversion will be considered in more detail in Chapter 2.

1.4.2 Biosonar in littoral waters

Many marine mammals are known to possess extraordinary biosonar capabilities. According to Au, "dolphins have biological sonar abilities that exceed those of any man-made system in an aquatic environment" [30]. As a result, many researchers have studied the biosonar abilities of dolphins, in the hopes of improving human-operated echolocation methodologies. Despite the amount of literature dedicated to so-called biomimetic sonars, it is not yet understood how dolphins navigate and hunt in limited-visibility bubbly water. To understand these abilities better, it seems logical that scientists should pursue focused studies on those animals which inhabit such waters exclusively. Indeed Odontecetes of the genus *Cephalorhynchus*, all of which have been echolocate actively, inhabit only littoral waters [31]. However, the acoustic abilities of the genus *Cephalorhynchus* remain relatively undocumented.

As will be discussed in Chapter 3, microbubbles, entrained by breaking wave action, remain within the water column of well-mixed littoral seas for several hours after the entrainment activity has ceased [23]. Thus, a hypothesis well worth investigating is the proposition that acoustically-active animals in this habit might have some ability to cope with microbubble scattering [32, 33]. A review of the literature concerning the acoustic behaviour of members of the genus *Cephalorhynchus* will be offered in Chapter 6. It will be shown that in fact that these species may be using a dual-pulse method [32, 34],

similar to that solution which was suggested by Leighton in 2004 [24], and which is the main subject of this dissertation.

1.5 Overview of the thesis

This thesis will proceed in six chapters. This first chapter has introduced the basic concepts relevant to this investigation. In the next chapter, a description of basic bubble dynamics will be used to prompt a review of the literature on the topic of bubbles and biomedical ultrasonics. The degree to which those acoustic methods which are used in biomedical ultrasound have also been applied to ocean acoustic studies will then be discussed. One of these methods, pulse inversion (PI), will then be used to form the basis of Twin Inverted Pulse Sonar (TWIPS), the first-known viable engineering solution for the detection of solid objects in bubble water.

Chapter 3 will discuss the sources and physical characteristics of bubble clouds found in the ocean. It will be seen that many of the methods used to study oceanic bubbles draw on or are identical to those methods presented in Chapter 2. Also reported in Chapter 3 is the development of an air/water mixing mechanism at the A.B. Wood Underwater Acoustics Laboratory. This bubble fluid generator (BFG) facilitated the creation and controlled distribution of bubbles clouds having a size distribution comparable to that distribution exhibited by oceanic clouds.

The discussion of the viability of TWIPS will continue in the following chapter with a report on an experiment designed to investigate the operating characteristics of that sonar. Experimentally acquired data will be used to show that, in detecting solid objects in bubbly water, TWIPS outperforms the state-of-the-art technology. The chapter will continue with a comprehensive analysis of the experiment results. Chapter 5 will be used to the results of a field study performed to justify the claim that TWIPS detect the seafloor when obscured by a bubbly ship wake.

Chapter 6 will contain a study of littoral biosonar. This topic will be introduced because, after successful target detection using TWIPS-pulses had been simulated and published [33], the ISVR research team became aware[2] that some cetaceans in fact use TWIPS-like pulses when echolocating in bubbly water. This discovery prompted a review of the literature concerning littoral cetacean biosonar, which will appear at the beginning of Chapter 6. That chapter will then continue with the study of some TWIPS-like biosonar sounds.

---

[2] Dr Marc Lammers of Oceanwide Science Institute pointed out to the authors in 2005 that surface reflections of echolocation signals generated by bottlenose dolphins are an oft-encountered artefact with which bioacoustics researchers are generally familiar. This dialogue took place at the First International Conference on Measurements in Acoustics in Heraklion, Crete.

In the conclusions section (Chapter 7), the successes of this investigation will be summarised. The information presented in the preceding chapters will be synthesised and used to show how research in this field might move forward.

At the end of the volume appears an appendix comprised of two parts. The first is a treatise on the nature of receiver-operating characteristic (ROC) curves. The second part is a reproduction of all publications which the author has written or co-written whilst completing his PhD.

2 A method for searching for solids in bubbly water

> *Two sorts of truth: trivialities, where opposites are obviously absurd, and profound truths, recognised by the fact that the opposite is also a profound truth.*
>
> -Nils Bohr[3]

In this chapter, a potential algorithm for the detection of solid objects in oceanic bubbly water is described. First, the state of the art will be discussed, and it will be established that the presence of bubble clouds in the water greatly reduces the degree to which modern sonar systems are effective. Second, the dynamics of bubbles under acoustic excitation will be discussed, and it will be shown that bubbles tend to scatter in a highly nonlinear manner. Following the section on bubble dynamics there is a review on the topic of bubble contrast enhancement in the field of biomedical ultrasound. This section is punctuated with a discussion on the methodology behind "pulse inversion" technology.

---

[3] As quoted by his son Hans Bohr, in:

S Rozental, Niels Bohr. His Life and Work as Seen by His Friends and Colleagues, Amsterdam: North-Holland Publishing Company, (1967), p 328.

As was reasoned in Chapter 1, scattering suppression is not altogether divorced from scattering enhancement. The discussion here will build upon that logic, and lead from the review of literature on pulse inversion into the proposal for a new method, based on a pseudo-reversal[4] of the pulse inversion approach. The feasibility of this new method, the Twin Inverted Pulse Sonar (TWIPS), will be analysed in the third section. This will be accomplished by using the results of simple computational studies to differentiate between the acoustic scatter from a target and a single bubble. Fourth, that computation will be expanded to simulate the acoustic search for a single fish surrounded by tens of millions of bubbles per cubic meter beneath a breaking wave.

2.1 The state of the art

Active sonar technology developed for the detection of objects hidden in or on the seabed has tended towards the production of images based on scanning technology. As technology improves, scanning sonars tend to the employ ever-higher frequencies. This is because wavelength varies inversely with frequency; therefore higher frequency scanners allow for higher resolution images (this will be explained in

---

[4] The term "pseudo-reversal" is used here to express the fact that, although a literal reversal of pulse inversion technology is the logical predecessor of the TWIPS method, further improvements are required to reveal the presence of solid objects in bubbly oceanic water, as developed within the body of the text.

more detail within section 2.7.1.2). In clutter-free conditions, the practical upper limit for sonar scans is limited according to the signal-to-noise ratio (SNR). Clutter, ambient noise, and absorption all contribute to the diminution of the SNR. In bubble-free seawater, absorption increases by roughly an order of magnitude for every order of magnitude increase in frequency [21], thereby limiting the usefulness of very high frequency (VHF) sonar systems. Currently, a wide variety of side-scan sonars are available which operate from 30-100 kHz (for long range surveys) up to 500-1000 kHz (for close-range high-resolution scans).

Scanning sonar was developed for target identification and for ocean-bottom surveying. In oceanic scanning, bubbles are generally perceived as sources of noise and acoustic signal loss. Thorpe [23] was innovative in realising that the tendency for bubbles to backscatter sound could be exploited in the study of bubble plumes in Loch Ness. Thorpe observed that bubbles, once generated by mild wind-induced surface turbulence, were then dragged down several meters within the water column, and persisted for several minutes after the winds subsided. Bubbles scatter target-finding sonar undesirably, so this physical observation suggested that sonar might be difficult to use in both rough waters, and also in calm waters following periods of surface disruption (such as that generated during a high-wind period). This study represented an important advance in terms of understanding the evolution of bubble clouds within the sea.

The success of Thorpe's method depended principally on the fact that the properties which make scanning sonar inadequate when one seeks to find a target in bubbly water can be exploited for the study of oceanic bubble plume evolution.

While the prevailing technology in MCMs is dependent on the high-resolution images created using high-frequency acoustics [35], some competing technologies rely on mid-frequency (1-10 kHz) resonant scatter by targets for detection [36]. High-frequency target imaging is capable of revealing the visible profile of an unburied or only partially-buried object but does not facilitate the perception of any information concerning target construction. However, resonance scattering by a target in the range of $4<kL<30$ (k is the wavenumber and L is the characteristic length of the object) makes it possible to obtain information concerning the structural features of targets such as wall thickness and elastic properties [37]. Furthermore, when compared to the frequencies used for imaging, frequencies of this order (1-10 kHz) offer improved seabed penetration [36]. In the case where the structural behaviour of targets within the scanned location is understood, this improved seabed penetration means that resonant scatter detection systems are theoretically well-adapted to the detection of fully-buried objects. Resonance detection will not be exploited in the experiments conducted in connection with this study, because only non-resonant targets were available for testing. However, because of the frequency range eventually employed for

TWIPS, it will be seen in later discussions that this topic will become relevant.

Bubble scattering problems are not isolated to the upper part of the water column. Bubble clouds trapped within sediment will tend to interrupt acoustic propagation in the sea-bottom (regardless of whether one is attempting to locate sub-bottom objects using sidescan sonars, resonant scatter detection systems, or another technology). The solution, as this document has already suggested, might be to exploit the ability of bubbles to scatter nonlinearly. The next section will discuss methods in use in biomedical ultrasound which take advantage of nonlinear scatter for the purpose of bubble scatter enhancement. It will then be argued that one of these methods, pulse inversion, can be in a sense reversed for the purpose of bubble scatter suppression. This hypothesis will then be tested using a computer simulation.

2.2 Dynamics of an acoustically excited bubble

In response to low-amplitude acoustic excitation, bubbles will act as simple linear oscillators. Consider a single degree of freedom system, as depicted in Figure 2.1.

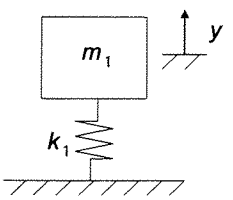

Figure 2.1 A single degree of freedom system

The equation of motion for the single degree of freedom system shown above is given by the following well-known equation [38].

$$F(t) = m_1 \frac{d^2x}{dy^2} + c_1 \frac{dx}{dy} + k_1 x \tag{2.1}$$

For this oscillator, the resonance frequency can be obtained via the expression $f_{res} = (k_1\ m_1^{-1})^{1/2}$. With respect to the driving signal, the frequency spectrum is comprised of three regions [39]. At frequencies much below resonance the system is said to be in the stiffness region, as the stiffness of the spring determines the motion of the mass. In the stiffness region, the system mobility (the ratio of velocity and force) is proportional to $\omega\ k_1^{-1}$, where ω is the radial driving frequency and k_1 is the system stiffness. At resonance, the system will exhibit damping-limited unstable oscillation. At frequencies much above resonance, the system is said to be in the inertial region, as the motion is dictated mostly by the properties of the mass. In the inertial region, the system mobility is proportional to $\omega^{-1} m_1^{-1}$, where ω is the radial driving frequency and m_1 the system mass. A bubble can be modelled as a single-degree of freedom system where the stiffness is given by the compliant gas volume and the mass term refers to the inertia of the fluid entrained in the motion observed as the bubble pulsates [11]. The formula for the resonance frequency of a bubble is of the same form as that for a mechanical system, but the stiffness and mass terms are replace respectively by the bubble stiffness and the sum of the bubble mass and the radiation mass [11]. Radiation mass here refers a quantity equal to three times the mass of the water

displaced by the pulsating bubble [11]. If the bubble is assumed to be spherical, the system is treated as adiabatic, and the mass of the bubble is assumed to be insignificant in comparison to the mass of the water entrained in oscillation, then the bubble resonance ω_o is given by [11]

$$\omega_o = \frac{1}{R_o}\sqrt{\frac{3\gamma p_{i,e}}{\rho} - \frac{2\sigma}{\rho R_o}} \qquad (2.2)$$

In this expression, R_o is the radius of the undisturbed bubble, σ is the liquid surface tension, γ is the ratio of the specific heat of air at constant pressure to that at constant volume, $p_{i,e}$ is the pressure inside the bubble when undisturbed, and ρ is the density of water.

When an acoustic wave encounters a static object, the incident acoustic energy is either reflected, transmitted, or absorbed in accordance with the relation between the geometry of the object and the wavelength of the ensonifying energy [21]. The same holds true when an acoustic wave encounters a dynamic object (such as a bubble), although in addition an ensonified dynamic object will also reradiate sound [11]. This reradiation is driven by oscillatory excursions in the radius of the bubble, which will also result in scattering. However, since bubbles are nonlinear oscillators, the type of sound scattered by bubbles is classified as being nonlinear scatter. Defintions of by linear and nonlinear scattering will now be given.

A linear system is defined according to the principles of superposition

[40]. If $y_1[n]$ and $y_2[n]$ are the responses of a system when $x_1[n]$ and $x_2[n]$ are the respective inputs, then the system is linear if and only if

$$T\{x_1[n] + x_2[n]\} = \{Tx_1[n] + Tx_2[n]\} = y_1[n] + y_2[n] \tag{2.3}$$

and

$$T\{ax[n]\} = aT\{x[n]\} = ay[n] \tag{2.4}$$

where a is an arbitrary proportionality constant. The relationships expressed in equations (2.3) and (2.4) are known respectively as the properties of *additivity* and *scaling*. The properties can be combined to express the principle of superposition, which can be written as

$$T\{ax_1[n] + bx_2[n]\} = aT\{x_1[n]\} + bT\{x_2[n]\} \tag{2.5}$$

A target does not need to be perfectly rigid or non-porous to scatter linearly, but such an object will indeed scatter all sounds in a linear manner. When a target is not perfectly rigid, then the dynamics of the target structure will influence the scattered field. In the case of a target of weakly elastic material such as steel of a few millimetres thickness excited by low-intensity, audio frequency[5] sounds, the structure can be expected to exhibit resonances. At these resonances, the target will "ring", and this will influence the re-radiated signal in both the frequency and time domains.

---

[5] The audio frequency range is generally accepted to be roughly 20 Hz - 20 kHz. Here, the term 'low-intensity' pertains to a sound of a level which would be audible but not uncomfortable for a listener.

Bubbles are nonlinear oscillators as pointed out above [11]. A simple example of a nonlinear system can be expressed by stating that a system's response is related to the driving force through a power series expansion:

$$\Psi(t)=s_1 fi(t)+ s_2 fi^2(t)+s_3 fi^3(t)+ s_4 fi^4(t)... \quad (2.6)$$

where Ψ is the general response of the oscillator, and fi is the driving force. The parameters s_1, s_2 *etc.* are coefficients. Consider a single frequency driving pulse defined as $P(t) = P_A \cos\omega t$, where ω is the angular frequency, P_A is the amplitude, and t is time. If this signal is substituted into (2.6), it can be seen that frequencies which are integer multiples of the fundamental driving frequency will be generated. It should be noted that the power series expression of bubble nonlinearity is useful, but incomplete. It does not for instance predict subharmonics, which have been shown to be produced by nonlinearly oscillating bubbles [41], or any dynamics following the end of the excitation pulse (so-called 'ringing').

Rayleigh first showed bubbles to be nonlinear oscillators in a 1917 publication [42], and Plesset was the first investigator to apply this equation to cavitating bubbles [43, 44]. The following result, which has been reproduced in several places [11, 45], is thus known commonly as the Rayleigh-Plesset equation:

$$R\ddot{R}+\frac{3\dot{R}^2}{2}=\frac{1}{\rho}\left\{(p_o+\tfrac{2\sigma}{R_o}-p_v(\tfrac{R_o}{R})^{3\kappa})+p_v-\tfrac{2\sigma}{R}-p_o-P(t)\right\} \quad (2.7)$$

In the equation above, R is the bubble radius, $\dot{R}$ is the first derivative

of the bubble radius, $\ddot{R}$ is the second derivative of the bubble radius, ρ is the density of gas within the bubble, κ is the polytropic index, σ is the surface tension of the liquid, p_o is the hydrostatic liquid pressure outside the bubble, and $P(t)$ is the time-varying driving acoustic pressure. This result accounts for viscous damping, but not radiation damping. More advanced formulations for the nonlinear response of a driven bubble have been derived by several investigators to take radiation damping, including a family of formulations known as the Herring-Keller/Keller-Miksis equations. The Herring-Keller equation [46] [47] is the result which was used to develop the numerical output presented later in this chapter:

$$\frac{3\dot{R}^2}{2}\left(1-\frac{\dot{R}}{3c_w}\right)+R\ddot{R}\left(1-\frac{\dot{R}}{c_w}\right)= \left(1+\frac{\dot{R}}{c_w}\right)\frac{1}{\rho_w}\left(p_L-p_0-P\left(t+\frac{R}{c_w}\right)\right)+\frac{R}{\rho_w c_w}\frac{\mathrm{d}p_L}{\mathrm{d}t} \tag{2.8}$$

where values are defined for the variables as above, c_w indicates the sound-speed in the liquid, ρ_w indicates the density of the water when undisturbed, and p_L is the pressure within the liquid just outside the bubble.

2.2.1 Scattering cross-section of a bubble

If a plane-wave were to travel from left to right through a field free of any inhomogoneities, it would be expected that no energy would be reflected to the left. However, if the wave were to encounter a rigid, normal plate of cross-sectional area Ω, then all of the sound incident

on that surface would be reflected to the left; it could be said then that the plate has a scattering cross-section of area Ω. If that plate were to vibrate, then further energy would have to be supplied by the acoustic field to sustain the vibrating motion. This increase in supply of energy to the plate could be accounted for by increasing the effective size of the plate to give a larger effective scattering cross-section. For a bubble, the time-averaged scattering cross-section Ω^{scat}_{b} is

$$\Omega^{scat}_{b} = \frac{\omega_1^4 4\pi R_o^2}{\Pi^2} \quad (kR_o<<1) \tag{2.9}$$

where ω_1 is the driving frequency, R_o is the equilibrium radius of the bubble, Π is a function describing the frequency response of the forced bubble, and k is the wavenumber. The function given above in (2.9) is shown in graphical form in Figure 2.2 below. In Figure 2.2, q indicates the so-called quality factor, which is defined as the number of radians required for the energy to decay by a factor of e^{-1}

$$q = \frac{\omega_{damped}}{2\beta} \tag{2.10}$$

where ω_{damped} is oscillatory frequency of the damped system and β is the damping factor. Note that the natural system resonance in the absence of damping ω_o is related to the damped oscillation frequency via $\omega_{damped} = (\omega_o^2 - \beta^2)^{1/2}$.

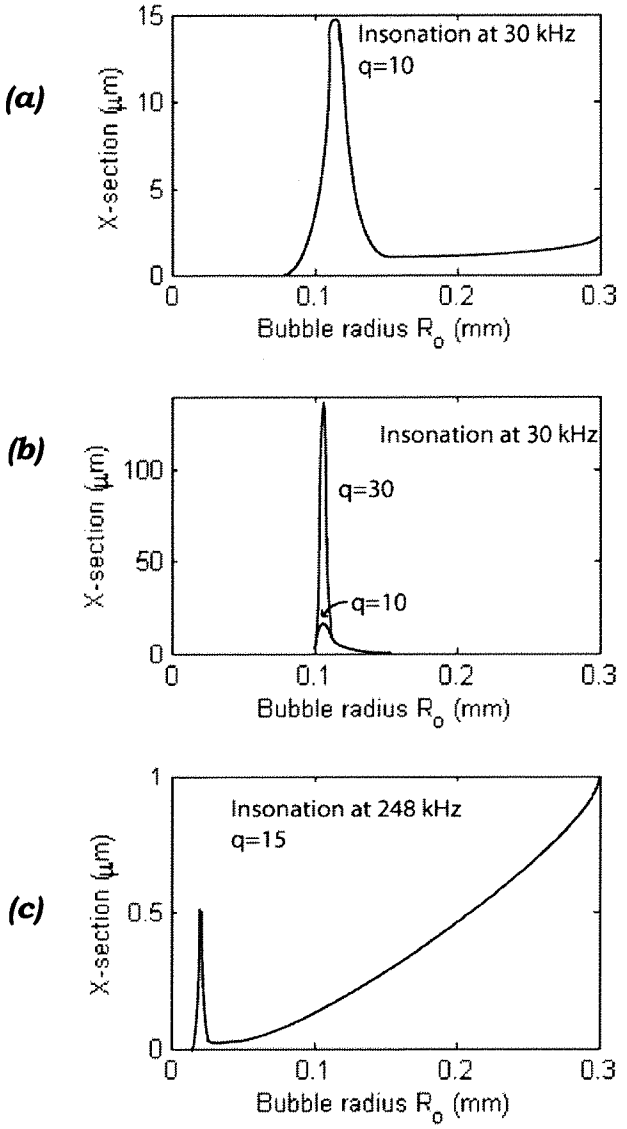

Figure 2.2 The scattering cross-section of a bubble, for which the damping is assumed to be constant with frequency. Linear harmonic bubble pulsations assumed. *(a)* Insonation at 30 kHz with q=10. *(b)* Insonation at 30 kHz for bubbles having *q*=10 and *q*=30. *(c)* Insonation at 248 kHz for *q*=15. (Figure and caption after Leighton [11]; in this figure, *q* indicates the quality factor as defined by the number of radians required for the energy to decay by e^{-1}).

An analysis of Figure 2.2 leads to some interesting conclusions. For a bubble cloud containing bubbles of many sizes and ensonified at frequency ω_1, it might be hypothesised that the only bubbles to

respond and thus cause variations in the sound field would be those having a resonance frequency $\omega_0 \approx \omega_1$. The resonant peak in Figure 2.2 *(a)* makes it clear that these resonating bubbles would indeed respond. However, this resonant peak is only a local maximum, as is shown in Figure 2.2 *(c)*. In that figure, the rising tail on the cross-section plot shows that with increasing insonation frequency, the cross-section may attain values comparable or greater than the resonance value [11]. This is a result of the fact that as the bubble dimensions approach the wave size, geometric effects (such as shadowing) begin to dominate even though physical effects on the bubble caused by the sound may be relatively imperceptible. Usefully, at low insonation powers, the emission of the second harmonic is a global maximum when the insonation frequency coincides with the bubble resonsance [11]; a point which will be expanded upon later in this chapter. The next section will show how the physics of acoustically excited bubbles can be taken advantage of for the purpose of detecting the presence of bubbles in the blood stream.

2.3 Bubble scatter enhancement in ultrasound

Blood flow is essentially transparent to *in vivo* ultrasound measurements. This is a result of the fact that the mismatch of acoustic impedances is relatively low at the interfaces between blood and tissue ($z_{water}/z_{tissue} \approx 2.25$ MRayl/1.5 MRayl [48] where z_{water} and z_{tissue} are the specific acoustic impedances of water and tissue respectively, and a Rayl is a Pa s m^{-1}, known as a Rayleigh). As such,

sonographers and other practitioners of biomedical ultrasound have long sought ways to improve blood flow-measurements. Gramiak and Shah provided a breakthrough in 1968 when they reported that, during M-mode cardiography[6] [49], they noticed the appearance of a cloud of echoes during intracardiac injections of indocyanine green dye - a substance used to trace blood flow [50]. It was later discovered that this contrast effect could reproduced by injecting almost any liquid into a flow through a needle or catheter; and that the contrast was caused by bubbles introduced into the flow in the injection process. This detection resulted from the effects of impedance mismatch and bubble scattering as described above.

2.3.1 Doppler imaging

Nishi [51] improved the contrast between bubbles in the bloodstream and their static surroundings by taking advantage of the Doppler effect. When driving a field at a frequency f, the motion of ensonified bubbles within the blood stream results in the generation of reflections at shifted a frequency f' which is given by:

$$f' = (c/(c+V_b))\, f \qquad (2.11)$$

where c is the sound speed, f is the operation frequency, and V_b is the

---

[6] M-mode, or "Motion-mode", ultrasound is the study of the acoustic returns from a single acoustic beam. In this mode, the acoustic beam is projected onto an object, which provides a single acoustic return. Any motion of that object will cause a variation in the time-history of the reflection of the acoustic beam.

velocity of the bubble along an axis extending between the bubble and an observer. The system response may then be filtered for energy at the Doppler shifted frequency f', thereby increasing bubble contrast by suppressing the response of any non-moving objects which will would have reflected energy at the input frequency f. It should be noted that the ability of Doppler methods to increase contrast is limited as a result of the fact that body tissue is not entirely static. As a result, tissue echoes may also exhibit some frequency shift [52].

2.3.2 Resonance imaging

Fairbank and Scully [53] attempted to use resonance scattering to identify pressure variations in the heart. They hypothosised that pressure excursions in the heart would lead to a shift in the resonance of bubbles contained within the bloodstream (see equation (2.2), where the undisturbed bubble radius R_0 is a function of the equilibrium pressure). This hypothesis is borne out by theory and experiment. However the analysis of Fairbank and Scully does not take into account that resonant bubbles will not be the only ones to respond to the input pulse. According to Figure 2.2 *(c)*, it may occur that the response measured from an ensonified bubble cloud containing a wide size distribution[7] would be dominated by bubbles

[7] Greater in radius by more than about an order of magnitude

much larger than those at resonance[8]. This is a result of the fact that the resonant peak in scattering cross-section is only a local maximum as shown in Figure 2.2. A problem therefore presents itself which limits the applicability of both the method of Fairbank and Scully and that of Nishi to only those clouds displaying a narrow size distribution. It should be noted that in the tests of Fairbank and Scully [53], the population distribution is reported to have only extended from 30 μm to 40 μm, so the issue mentioned here no way invalidates the results reported in that publication. This argument merely limits the variety of bubble clouds to which resonance methods can be applied succesfully.

2.3.3 Second harmonic[9] imaging

One way of in which the limits of resonance imaging can be overcome is by taking advantage of second harmonic emissions. As discussed

---

[8] Larger by more than about an order of magnitude.

[9] In some texts concerning manners of acoustics, there is an ambiguity regarding the meaning of "second harmonic". In many writings on music and musical acoustics, "second harmonic" is used to refer to the third frequency peak which would appear on the frequency spectrum appropriate to a particular compound sound, such as that generated by a musical instrument (see for instance Olson, Music, Physics, and Engineering). Here as in many treatises on biomedical ultrasound and sonar, "second harmonic" is used to indicate the second peak in the ascension of the harmonic series for a given sound (the frequency which is one octave above the fundamental; also $2\omega_1$ where ω_1 is the driving frequency).

earlier, bubbles are nonlinear oscillators, the scatter of which can be represented by using a power series representation as shown in equation (2.6). It was shown that if a bubble is driven by a sinusoidal signal such as $P(t) = P_A \cos\omega t$, frequencies which are integer multiples of the fundamental driving frequency can be generated by the scattering bubble. At low driving amplitudes, the bubble size corresponding to resonance will act as the global maximum for scattering cross-section if the signal is filtered for the *second harmonic*.

Miller [54] took advantage of this fact when developing his resonant bubble detector in 1981. Miller produced a cloud with a bi-modal size distribution, and was able to use second harmonic emissions to distinguish between bubbles with radius on the order of microns, and the larger bubbles with radius on the order of hundreds of microns. Vacher *et al.* [55] produced a device which operated on the same principle, but used a frequency sweep in the source and a corresponding sweep in the receiver (always higher than the source frequency by a factor of two) so that bubbles of a large size range could be monitored accurately. The success of these methods gave way to the development of bubble design for the purpose of ultrasound contrast enhancement. The first commercial version of these so-called ultrasound contrast agents (UCAs) was developed by Meltzer *et al.* (all of whom worked concurrently for Rasor Associates and Stanford University) [56]. The bubbles designed by Meltzer *et al.* were reported

to be of diameter 75 +/- 25 μm.

A significant shortcoming in the application of second harmonic imaging is that this method inherently involves a trade-off between contrast and spatial resolution [52]. If a single-frequency, long-length (50+ cycle) continuous-wave (CW) pulse is used for ensonification, then it is possible to obtain very narrow frequency bandwidth in the output signal, and so there will be a narrow frequency peak in the second harmonic. However, in a dynamic environment it is not practical to employ long-length CW pulses, because the physical system may change considerably in the time period during which the system is still being ensonified giving way to ambiguous result. Such an approach would allow for excellent frequency resolution, but spatial information of little or no use. Thus, in a dynamic system short echolocation pulses are used. Short pulses reduce the "smearing" of the returned signal which will occur as a result of the presence of moving targets and decrease the blind time for the sonar, but at the cost of broadened input pulse bandwidth. Any broadening in the bandwidth of the driving frequency will result in result in a two-fold broadening of bandwidth in the harmonic.

To illustrate the signal degradation that will follow as a result of this fact, consider an outgoing pulse with half-power upper and lower frequency limits from ω_a and ω_b, respectively. The outgoing signal then has a half-power bandwidth of $\omega_b - \omega_a$. The second harmonic will

therefore have half-power upper and lower limits of $2\omega_a$ and $2\omega_b$, so that the bandwidth is now $2(\omega_b - \omega_a)$ – twice that of the outgoing pulse. This may result in a reduction the amount of usable bandwidth: If ω_b is greater than or nearly equal to $2\omega_a$, then an ambiguity will be present in the crossover region between the upper frequency limits of the emitted pulse and the lower limits of the received pulse.

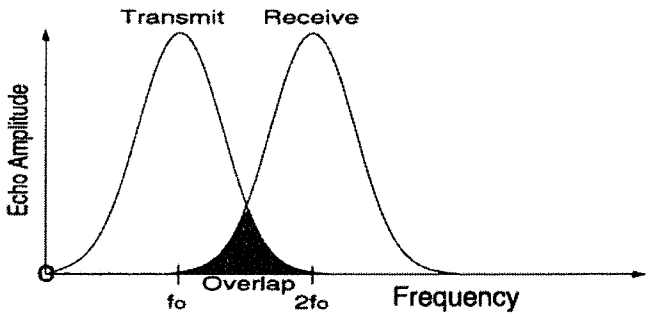

Figure 2.3 Overlap between the transmit and receive passbands results in harmonic mode (This figure and caption taken from Simpson *et al.* [52] who in turn cited Powers *et al.* [57])

To summarise these points, this method may be useful in certain restricted situations - especially where harmonic data becomes available opportunistically within the results of other measurements. However in those situations where an echolocation signal and send/receive transducer can be custom-built, more advanced methods such as pulse-inversion out-perform the second harmonic approach.

2.3.4 Combination frequency techniques

As stated earlier, the echo from a nonlinearly driven bubble can be approximated by a power series $\Psi(t)=s_1.fi(t)+ s_2.fi^2(t)+s_3.fi^3(t)+ s_4.fi^4(t)...$ (2.6). If such a system is driven using two multiple frequencies, then

the system output will result in the presence of so-called sum and difference frequencies. If two insonating frequencies are used, then bubbles can be detected and sized [11]. Consider a driving pressure P_{comb} consisting of two coherent pressure waves

$$P_{comb} = P_\alpha \cos \omega_\alpha t + P_\beta \cos \omega_\beta t \qquad (2.12)$$

where $\omega_\alpha > \omega_\beta$. If this input is substituted into the above power series formulation, a result is obtained which contains a quadratic component. This component can be expanded to show sum and difference frequencies

$$2P_\alpha P_\beta \cos \omega_\alpha t \cdot \cos\omega_\beta t = P_\alpha P\beta[\cos (\omega_\alpha + \omega_\beta)t + \cos (\omega_\alpha - \omega_\beta)t \,] \quad (2.13)$$

Based on this phenomenon, Newhouse and Shankar described this method, labelling the lowering frequency (selected near resonance) as a "pumping" frequency, and the higher frequency as an "imaging" frequency [58]. Shankar *et al.* [59] employed this method to successfully size UCAs and thereby monitor fluid pressure fluctuations.

2.3.5 Pulse Inversion Doppler

Pulse-inversion (PI) Doppler, developed by Simpson *et al.* [52], combines the advantages of nonlinear harmonic generation and Doppler filtering to obtain results which can be superior to those garnered when either of those technologies are exploited on their own. Simpson *et al.* claim that PI Doppler can improve 3 to 10 dB more agent to tissue contrast than harmonic imaging with similar pulses. Further, they claim that so-called broadband PI Doppler can provide

up to 16 dB greater contrast than conventional Doppler filtering. Their approach is presented here in two parts: first the theory of PI will be presented, and then it will be shown how Doppler shift can manifest itself uniquely within PI data.

2.3.5.1 Pulse Inversion

Consider the result when a linear and a nonlinear scatterer are each exposed to two pulses in succession, the second of which is the switched polarity version of the first pulse, as shown below in Figure 2.4.

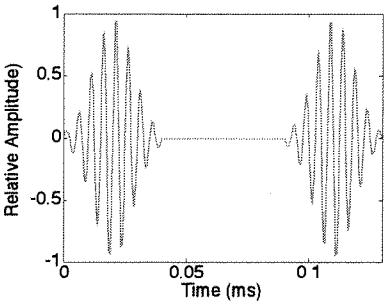

Figure 2.4 A pulse-inverted signal consists of two pulses in succession, the second of which is the switched polarity version of the first. The driving frequency in the example shown is 200 kHz.

For the purpose of this initial analysis, assume that the linear scatterer is highly damped, and so exhibits no ringing. In response to the incident pressure signal (P_{pos} or P_{neg}) a heavily-damped linear scatterer will return a signal ($P_{pos,l}$ or $P_{neg,l}$), a phase-identical version of the incident pressure signal which has been scaled by a factor s_T. A nonlinear scatterer approximated using a power series will return signals $P_{pos,nl}$ and $P_{neg,nl}$ of the form shown in the third column in Table 2.1.

Table 2.1 Harmonic suppression and enhancement

Incident Pulse	Linear Scatter	Nonlinear Scatter
Positive	$P_{pos,l} = s_T P_{incident}$	$P_{pos,nl} = s_1 P_{incident} + s_2 P_{incident}^2 + s_3 P_{incident}^3 + s_4 P_{incident}^4 + \ldots$
Negative	$P_{neg,l} = -s_T P_{incident}$	$P_{neg,nl} = -s_1 P_{incident} + s_2 P_{incident}^2 - s_3 P_{incident}^3 + s_4 P_{incident}^4 + \ldots$

Consider the linear scattering described in Table 2.1. The sum of the returns (P_+) from the linear scatterer is field described by

$$P_{pos,l} + P_{neg,l} = P_+ = 0 \tag{2.14}$$

while the difference of the returns is

$$P_{pos,l} - P_{neg,l} = P_- = 2\, s_T P_{incident} \tag{2.15}$$

It can be seen from equations (2.14) and (2.16) that in the absence of nonlinear scattering, P_+ suppresses the all information. Conversely, equations (2.15) and (2.17) show that P_- enhances the signal by a factor of two. The results become more interesting when nonlinear scattering is taken into account. In that case, adding the scattered terms suppressed the odd-numbered terms

$$P_{pos,l} + P_{neg,l} = P_+ = 2\,(s_2 P_{incident}^2 + s_4 P_{incident}^4 + \ldots) \tag{2.16}$$

And subtracting the scattered terms suppresses the even-numbered terms

$$P_{pos,l} - P_{neg,l} = P_- = 2\,(s_1 P_{incident} + s_3 P_{incident}^3 + \ldots) \tag{2.17}$$

Simpson *et al.* [52] argue that body tissue scatters mostly linearly, and so will only exhibit acoustic scattering at the driving frequency. Since the driving frequency only appears in P_- and not P_+, the nonlinear scatterers present within the system (UCAs) will theoretically be the only signal present in P_+.

The contrast gained through PI, argue Simpson *et al.* [52], can be enhanced by taking advantage of the Doppler effect. As discussed previously, Nishi [51] sought a Doppler shift based on the driving frequency; an approach which is limited in applicability as a result of the fact that under clinical ultrasound conditions, the body tissue surrounding the bubbles is not necessarily static [52]. Simpson and Burns [28] and Simpson *et al.* [52] instead searched for Doppler shift on the pulse repetition frequency (PRF), as explained here.

2.3.5.2 Doppler shift of the pulse repetition frequency

Having established above that a twin input pulse consists of two portions, P_{pos} and P_{neg}, the echoes from those driving pulses are now denoted as follows:

$$e_1(t) = \text{Echo}[P_{pos}] \tag{2.18}$$

$$e_2(t) = \text{Echo}[P_{neg}] \tag{2.19}$$

Where scattering is linear, successive echoes m will take the following form:

$$e_{m+1}(t\,(m\text{-}1)\,\tau) = -e_m(t - m\,\tau - \Delta\,\tau_{detect}) \tag{2.20}$$

where τ is the interpulse delay, and $\Delta\tau_{detect}$ is the change in echolocation delay caused by the interpulse axial motion of a detected object. The quantity $\Delta\tau_{detect}$ can also be expressed according the amount of motion as $\Delta\tau_{detect} = 2\Delta d_{detect} c_o^{-1}$, where Δd_{detect} is the axial distance the detected object travelled in the interpulse time and c_o is the speed of sound in the detection medium. The phase shift between successive echoes $\Delta\tau_{detect}$ measured relative to the operating frequency

f_{op} will then be

$$\Delta \varphi_{detect} = 2\pi f_{op} \Delta\tau_{detect} + \pi \qquad (2.21)$$

where the additive π is a result of the negative sign in front of e_m in (2.20). Next is introduced the pulse repetition frequency $f_{pr} = \Delta\tau^{-1}$. The Doppler shift f' (see (2.11)) can then be formulated as

$$f' = f_{pr} \Delta \varphi_{detect} / (2\pi) = f_{op} * 2 V_{detect} / c_o + \tfrac{1}{2} f_{pr} \qquad (2.22)$$

where V_{detect} is the relative axial velocity of the detected object with respect to the transducer. Recall that echoes received as a result of nonlinear scattering appear a shown in Table 2.1, so that the odd harmonics are added to the positive incident pulse and subtracted from the negative incident pulse. The Doppler shifts for the two components can be formulated according to the previous equation as

$$f'_{odd} = f_{op} * 2 V_{detect} / c_o + \tfrac{1}{2} f_{pr}$$

$$f'_{even} = f_{op} * 2 V_{detect} / c_o \qquad (2.23)$$

According to this formulation, the even harmonics have a Doppler shift which is the same as that produced by conventional Doppler. The limiting factor in this approach is the velocity of all moving scatters must obey the limit caused by the folding frequency limitation, which in this case is have of the conventional limit

$$f_{op} * 2 | V_{max} | / c_o \leq \tfrac{1}{4} f_{pr} \qquad (2.24)$$

This form of Doppler gives a spectrum wherein the region between $-\tfrac{1}{4}f_{pr}$ and $\tfrac{1}{4}f_{pr}$ contains only Doppler signals arising from nonlinear scattering, whereas the remaining half of the Doppler spectrum will contain Doppler signals arising from both linear scattering and possible higher order nonlinear scattering. Thus, the PI Doppler

approach takes advantage of a two pulse technique through both signal combination and Doppler filtering.

2.3.6 Section summary

The evolution of ultrasound bubble scattering detection techniques has been presented. It was shown that basic resonant techniques and Doppler filtering can be used to reveal the presence of bubbles in a system, but are not necessarily effective at selectively highlighting bubble scattering while neglecting tissue scattering. The contrast between the two media can be increased by taking advantage of the nonlinear scattering abilities of bubbles. Three methods for taking advantage of nonlinear scattering were presented; second harmonic imaging, combination input frequencies, and pulse inversion. Second harmonic imaging is more effective than resonant imaging because the acoustic cross-section for a resonant bubble is a global maximum for all bubble sizes at the second harmonic, but not at the fundamental frequency. Second harmonic imaging however yields images poor resolution. Pulse inversion takes advantage of nonlinear scattering in a more comprehensive manner than does second harmonic imaging, and can be combined with Doppler filtering to produce pulse inversion Doppler (PID). For the purpose of imaging, Pulse inversion Doppler offers superior output when compared to all of the other technologies discussed here.

2.4 Oceanic bubble-cloud contrast enhancement and suppresion

It was shown that bubble scattering can be used to differentiate bubbles from surround tissue so that the bubbles act as ultrasound contrast agents (UCAs). While the purpose of this investigation is to develop a bubble scatter suppression technology, it has already been argued that such a task might be made easier if bubble scatter enhancement can be harnessed in the denominator of some detection algorithm. On that basis, this section will now consider ways in which it might be possible to enhance and suppress the contrast of bubble clouds in oceanic sonar studies. The previous section described the way in which linear and nonlinear bubble scattering of ultrasound was exploited by various researchers to investigate micro-bubble behaviour. Not all of these techniques translate well from the ultrasonic laboratory to the oceanic setting.

2.4.1 Previous oceanic bubble cloud studies based on linear dynamics

Of the UCA detection methods discussed, two rely on linear dynamics, resonance imaging and Doppler filtering[10]. Resonance imaging has

---

[10] While Doppler can of course be applied to systems exhibiting nonlinear scatter, filters of this type do not capitalise on information gained in driving the bubbles nonlinearly. The exception to this is Pulse Inversion Doppler which, when discussed

been applied in the ocean with limited success [60]. This approach was already shown to be unreliable for those cases where the bubble cloud may contain bubbles of a wide size distribution, as do those clouds which are encountered in the ocean (see Chapter 3). Doppler filtering might be useful in the ocean in cases where the median bubble speed is high enough to overcome input signal bandwidth limitations. However, the fact that the terminal rise speed of the smallest oceanic bubbles (which make up the vast majority of oceanic bubbles [11]) is on the order of 1/10000 as compared to the oceanic sound speed suggests that such an approach is not appropriate for the solution sought here.

2.4.2 Previous oceanic bubble cloud studies based on nonlinear dynamics

Two of the nonlinear approaches used for the study of biomedical UCAs have also been applied in the oceanic environment: combination input frequencies [61, 62] and second harmonic methods (Sutin *et al.* [63] cite Ostrovsky and Sutin [64, 65] as having applied a second harmonic approach in oceanic waters, but the author was unable to obtain these publications). Before this investigation [66], pulse-inversion had not yet been applied to oceanic bubble clouds. In order to take advantage of any of the three above-mentioned methods,

---

in this document, is always referred to in its complete form (PID).

investigators must be able to drive oceanic bubble clouds nonlinearly. This task is considerably more different in the ocean than in the biomedical environment: in the ocean, clouds may have primary dimensions of several meters and contain bubbles spanning four orders of magnitude in radius, while in the body manufactured bubbles of a size range varying by only +/- 10 microns can be presented, and then only occupy a region of a few square centimetres.

2.4.3 Driving a large bubble cloud with the intention of causing nonlinear scattering

In order to obtain a nonlinear response from the bubbles within in a cloud by means of an acoustic source, some consideration must first be given to the appropriate driving frequency. The response to an acoustic excitation by a bubble is dependent on the frequency, amplitude, and duration of the input signal. Since the amplitude of response is maximal at resonance, the effects of nonlinearity are most apparent for a bubble excited at the resonance frequency. A formulation for the resonance frequency was given above in (2.2), and is approximately proportionate with the reciprocal of the radius, especially for larger bubbles (R_0>~10 μm) where surface tension effects are nearly negligible [11].

Assuming negligible surface tension, Minnaert [67] derived bubble resonance as

$$\omega_M = \frac{1}{R_0}\sqrt{\frac{3\gamma p_0}{\rho}} \qquad (2.25)$$

where ω_M is the Minnaert resonance frequency, R_0 is the bubble equilibrium radius, γ is the ratio of specific heats for air, p_0 is the equilibrium pressure, and ρ is the density of water. If the bubble is driven with a sufficiently low amplitude signal, that system will scatter nearly linearly. As the driving frequency approaches zero (and the system is being driven in the stiffness region), the output gain across the system approaches unity. Above resonance however (in the inertial region), the system transfer function exhibits a 6 dB octave^{-1} reduction (20 dB decade^{-1}) [68]. Therefore a bubble responds to driving signals at frequencies far below resonance much more readily than to those driving signals far above resonance [25]. This means that to drive a given bubble non-linearly, less input force is required at frequencies below resonance than would be required were the same bubble driven above resonance. Since resonance frequency varies with inverse proportion to the size of a bubble, it would seem that the optimum frequency for driving a polydisperse bubble cloud nonlinearly would be the resonance frequency of the largest bubble.

In using the plots showing the scattering cross-section of a bubble versus frequency Figure 2.2, it might appear as if the use of a very low frequency (much less than the resonance of any present bubble) is in fact) would make any bubbles present complete invisible to the detection system. This conclusion is reasonable, however it will be

seen in the next chapter that the size distribution of bubbles within a cloud covers many orders of magnitude, and that the largest oceanic bubbles have a resonance on the order of a few kHz. In order to render the bubbles inconsequential in terms of scattering, a frequency on the order of a few hundred Hz would have to be used. While some sonars do exist which use very low frequencies [69], such systems are impractical in shallow water where the wavelengths of such low frequency signals would be of the same order of magnitude as the relevant depths. This conclusion provides motivation for the use of signals on the order of a few kHz in applications where it is desired to drive the bubbles within an oceanic cloud nonlinearly [70]. This approach is contrary to the current trend of using the high frequency sonar so adept at creating visually detailed images (see 2.7.1.2), but commensurate with the use of low frequencies for resonance detection [36]. The next section describes some limitations of low-frequency sonar.

2.4.4 Sonar blindspots

In an active detection system, the total length of the outgoing pulse (wavelength multiplied by the number of cycles) dictates the nearest perceptible objects. This can be illustrated by considering the physics involved in a simple sonar scenario. Consider a sonar system operating in a noise-free acoustic free-field which contains a single linearly scattering object (for instance, a rigid wall) at a distance of 10 meters from the target. For the purposes of this illustration, the

operation frequency will be 1500 kHz so that the wavelength is 1 m. The outgoing pulse will generally contain more than one acoustic cycle so as to minimize driver overloading, improve phase-matching in the detection algorithm, and minimize the frequency bandwidth of the pulse. However, if the pulse is too long (in this example, more than 10 cycles), then the time periods during which the first echo is returned from the wall will coincide with the period during which the acoustic driver will be active. In this case, it will be impossible for the receiver system to discern between the outgoing pulse and the received pulse. Therefore, the sonar system will have a 'blind spot' of range corresponding to the amount of space occupied by the echolocation signal within the detection environment. Consider now the case where the detection pulse has two parts separated by a time $\Delta\tau$, as in PI. The maximum lengths of the individual components of the output pulse are limited by the same constraints as for the single pulse system. However, the inter-pulse time $\Delta\tau$ is determined by the constraint that any detectable feature should not be ensonified by both halves of the output pulse at any one time. In summary, the limiting factor for the length of any ensonification pulse is determined by the one-way travel distance from the sonar to the nearest detectable target, whereas the minimum usable inter-pulse time is determined by the two-way signal travel time to the nearest detectable target. The next section shows how it might be possible to take advantage of the *en masse* nonlinear behaviour of bubbles within a cloud to give way to a method capable of suppressing bubble scatter.

2.5 The Twin Inverted Pulse Sonar

Pulse Inversion (PI) is a technique which is used to solve a problem which is essentially the opposite of target detection in oceanic bubble clouds [29] as discussed in 2.3.5. PI depends on the enhancement of nonlinear scatter by so-called biomedical ultrasound contrast agents (UCAs), which were discussed earlier in this chapter. However, oceanic target detection in bubbly water is more complex than UCA detection for two reasons. First, PI techniques are designed to *enhance* the scatter from many bubbles, the radii of which might span *a few micrometers*. By contrast, in oceanic target detection, the goal is to *diminish* the scatter from millions of bubbles the radii of which span *several orders of magnitude*, whilst searching for a *single* target. A second complication presents itself as a result of frequency response consideration. In UCA detection, the bubbles will tend to scatter in a strongly nonlinear manner, while the tissue will only scatter linearly (though some nonlinear propagation may occur within tissue [70]). However, in oceanic target detection, both the bubbles and any linearly scattering target will respond together at the fundamental. Practically, TWIPS depends on the existence of an amplitude range where scattering by bubbles in nonlinear, but for that same range, scattering by the semi-rigid structures of interest is linear. It is proposed that PI output can be reversed for the purpose of enhancing linear scatter and suppressing nonlinear scatter. Such a notion was first published by Professor T G Leighton [24, 71] and was followed by

several related publications and a patent, all of which were published by Leighton, Finfer, and White [33, 70, 72-79]. The topic of twin-pulse processing is now reintroduced as a model for oceanic bubble scatter suppression, instead of UCA scatter enhancement, and the derived system is referred to as the Twin Inverted Pulse Sonar, or TWIPS.

2.5.1 Scattering of phase-reversed pulses

Re-consider the result when a linear and a nonlinear scatterer are each exposed to two pulses in succession, the second of which is the switched polarity version of the first pulse, as described in 2.3.5. Earlier it was shown how the echoes from the individual components of this pulse-pair can be manipulated to produce the sum and difference quantities according to the method of Simpson and Burns [28]. The difference of the returns, P_- will retain odd harmonics (including any linear scatter), while the sum quantity P_+ will retain even harmonics. Assuming that the bubble cloud can be driven nonlinearly on the logic of 2.4.3, P_+ will contain both bubble scatter (at the fundamental frequency as well as at the higher odd harmonics) and the target signal, while P_- will contain only the bubble signal. This means that P_+ is a less efficient discriminator than is P_-. The system is summarised below in Figure 2.5.

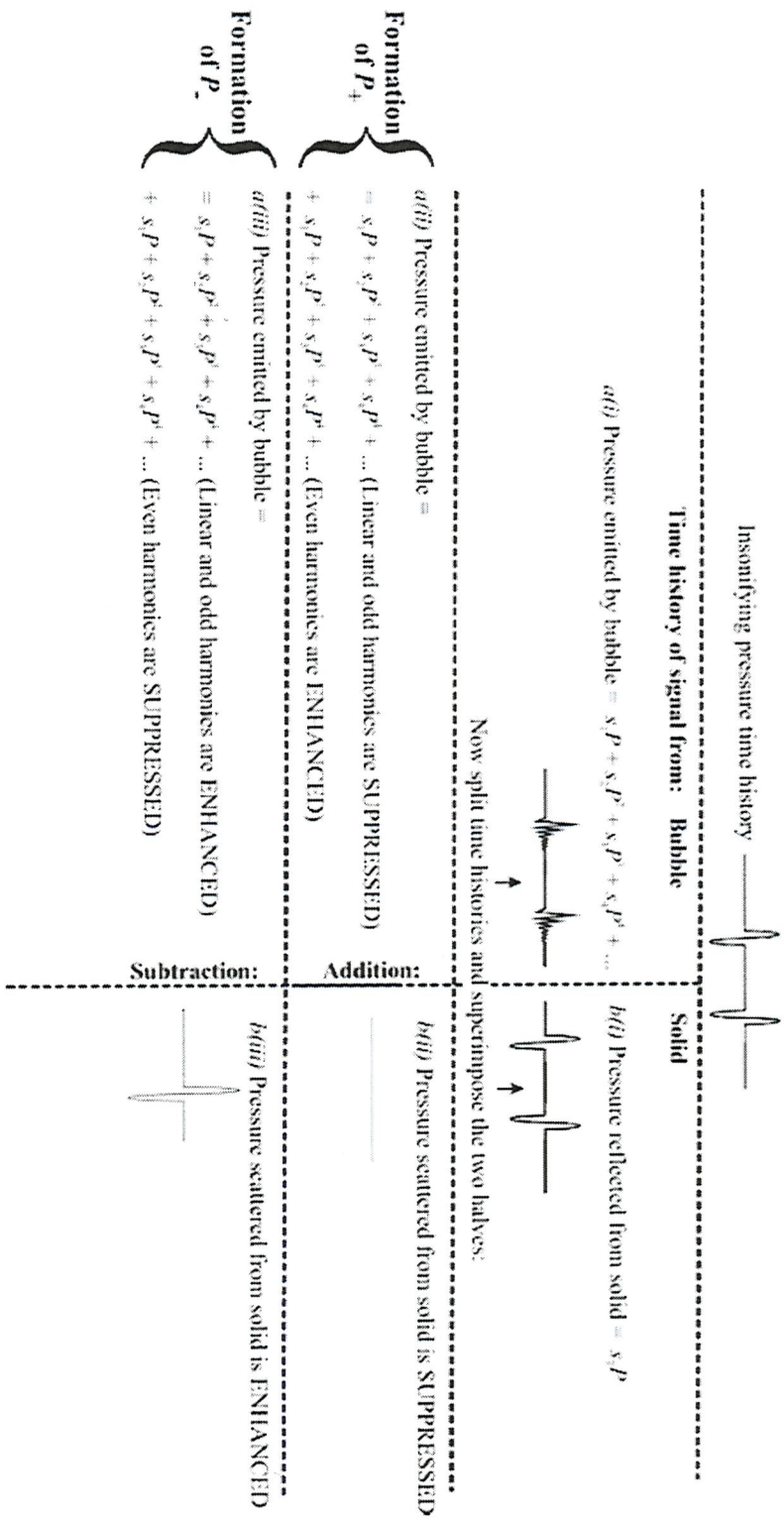

Figure 2.5 Summary of the formation of P_+ and P_-. Figure drawn by T G Leighton.

In the case where a target is being sought within a bubble cloud, P_-

contains both the desired information (the target scatter) and undesired information (the bubble scatter). Thus an algorithm is sought which will minimise the bubble scatter energy which appears within the system output. This will be accomplished by manipulating the physical system, employing a suitable low-pass filter, and using a novel signal processing technique, as will now be described.

The physical system of interest – a bubble cloud – can be manipulated to reduce undesired bubble scattering at odd harmonics (*e.g.* the undesired signal in P_-). The problem is two-fold: if the elements within the bubble cloud are excited nonlinearly, P_- will contain energy scattered by bubbles at both *the fundamental* and at *higher odd harmonics*. To reduce the amount energy scattered at the fundamental is fairly straightforward. At the beginning of section 2.2, it was stated that a bubble which is excited in a limited manner such that the radial excursions are much less than the radius of the undisturbed bubble will tend to scatter in a pseudo-linear fashion [11]. As the magnitude of radial excursions increases, so increases the nonlinearity present in the bubble dynamics. As the dynamic nonlinearity increases, the bubble scatter will exhibit harmonics of increasing amplitude. Thus, as the input power at the fundamental frequency increases, the bubble will begin to "pump" energy to higher frequencies [11, 80]. Input power in an acoustic system comes from the driving source; so that increasing source power will result in overall increase in the relative amplitude of harmonics, and thereby

decrease the relative amplitude at the fundamental frequency. This however does not solve the problem of higher harmonics within P_-. This simplest solution to this physical problem is the employment of a digital filter on P_- for frequencies above the fundamental. This approach has been termed as Twin Inverted Pulse Sonar 1, or TWIPS1.

$$\mathbf{T1}(t) = g(P_-) \tag{2.26}$$

where **T1** is TWIPS1 and P_- represents the difference of two halves of a pulse pair. The function g represents a generic normalisation and convolution routine, in addition to a filter of the type discussed above.

Up to this point in the development of the algorithm, only the ability for P_- to retain the target signal has been employed. It is instructive to consider then how P_+, the quantity used in PI to enhance bubble scatter, might be used to enhance the detection of linear scatterers. Since P_+ will theoretically contain no signal corresponding to target scatter, the reciprocal of this quantity could be used to suppress further any bubble scatter present within P_-. Detection methods based on this ratio are termed as TWIPS2.

$$\mathbf{T2a}(t) = g(P_-)\, g^{-1}(P_+) \tag{2.27}$$

Where **T2a** is TWIPS2a, and P_- and P_+ respectively represent the difference and sum of two halves of a pulse pair. The function g represents a normalisation and convolution routine similar to that discussed in conjunction with TWIPS1.

Consider two types of systems: (a) an environment containing no nonlinear scatterers or (b) the responses caused by linear scatters and nonlinear scatterers are temporally exclusive. If phase-matching is perfect (*e.g.* the sample rate is infinitely high, and the acquisition system presents no phase distortion), system (a) will return a response for TWIPS2a which is infinite at all points. In this case, TWIPS1 could be used to identify targets. System (b) however will return an infinite result at only those points where a linear target is present. In reality however such infinite results are not likely as P_+ is calculated based on two echoes generated under conditions which are not necessarily identical. Since the system requires two successive pulses, there is necessarily some delay between the playback of each half of the input pulse. The bubble cloud may evolve during this delay, meaning that the physical conditions encountered by each half of the pulse will not be identical. Further, in a controlled laboratory or in calm oceanic conditions, the ambient and electronic noise during the acquisition of each of these signals may be continuous and stationary, but will be still be stochastic. The noise observed during the response to the two successive sounds will not be identical, preventing the envelope of the amplitude of P_+ from being zero.

Therefore, TWIPS2a offers the potential for good results, but the technique is prone to unsteadiness as a result of its sensitivity to noise and variation in boundary conditions. In contrast, success with biomedical pulse inversion methods suggests that the TWIPS1

approach is robust, but considerably less statistically successful than a perfectly operating TWIPS2a system.

A steadying function can be introduced to reduce the impact of rogue minima in the denominator of TWIPS2a (which might result in misleading maxima in T2a output). When this steadying function is in the form of TWIPS1, the system is termed as being of the type TWIPS2b, **T2b**

$$\mathbf{T2b}(t) = g^{\xi_a}(P_-)g^{-\xi_b}(P_+) \qquad (2.28)$$

where all variables are as for equations (2.26) and (2.27). In equation (2.28), ξ_a and ξ_b act as control variables which alter the extent to which the respective algorithms TWIPS2a and TWIPS1 dominate the system output.

2.5.1.1 Signal amplitude range independence

It is interesting to note that time series which are returned to a sonar or radar system often suffer from a common characteristic: dependence of signal amplitude on range. Consider a monostatic[11] radar system mounted at an observation station which is being used to examine two objects; the first object is a tank and is at a range of 1 mile from the station, and the second object is an identical tank located 15 miles from the station. The effects of geometric signal

[11] *Monostatic* is used here to indicate that the source and receiver are co-located.

spreading and attenuation are such that the signal which is reflected by the furthest tank will be lower in amplitude than that signal which is reflected by the nearer tank. To generalise the idea, those objects closer to the source/receiver will return a signal which is disproportionately high in level when compared to the response corresponding to similarly-shaped objects at a greater distance. This means that the amplitude of the signal received at the radar station will have a range dependence, and that the energy within time series resulting from successively further reflectors will exhibit a downward sloping trend. This range dependence can be reduced by increasing signal directionality and/or using source directionality information in conjunction with estimates of the amount of absorption which may have affected the signal. Amongst sonar developers and users, this method of correction is known as "Time Varying Gain (TVG)" [81]. In non-littoral waters where there is only limited attenuation by bubbles and suspended sediment, it is reasonably straightforward to predict the signal attenuation, and it can generally be assumed that the TVG should remain constant from minute to minute. However, in shallow, dynamic waters, much more uncertainty is introduced by making estimates of the attenuation; and the applicability of assumptions concerning steady-state conditions must be called into question if there is any significant wave breaking and/or sediment transport in progress.

One interesting feature of TWIPS2 is that there is no such dependence

of range on amplitude, and so there is no need to introduce TVG. This is because, in that algorithm, the entire range-dependent vector representing the quantity P_- is normalised by another vector with identical range-dependence, that of the vector representing the quantity P_+. As per the above-explained limited applicability of TVG in shallow water, this feature contributes to the suggestion that the hypothesised sonar may be well-adapted to shallow water.

The feasibility of using TWIPS to detect solid objects in bubbly water was assessed first by using a very simple simulation employing a single bubble and a single pulse-pair. This simple simulation and its results will be now be discussed.

2.6 The single bubble simulation

The case presented in this section concerns only a single bubble. For the case shown here, a bubble of radius 22.5 microns was driven in the stiffness region at $f_{res}/2$ = 65.7 kHz.

Figure 2.6 summarises the results of the calculations used to show one way in which nonlinear bubble dynamics might indeed be exploited to differentiate linear from nonlinear scatterers. Figure 2.6 *(a)(i)* and *(a)(ii)* show the response by a solid object ensonified by the outgoing pulse shown previously in Figure 2.4. Both the positive and negative inputs result in scattered signals which are nearly identical to the input signals. Figure 2.6 *(c)(i)* and *(c)(ii)* show that the bubble of

radius 22.5 microns, when excited by the same type of signal, responds very differently. The successive responses by the linear scatter can be added to give a result with a theoretical limit of zero (Figure 2.6 *(b)(i)*). In contrast, successive responses by the bubble, when added, give a complex odd-harmonic suppressed signal (Figure 2.6 *(d)(i)*), as predicted in the previous section.

When any pair of phase-reversed responses are subtracted, the linear scatterer returns a signal which is of the same frequency content and amplitude modulated shape as the input signal (Figure 2.6 *(b)(ii)*), while the dynamic bubble returns a signal which is odd-harmonic enhanced (Figure 2.6 *(d)(ii)*). The maximum amplitude of the odd-harmonic enhanced signal is only half that of the amplitude of the odd-harmonic suppressed signal, as bubble dynamics have in the case dictated that energy be pumped from the first harmonic (which is odd) to the second harmonic (which is even).

The difference between the results obtained using odd-harmonic enhancement and odd-harmonic suppression suggest that nonlinear bubble dynamics might indeed be one way in which bubbles can be distinguished acoustically from solid objects. However the question of application still remains largely unanswered: how can the technique described using the single bubble model be expanded to facilitate the design appropriate for the ocean? To study the effect on the algorithm of complicating factors encountered in the ocean, the results of the

single bubble model were expanded into a simulation which attempts to describe the bubble acoustics beneath a breaking wave. This breaking wave simulation is described in the following section.

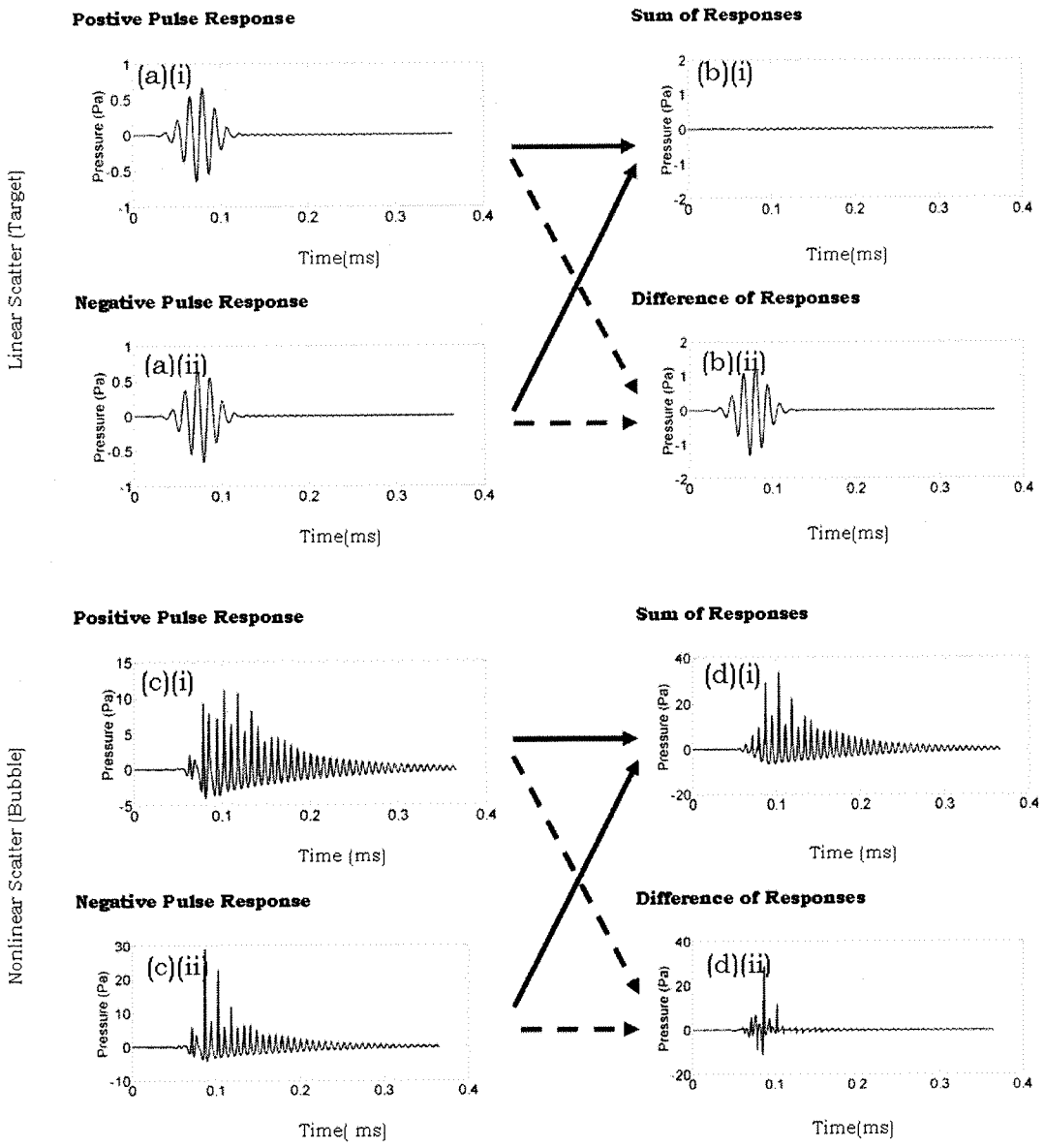

Figure 2.6 The scatter that follows following insonification by the pulses from Figure 2.4 The figure shows the linear scatter from the target (above the horizontal dashed grey line, in (a) and (b)), and the scatter from a bubble (below the horizontal dashed grey line, in (c) and (d)). The graph on the left in each case (i.e. (a) for the target; (c) for the bubble) shows the scatter from the pulses from Figure 2.4: the upper plot (i) shows the scatter when excited by the 'positive' pulse of Figure 2.4; the lower plot (ii) shows the scatter when excited by the 'negative' pulse of Figure 2.4. The solid arrows indicate the process of addition, and the dashed grey arrows indicate the process of subtraction. The air bubble has radius 22.5 microns and is in water under a static pressure of 1 bar, insonified at its resonance frequency. (Figure and caption after Leighton et al. [72])

2.7 The breaking wave simulation

The single bubble simulation showed that the theory presented in section 1.1 transfers well to the physical situation when the bubble dynamics are calculated rigorously. However the problem of finding a solid object within bubbly water is much more complex than section 1.2 might suggest. For instance, according to Phelps and Leighton [82] a 1 m^3 section within a breaking wave contains some 35 million bubbles ranging in diameter from 1 micron to 1 cm. Each of these bubbles scatters and absorbs sound, making it difficult to interpret information gleaned from active acoustic systems used in bubbly water.

It is difficult to find data in the literature on active sonar beneath coastal breaking waves, largely because of the fact that such data is difficult to gather. However, considerable effort has been made to understand active sonar in boat wakes [22, 83, 84], which like breaking waves contain large numbers of microbubbles and interfere with scanning sonar. According to those studies, the degree to which sonar is disrupted by a boat wake depends largely on the craft speed, time since the craft has passed, and the below-waterline dimensions of the craft. Additionally, a study by Trevorrow [84] showed that the manoeuvrings of a ship can influence the way in which wake-borne microbubbles are distributed. In that study, the acoustical environment in the wake of a ship performing 90° turns was studied.

It was observed that interference tended towards a maximum at the outer edge of the wake. It can take several minutes for the interference introduced by the bubbles within a ship's wake to subside, as shown below in Table 2.2.

The papers reviewed, and the insight offered into bubble plume evolution by Leighton [11], were used to inform the development of the computations which will now be presented. The simulation developed here is unique, and will be presented transparently so as to justify the validity and applicability of the results.

Table 2.2 Wake persistence statistics for three different ships, after Trevorrow, *et al.* [22]

	USNS de Steiguer	**CSS Parizeau**	**CSS Vector**
Length at waterline	63.5 m	64.5 m	39.65 m
Beam	12.1 m	12.2 m	9.46 m
Draft	5.5 m	5.4 m	4.27 m
Wake depth	5.3 m	6.2 m	6.4 m
Max bubble depth (10 kn)	9.0 m	9.0 m	12.4 m
Average wake persistence	6.8 ± 0.5 min	7.3 ± 0.5 min	8.0 ± 1.0 min

2.7.1 Simulation components

2.7.1.1 Bubble populations in the surf zone

Bubbles are the most acoustically active entities in the ocean, and breaking waves are the most significant natural sources of bubble entrainment in the ocean [11]. An accurate model of the acoustic

environment beneath a breaking wave therefore requires an accurate count of the number of bubbles that will be beneath such a wave. The simulation developed for this study uses the results of Phelps and Leighton [82], who showed that the bubble population encountered beneath a breaking wave can be approximated by:

$$n_b = 6\times10^6 e^{-0.02(R_0/1\mu m)} \qquad (2.29)$$

where $n_b(R_o)dR_o$ is the number of bubbles per unit volume having a radius between R_o and R_o+dR_o, and where R_0 (which must be expressed in microns for use in (2.29)) is the equilibrium radius of the bubble at the centre of each radius bin in a discretised bubble population. To simplify the computing process, the entire bubble cloud was discretised and approximated as being comprised of bubbles within 6 discrete logarithmically spaced radius bins with the following centre radii: 10 μm, 50 μm (which would be the resonance radius under 1 bar static pressure), 100 μm, 500 μm, 1 mm, and 5 mm. Using these centre radii, equation (2.29) was found to give void fractions (the ratio of the volume of gas within a cloud to the total volume occupied by the cloud) on the order of 10^{-7} (i.e. 10^{-5}%). The bubble population used to produce the simulation output presented in this paper is shown in Table 2.3 below.

Table 2.3. Bubble population used in the simulation.

Bubble radius (μm)	Size bin radius limits (μm)	Number of bubbles in size bin per cubic metre of seawater
10	$10^{0.75} \leq R_0 < 10^{1.25}$	3.5×10^7
50	$10^{1.25} \leq R_0 < 10^{1.75}$	3.3×10^6
100	$10^{1.75} \leq R_0 < 10^{2.25}$	3.0×10^4
500	$10^{2.25} \leq R_0 < 10^{2.75}$	3.1×10^2
1000	$10^{2.75} \leq R_0 < 10^{3.25}$	3×10^0
5000	$10^{3.25} \leq R_0 < 10^{3.75}$	0

2.7.1.2 Source pulse design

2.7.1.2.1 Operating frequency

As stated at the beginning of the chapter, scanning sonars tend to be designed to exploit the benefits of high-frequency scattering. Low frequency sonars are poor at detecting small objects unless those objects scatter in a resonant manner. This is partly a result of the fact that an object which scatters according to Rayleigh scattering[12] is essentially acoustically invisible. At the outset of the chapter, it was pointed out by increasing the sonar frequency of operation, it is possible to increase the amount of detail in a sonar image. However, there are practical limitations for the upper operation limit of a scanning sonar system, since absorption increases by roughly an

[12] Rayleigh scattering occurs where product of the wavenumber k and the primary object dimension L is very small; *e.g.* $kL<<1$.

order of magnitude for every order of magnitude increase in frequency [21]. As was highlighted when discussing Thorpe's method of scanning the reflection by bubble clouds [23] (see section 2.1), scanning sonars are well-adapted for establishing the presence of bubble clouds – though not for looking finding objects within such clouds. If $kL>>1$, a bubble will scatter linearly, making each bubble within a large cloud appear as a target. But scanning sonar systems do not require the response of the elements within the water to be non-linear. This special requirement can be used to justify working instead at frequencies on the order of 10 kHz (see section 2.4 for the justification of this statement), where only coarse images can be obtained, but attenuation by bubble clouds is reduced considerably (as shown in Figure 2.7).

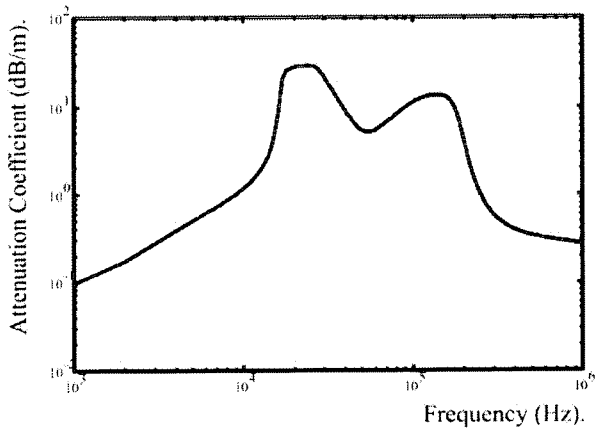

Figure 2.7 Attenuation as a function of frequency typical of an oceanic bubble cloud (bubble size distribution shown in Figure 2.8) [85]. Note the steady reduction in attenuation as frequency is reduced from about 15 kHz (Figure from [72]).

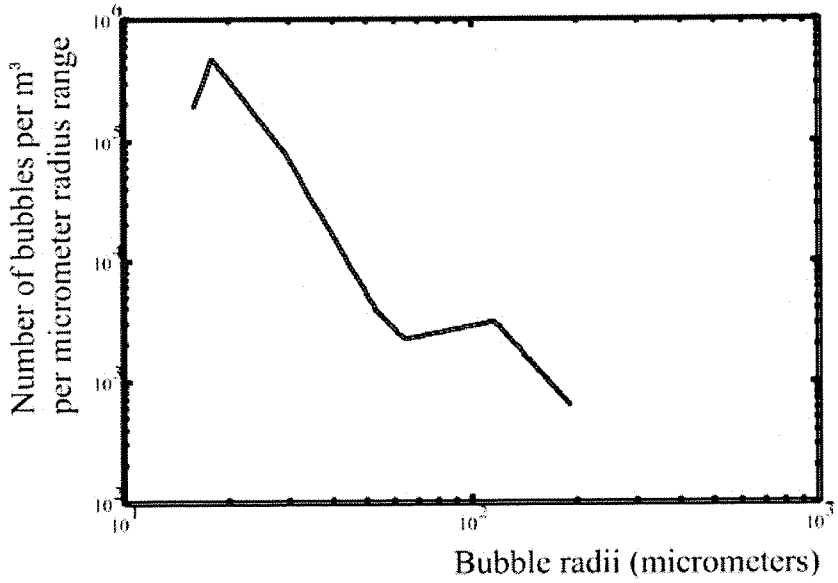

Figure 2.8 Bubble size distribution used to calculate the attenuation shown in Figure 2.7 (Figure from [72]).

2.7.1.3 Calculation of the acoustic response by the cloud to the input pulse

The ensonifying wavetrain is shown in Figure 2.9. It consists of two pulses of 50 kPa (zero-to-peak), identical except that the second (the 'negative') pulse has opposite polarity to the first (the 'positive') pulse. The input pulse used for the simulation was a Gaussian-shaped multiple cycle pulse. The use of multiple pulses increases the amount of time during which each bubble is driven and so enhances the degree to which nonlinear effects are realised. The Gaussian window was used because the low amplitude at the beginning of the Gaussian window reduces the initial inertial load on the acoustic driver, and the overall shaping is useful for phase-matching acoustic returns when locating objects [86].

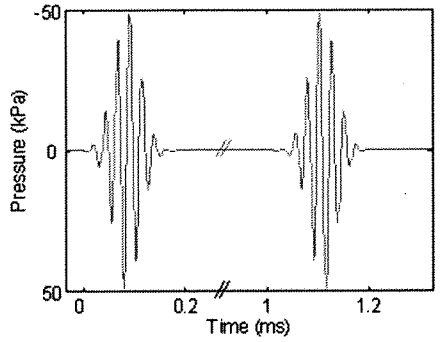

Figure 2.9 Simulation input pulse

Bubble-wall displacement time histories were for bubbles of each radius using a modified non-linear Herring-Keller expression (see equation (2.8)) [87]. Once the displacement, velocity, and acceleration of the bubble wall are calculated, the pressure radiated by the bubble can be calculated. In an incompressible fluid, the pressure at any distance r from the bubble centre when the instantaneous bubble radius is R is:

$$\left(\frac{p}{p_\infty}-1\right)\frac{p_\infty}{\rho}=\frac{R}{r}\left(\ddot{R}R+2\dot{R}^2\right)-\frac{\dot{R}^2}{2}\left(\frac{R}{r}\right)^4 \qquad (2.30)$$

where p_∞ is the pressure in the liquid at some distance far enough from the bubble to be undisturbed by the excitation; $\dot{R}$ and $\ddot{R}$ are respectively the velocity and acceleration of the bubble wall [11]. The final term in (2) is related to the kinetic wave, which is normally treated as negligible at distances far from the bubble, although this assumption breaks down for high amplitude pulses.

Figure 2.10 shows the radiated pressures from the bin-centre bubble sizes (see Table 2.3) in response to the positive portion of the 60 kHz

twin wavetrain which was shown in Figure 2.9. Both the 10 μm and 50 μm bubbles clearly exhibit nonlinear behaviour. The larger bubbles respond linearly, and return a signal that is identical in form to the input pulse (Fig. 5(c)-(f)). In the computation, each 1.1 ms pulse is comprised of 1600 points, giving a simulation resolution of 1.49 x 10^6 samples/second.

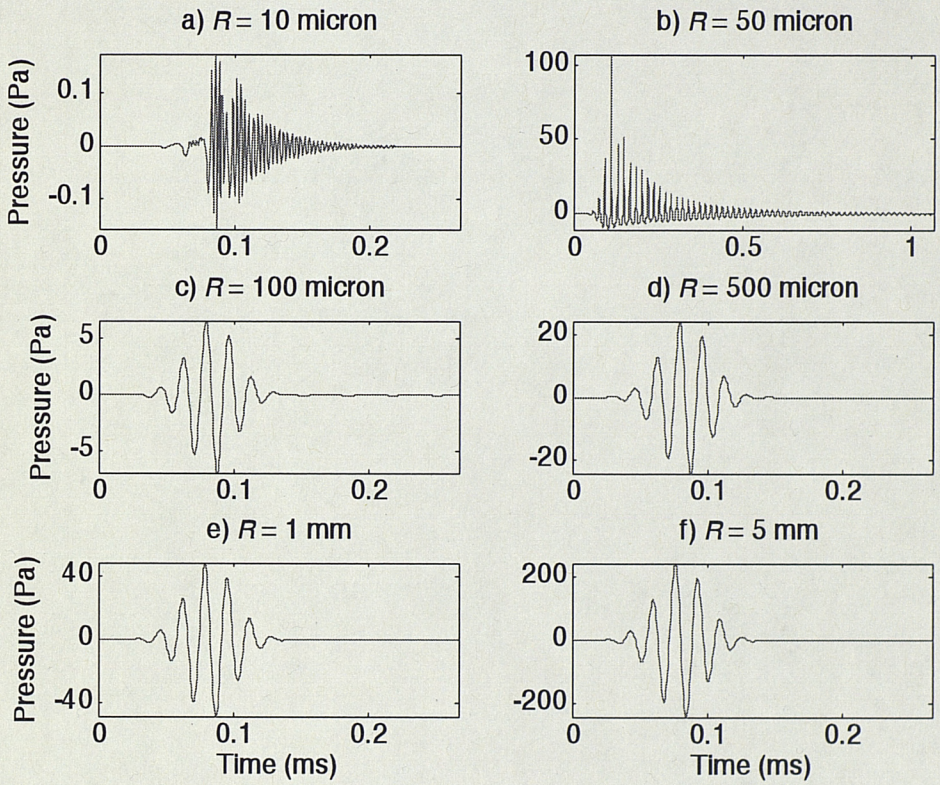

Figure 2.10 Pressures radiated at 1 m range from single bubbles of varying sizes in response to insonification by the 'positive' pulse only (shown Figure 2.9).

As the twin pulse signal is comprised of two pulses, it was necessary to calculate the bubble response for both portions. The response was then calculated from a region of seawater containing spherical cloud of bubbles of radius 1 m, centred on the target (which was at a range

of 10 m from the transducer) (Figure 2.11). The bubbles were randomly distributed within the perimeter of the cloud, but with no bubbles outside its spherical outer boundary. The object the detection of the target within the bubble cloud. In the model, this cloud does not evolve significantly in the 1 ms interval between a given 'positive' pulse and the subsequent 'negative' pulse. However after each 'negative' pulse, the cloud is allowed to evolve in keeping with known oceanic behaviour [87] (with the restriction that the total number of bubbles in the cloud does not change).

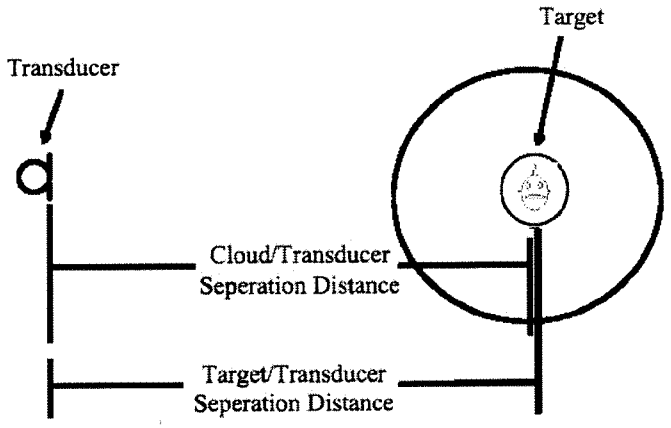

Figure 2.11 Diagram of simulation geometry for transducer, target and spherical bubble cloud.

Having calculated the amplitude appropriate impulse response shown in Figure 2.10, the following process was then followed for each bubble size bin. The time limits for an acoustic response by the cloud to an input pulse were calculated using the two-way travel time appropriate to the near and far boundaries of the bubble cloud with respect to the send/receive transducer. The time limits were approximated assuming a constant sound speed for the entire region

as would be found in clear water. The probability of a bubble being excited at any instant during input wave propagation was calculated to give a single number, an average bubble response time rate. This bubble response time rate was then put in the form of a temporal probability vector, with each position in the vector representing the number of bubbles responding at a given instant in time according to the sampling rate. The generic scattering waveform was then convolved with the temporal probability vector to give the time history at the source/receiver location. The total response for the bubble cloud was then found by adding the set of responses calculated for each bubble size.

2.7.1.4 Target

The simulation requires the use of a simulated target; a device which, when ensonified by a pressure wave of any amplitude, will scatter linearly and predictably. For this study, a non-resonant scatterer has been used so that the acoustic reflection from the target is of the same temporal shape as that of the incident pulse, but will is scaled by amplitude according to the two-way distance from the source to the target. In the absence of inhomogenities within the water column, the amount by which the amplitude of this acoustic return is reduced as compared to the input pulse is dependent on the total source-target-receiver path length and the target strength.

The target strength TS is defined by Pierce [3] as

$$\mathrm{TS} = 10\log\frac{\sigma_{\mathrm{scat}}}{4\pi L_{\mathrm{REF}}^2} \tag{2.31}$$

where σ_{scat} is the scattering cross-section and L_{REF} is the reference length. Most modern literature uses a reference length of 1 meter, though Pierce notes that some earlier literature uses L_{REF} as 1 yard which is usually taken to be 1 meter. Note that σ_{scat} the scattering cross section is larger than σ_{back} the backscattering cross cross-section by a factor a 4. The 4π arises here by considering the solid angle ratio; where scattering is omnidirectional, backscatter only takes into account that energy which is directed back to the source [2]. The target used in the simulation has a target strength TS = -20 dB. It should also be noted that the concept of target strength is not valid for resonant scatterers [3].

2.7.2 Output

The results of this study were published initially in 2005 [33]. For conventional sonar (Figure 2.12 (*a*)), TWIPS1 (Figure 2.12 (*b*)) and TWIPS2b (Figure 2.12 (*c*)), 50 pulse pairs were projected at the cloud, spaced at intervals of 10 ms. The processed echoes were then stacked, one above each other, to form an image. As a stationary feature in the display, detection of the target in every ping would correspond to the observation of a vertical white line which is visible when the target is present, but absent from the corresponding sonar plot when the target is absent.

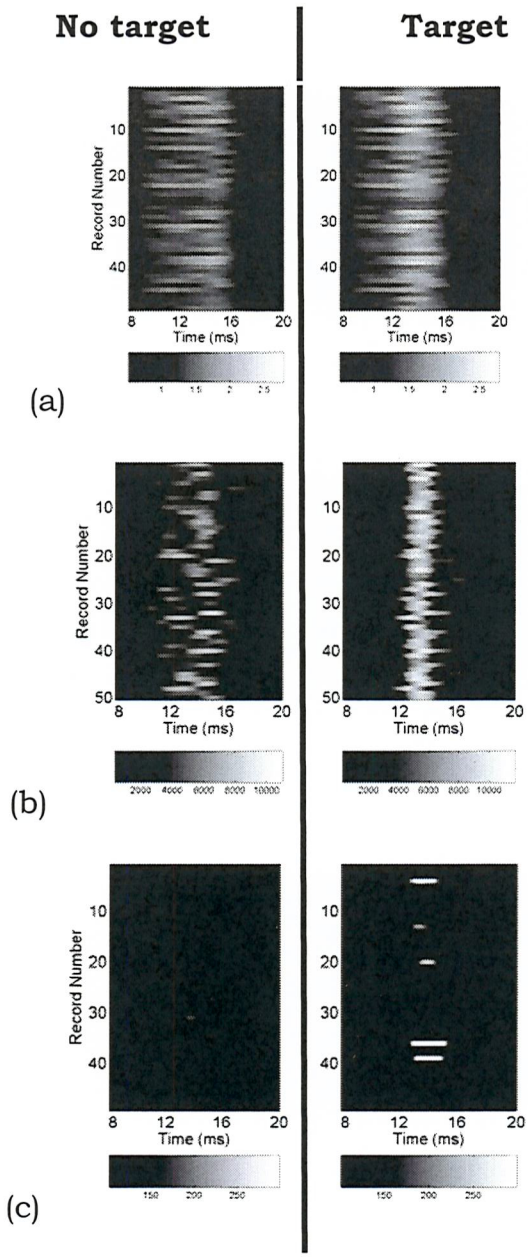

Figure 2.12 Fifty pulse pairs were projected at the cloud, spaced at intervals of 10 ms, and the echoes processed using (a) conventional sonar deconvolution techniques, (b) TWIPS1 and (c) TWIPS2b. Complete figure description given within the body of the text. (Figure from [33])

In Figure 2.12 the plot on the left in each panel shows the case when there is no target present, and the right plot shows the case when a target is inserted at the cloud centre (TS = -20 dB). The cloud, of 1 m radius, contains 35 million bubbles, and evolves appropriately between each echo, as described earlier. A single average was formed

from the two pulses that make up each pulse pair, such that 50 averages are available for plotting. Each average was plotted as a time history on a line, with a greyscale such that the amplitude of the signal at the corresponding moment in the time history was displayed. These processed echo time histories were then stacked, one above each other, to form an image. In Figure 2.12 (*b*), the results of TWIPS1 processing of the 50 pulse pairs (no averaging) are displayed similarly, by stacking the consecutive grey-scale time series one above the other. The TWIPS1 processed echoes were plotted, each as a time history on a one-dimensional line, as in Figure 2.12 (*a*). In Figure 2.12 (*c*) TWIPS2b processing is used (no averaging) and the image displayed as in Figure 2.12 (*b*).

The left hand plots in the individual panels of Figure 2.12 correspond to the cloud when there is no target present, and the right hand plots of each panel in Figure 2.12 correspond to the bubble cloud when the target (TS = -20 dB) is present. In visually comparing the results[13], it is inappropriate to compare against each other the 'target present' plots in (*a*)-(*c*). Rather, one should consider the decision-making process followed by a sonar operator, and consider the *distinctions*

---

[13] Statistical analyses are performed on the experimental results. The goal here is to establish proof-of-concept using the computational models, which can in turn be used to justify the development of an experimental study.

between the left and right plots in each panel.

On a visual basis, standard sonar processing fails to detect the target: There is insufficient difference between the two plots in Figure 2.12 (*a*) because scatter from the bubbles masks the presence of the target. TWIPS1 detects the target on almost every occasion, such that there is a vertical line on the right of Figure 2.12 (*b*) compared to the plot on the left (where, importantly, it has suppressed the bubble signal). In Figure 2.12 *(c)*, it can be seen that TWIPS2 fails to detect the target within the majority of echoes. However when it does detect one, the amplitude is very high; when the target is not present (left hand plot), it rarely delivers a high amplitude return, very effectively suppressing the returned signal. The plots all have a linear greyscale and no thresholding has been applied. By comparing the computation results with those from the tank tests (Chapter 3) and the field studies (Chapter 5), it will be seen this sporadic detection ability is characteristic of the TWIPS2 algorithm. An explanation for the behaviour is offered in the system analysis at the end of Chapter 5.

TWIPS covers a range of processing techniques, with different capabilities. All are designed to enhance contrast of targets in bubble clouds, both by increasing the scatter from the target and, very importantly, at the same time suppressing the signals from the bubbles. TWIPS1 is designed always to enhance target contrast, producing a reliable enhancement with every ping. TWIPS2b gives

much greater contrast enhancements, but not with every ping: the particular form demonstrated here 'glints' on about 10% of pings. However the contrast enhancement is much greater than occurs with TWIPS1. It is particularly useful for sources that are capable of ensonifying a region with multiple pings.

2.7.3 On the greyscales employed for visual comparisons in this thesis

A relative greyscale was used to produce the contrasts visible in Figure 2.12. The numeric scale used to produce that image, and the others like it presented throughout this thesis, is linear and relative. The absolute values to which each gradation within the greyscale maps are meaningless, as the standard sonar and TWIPS were not calibrated during the course of this investigation. A calibration would have required continual monitoring of bubble size distributions – a facility which was not available except in certain instances. As such, the individual sonar output plots presented throughout this document cannot be compared to each other in an absolute sense except where the bubble size distribution is available (as indicated where appropriate).

2.8 Potential non-oceanic applications of TWIPS

A twin-inverted pulse-based technology designed for the purpose of acoustic bubble-scattering suppression has been presented. The power of this method is rooted not in its specific suitability to bubble-

scatter suppression, but in its general ability to reduce (or enhance by inverse application) nonlinear scatter from any type of radiation. Therefore, TWIPS might find application not only in the oceanic environment, but might also be exploite in biomedical ultrasound, RADAR, and LIDAR as considered here in brief.

2.8.1 Biomedical ultrasound

In biomedical ultrasound, bubbles are employed for a wide variety of applications [88], including contrast enhancement (as described above), drug delivery (via micro-encapsulation, where the bubble is "wrapped" with a particular drug and then driven to a particular location) [89], and cavitation (for the destruction of unwanted bodies, such as kidney stones or circulatory clots) [90, 91]. Both contrast enhancement and drug delivery applications require bubble scatter enhancement, and so would not stand to benefit from TWIPS directly, but rather from the process used to select the operating frequency in the development of the computational study described above. Oceanic bubble clouds contain bubbles with radii spanning several orders of magnitude, whereas the bubbles used in biomedical bubble contrast and drug delivery are monodisperse. It is straightforward to cause the bubbles with in a monodisperse cloud to oscilate nonlinearly – one can merely excite the system at or near the resonance frequency of the individual bubbles. However, in a polydisperse cloud, it is necessary to consider the bubble size distribution before designing the input signal. It was shown here that for a cloud containing bubbles of an

oceanic-type size distribution (where the distribution is inversely proportional to the radius), it is possible to achieve nonlinear scattering across several orders of magnitude of radius by driving the cloud at the resonance frequency of the largest bubbles. This might be used to facilitate any application of bubbles in biomedicine where a polydisperse bubble population is desired.

One such application is cavitation-enhanced heating, where bubbles "convert acoustical energy into mechanical energy which is subsequently deposited as heat" [88]. In this application, high intensity focused ultrasound (HIFU) is used to induce cavitation for the purpose of lesion destruction. The bubble clouds used for this HIFU-induced heating are typically not introduced from an external, engineered source as in contrast enhancement. Rather, the source of these bubbles is either pre-existing gas bodies, or the coaelesence of gas already present within the tissue [92, 93]. The size distribution of the active bubbles in this application is not well-known [94]. However, the size of the largest active bubbles might be used to design an ensonation pulse which is capable of maximizing the response of all bubbles present, following the method employed in section 2.4.3.

2.8.2 LIDAR

Lidar (Light Detection And Ranging) involves the use of laser systems for the detection of media. Interest in the use of lidar for remote sensing in industrial, environmental, and homeland security

applications has increased since the early 2000's [95]. The systems employed for long-range detection operate at powers on the order of terawatts (10^{20} W/cm^2), and are capable of investigating targets at ranges on the order of tens of kilometres [96]. It has been shown that some bioagent stimulants can scatter lidar energy nonlinearly [97]. This nonlinear scattering can be harnessed for aerosol detection [98], a result of particular importance as "the deadliest form of a biological attack is aerosolized agents dispersed into the atmosphere. Early detection of aerosolized agents is important for defense against these agents" [99]. It is hypothesised that twin-pulse method could be applied to lidar, thereby enhancing the ability to monitor for nonlinear scattering with implications (for example) in environmental monitoring.

2.8.3 RADAR

Radar can cause certain features (such as electrical circuitry) to scatter nonlinearly. This so-called 'rusty bolt' effect arises in air gaps, of width 1-10 nm, in for example imperfect riveting or welding [100]. Over time, the exposed metal surfaces are oxidised and metal-insulator-metal (MIM) junctions are formed. When these are exposed to radar or similar radiations, they can scatter nonlinearly as a result of electron tunnelling through the insulator [101]. This widespread phenomenon is simple to demonstrate [102], and affects many types of radio- and micro-wave communications [101, 103]; including radio, television, radar, and global positioning systems [104].

The methods contained in this report could be used to detect such MIMS junctions, whether their presence is intentional or not, by enhancing the scatter from the nonlinear components with respect to the linear ones. The applications could range from exploiting electromagnetic radiation of the correct frequency range to test weld strength or for crack detection, to allowing radar to detect complex electrical circuitry in possible targets. Alternatively, it might be used to suppress from the signal spurious 'noise' generated by such nonlinearities (in for example, radomes or antennae).

In fact it could be suggested that the problems inherent in TWIPS2a make it a technique better suited for radar than for sonar. In water, sound travels at approximately 1500 m s^{-1}. The frequency of interest for the duration the TWIPS experiments (see Chapter 3) is 6 kHz, giving a wavelength λ of 0.25m. Through the analysis related to testing, it will be seen (in 4.1.5 and 5.5.1) that the largest (that is, the fastest-rising) oceanic bubbles rise under buoyancy at a rate of about ½ wavelength during a single interpulse pause. In contrast, consider an observation plane. The speed of light is approximately 3×10^8 m s^{-1}. The two-way time for a signal emitted from the plane and reflected off the observed ground-based target in that case is 4×10^{-5} seconds. If an operation frequency of 100 MHz is used, the wavelength is about 3 meters. If the target or target field is moving a few meters per second, and an interpulse time equal to the two-way travel time is used, then

the target or target field only moves by some 0.001% of a wavelength between pulses. Radar applications of TWIPS are considered further in the relevant patent application [70].

2.9 Conclusions

It was established in Chapter 1 that MCM systems capable of coping with bubble scattering in littoral waters are not yet commercially available, and that the US Department of Defense is particularly interested in rectifying that situation [13, 17-19, 105]. On that basis, this chapter was used to introduce the theoretical basis and computational justification for a new sonar method which is theoretically capable of acoustically deciphering solid objects from bubble clouds. The chapter began with a review of current technologies which might be used in a sonar context when hunting for mines in the presence of bubbles.

Next, the methodology used currently in biomedical ultrasound to highlight bubble contrast was presented. It was shown that both second-harmonic imaging and pulse-inversion are useful for contrast enhancement. Both of these methods require that the bubbles in question be driven nonlinearly. In practice, this goal is straightforward to achieve as biomedical bubbles are designed to exhibit a narrow size distribution, so all relevant bodies can be driven near resonance to give high-amplitude responses. It was additionally

shown that second-harmonic imaging suffers performance-wise as a result of bandwidth considerations which in turn result in poor image resolution.

Following the discussion of pulse inversion, it was argued that it would be possible to suppress bubble scatter while enhancing that scatter generated via rigid objects (linear scatterers). This concept was then given the name "Twin Inverted Pulse Sonar" (TWIPS). The application of TWIPS to the oceanic environment was seen to be complicated by the fact that, while biomedical bubbles are of a narrow size distribution and their location is contained by blood-flows which are somewhat predictable, oceanic clouds contain hundreds of millions of bubbles spanning several orders of magnitude in radius. Thus, a consideration had to be given to the type of signal which would be capable of generating nonlinear bubble-wall oscillations throughout an oceanic cloud. One approach to this issue, it was argued, is to drive all bubbles either at or below resonance, as it is considerably easier to invoke a high-amplitude response for a given dynamic oscillator in the mass-controlled frequency regime when compared to attempts to perform the same task in the stiffness-controlled regime.

After establishing the theoretical basis for TWIPS, a simulation was then developed to test the TWIPS hypothesis. It was found that the system is capable of out-performing standard sonar in attempting to

identify a target of strength -20 dB in a cloud of some 50 million bubbles having a size distribution which is realistic for the oceanic environment. The TWIPS algorithm at this point appears to be a promising solution for the detection of solid objects in bubbly water.

A brief treatise on the potential application of TWIPS-type systems for use in biomedicine, radar, and lidar was offered. It was shown that this algorthim, while promising for sonar, might in fact be even more well-suited to radar applications.

The next chapter will be used to develop a method for the production of oceanic bubble clouds in a controlled environment. In Chapter 4 the results of the computational study developed here will be combined with the developed bubble production technology to facilitate the testing of the TWIPS hypothesis in a laboratory setting.

3 Bubble clouds

Sophie opened her mouth, and very gently the BFG tipped the bottle forward and poured some of the fabulous frobscottle down her throat.

And gosh, how delicious it was! It was sweet and refreshing. It tasted of vanilla and cream, with just the faintest trace of raspberries on the edge of the flavour. And the bubbles were wonderful. Sophie could actually feel them bouncing and bursting all around her tummy. It was an amazing sensation. It felt as though hundreds of tiny people were dancing a jig inside her and tickling her with their toes. It was lovely.

"It's lovely!" she cried.

"Just wait," said the BFG, flapping his ears.

Sophie could feel the bubbles travelling lower and lower down her tummy, and then suddenly, inevitably... the explosion came. The trumpets sounded and she too made the walls of the cavern ring with the sound of music and thunder.

"Bravo!" shouted the BFG, waving the bottle. "You is very good for a beginner! Let's have some more!"

from The BFG, by Roald Dahl

In the previous chapter, computational models were used to support the claim that TWIPS might offer a solution to the problem of target detection in bubbly water. On those grounds, the discussion now turns to consider the nature of oceanic bubble clouds. This chapter will begin with a review of the results classic bubble-propagation laboratory experiments. A short review will then follow on the topic of sea trials conducted for the purpose of understanding oceanic bubble clouds and acoustic propagation therein. Finally, the focus will turn to the way in which a device (the Bubbly Fluid Generator, or BFG) was developed for this project to reproduce oceanic-type bubble clouds inside a controlled environment at the A B Wood Underwater Acoustics Laboratory.

3.1 Early laboratory experiments

Over the past 50 years, many attempts have been made at measuring the change in phase speed and attenuation in the presence of bubbles [87, 106]. The bubble population can be estimated by inverting these measured characteristics using a model. The significant interest in understanding bubble clouds has a wide variety of applications; to quote Medwin, "A knowledge of bubble populations in the sea is important in understanding such superficially diverse subjects as sources of airborne salt nuclei, sea slicks and wind-rows, cavitation, sea surface chemistry, and underwater sound scatter from the sea surface" [107].

The first experimental work to quantify the effect of bubbles on underwater acoustic propagation was by done in Germany by Meyer and Skudryzk in the late 1930's, but was not published until 1953 [108]. Meyer and Skudryzk made bubble clouds in three different ways: by pumping air thorough a porous material, electroloysis, and by using a "pumping device". They then used reverberation times to calculate the phase-speed and attenuation through the bubble cloud - results which agreed with their own theoretical predictions. Carstensen and Foldy [109] also developed a theory for propagation of sound through bubbly water, and performed experiments using a pumping device they called the "microdisperser" - a device which will be discussed in more detail later in this chapter.

In their theoretical analysis, Carstensen and Foldy [109] treated the bubble screen as region of uniform bubble distribution with two parallel plane surface boundaries, and then proceeded using standard two-dimensional acoustics [110]. A particular weakness of this approach, which the authors recognised, is that bubble clouds do not in fact have "sharp boundaries" [111, 112]. Also contributing to the lack of agreement between their theoretical predictions and experimental results is insufficient description of the increased backscattering cross-section of a bubble at resonance, a principle described in section 2.2.1. Carstensen and Foldy commented that their model "could easily" account for the discrepancies between the observed and calculated attenuations if the boundary conditions were modified to account for gradual velocity gradients through the bubbly/bubble-free water interface. Carstensen and Foldy reported bubble-size distributions based on both optical observations and the results of an acoustical inversion. Their results indicate (1) a disproportionatly low number of microbubbles (a trivial number of bubbles less than 0.1 mm in diameter, whereas it will be seen that the majority of oceanic bubbles are less than 0.1 mm in diameter) and (2) a void fraction of around 3% (whereas void fractions in oceanic bubble plumes are typically 100 to 1000 times lower than that figure [11]).

Fox *et al.* [113] were successful in obtaining phase-speed and attenuation results which they reported to be "in fairly good

agreement" with the theories of Carstensen and Foldy [109] and Meyer and Skudryzk [108], though they did not statistically justify this statement. Fox *et al.* pointed out that the measurements of absorption by Carstensen and Foldy indicate that the theoretical approach by Meyer and Skudryzk underestimates acoustic attenuation in the frequency region near bubble resonance.

Fox *et al.* used three methods to attempt to characterise the bubble size distributions produced in their laboratory: direct observation using a telescope, measurement of the bubble rise time in water, and finally photography. It should be noted that, at the time of that study, it was not know what type of bubble size distribution were found in oceanic conditions. Fox *et al.* reported that "no bubbles in the region of the sound beam were larger than 0.015 cm in diameter, but in some instances small bubbles of diameters as low as 0.003 cm were observed in quantity" [113]. This is consistent with the bubble size distributions used by Carstensen and Foldy [109], Meyer and Skudruzk [108]. It will be seen in section 3.2 that oceanic clouds are comprised mostly of microbubbles [87]. Thus, while the results of this generation of these investigations were critical for advancing the state of the art, the actual phase speeds and attenuations reported by Carstensen and Foldy [109], Meyer and Skudruzk [108], and Fox *et al.* [113] are in fact not representative of the phase speeds and attenuations encountered in oceanic bubble clouds. It should be noted, however, that Fox *et al.* measured a void fraction of 0.06% - a

void fraction which is of the same order of magnitude as those encountered in oceanic bubble clouds.

3.2 Measurements of oceanic bubbles at sea

Turner [114] noted that microbubbles (bubbles having radii on the order of micrometers) persisted in his freshwater tank for much longer than accounted for by classical theory. His investigation was performed by measuring the attenuation of an ultrasonic beam operating at 5.125 MHz. The implication of this work was the realisation that very small bubbles, which had gone virtually unnoticed in previous work, might be present in large number and in fact have a substantial effect on acoustic propagation in bubbly water.

Medwin made acoustic measurements of bubble populations in coastal ocean waters in 1970 [107]. Before that investigation, "conflicting statements about the persistence of bubbles at sea" [107] had appeared in the literature. To facilitate the proper design of the acoustic system, Medwin undertook a preliminary photographic study of bubble populations beneath white caps. The photographs revealed the presence of millions of bubbles per cubic meter having a radius between 10 and 100 microns.

Oceanic bubble clouds are primarily generated by surface turbulence though some instances of some sub-surface sources appear within the literature. Surface turbulence can be the result of either natural

mechanisms, such as breaking waves [23], or can be through artificial means, such as through boat/propeller hydrodynamics [22]. The first portion of this section will be concerned with observations and measurements of naturally-generated bubble clouds. As the experimental methods developed for studying surface turbulence-generated clouds were only later applied to the study of ship-wakes, so too will this section use the concepts built up in the first portion of the discussion to put artificially-generated bubble clouds in context.

3.2.1 Naturally generated bubble clouds within the water column

Quantitative knowledge concerning the physical characteristics (especially population and size-distribution) of wave-generated bubbles has been developed only in the past 30 years. In 1982, Thorpe [23] wrote that "knowledge of wave-generated bubbles in the sea is meagre and measurements few." Since then, several investigators have used a variety of acoustic methods to establish roughly the bubble size distribution beneath a breaking wave; as shown in Figure 3.1 below.

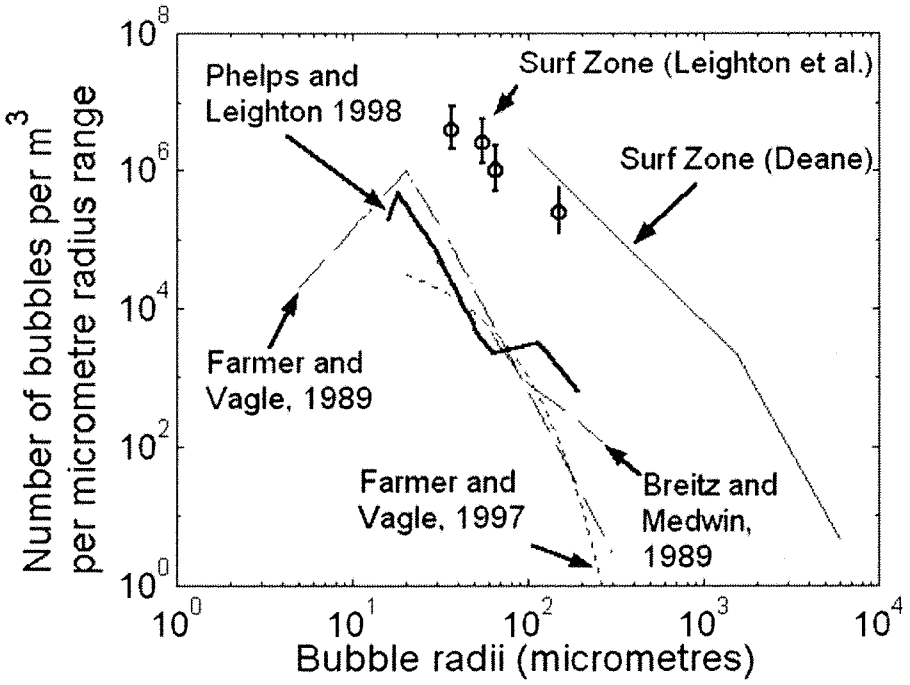

Figure 3.1 Bubble size distribution estimates based on field measurements by Breitz and Medwin [115] and Farmer and Vagle [116, 117], Phelps and Leighton [82], Deane [118], and Leighton *et al.* [87] (figure from [87], reproduced here with permission).

3.2.2 Gas pockets trapped within sediment

Researchers and surveyors interested in sub-bottom profiling for the purposes of resource exploration, geological study, buried object location, or other endeavours are often limited in their efforts as a result of gas pockets which are trapped with the sediment layer [119]. These gas pockets, known to some practitioners as "acoustic blanks" because of their appearance on side-scan images [120], can give way to discontinuous data which may be difficult to interpret. Therefore, although a surveyor operating a high-amplitude sonar source might generally be able to see tens of meters below the seabed, acoustically impeneatrable gas pockets can limit their ability and effectively blind sonar scanners.

In Figure 3.2, the effect of gas deposits in the sea bed on sonar performance is shown using a sonar image developed using a high-amplitude acoustic source in conjunction with a high resolution receiving array (240 hydrophones in a plane of dimensions 2.5 m x 2.0 m) [121]. In that figure, the sea bottom is visible as a bold line running continuously across the top of the image. Below that line lie several faint, semi-parallel lines. These lines represent interfaces within the sediment layer where the composite type alters suddenly with depth. Shallow gas deposits have been labelled as such. They appear as dark amorphous bodies because they occupy large volumes of the sediment, and they reflect most of the sound which is incident upon them. As a result of this reflection, very little energy penetrates through the clouds. This results in a general lack of information concerning the spatial distribution of sediment layers below the gas; apparent on the figure below as breaks in sediment contours below the gas clouds.

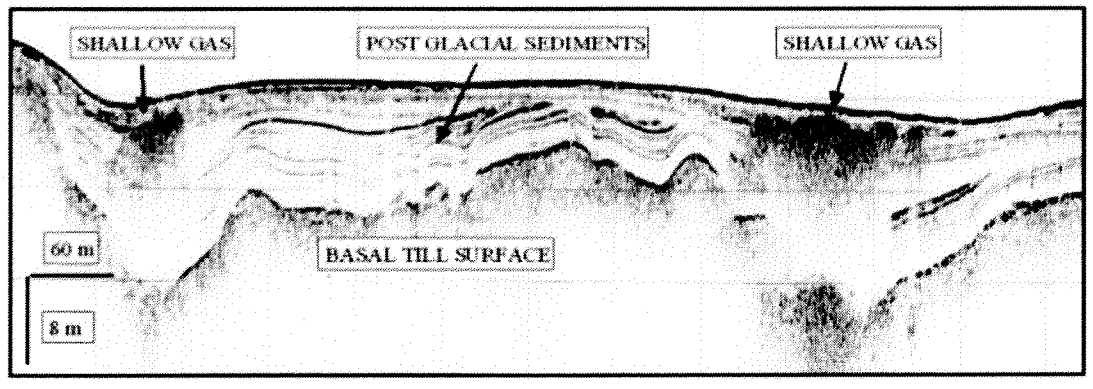

Figure 3.2 A sonar image, showing a cross-section of the seabed (maximum penetration approximately 20 m) in Strangford Lough, Northern Ireland. Reproduced by permission of National Oceanography Centre (J.S. Lenham, J.K. Dix and J. Bull). The depth of the water was estimated to be 15.5 m.

3.2.3 Ship-generated bubble clouds

Large vessels are known to generate visible "surface scars" which can extend several miles behind the ships by which they were generated (See **Figure 3.3**). These surface scars are visible as regions of slightly discoloured water, and, at distances beyond about one ship-length behind the ship, typically exhibit reduced surface wave activity when compared to immediately surrounding waters. Surface scars have been detected using high-altitude photographs taken by NASA at distances up to 100 km behind ships [122]. Microbubble-wall surfactants are at least partly responsible for these surface scars[14] [11].

However, regardless of the fact that surface scars are not well-

[14] There are at least two competing theories for the source of these tracks – turbulence; and microbubble-wall surfactants. The turbulence theory is as follows: as a surface ship passes through a region of water, the combined effect of the bow-wake, screws, and after-wake is to generate large-scale, high Reynolds number turbulence which can extend ship-depths below the vessel. This turbulence successively causes smaller-scale turbulence - a process which is repeated until the flow energy is lost to thermal-viscous losses within the water column. This theory, however, does not explain why the surface of ship-wake exhibits reduced surface-wave activity at a distance of more than about a ship length behind the ship. This "smoothness" can however be explained by the microbubble-wall surfactant theory, explained later in the main body of the text.

understood, it is known that ship wakes contain large numbers of bubbles [22, 84]. Sailors have long been aware of the effects of acoustic scattering and attenuation by ship-generated bubbles: When a vessel passes through a wake (generated perhaps by another ship), the high-frequency echo-sounder will tend to fail, as its self-produced signal becomes obscured as a result of its interaction with the local bubble cloud. The scattering of sound in ship wakes has been documented by Trevorrow *et al.* [22] and Trevorrow [84], but the bubble size distribution within such clouds is not well-known.

Figure 3.3 A surface scar visible behind amphibious assault ship USS Bonhomme Richard in the Indian Ocean, Jan 2005 (Photo credit: Photographer's Mate 1st Class Felix Garza Jr., via US Navy News website).

However, two facts suggest that the extended wake region contains large numbers of microbubbles (comparable to the population densities of microbubbles found in shallow waters following plunging wave activity):

(1) Trevorrow [84] demonstrated that ship wake scattering continues for several minutes after the turbulence

source has passed. This is consistent with the fact that, while large bubbles (radius greater than about 500 microns) rise quickly under buoyancy, small bubbles can be trapped by local turbulence and remain in the water column indefinitely [11].

(2) Microbubble stability in the water column will be further enhanced by the large quantities of surfactant which is present the water column in salt water [11] and is scoured by rising bubbles onto their surfaces [123]. As the microbubbles injected into the water by the ship slowly rise to the sea-air interface, they will transport those surfactants to the surface, leaving behind a region of water in which there will be increased surface tension when compared with immediately surrounding waters. This is consistent with the observation of smooth water in ship wakes.

Thus, it can be concluded that microbubbles are present in large numbers both beneath breaking waves and in ship wakes. If one wishes to recreate the conditions in those environments, one must be capable of generating large numbers of microbubbles. Since one of the eventual goals of this study is the injection of ocean-like bubble clouds into a controlled environment, this chapter will now discuss the way in which such a cloud can be created and one way in which those bubbles can be measured. The results of such a measurement technique will then be used to show that the bubble-generation

method described here does in fact generate bubble clouds having void fractions and bubble size distributions similar to those encountered in the ocean.

3.3 Reproduction of ocean-like bubble clouds in a laboratory environment

A variety of methods have been used by various experimenters in attempts to generate bubble clouds in experimental tanks. The advantages and disadvantages of a few of those methods are considered here. Then, an advanced method is developed and examined.

3.3.1 Background

Investigators have pursued a many different methods of bubble production in experimental tanks. A few are reviewed here.

3.3.1.1 Microdisperser

Cartensen and Foldy [109] developed bubble clouds using a device which they called a microdisperser. They described their bubble production process as follows (an extraneous parenthetical bracket has been removed from the quote):

> To produce the bubbles, a device called a microdisperser, was used, which consists of two concentric glass tubes. The central one, of capillary dimensions, 0.01 cm [inner diameter] carried air under a pressure of from 5 to 7 lb in^{-2} above atmospheric pressure or roughly 0.5 to 2.5 lb in^{-2} above hydrostatic pressure at the mouth. The outer tube directed a flow of water

> about the capillary. The effect of the water flow was to tear off the bubbles of air as soon as they were formed at the end of the central air tube. A rough control over bubble size was thus possible, for by increasing the velocity of water flow, and consequently the rate of bubble formation, it was possible to decrease the average size of the bubble produced."

Several of these devices were set up in parallel at the bottom of a tank to produce the bubble cloud which was used for their tests. The clouds produced by Cartensen and Foldy contained far fewer relative numbers of microbubbles when compared to oceanic clouds. However their size distribution measurements were made using an optical method. Visual methods for the measurement of bubble size distributions should be treated with care lest they skew measurements towards larger radii, as per the following analogy, adapted from Leighton [124]:

> Consider a traffic policewoman standing atop an overpass, performing a survey on the speed at which traffic travels on a given road. She plans to count cars and measure their individual speeds using a standard radar gun. After one hour, she draws a histogram showing the number of cars versus car speed. Thinking she has characterised the traffic speed distribution, she publishes the results. However, she is mistaken. In one hour, she has sampled 70 miles of road corresponding to those travellers going at 70 miles per hour, but only 45 miles of road for those cars going 45 miles per hour. She has in fact skewed the data and under-represented the number of slow cars.

Thus, when one wishes to characterise the bubble size distribution in a given bubble cloud, one must be aware of the fact that big bubbles rise faster than small ones. Depending upon the method applied, it may be necessary to use a correction to account for under-representation of slow-travelling bubbles. To summarise, the microdisperser bubble production method is unsuitable for modelling the oceanic environment for three reasons (1) the resultant void fraction is too high (see 3.1); (2) almost no bubbles with a radius of less than 100 microns are present; and (3) steady-state conditions can not be achieved.

3.3.1.2 Aqualungs and pressure hoses

An aqualung (also known as a scuba-tank) can be used to make a concentrated bubble screen. The aqualung (nominally pressurised to 3 kPSI, or about 20 kPa) is simply placed at the bottom of a water-tank, and opened. The ensuing bubble screen will continue to develop as long as the tank contains pressurised air. Aqualungs tend to make very large bubbles, and only release over a limited area (as determined by the orifice size). The footprint over which bubbles are released can be increased, but the author knows of no way to reduce the mean bubble size.

Conceptually similar to an aqualung is a pressurised air-hose with a free-end open to the water. Such a system will tend to generate very large bubbles, but is capable of distributing bubbles over a large

footprint, as shown in Figure 3.4 and Figure 3.5 below.

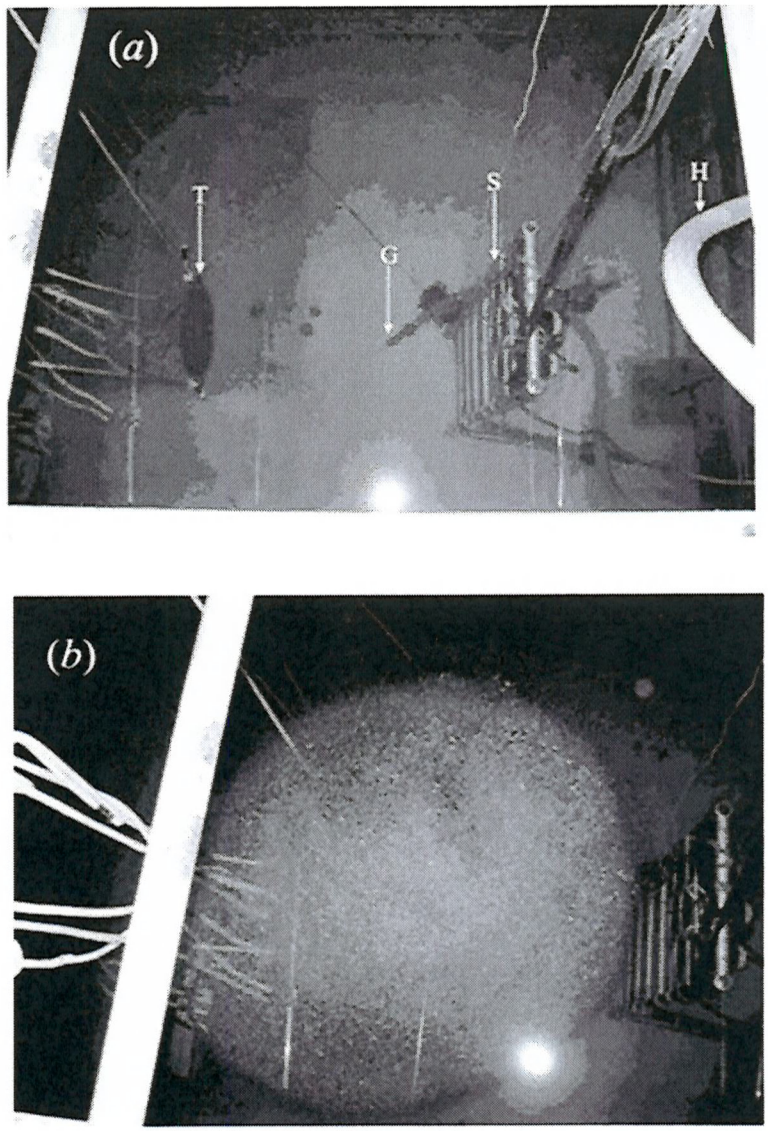

Figure 3.4 A submersible pump, lowered into the above-ground mixing tank, is used to pump air into the below-ground experimental tank. As a result of the height differential between the surfaces of the two tanks, there is air in the pumping hose between the surface of the experimental tank and the surface of the mixing tank, as shown in Figure 3.9. When the submersible pump is turned on, this air is forced to the bottom of the tank. It is this air, not the aerated water, which causes the impressive-looking bubble cloud shown here. (a) Photograph looking down into the water tank from above. The source is on the right. The target (T) and source (S) are labelled. The hose (H) leads down to the bubble generator, whose tip is arrowed (G). The bubble cloud can just be seen forming in front of this tip. (b) A similar view to part (a), but here the target is obscured by the rising bubble cloud, which fills most of the space between the source and target, and in which the target is enveloped. The ropes upon which the target is suspended can be seen disappearing in to the cloud. The rig holding the source is still visible. In this figure the target is at a range of 1.42 m from the source [70].

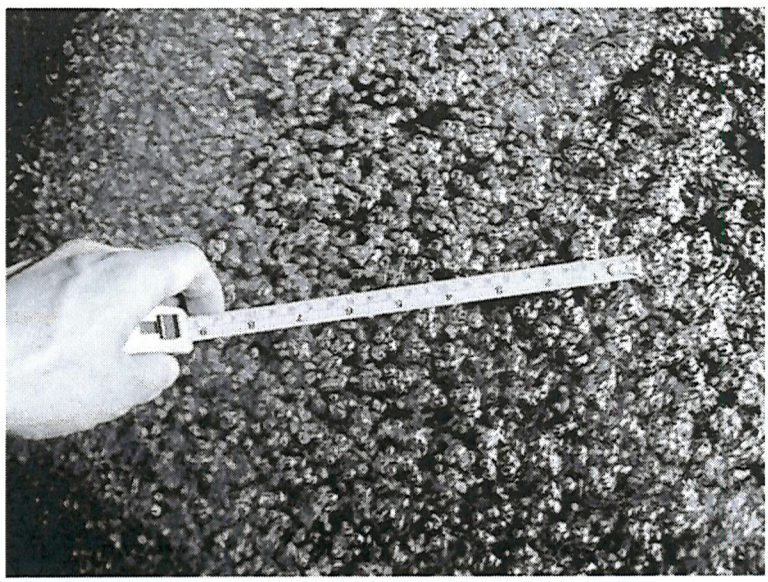

Figure 3.5 A tape measure held at the surface of the A.B. Wood Tank while the transient bubble cloud rises. This high void-fraction cloud does not contain a significant number of microbubbles, and is unsuitable for reproducing the conditions below a breaking wave.

3.3.1.3 Porous ceramic

It is possible to generate very high void-fraction clouds by pressurizing porous ceramic tubes [113] (or porous plates [63]) which have been placed at the bottom of a tank. The pressurized air will be forced out the microscopic holes, and will cause bubbles to develop. Surface tension will cause these bubbles to cling to the tube, and allow them to continue to grow until the buoyancy of each bubble overcomes the local surface tension. When that occurs, the bubbles will rise, leaving behind regions in which further bubbles can develop. This method tends to give very high void fractions, but the high amount of buoyancy needed to overcome surface tension means that the bubbles will generally grow to a very large size (radius >500 μm) before they are able to float to the surface. As a result, virtually no

micron-sized bubbles will be formed when this method is used.

3.3.1.4 Electrolysis

Electrical currents can be used to generate hydrogen and oxygen bubbles. Electrolysis methods can be effective in producing micron-size bubbles [63], but high currents are required in order to achieve oceanic void fractions greater than about 10^{-7}. The footprint of the bubble cloud generated using this method is limited to the region over which electrolysis can be produced.

3.3.1.5 Hydrogen peroxide

Over time, a hydrogen peroxide solution will eventually break down into water and oxygen. In the presence of a suitable catalyst, this process can be sped up so that a bubbly solution can be produced:

$$2H_2O_{2(aq)} \xrightarrow[MnO_{2(s)}]{} 2O_{2(g)} + 2H_2O_{(l)} \tag{2.1}$$

This method of bubble production, termed "Sedna's Raven" within the ISVR underwater acoustics group, is extremely effective in carefully controlled environments, but is difficult to scale up for at least two reasons:

(1) Hydrogren peroxide can be dangerous in large quantities.

(2) The reaction requires that the catalyst have continual contact with the hydrogen peroxide. This is straightforward to achieve in a sterilised glass with distilled water. However, in the A B Wood tank, the water contains particulates which tend to settle on top of the catalyst. Bubbles tend to cling to the

settled particles as a result of surface tension, creating a layer of air between the catalyst and the reaction solution. This effectively grinds the desired reaction to a halt, while allowing the hydrogen peroxide to escape from the desired region and dilute into the tank reservoir.

Nonetheless, in the sterilised laboratory, the reaction can give way to the production of a spectacular number of microbubbles in a very short time. This is depicted in Figure 3.6.

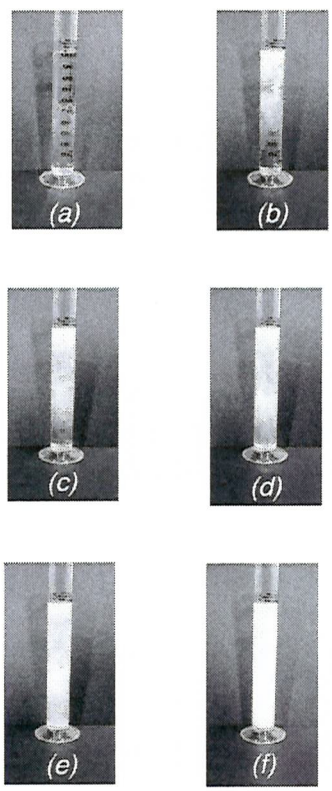

Figure 3.6 The generation of high concentrations of minute oxygen bubbles in liquid (without the production of any large bubbles) by means of "Sedna's Raven" in a 100 ml measuring cylinder. The whole sequence of photographs (a) to (f) was taken in under a minute. The system was devised with TGL and DCF by Dr Peter Birkin of the School of Chemistry, University of Southampton using hydrogen peroxide over Manganese dioxide (MnO_2) for the purpose of scaling oceanic bubble populations. The results still posses the dynamics of bubbly water, whereas froth would not.

3.3.1.6 Boston University method

Researchers at Boston University have developed a method for bubble generation which takes advantage of the porous ceramic concept described above, but with an improvement. Microbubble generation is facilitated by the incorporation of a fluid flow which allows shear forces to reduce the amount of time between when air is ejected from the ceramic and subsequently released into the fluid. This reduction in time results in a reduction in median bubble size. The complete method is shown as a sketch below in Figure 3.7.

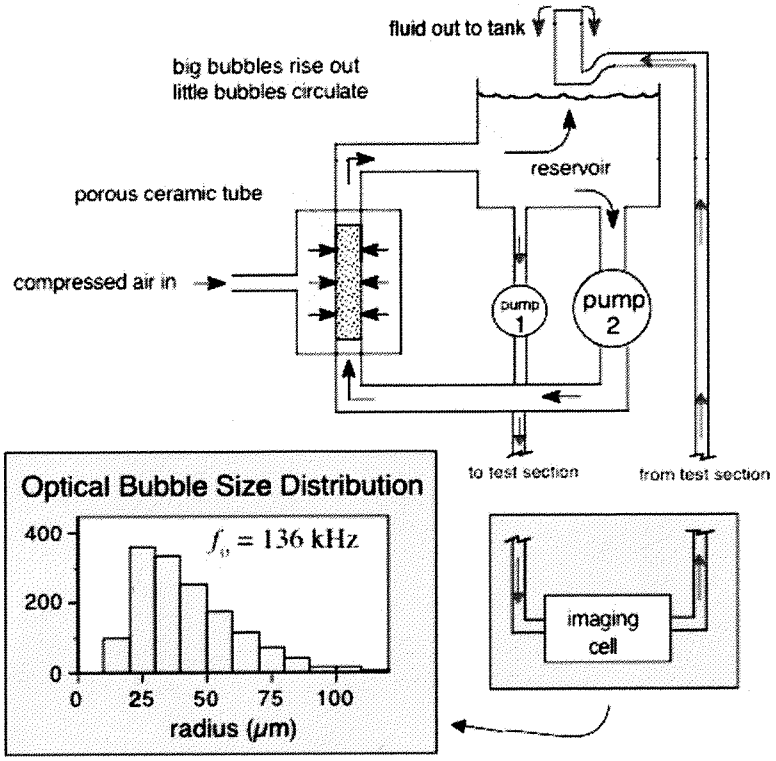

Figure 3.7 A visual description of the bubbly fluid generator used at Boston University. As per the diagram at top, Pump 2 passes water in a circuit past a region where compressed air is supplied to the fluid. The flowing water shears bubbles away from the porous ceramic tube, and into the reservoir. In the reservoir, the large bubbles rise out, and the remaining fluid is then either re-circulated past the air source or pumped to the test section. In the scenario depicted, an imaging cell is being used to give real-time bubble size distribution measurements. The fluid is then released to the tank at the end of the cycle. (Image supplied by P Wilson, University of Texas at Austin).

3.3.2 Bubble production the A B Wood Tank

As shown above, it is difficult to produce artificially large numbers of micron-sized bubbles such as are found in oceanic bubble clouds. It is even more difficult to perform this task in freshwater, as there are fewer naturally occurring surface-active materials (surfactants) within freshwater than in sea water. The reduction in surfactants means that bubbles are more likely to coalesce and become too large to represent oceanic clouds [11]. Several months were invested in researching and in some cases testing the above listed methods so as to identify an appropriate method for the repeatable generation of steady-state ocean-type bubble clouds in the A B Wood Tank. It was observed by the author that experimental physical oceanographers are not the only types of practitioners which encounter this challenge – the same problem is dealt with by fish farmers. Within the aquaculture industry, steps must be taken to ensure that farmed fish are able to breathe. To this end, several companies manufacture machinery specially designed to "aerate" water. Aeration, as it is known in the aquaculture industry, is the introduction of many small bubbles into a volume of water. The bubbles are typically small enough that they do not rise in a straight-forward manner, their motion being dictated by local turbulence effects (note that microbubbles tend to be taken out of the water column by dissolution as opposed to rising to the surface [11]). Thus it was decided that such an aquaculture machine might in fact be appropriate for this study, provided that a bubble distribution method could be developed

to distribute the gas-liquid mixture into the acoustic test tank.

A design was sought which would maximize water aeration and facilitate the generation of high-void fraction clouds containing large numbers of microbubbles at minimum cost. In designing a solution, some guidance was borrowed from Henry's law: If species **A**, a gas, is only weakly soluble in a liquid, species **B**, Henry's law may be used to relate the mole fraction of **A** in the liquid to the partial pressure of **A** in the gas phase outside that liquid:

$$x_{\mathbf{A}} = \frac{p_{\text{species A}}}{H_{\text{sol}}} \qquad (1)$$

The constant H_{sol} is temperature dependent, and pressure independent up to about 5 bar. The purpose of showing this relation here is simply to establish that, when building a system for the purpose of aerating water, there are clear benefits to building a pressure vessel capable of withstanding pressures above atmospheric pressure. To recreate a surf zone bubble cloud, Aqua Systems of Renfrewshire, Scotland was commissioned to build a water aerator as shown in Figure 3.8.

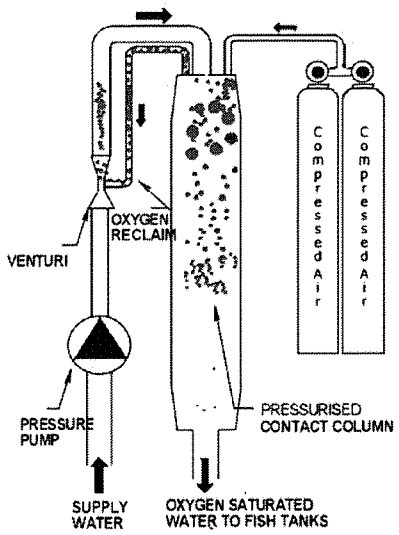

Figure 3.8 - A sketch showing the operation of the bubbly fluid generator. This image was produced by the manufacturer (Aqua Systems, Renfrewshire, Scotland) and is available from their website: www.aquasystems.co.uk.

The bubbly fluid generator operates via the following process: Water is pumped from the bottom of an above-ground mixing tank across a pressure drop (the venturi shown in Figure 3.8). To reduce equipment costs, a self-priming pump was not selected for the system. As such, the water within the above-ground tank provides the pressure head necessary for system operation. The tube labelled "oxygen reclaim" in Figure 3.8 is filled initially with air, which allows air to mix with the turbulent water immediately downstream of the pressure drop. The bubbly mixture is then pumped into the pressurised contact column, where further air/water mixing occurs per Henry's law [125]. Large bubbles, which are unsuitable for the experiment, float to the top of the contact column and refill the "oxygen reclaim" tube. The air/water mixture is then pumped into a large (6700 liter) mixing take (as shown in Figure 3.9), where the mixture is then either recirculated through the aerating system, or pumped into the acoustic test tank.

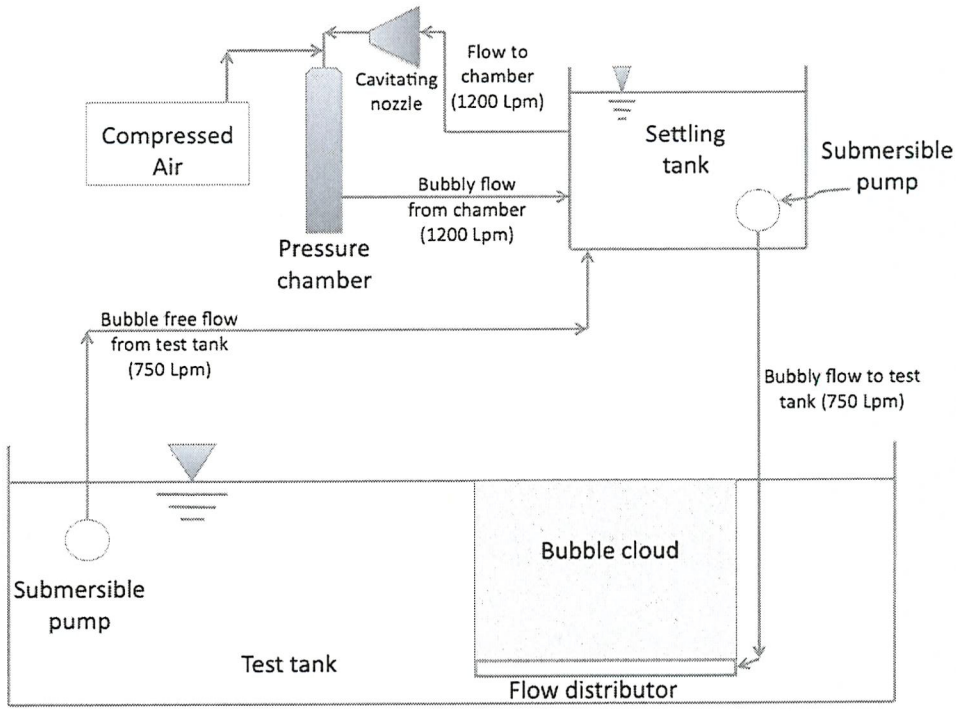

Figure 3.9 – A sketch showing an approximate layout for the bubbly fluid generator/mixing tank flow cycle. Note that the tank shown in the diagram is a mixing tank, not the experimental tank. Bubbly water is pumped from the mixing tank to the bottom of the mixing tank, where controlled bubble clouds are then produced.

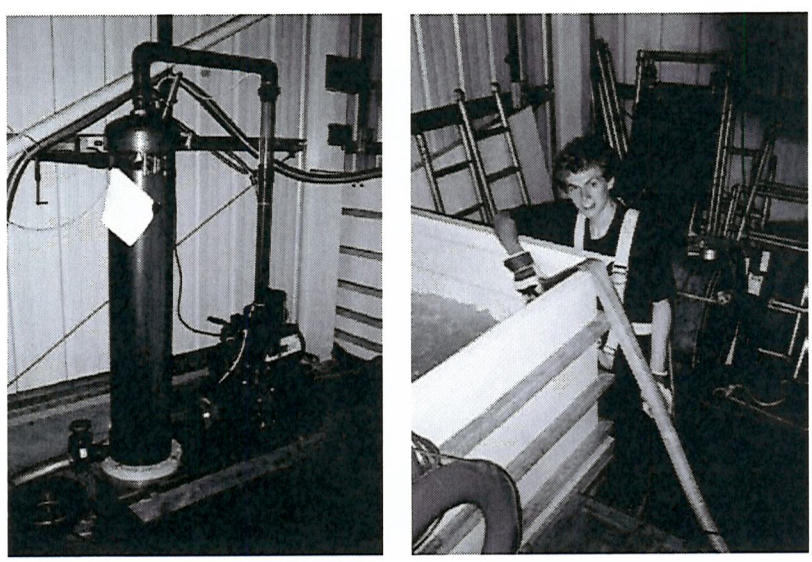

Figure 3.10 – (Left) A photo of the high pressure chamber used to mix compressed air and water which has been cavitated by pumping it through a nozzle at high speed. (Right) Mr D C Coles manages the line delivering bubble-free water from the test tank back to the mixing tank.

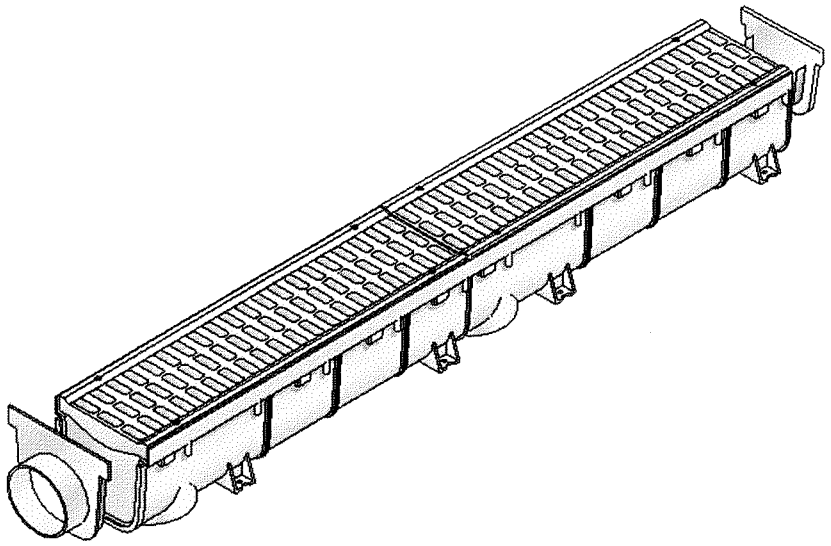

Figure 3.11 – An engineering drawing of the PVC drainage gutter used for bubble distribution. The drain measures 0.10m x 0.10m x 1.5 m (drawing source: NDS Inc., Lindsay, CA, USA)

As an illustration of the effectiveness of the bubbly fluid generator, the machine is capable of reducing the visibility within the mixing tank from effectively clear to less than 12 inches in about 5 minutes as illustrated in Figure 3.12. As the flow cycle introduces no substantial amount of particulates, this change in visibility is due entirely to the introduction of microbubbles into the water.

The bubbly fluid emitted into the test tank varies with time in terms of void fraction, foot-print, and bubble-size distribution. While careful use of the BFG can minimise the variation in these characteristics, variations in the bubble cloud tended to occur when the system was operated for several hours at a time. Therefore, a pseudo-steady state was generally sought during testing. The pseudo-steady state was characterised by a well-balanced level within the mixing tank, relatively unchanging surface activity within the test tank, and no

large bubbles (> 1 cm radius).

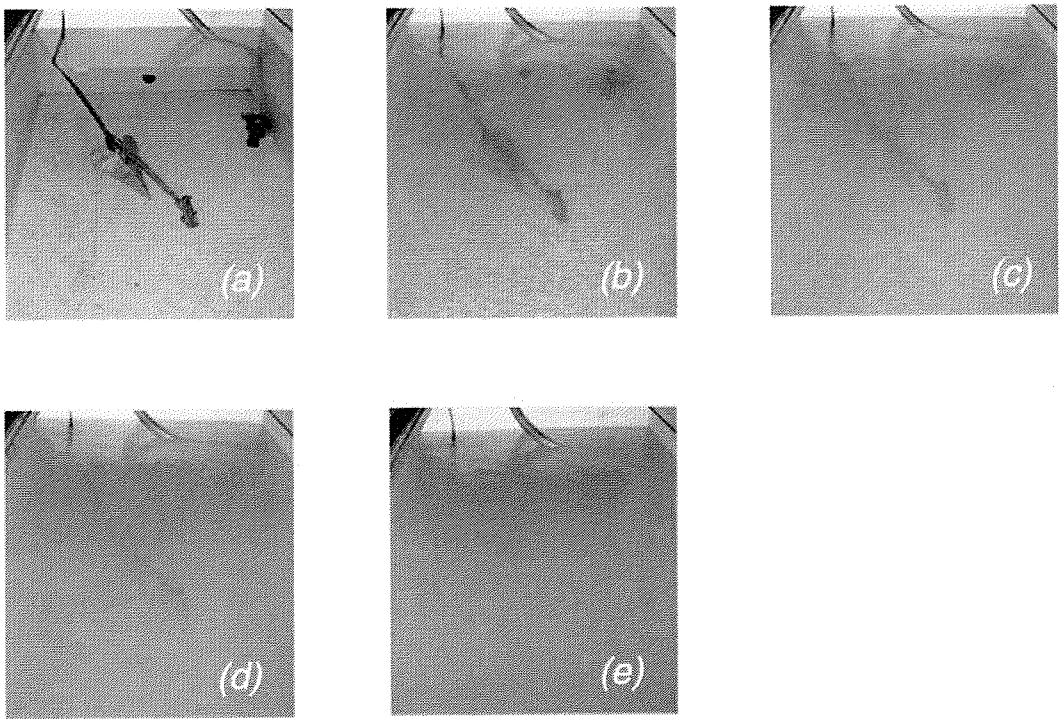

Figure 3.12 A large-scale generator of small bubbles implemented by the authors, the images corresponding to times of (a) 0, (b) 1 min, (c) 2 min, (d) 3 mind and (e) 4 min after activation of the generator. They show the system filling a tank of normal fresh water (measuring 1.5m by 2.5m by 1.5m) with a dense cloud of minute bubbles, without the production of large bubbles. As a result, the initially clear water turns milky white, obscuring from view the Delta 22 anchor which lies under 1.5 m of water and measures 695mm end-to-end and a maximum of 310mm between the fluke tips. No chemicals were used.

3.3.3 Measurements

Bubble-size measurements were made using the acoustic method which was published by Leighton *et al.* [87], and applied by Coles and Leighton [126]. Coles and Leighton described two test equipment configurations: one for the open water, and one for an experimental tank. The latter configuration was used for monitoring the cloud used here. A complete explanation of that method is beyond the scope of this document, but a brief overview is given here. Acoustic tones were

emitted into the water, and the attenuation and propagation speed of those pulses were monitored by an array of hydrophones placed within the bubble cloud and directly in the beam of the source transducer. A schematic of the test setup is shown in Figure 3.13.

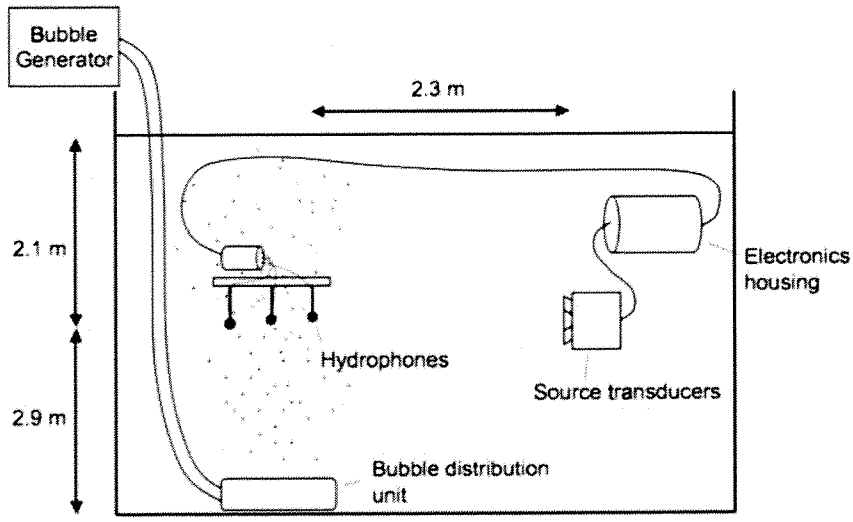

Figure 3.13 Schematic showing side-view of the A B Wood tank during bubble size distribution measurements (drawing reproduced from Coles and Leighton [126] and used here with permission).

The tone-burst pulse train used for these measurements is shown below in Figure 3.14.

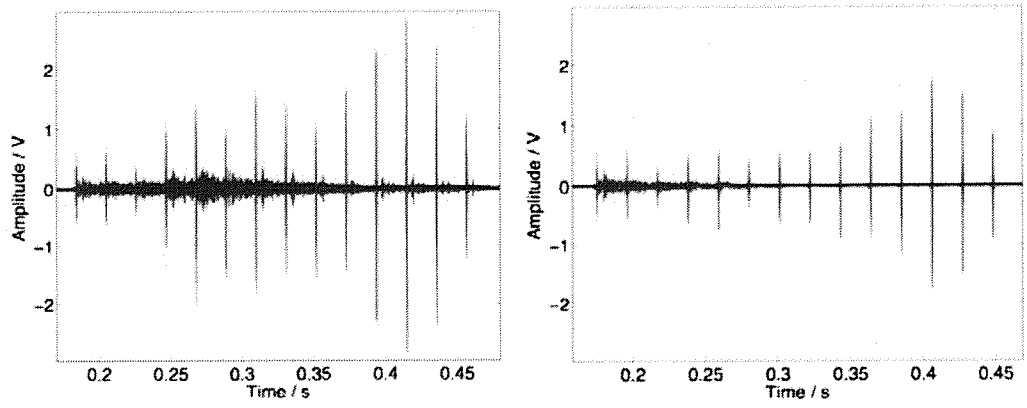

Figure 3.14 *(a)* The pulse train measured at the second hydrophone with no bubbles present *(b)* The increased attenuation at the same hydrophone with bubbles present (drawing reproduced from Coles and Leighton [126] and used here with permission).

Measurements were made prior to the beginning of any TWIPS experiments to ensure that the cloud was reasonably in accordance with those which might be encountered at sea. Upon successful completion of these measurements, the system was adapted so as to be compatible with the equipment required for the TWIPS tests. It was therefore possible to monitor the bubble size distribution during the course of many[15] of the laboratory tests conducted in conjunction with this study.

3.3.4 Results

The bubble clouds generated using the BFG seemed to be generally consistent with the types of bubble clouds measured during sea trials. The data reported here, which was recorded as explained in the previous section, was published by Coles and Leighton [126] and is labelled as such in the figure below:

Figure 3.15 summarises the acoustic bubble-size measurements, which were made according to the method explained in the previous section. Note that all of the measurements to which those of Coles and Leighton are compared in Figure 3.15 were taken in open water during sea-trials in salt water. The bubble size distribution obtained

---

[15] Occasional system failures, equipment shortages, and personnel limitations dictated that it was not always possible to monitor the bubble size distribution during TWIPS tests.

in the controlled experiment is therefore comparable to that which might be encountered at sea. This result is favourable, in that it reduces the difficulty encountered when attempting to use the results of the tank experiment (Chapter 3) to inform the development of a reasonable open water sea-trial (Chapter 5).

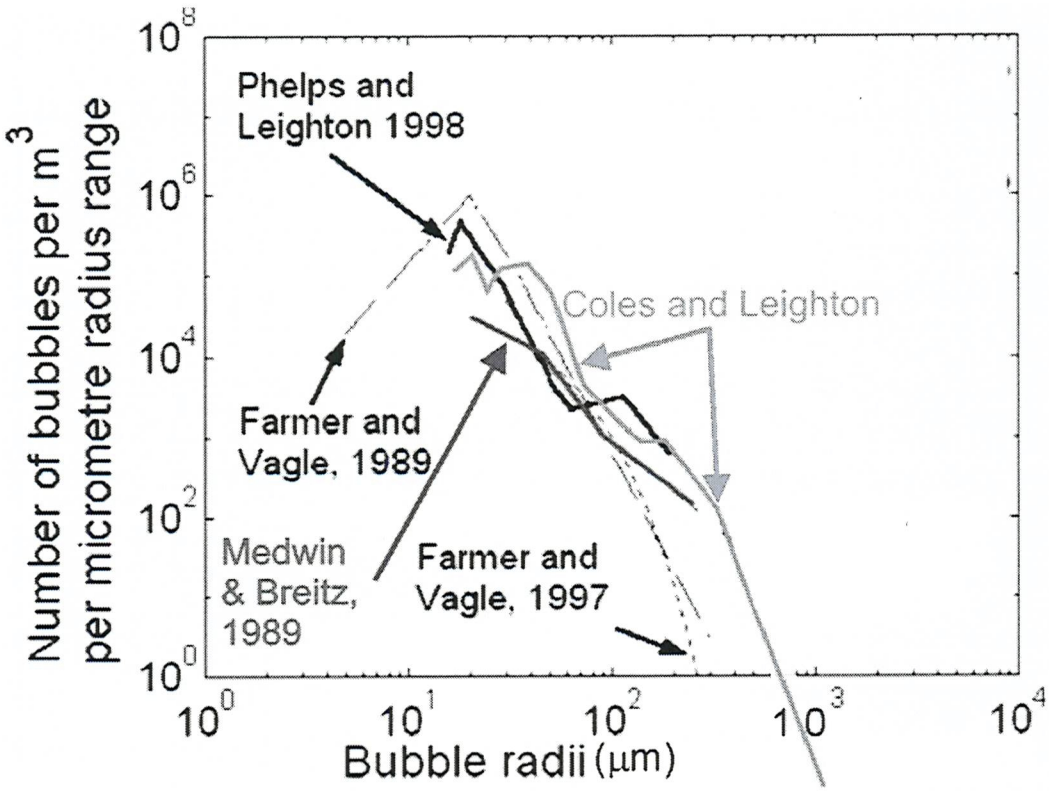

Figure 3.15 The bubble size distribution used in the experiment is labelled Coles and Leighton [126]. It compares well with a range of bubble populations measured at sea, by Farmer and Vagle [116, 117] and Medwin and Breitz [115], and Coles and Leighton [126].

4 Experimental detection of linear scatterers in bubbly water

It was shown using the computational model presented in Chapter 2 that TWIPS might make possible the detection of linear scatterers in bubbly water. On this basis, it was deemed appropriate to design an experiment for the testing of the technique. To that end, the development of a machine capable of producing ocean-like bubble clouds was described in the previous chapter. The purpose of the development of that machine was to facilitate a test of TWIPS in a controlled environment. That endeavour and its outcome are described in this chapter.

4.1 Experimental setup

The experiment was performed in the AB Wood tank, a rectangular freshwater tank measuring 8m x 8m x 5m deep (320 m^3), as pictured below in Figure 4.1.

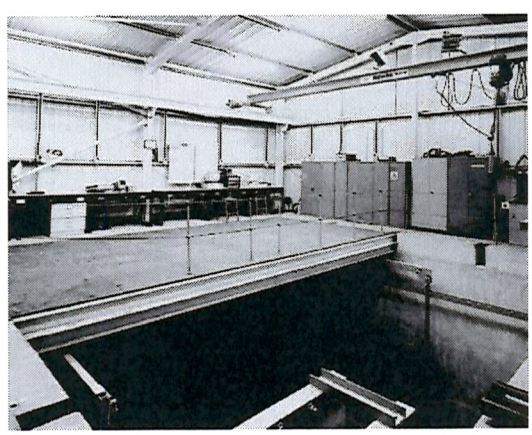

Figure 4.1 A photograph of the A B Wood Underwater Acoustics Laboratory. The tank is shown here as being empty.

4.1.1 Geometric layout

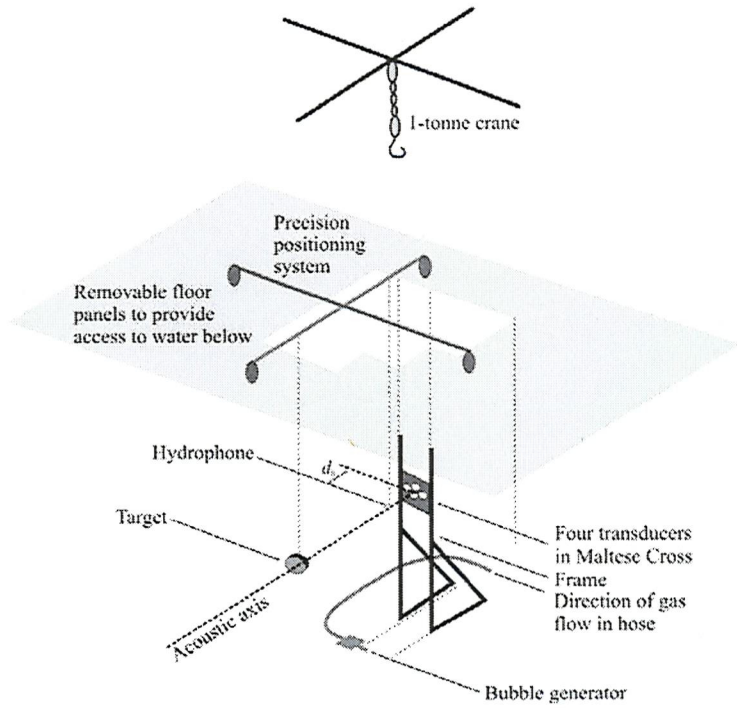

Figure 4.2 Schematic of tank layout during initial testing. The shaded plane corresponds to the floor of the laboratory, below which is an underground water tank measuring 8 m × 8 m × 5 m deep. Four transducers are mounted in a Maltese Cross configuration, held on a rigid frame. Aligned on the acoustic axis are a hydrophone (at range d_h=0.03 m from the source) and a removable target (at range 2.19 m from the source). (Figure and caption by Prof Leighton).

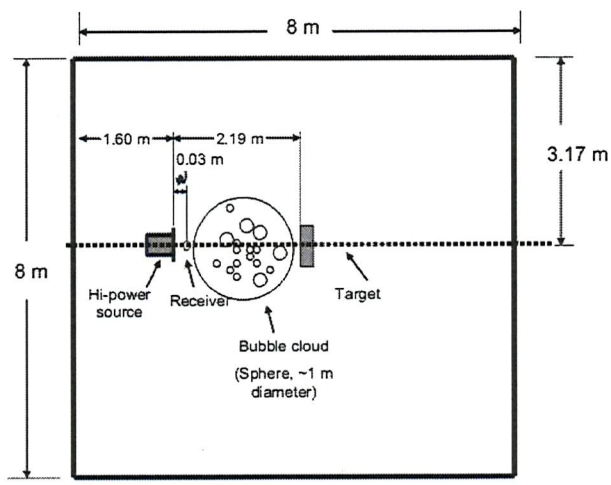

Figure 4.3. Overhead schematic of the tank during tests. Note that the size and number of the bubbles shown within the sketch are distorted for visibility within the diagram.

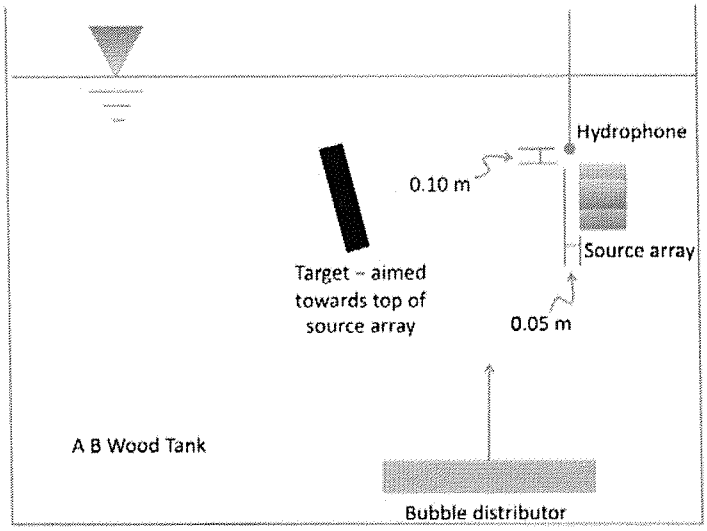

Figure 4.4. Elevation schematic of the tank during tests. Note that the hydrophone is located above the source array.

4.1.2 Source signal and transducer

This section will describe the signal production method used during the TWIPS experiments. The experiment required the regular generation of two high-amplitude pulses in rapid succession, the second of which had to be opposite in phase to the first. It was pointed out by Paul Doust, a recognised transducer expert and student within the Ultrasonics and Underwater Acoustics research team, that the acoustic requirements for our source would pose quite a challenge for most off-the-shelf systems. He stated that the electroacoustic production by a compact source system of two phase-reversed high amplitude pulses, each no longer than a few milliseconds, would require the development of specialised equipment [127] which could cost several tens of thousands of pounds. In response to this information, it was questioned whether surface reflections might be used to generate the phase-reversed signals. The

merits of a reflection-based approach and the eventual decision to acquire specialised acoustic equipment of the type suggested by Mr Doust will now be discussed.

4.1.3 A surface-reflection approach to TWIPS pulse generation

The reflection from a pressure-release surface will be opposite in phase to the incident pulse [110]. It follows that the reflection from a pressure release surface might be an effective way to generate a pulse which is nearly equal in amplitude to, though 180° out of phase with some incident pulse. The practicability of this statement can be evaluated using the results of a study by Medwin conducted in 1966, and entitled "Specular scattering of underwater sound from a wind-driven surface" [1]. In that study, specular reflections were generated using an upward-firing send/receive transducer placed at the bottom of a wave-tank, as shown in Figure 4.5. The amplitude of these reflections was then compared with that of the incident pulses in order to determine the relationship between surface wave size/shape and reflection amplitude[16]. Concisely, it was shown that for anything more than trivial surface disruptions, the probability of encountering a specular reflection equal in amplitude to the incident pulse is very low. This is illustrated below in Figure 4.6, which has been reproduced from the original publication [1].

---

[16] In this experiment, Medwin did not attempt to change the size scale of the surface waves, but rather increased the frequency of the incident waves.

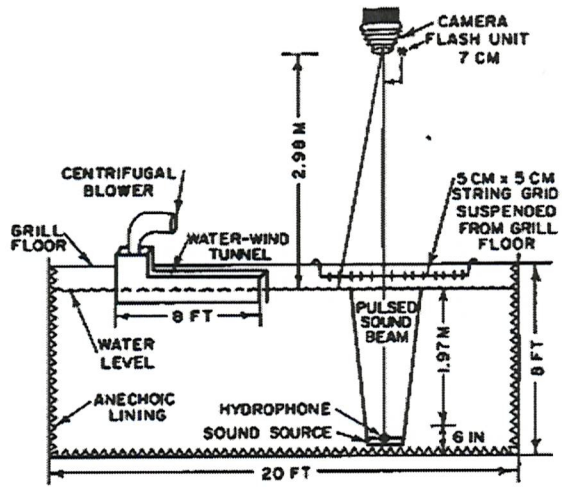

Figure 4.5 Diagram of the specular reflection experiment conducted by Medwin (after Medwin [1])

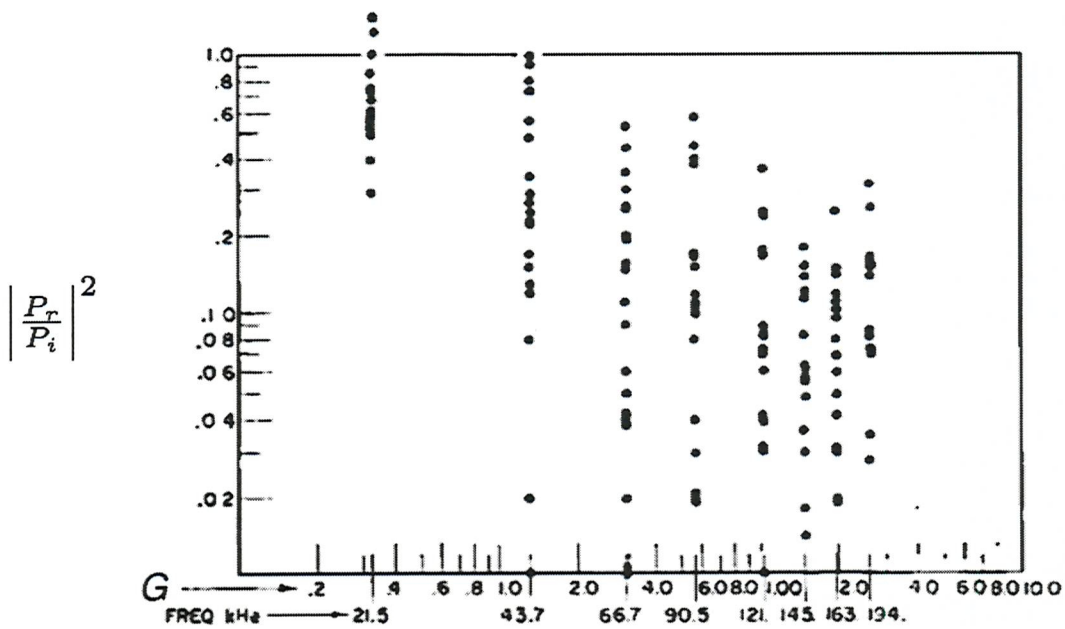

Figure 4.6 Results of the specular reflection experiment conducted by Medwin (after Medwin [1]). The results shown here indicate use of a two metrics. Along the abscissa, the surface roughness is indexed according the roughness parameter, *G* (defined in text below). For the ordinate, the reflection amplitude is expressed as the square of the magnitude of the reflected pressure wave P_r relative to the amplitude of the incident wave, P_i.

In Figure 4.6 above, the normalised magnitude of the pressure of the reflected wave has been plotted as a function of the surface roughness, *G*, which is defined as:

$$G = 2\pi(\varsigma/\lambda)(\cos\theta_i + \cos\theta_r) \qquad (4.1)$$

where ς is the root-mean-square of the wave height, λ is the wavelength, and θ_i and θ_r are the angles of incidence and reflection. The angles of incidence and reflection are measured against a vector parallel to the sea-air interface, and are both zero according in the experiment schematic shown Figure 4.5. In the results of Medwin, at G = 0.2, of the ordinate values are greater than unity. This suggests that the reflected energy was greater than the incident energy – a non-plausible conclusion. Such a result could be explained through the effects of focusing and constructive interference.

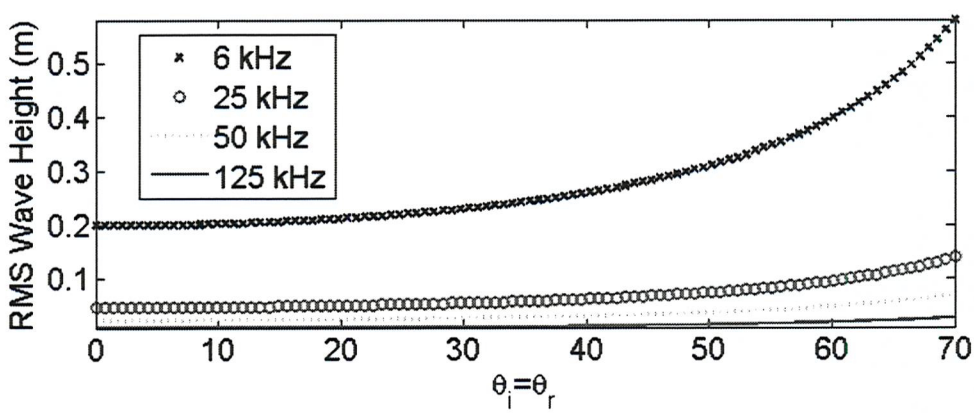

Figure 4.7 These curves describe for angles of incidence from $0\ ^\circ \le \theta_i \le 70^\circ$ the wave-height which will give perfect reflections for no more than about 5% of incident rays (based on extrapolation from Medwin [1]. Higher wave heights can be tolerated at angles greater than 70°, but high angles are impractical from a design perspective because (1) for short range detection (necessary to maintain the high pressure amplitudes necessary for this technique) the source must be placed prohibitively close to the sea-air interface, thereby altering the directivity of the source and (2) the exploitation of grazing angle incidence will tend to reduce the inter-pulse delay, necessitating either unrealistically short detection pulses or resulting in inter-pulse interference.

The likelihood of a specular reflection with increasing surface roughness is shown above in Figure 4.6. That result shows an

exponential reduction in the likelihood of a specular reflection with increasing surface roughness. In Medwin's data, no perfect[17] specular reflections resulted for a surface roughness of greater than about 1.2. In real terms, this means that at 6 kHz (λ=0.25 m) for an RMS wave height of greater than 17 cm, Medwin found approximately a 5% chance of a perfect reflection. The function shown as equation (4.1) has been plotted in Figure 4.7 using G =1.2. Since regular, controlled reflections are the issue of interest here, the condition $\theta_i = \theta_r$ according to Snell's law was enforced in the calculations performed to generate Figure 4.7. This value has been used for surface roughness because, in Figure 4.6, that is the maximum G for which a perfect reflection was obtained. From this analysis, one can conclude that in the A B Wood Tank, where there is only low-amplitude surface disturbance when the bubble-generator is functioning, it might be possible to take advantage of surface reflections to obtain twin inverted pulses, but the system would only operate intermittently[18]. Such a system would be

---

[17] "Perfect" is used here to indicate a reflection which is equal in amplitude and exactly out of phase with the incident wave.

[18] Even with Medwin's lucid results as a guide, the exact degree of this intermittence is difficult to determine analytically. It would depend on the exact depth of the source depth and the target, and the amplitude of surface ripples. Based on the configuration which was finally employed for this experiment, it can be estimated that $G=2\pi(0.02\text{ m})/(1500\text{ m s}^{-1}/6000\text{ Hz})(2\cos(22^\circ)) = 0.94$ was present during experiments. According to the experimental results of Medwin shown above, the likelihood of a

inadaptable to open-water conditions as a result of the increased surface turbulence encountered in that environment. Further, a twin-inverted pulse system which is dependent on surface reflection for production of the second pulse would almost never function properly were a high operating-frequency to be used. Although this high-frequency result is not related to the immediate discussion, it will be re-introduced in Chapter 6, where cetacean biosonar is considered.

4.1.4 Electroacoustic production of TWIPS pulses

As was argued in the previous section, a sea-air interface which is even slightly disturbed will not tend to give a predictable, equi-amplitude acoustic reflection. Thus, an electro-acoustic source capable of meeting the requirements unique to this investigation was sought. Dr Justin Dix of the National Oceanography Centre, Southampton, agreed to loan to our research team a GeoAcoustics Chirp II transducer and transceiver system [128].

The 3D-Chirp source consists of four separate high power transducers, which can be mounted into whatever configuration the user deems appropriate. They are powered by a matched amplifier which is controlled by a trigger box and, in turn, a personal computer (PC). The source characteristics have been documented by previous

---

perfect reflection was then somewhere between 5% and 30%.

investigators, making it straightforward to select and mount the transducers in the manner that would most benefit our experiment. Bull *et al.* [129] showed that for the four transducers in question, when mounted in a plane and fired simultaneously, the far-field level is maximized if the sources are arranged in a Maltese Cross. This arrangement gives the directivity pattern shown in Figure 4.8.

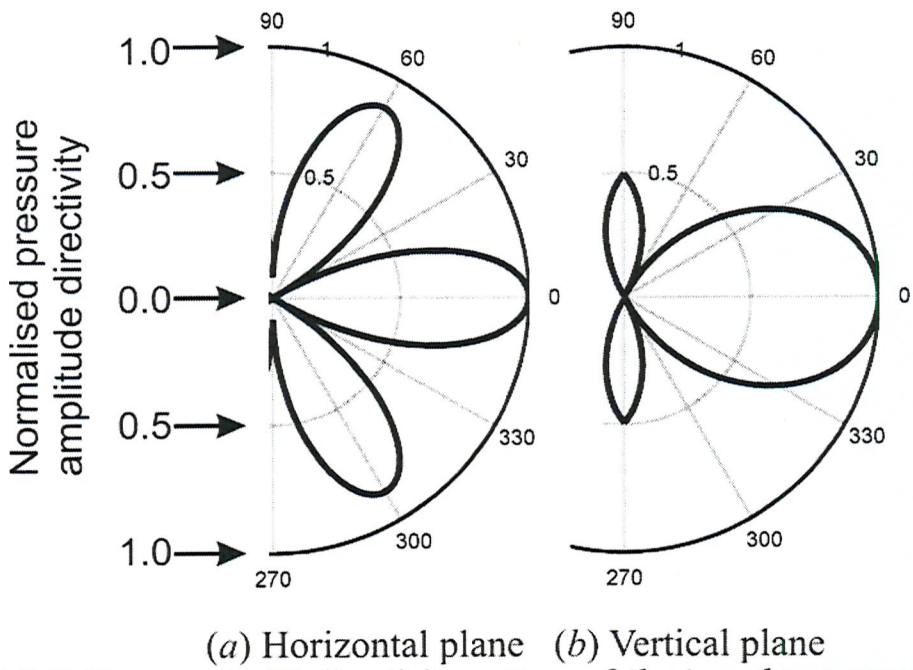

Figure 4.8 Half-power (-3 dB) directivity pattern of the transducer array when configured as shown in Figure 4.9 and each driver is fired simultaneously.

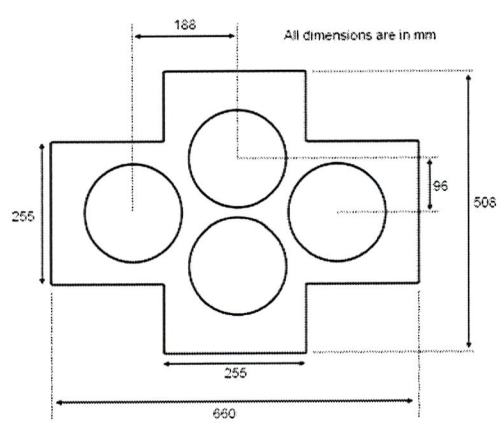

Figure 4.9 The Maltese Cross configuration in which the acoustic transducers were arranged for this test. The transducers were held in place by a steel frame having the dimensions shown in the sketch (Figure drawn by David Coles of the Institute of Sound and Vibration Research).

For the TWIPS experiment, it was necessary to mount the transducers so that they would be side-firing. The mounting rig that was built for the experiment is shown in Figure 4.10.

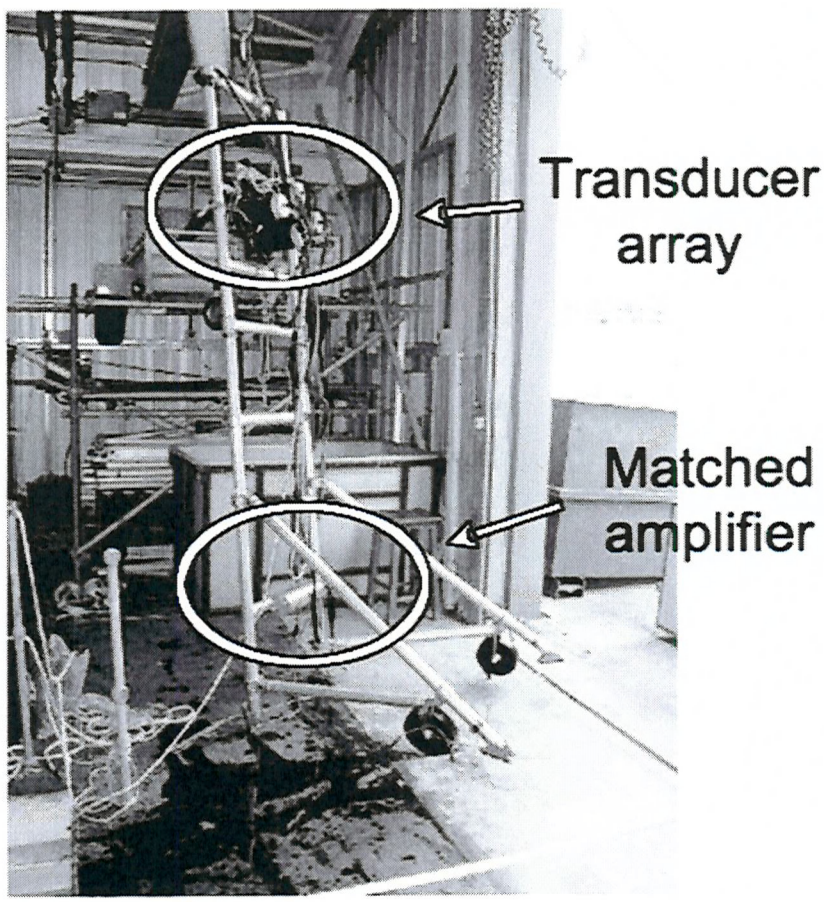

Figure 4.10 Photograph of the scaffolding used to support the acoustic transducers within the A B Wood Tank. At top can be seen the transducer array (facing the left edge of the photo). The matched amplifier (the 'bottle') can be seen suspended from the lowest scaffold rung. The complete transducer stand measures approximately 3.3 m high.

For testing within a confined water tank, the minimum operation frequency is limited by the tank dimensions, while the maximum operation frequency is limited by the size of the largest bubbles. If, in the case of the long wave, a very long pulse is used within a very small tank; wall, surface, and bottom reflections will be individually

indecipherable as a result of superposition and the associated destructive/constructive interference. In the case of the short wave, an operating frequency much greater than the resonance of the largest bubble will turn the largest bubbles into linear scatterers, and will reduce greatly the decipherability of solid objects from large bubbles.

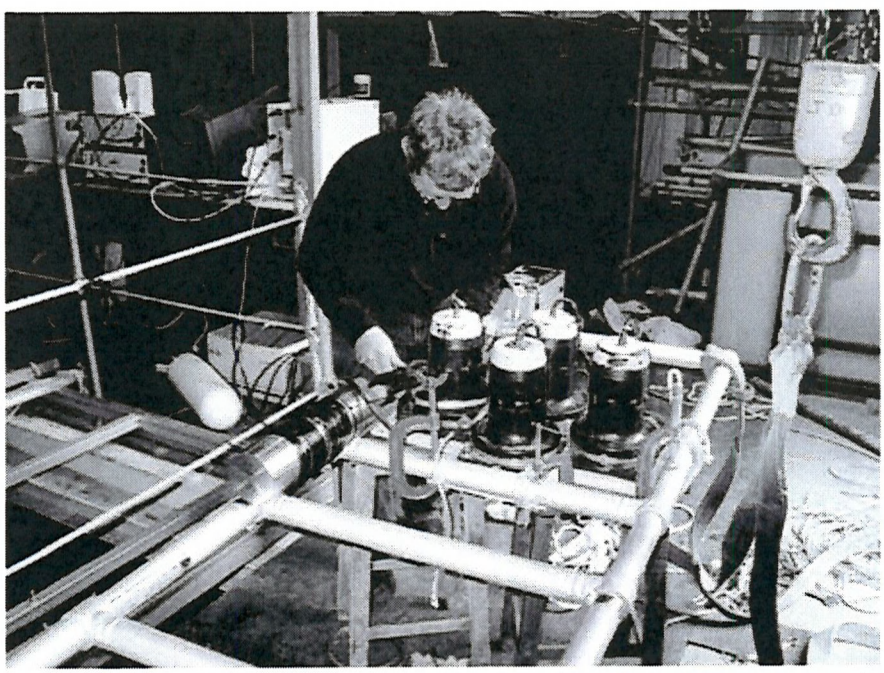

Figure 4.11 Dr J Dix of the National Oceanography, Southampton assists in setting up the transducer array. In the iteration of the scaffold rig shown here, the matched amplifier (the 'bottle') has not yet been placed in the final location (where it was depicted Figure 4.10).

Sounds which are to be produced by the transducers used in the TWIPS tests must first be soft-written to the matched amplifier (the 'bottle') before they can be produced acoustically. It is not possible for users of the 3D Chirp system to write sound files directly to the bottle. The desired outgoing sound pulses must be first be written as ASCII files, sent to a electronically to the corporate headquarters of the system manufacturer, encoded by company technicians, sent back to system owner, and then encoded onto the bottle. A trigger box is then

used to tell the bottle when to power the transducers with the desired pulse. The pulse designed for this experiment consisted of three components: *(1)* an eight-cycle Gaussian modulated pulse; the 'positive pulse'; *(2)* pause; *(3)* An exact opposite of *(1)*: a pulse equal in amplitude to but π-radians out of phase with the first pulse; this is known as the 'negative pulse'.

The pulses generated are shown, without the pause time, in Figure 4.12. The amount of time needed for the pause requires consideration of the physical environment in which the method is being applied. Those considerations appropriate to the A B Wood Laboratory will now be discussed.

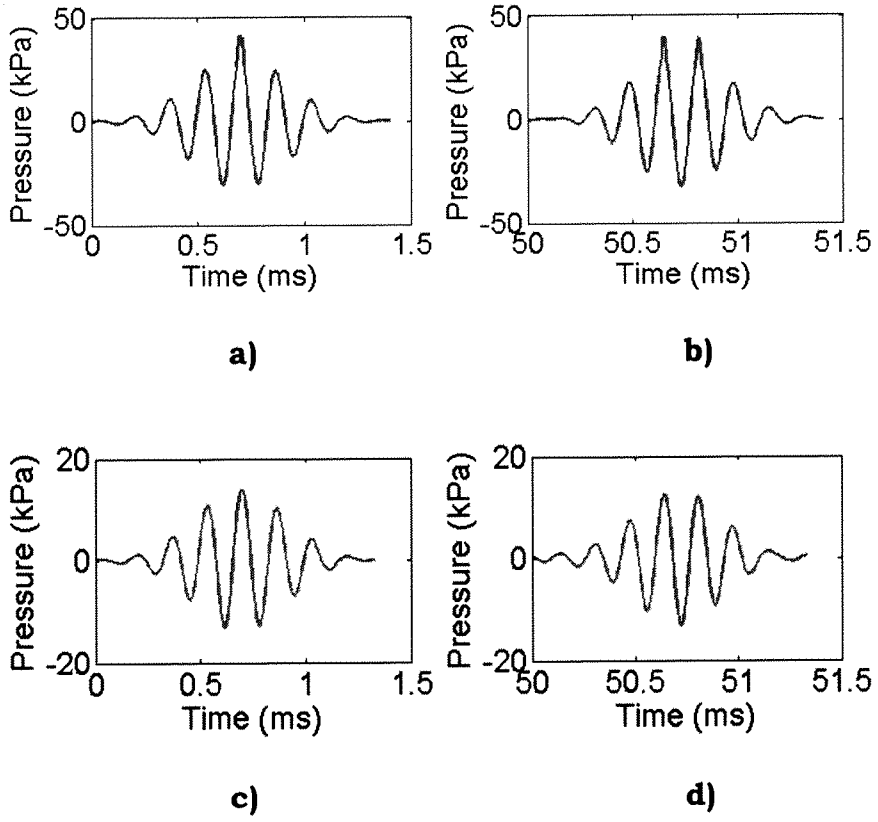

Figure 4.12. Reference signals as recorded in the AB Wood Tank in the absence of bubbles. *a)* First half of out-going signal at a distance of 1 m from

the source. *b)* Second half of out-going signal at a distance of 1 m from the source. *c)* First half of outgoing pulse as measured at target location. *d)* Second half of outgoing pulse as measured at target location.

4.1.5 Inter-pulse delay

The upper limit for pulse-pair spacing τ is based on the rate of bubble-cloud evolution. The TWIPS method assumes that there is insufficient change in the bubble population and target position during the time expired between the two pulses to degrade the correlation of the boundary conditions which dictate scattering returns from the two pulse halves. In the current experiment, the cloud in the beam will evolve as a result of both buoyant rise and size change in response to the steadily decreasing hydrostatic pressure. Therefore it might reasonably be expected that the upper limit for pulse-pair spacing *(τ)* will be based on the rate of bubble-cloud evolution. If scatterers in the acoustic field are allowed to move considerably during the pause between the two outgoing pulses, then the physical parameters dictating the scattering apparent in the first pulse return will not correlate well with those dictating the scattering within the second pulse return. In the tank, where the experiment has been designed to allow the bubbles to rise through buoyancy forces (and not under convective flow forces), an interpulse interval might be sufficiently long to degrade the TWIPS pulse if enough bubbles rose through a significant fraction of a wavelength.

A simulation of the effect of phase on the success of the TWIPS

algorithm was conducted. The goal of this study was to establish the degree to which system performance is degraded if the phase relationship of the two-portions of the excitation pulse are not identical. To conduct this study representative bubbles sizes were selected from the entire bubble size distribution with radii of 10 μm, 50 μm, 100 μm, 500 μm, 1000 μm, and 5000 μm. Each of these were excited by a wave of phase ϕ, and by and opposite wave of phase $\phi+\Delta\phi$. By varying $\Delta\phi$ until nonlinear suppression reduced by 50%, it was seen that the maximum tolerable motion for a bubble between two halves of a TWIPS pulse is about 0.37 of a cycle at the driving frequency (at the operating frequency of 6 kHz used here, 0.37 wavelength corresponds to about 92 mm if the sound speed were around 1500 m s^{-1}).

Estimates of the speed at which a bubble rises are made somewhat complex by the fact that the drag coefficient of a bubble varies with bubble size, shape, and speed of travel [11, 44]. To estimate the speed at which a bubble encountered in the tank will rise, an iterative approach can be taken. This calculation will be made for a wide range of bubble sizes, according to the range encountered in oceanic conditions and the tank experiment. The bubble rise speed can be determined to a first approximation using Stoke's law [44]:

$$V_{St} = \frac{2gr^2}{9\nu} \tag{4.2}$$

where V_{St} is the velocity according to Stoke's law, g is the acceleration

due to gravity, r is the bubble radius, and υ is the kinematic viscosity of water (10^{-6} m^2 s^{-1} [27]). Results obtained using this method tend to largely underestimate the drag coefficient of a bubble (by as much as an order of magnitude) as can be seen from Figure 4.13.

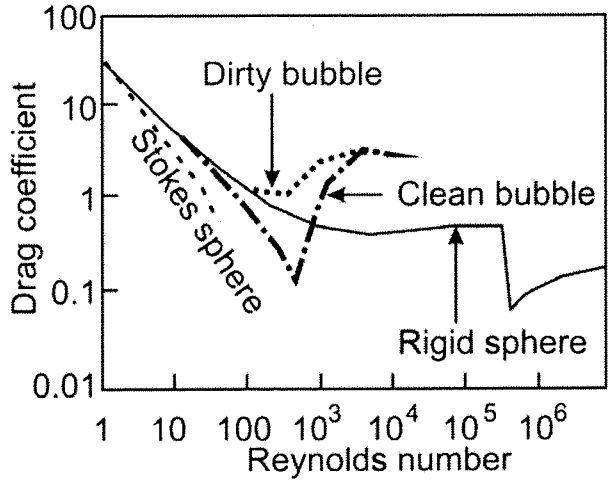

Figure 4.13 The variation in drag coefficient with Reynold's number for four types of sphere (copied from Leighton [11], which was based on data of Clift *et al.* [130]).

In the first iteration, the estimated velocity V_{st} can be used to estimate the Reynolds number which can in turn be used to find a first estimate for the drag coefficient of the bubble. Further iterations then use the terminal velocity calculated via the drag coefficient to re-assess the estimated Reynolds number, and so on. The Reynolds number Re is calculated as the ratio of inertial forces to viscous forces, and indicates the relative turbulence of a given environment:

$$Re = \frac{V_s L}{\nu} \tag{4.3}$$

In the above expression, V_s is the bubble velocity, L is the length scale of the system (for a sphere, the diameter can be used to represent the length scale), and ν is kinematic viscosity of water. Having obtained

the Reynolds number, the drag coefficient can be estimated from Figure 4.13. This can in turn be used to calculate the drag force F_d on the rising bubble

$$F_d = \frac{1}{2}\rho_w V_t^2 C_d A \tag{4.4}$$

where ρ_w is the density of water, V_t is the terminal velocity of the bubble, C_d is the drag coefficient of the bubble, and A is the cross-sectional area of the rising gas volume. The net downward force on the bubble is equal to the mass of the gas within the volume of the bubble plus the drag force, while the net upward force on the bubble is that of buoyancy. At terminal velocity, the upward force is equal in magnitude to the downward force:

$$F_d + F_g = F_b \tag{4.5}$$

where F_g is the weight of the bubble, and F_b is the upwards buoyant force on the bubble by the surrounding water, equivalent to $\rho_w V g$, the product of the water density, the bubble volume, and the acceleration due to gravity. This expression can then be solved for velocity, which can in turn be used to re-calculate the Reynold's number, the drag coefficient, and so-on. The output from this iterative calculation shows that the largest bubbles in the tank (those with a radius on the order of 1 cm) will rise the fastest at a rate of approximately 1.1 m s^{-1}.

Recall that the goal here is to establish the maximum interpulse interval such that the fastest-moving bubbles do not travel more than about 0.37 of a wavelength at during the interpulse interval. On this

basis, with an operating frequency of 6 kHz and a sound speed of approximately 1500 m s^{-1}, the maximum allowable interpulse interval before system performance will degrade by 50% can be argued to be 84 ms. This information was used to inform the design of the pulse used during tests, but practical equipment considerations limited the maximum interpulse interval to 100 ms.

In summary of this section, buoyant rise speeds in water are not simple, and a complete description is beyond the scope of this discussion. In general the largest bubbles rise the most rapidly unless group effects occur [44]. From such considerations, it was calculated that an interpulse interval of 100 ms (the largest used in this thesis) would present the TWIPS pulses with a sufficiently stable environment. In a confined space such as a laboratory tank, the lower limit of the interpulse delay can be determined by the length of the reverberation tail. The reverberation time of a space is defined according to Sabine as the amount of time it takes for the level in a space resulting from an impulse to decrease by 60 dB [131]. By analysing the decay of the first 15 dB, and extrapolating linearly, it is possible to estimate the reverberation time via the so-called T_{15}. In Figure 8, the reverberation tail for the tank is shown, and has been smoothed after the method of Pierce [3]:

$$P_{\mathrm{rev}}(t) = 10\ \log[\frac{1}{T_{\mathrm{ref}}}\int_{t}^{\infty}\frac{p(t)^2}{p_{\mathrm{ref}}}dt'] \qquad (4.6)$$

where t' is time. t is the start time, $p(t')$ is the pressure in the tank as a

function of time, p_{ref} is an arbitrary reference pressure (chosen here to be the maximum pressure), T_{ref} is an arbitrary reference time, and $P_{rev}(t')$ is the smoothed reverberation function.

From Figure 4.15, it can be seen that the T_{15} for the tank is 240 ms. Further, it can be seen that, in order for the time-averaged sound pressure level to reduce by 10 dB following a single band-limited burst of the type designed for the TWIPS tests, the interpulse delay must be least 65 ms. That is, if two acoustic pulses are released into the tank in close temporal proximity, and a delay of less than about 65 ms is used, a detectable amount of reverberation from the first signal will still be present when the second signal is introduced into the water. This is demonstrated in Figure 4.14, where the acoustic returns from pulses played at different timing intervals have been displayed to show clearly the interference resulting from reverberation. In Figure 4.14, it is shown that the reverberant energy from the first pulse diminishes the correlation between the first and second pulses unless a delay of at least around 50 ms is used. It is unsurprising that Figure 4.14 *(a)* shows poor correlation between the two pulses, as the reverberation curve shown in Figure 4.15 shows that the time-averaged reverberant energy within the tank is only reduced by about 3 dB after 20 ms.

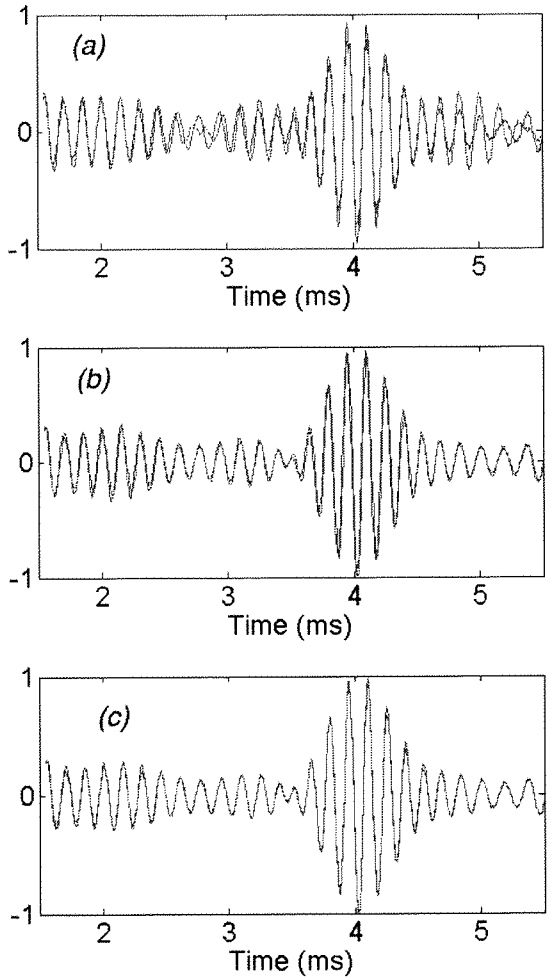

Figure 4.14. The effect of tank reverberation on pulse-pair matching. In each plot, the initial outgoing pulse has been drawn in dark blue, and overlaid by the inverse of the second pulse (which is an acoustical opposite of the initial pulse). Thus, if the second pulse is an identical opposite to the first, then in the plot shown, the red line should correlate perfectly with the blue line. The results are shown for three different pulse separation times, as follows:
***(a)* τ = 20 ms *(b)* τ = 50 ms and *(c)* τ =100 ms. The target is visible as a broad peak in the region of 4 ms. Increasing agreement is gained as the interval is augmented.**

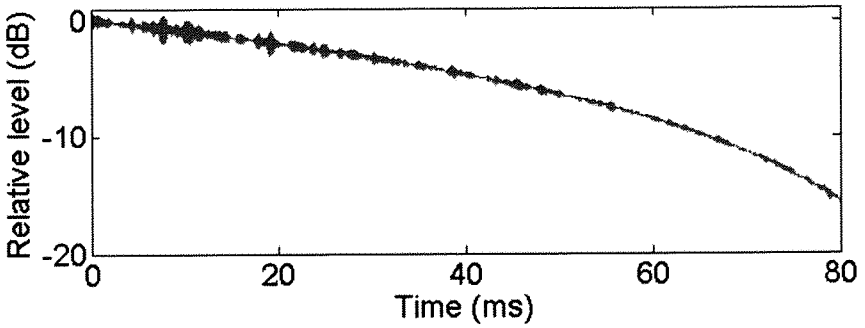

Figure 4.15. A reverberation curve for the A.B. Wood Tank. The T_{15} (reverberation time based extrapolation based on the rate of decay for the first 15 dB) for the A B Wood Tank at 6 kHz is 240 ms.

4.1.6 Receiver

A single hydrophone was used to receive TWIPS data; a Blacknor Technology D140, serial number 18938. That transducer was last calibrated by the National Physical Laboratory at Wraysbury Acoustic Laboratory on 30 June 2006. The results of that calibration are available on file at ISVR, and are summarised below in Figure 4.16. During experiments, the transducer was powered by a matched amplifier which was designed and built by Blacknor Technologies.

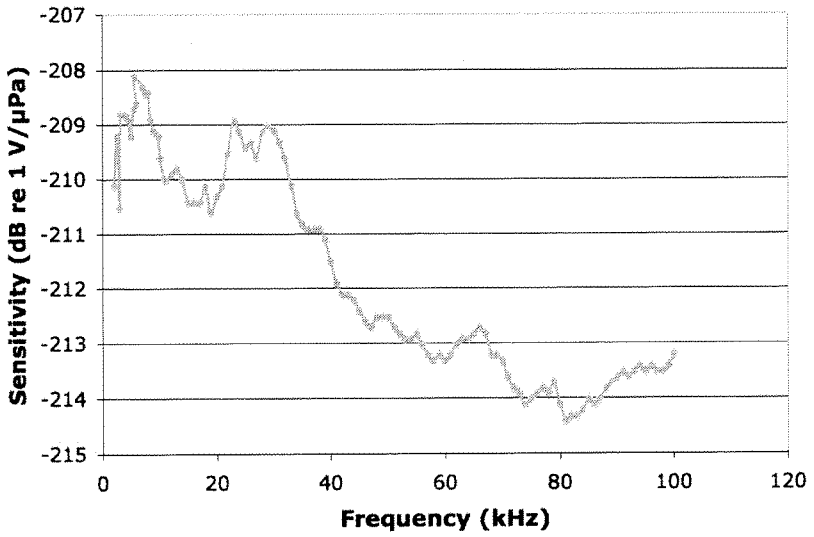

Figure 4.16 Calibration data for the Blacknor Technology D140 hydrophone/preamplifer used in experiments. In summary, the frequency response of the hydrophone/preamplifier was has flat to within +/-3.5 dB throughout the frequency range of interest.

4.1.7 Target

The target used in these experiments is shown below in Figure 4.17. The target was a steel disc of diameter 415 mm and thickness 50 mm. Its calculated target strength (see (2.31)) is -10 dB for a target/receiver along an axis extending normal to the face of the disc (that is, along an axis extending out of the page according to the orientation shown

in the figure below).

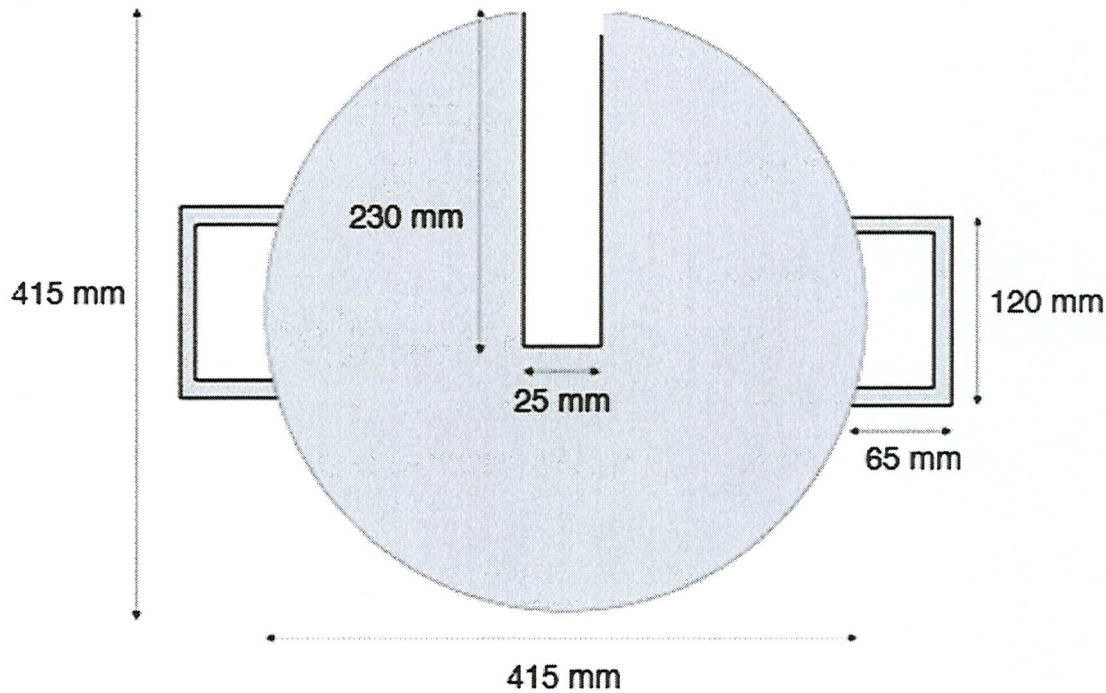

Figure 4.17 - The target used for TWIPS tests was a steel weight having the dimensions shown within the figure.

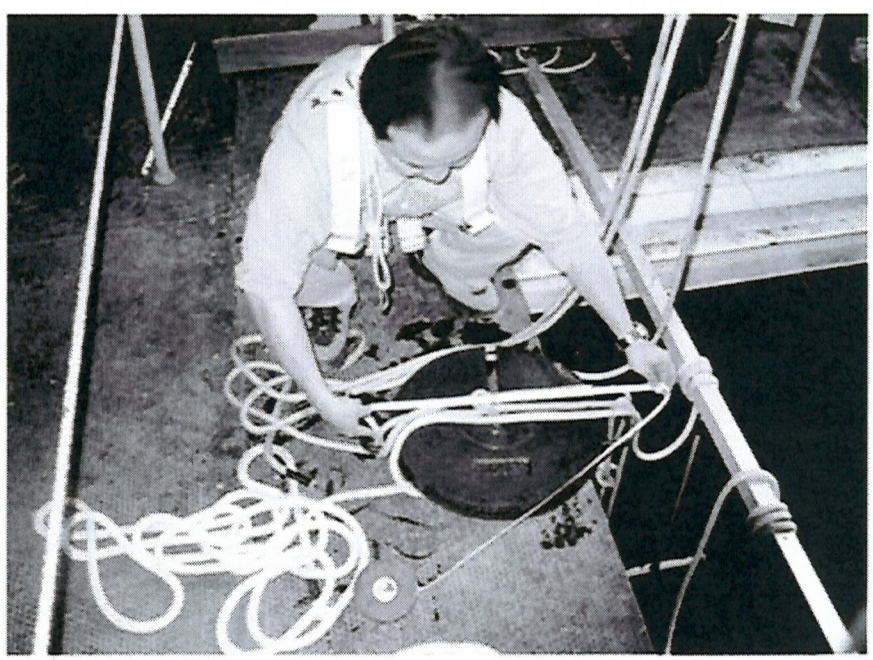

Figure 4.18 - Mr G T Yim of the Institute of Sound and Vibration Research assists by measuring primary dimensions of the target.

4.1.8 Data acquisition

Data was acquired onto a PC using a 4-channel National Instruments sound card acquiring data at 200 kilosamples per second per channel. One channel acquired a trigger signal from the trigger box, and the other two channels were set to acquire acoustic data. During TWIPS tests, only one acoustic acquisition channel was used. Acoustic signals were passed through a pair of Krohn-Hite model 3203 filter-banks. The high-pass was set at 0.2 kHz to eliminate mains contamination, and the low-pass was set at 100 kHz to avoid any frequency-folding effects.

4.1.8.1 Standard processing

As discussed in the introductory chapter, the commercially viable solutions for the detection of solid objects in bubbly water do not currently exist. It is therefore difficult to establish a baseline for the TWIPS measurements. A true baseline would probably involve the use of high frequency scanning sonar - but a scanning towfish was not available to our research group during the course of the experiments; and it is well-known that such systems are effectively blinded by bubble clouds [23] as explained in section 2.1. As such, a baseline was invented which would detect targets in bubble-free water, but would not take advantage of bubble dynamics (especially bubble cloud evolution and nonlinear oscillations) and in turn would most likely be confounded by the presence of a bubble cloud. The baseline technique, here-to-fore referred to as 'standard processing', relies on

the same data as the TWIPS technique, the difference being entirely in the processing. In summary, what is referred to here as standard processing is not necessarily the industry-standard problem solution, but is a laboratory-contrived attempt at establishing a performance baseline.

The standard processing technique involves three steps: matched-pulse filtering, signal smoothing, and finally averaging of two pulses. As the TWIPS approach takes advantage of the acoustic return from two pulses, it would be unfair to compare that output with the performance of a sonar system which only takes into account only a single pulse. Convolution, used to facilitate matched-pulse filtering and signal smoothing, is a linear process [40]. A 1 second delay always existed between any two input pulses used for the standard processing.

4.1.8.2 TWIPS

The TWIPS processing can be described in the following manner: First, P_+ and P_- are convolved with the 'matched pulse', a signal which is identical to the signal sent by the bottle to the transducers. There is a potential for error here caused by the distortion to the signal by the transduction process. However, the experiments reported here did not account for that factor, as highly variable loading was encountered by the transducer throughout testing (as a result of both changes in configuration and the presence of bubbles), and

accounting for the change in loading in each condition would have been prohibitively cumbersome. After convolving with the matched pulse to enhance regions in the time history which appear to resemble the output pulse, smoothing is accomplished by taking the absolute value of the Hilbert transform of the matched-processed signal, and convolving it with the envelope of the output (a Gaussian pulse with a length equal to that of the input signal).

4.1.8.3 Procedural comments

Measurements were performed in a variety of configurations. Those configurations were formed by varying the following variables in the ways described here:

Target presence. All measurements were performed with the target both in and out of the water. "Target in" measurements and their respective "Target out" measurements were never performed at intervals greater than 10 minutes. This was done to maximise the similarity in bubble cloud conditions for the two data sets.

Target position. The range from the source[19] to the target was altered by moving the target within the tank, both laterally and vertically.

---

[19] The source was never moved during the course of experiments.

Bubble cloud void fraction. Limited control of the bubble cloud void fraction was exercised via the valve controlling air flow from the air compressor into the pressurisation tank (see Figure 3.8). This control, while useful and effective, was not calibrated, and is sensitive to external variables such as air tank pressure, water level in the mixing tank, and flow rate through the cavitation nozzle. In some instances, an exceedingly high void fraction made it impossible to measure the bubble size distribution (the presence of excess bubbles increased attenuation to the point where no signal was available on the hydrophone furthest from the source).

To reduce the void fraction, the valve was constricted, and the test operator would wait until he had visually confirmed increased visibility within the mixing tank. If the observation had been made twice within 5 minutes, and a significant difference in visibility was not apparent, then the operator would accept the bubble cloud as being at pseudo-steady state.

4.1.9 Experimental accommodation of bubble measuring equipment

The system used for bubble size distribution (BSD) measurements was introduced in the previous chapter. Those measurements were made concurrently with TWIPS experiments in order to facilitate a clear

understanding of the bubble clouds in which the sonar was being tested. Here is described the method which was developed to minimise the interference presented by that system to the TWIPS system.

The BSD equipment was described as consisting of a driver, three hydrophones, and an electronic housing. The housing and driver were large enough to be detectable by the 6 kHz TWIPS signal, but were suspended at across the tank from and out of the main beampattern of the TWIPS transducer to minimise their visibility. The equipment needed to suspend the BSD hydrophones within the bubble cloud and capable of ensuring their stability within the high currents within that environment was too large and massive to obscure acoustically. Therefore it was decided that the BSD hydrophone array would be manually lowered into and raised out of the test tank each time a bubble size distribution measurement was desired. This system changeover was performed intermittently during tests as described within the body of the results section of this chapter.

4.2 Results

In this section, the output of the TWIPS algorithm will be compared to that of the so-called "standard" sonar. A short section explaining the way in which the data will be displayed precedes the reporting of that data.

To display the results of our testing, time histories are stacked and displayed using colour intensity to communicate amplitude. This process is shown in Figure 4.19. In the TWIPS experiments, a static target was used. This means a successful sonar system should show a vertical line (corresponding to the strong acoustic return from the target) when several time histories are stacked and viewed as an image.

Results are then processed according the "Receiver-operating characteristic" method described in detail in Appendix 1. The ROC curve is then studied for those properties which are advantageous to a sonar which would be employed in a littoral hidden-ordnance search.

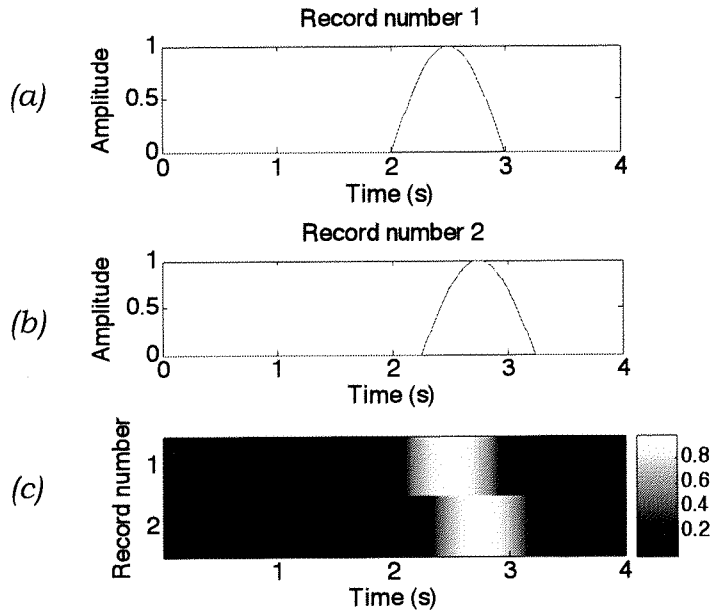

Figure 4.19 An example showing an image *(c)* to describe the time histories

shown in *(a)* and *(b)*.

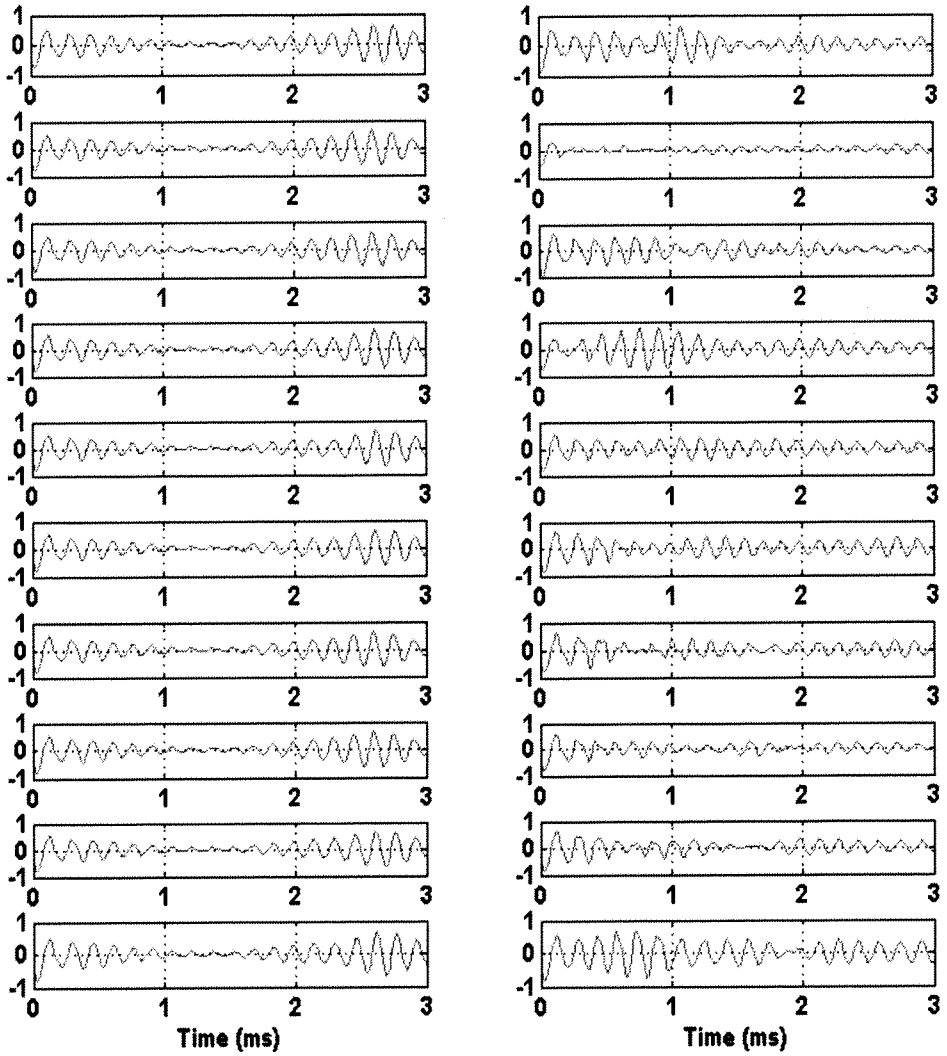

Figure 4.20. The effect of bubble scattering on target detectability. On the left are shown 10 echolocation traces taken in the A.B. Wood tank in the absence of bubbles. The target is clearly visible as a high amplitude region between 2.5 and 3 ms. On the right are shown 10 traces in the presence of bubbles. The bubbles, which are located between 0 and 3 ms, render the target invisible, and the time traces are highly inconsistent. The vertical axis in each case is a nondimensionalised pressure axis.

4.2.1 Bubble contrast enhancement results

As explained when introducing the TWIPS theory, the numerator P_- functions to enhance linear target scatter while suppressing nonlinear

target scatter. The denominator, P_+ does the converse. Therefore, it is instructive to examine the output of P_+ before examining the combined results of P_-/P_+^2.

The output of P_+ may prove to be critical for commercial applications of twin-inverted pulse sonar. In Chapter 2, the TWIPS method for detecting solid objects in bubble clouds was arrived at by first considering the pulse inversion method (used to highlight biomedical contrast agents in bloodflows), and then reversing that method and adapting it for the oceanic counter-analogy. However, the ability to detect of bubbles in the open water is a matter of potential interest to researchers in both environmental science [119] and defence technology [126].

To show the effect of reverberation interference on TWIPS results, the TWIPS experiment was repeated using the three different intervals used in Figure 9: 20 ms, 50 ms, and 100 ms. It was attempted to maintain a constant bubble cloud during these experiments. As explained above, TWIPS functions as a result of the successful performance of two tasks: target highlighting and bubble-scattering suppression in the numerator (via P_-), and bubble scattering enhancement in the denominator (via P_+). Reported here is the effectiveness of P_+, and the degree to which that effectiveness varies with the inter-pulse time.

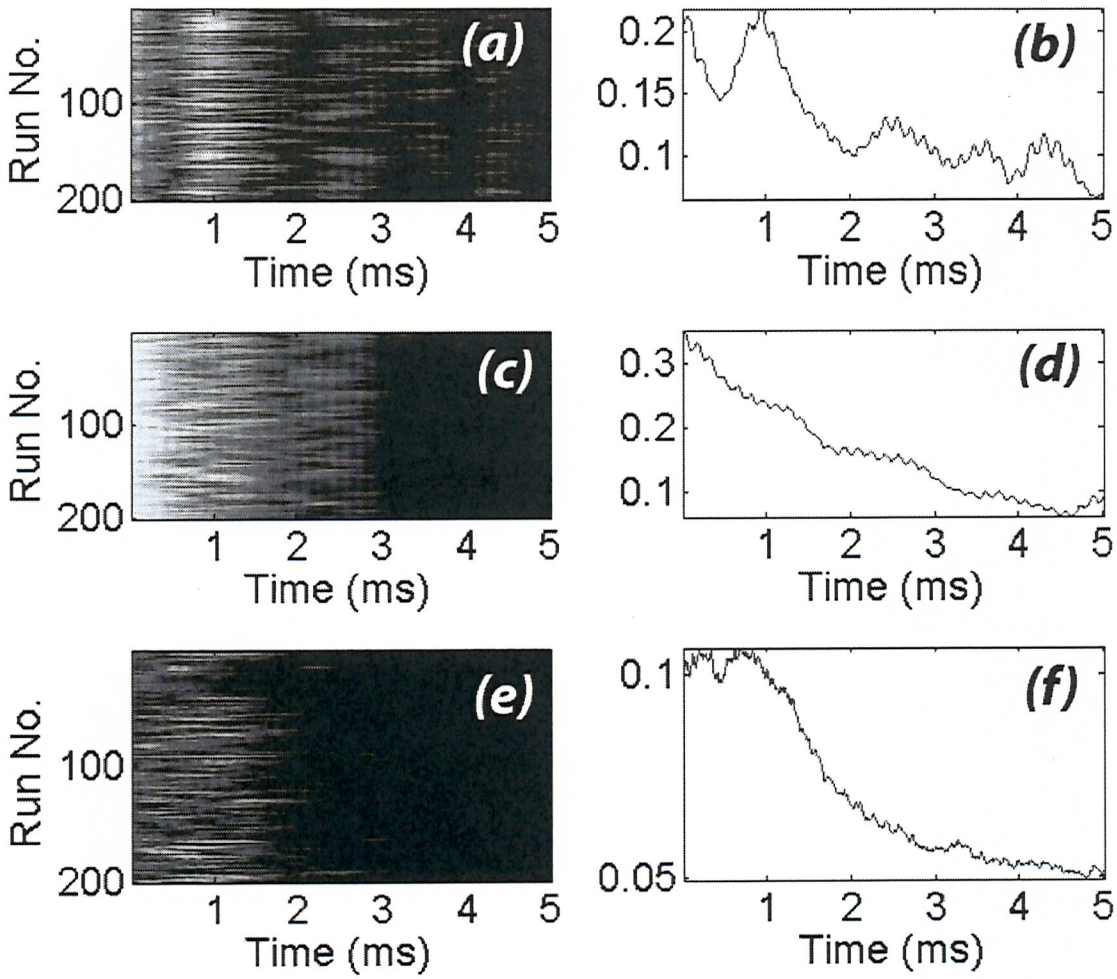

Figure 4.21. The effectivness of P_+ (bubble contrast enhancement) with varying interpulse times. The bubble cloud is located between 0 and 2 ms, and the target is between 2 and 3 ms.
***(a)* Intensity plot, P_+ for 200 pulse pairs; τ =20 ms *(b)* the median of all pulse pairs; τ =20 ms**
***(c)* Intensity plot, P_+ for 200 pulse pairs; τ =50 ms *(d)* the median of all pulse pairs; τ =50 ms**
***(e)* Intensity plot, P_+ for 200 pulse pairs; τ =100 ms *(f)* the median of all pulse pairs; τ =100 ms**

In Figure 4.21, the output of P_+ has been shown for varying interpulse times, τ. The only digital filtering applied to the signal in post-processing was a high-pass filter used to eliminate DC offset and some 50 Hz leakage. When τ is insufficiently short, reverberation from the first pulse affects the return from the second pulse. Figure 4.21 *(a)* and *(b)* show that this interference makes it difficult for P_+ to

distinguish between linear and nonlinear scatterers for τ=20 ms. As a result, while there is the desired broad peak indicating a bubble cloud between 0 and 2 ms, there is an undesired peak in the target location between 2 and 3 ms. Figure 4.21 *(c)* and *(d)* show that τ=50 ms functions much better as a bubble-cloud enhancer, but the gradual negative gradient from 0 ms to 3 ms is insufficiently resolute to show clearly where the bubble cloud lies. This gradual gradient presumably results from the fact that, while that τ =50 ms allows the algorithm to enhance the bubble scatter, the target signal suppression is incomplete. Figure 4.21 *(e)* and *(f)* show τ =100 ms to offer superior results. Figure 4.21 *(e)* shows consistent bubble cloud scatter enhancement, and it is clear from Figure 4.21 *(f)* that the target scatter has been virtually completely suppressed. It must be emphasised that these results should theoretically indicate the types of problems that one might encounter when using TWIPS. However, the ideal interpulse interval τ will vary from location to location, as dictated by the mean bubble speed and reverberation conditions encountered during a particular trial.

It has been shown that P_+ is capable of consistently enhancing bubble-scatter on the basis of nonlinear-scattering. An alternative nonlinear bubble-scatter enhancement method used extensively in biomedical ultrasonics is known as second-harmonic imaging. That method also requires the use of high-amplitude signals in a nonlinearly scattering environment, but requires only a single ping.

The return from that single ping is then band-pass filtered for second-harmonic energy to show the location of non-linear scatterers. The data used to generate Figure 4.21 *(a)* was reprocessed to study the effectiveness of second-harmonic techniques in a pseudo-oceanic environment. The results of this study are shown in Figure 4.22.

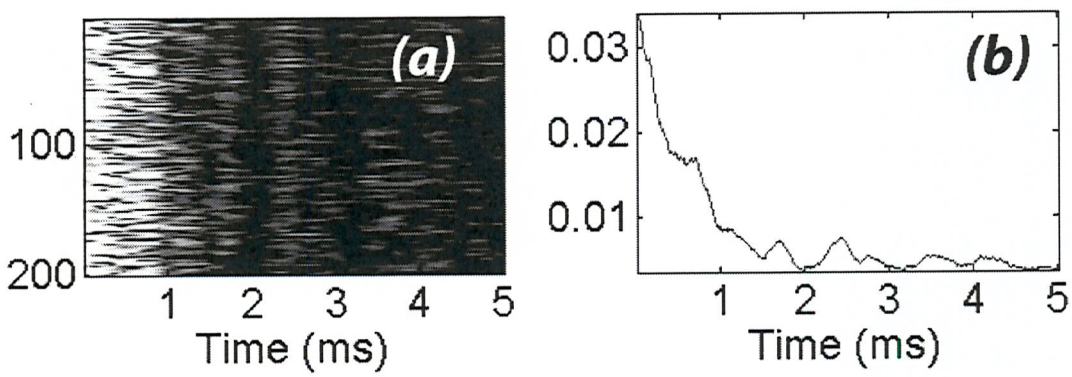

Figure 4.22. Second-harmonic imaging of a bubble cloud in the A B Wood Tank. Created using the same data that was used to generate Figure 4.21 (*a*). The bubble cloud is located between 0 and 2 ms, and the target is located between 2 and 3 ms; *(a)* An intensity plot for 2 pulse-pairs. *(b)* Median of the 200 pings.

The second-harmonic technique results shown in Figure 4.22 demonstrate that this technique is effective at suppressing the target scatter, but offers insufficient bubble-cloud enhancement. Observations during the experiment showed that the bubble cloud was located not just between 0 and 1 ms as suggested by Figure 4.22, but between 0 and 2 ms (a fact testified to by the results shown in Figure 4.21 *(e)* and *(f)*).

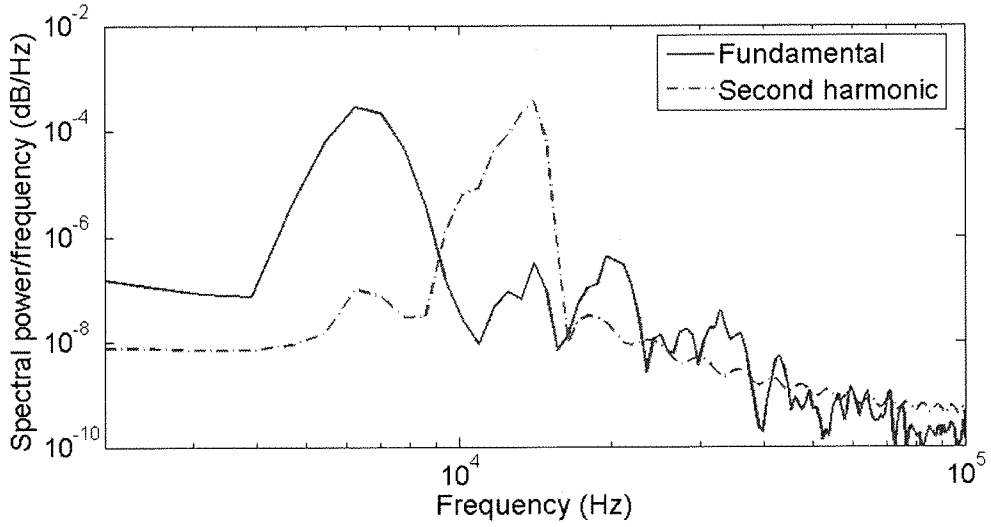

Figure 4.23. Harmonic content from line 1 of Figure 4.22, both unfiltered ('Fundamental') and filtered for the second harmonic ('Second harmonic'). This result shows the smearing encountered when using this approach. Information from the band corresponding to the fundamental frequency has 'leaked' into the second harmonic data. Narrow band-pass filters can be used to overcome this, with the side effect being that fewer bubbles will be detected. Note that the portion of the time record corresponding to the outgoing pulse has been time-gated out.

The cloud visibility obtained using the second-harmonic technique is limited when compared to the TWIPS output; this is a result of bandwidth considerations. Recall that no frequency filters were used to enhance bubble scatter in TWIPS. This means that any anti-phase information present in the second pulse return, regardless of frequency, will give contrast enhancement when inverted and combined with the return from the first pulse. The second-harmonic technique, however, can only give contrast enhancement when the bubble scatter is within the frequency constraints of the band-pass filter. As the output signal is limited in length (8 cycles at 6.5 kHz), the outgoing pulse is broad in frequency content. While those bubbles closest to the acoustic driver will tend to be very active at twice the rate of the centre frequency, the remainder of the cloud will tend to be

only weakly nonlinear as a result of attenuation, and may be relatively inactive within the limits of the filter. Therefore, limiting the bandwidth of the detector will limit the number of bubbles which can be perceived. The harmonic content of the first line of Figure 4.22 has been shown in Figure 4.23. This figure shows that it is difficult to filter effectively for the second harmonic using the driving pulse created for this experiment. Information from the band corresponding to the fundamental frequency has 'leaked' into the second harmonic data. Narrow band-pass filters can be used to overcome this, with the side effect being that even fewer bubbles will be detected.

Bubble detection and contrast enhancement has applications within both the biomedical ultrasound and oceanic sonar arenas. The ultrasound contrast agent (UCA) market is already well-developed, and accumulated revenues of just under $1 billion in 2006 [132]. That market, however, stands to benefit from advances in research as revenues in UCAs are expected to grow by 25-40% per year through 2010 [132]. By contrast, there is no record in the literature of a purely bubble-detecting oceanic sonar: one which is capable of highlighting only bubbles while suppressing reflections from linear scatterers such as the surface, the bottom, boats, mines, and pipes. Nonetheless, such a sonar could find application in environmental studies and underwater resource exploration, as will be discussed later in this chapter. Further, if bubbles are considered more generally as nonlinear scatterers, then it can be argued that a method

which is capable of revealing the presence of bubbles within an environment using acoustics might be applied to other types of radiation to reveal the presence of nonlinear scatterers in various media. Thus, TWIPS derivatives might find use in lidar, radar, and laser applications.

4.2.2 Target contrast enhancement

Having established that the TWIPS denominator is able to suppress bubble scatter, we now demonstrate that TWIPS2a can exploit this capability to perform target contrast enhancement. Presented here are the results of several tests along with their corresponding ROC analyses.

4.2.2.1 Results in the absence of bubbles

The first scenario presented here is that with and without the target present, but with no bubbles in the water (Figure 4.24 through Figure 4.27). Since the environmental conditions in that case were steady-state, the output is relatively constant, and only a few ping pairs were measured. To process the data in the ROC curve, the maximum value between 5 ms and 6.25 ms has been extracted for each block of 5 pings. This has been done instead of extracting the maximum for each individual pulse pair, as TWIPS output tends to be intermittent. The use of blocks made up of several pulse pair returns improves the system performance, but reduces the number of points available for the ROC curve (which is why the performance curves presented in this section are not smooth). In real-world applications, the use of such

blocks is somewhat disadvantageous, as the ability for the system to cope with dynamic physics is limited by the amount of time required for the acquisition of a single data block. In the tests presented here, 5 blocks of data corresponds to an elapsed period of between 5.02 and 5.10 s (dependent upon the length of the interpulse delay). Note that this does not mean that the algorithm will fail if the bubble cloud evolves during the acquisition of a data block, but that performance will suffer if the overall system geometry is changed during that time (that is if the relative position of the sources/acquisition devices and reflection surfaces are altered).

In the first scenario analysed here, the ROC is perfect (Figure 4.27); an unsurprising result, as there is a large metal target in the water located directly in front of the source and receiver, and no bubbles are present to scatter the sonar signal.

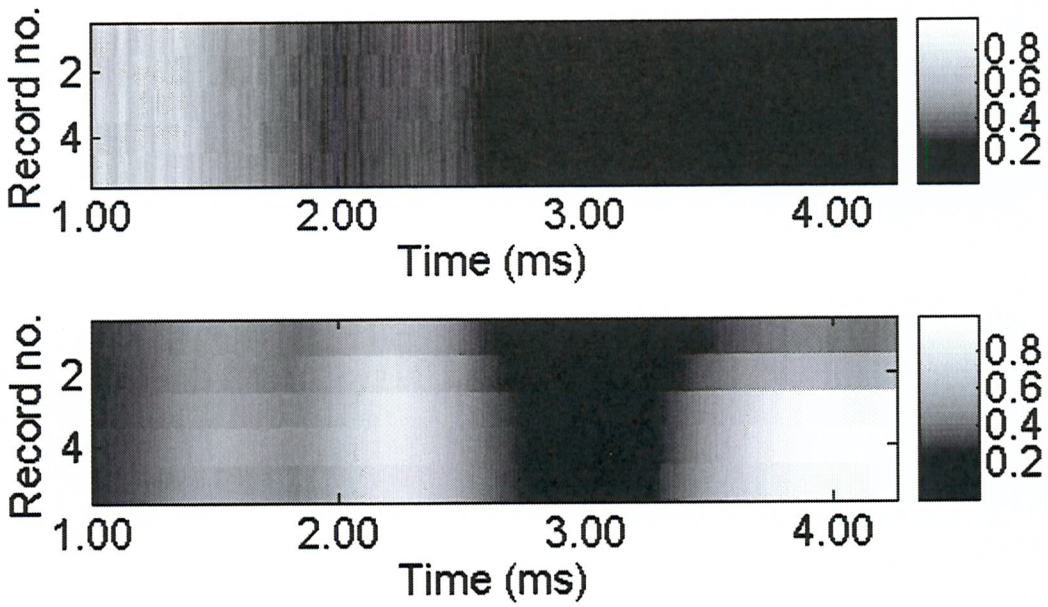

Figure 4.24 Tank data: no target present; no bubbles present. Top- Standard sonar; Bottom- P_-/P_+^2. Time-varying gain has been applied to the time history data before processing.

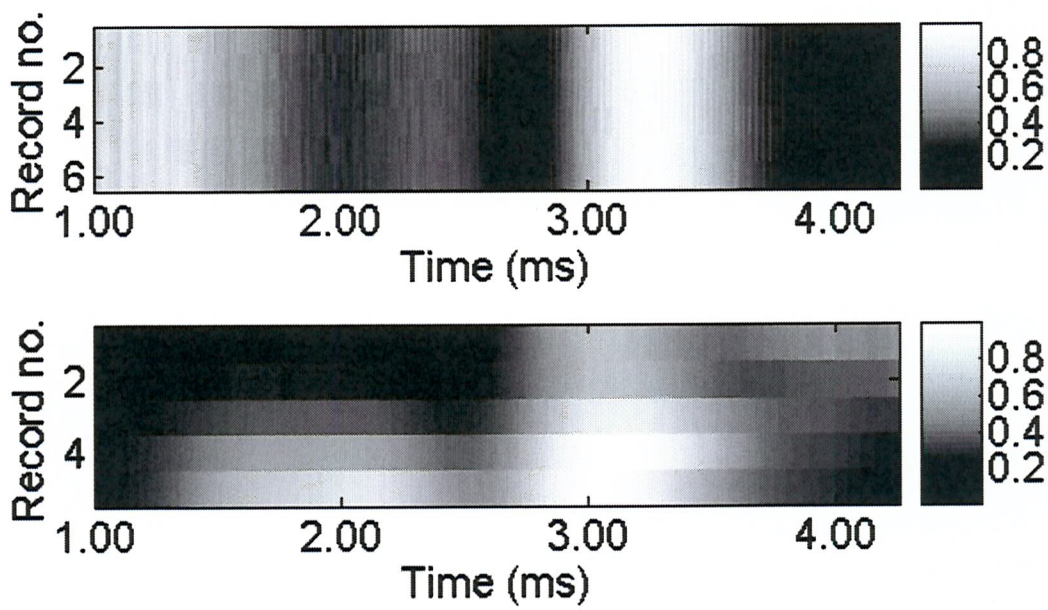

Figure 4.25 Tank data: target present between 3 and 3.5 ms; no bubbles present. Top- Standard sonar; Bottom- $P_./P_+^2$. Time-varying gain has been applied to the time history data before processing.

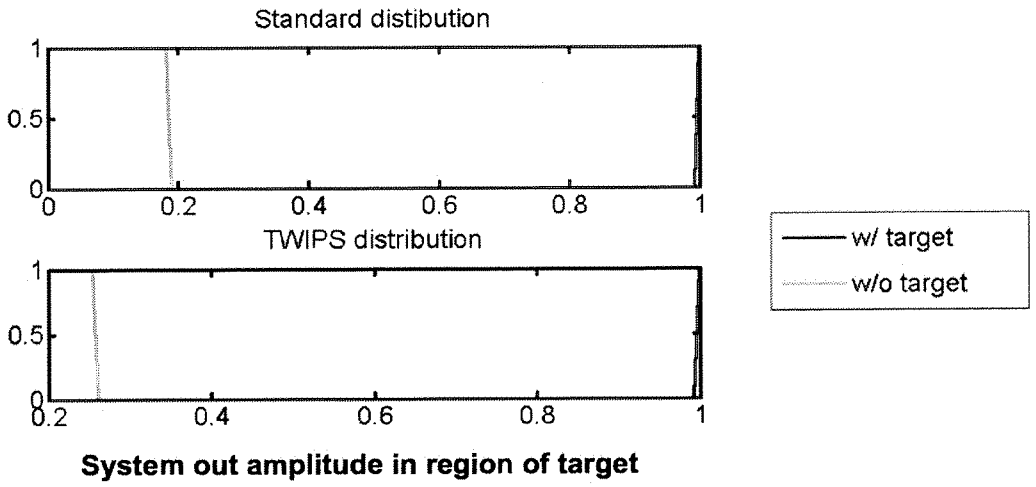

Figure 4.26 Amplitude distribution for the time window corresponding to the target location shown in Figure 4.25.

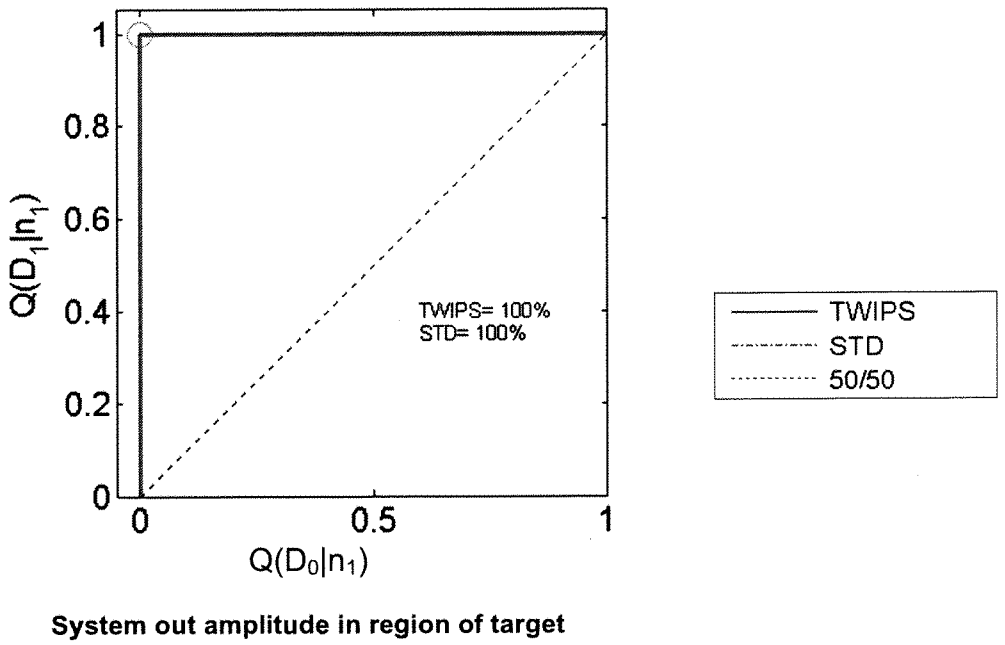

Figure 4.27 ROC analysis for data collected in the absence of bubbles, as shown in Figure 4.24 and Figure 4.25.

In the next experiment which is presented, bubbles were released into the water from a location nearly directly below the target. This allowed measurement of the degree to which TWIPS enhances target

detection in the presence of a bubble cloud.

4.2.2.2 Results in the presence of bubbles with targets of varying target strength

Here, the results of two experiments are contrasted wherein the target strength has been varied whilst the bubble size distribution and source/receiver-target distance have remained constant. In the two scenarios analysed here, the bubble cloud is located with its centre almost 1 meter in front of the target. The cloud extends only 0.75 meters in either direction along the acoustic axis. Therefore, there is a small transition zone from bubbly to bubble-free water in the region between the centre of the cloud and the location of the target. This configuration simulates the condition where an oceanic bubble cloud is not co-located with a target. Such a condition might be encountered when echosounding behind in the wake behind a ship, or when searching for an object in stormy waters where the depth is great enough that the void fraction approaches zero near the bottom.

In the geometry used to develop figures through Figure 4.29 - Figure 4.34, the target response occurs just after 3 ms, while the bubbly region extends from about 1 ms to about 3 ms (see Figure 4.28). As a result, the sound intensity of the field is greater in the bubble cloud than at the target location. If this effect were not corrected for, there would be an inherent energy bias favouring false positives (the bubble cloud) and it would be difficult to construct a fair ROC. To correct for

this effect in data analysis, a quadratic time-varying gain (TVG) has been applied directly to the time-history data prior to post-processing and to the production of ROCS. In the theoretical discussion of TWIPS2, see section 2.5.1.1, it was argued that an advantage to this particular algorithm is that TVG is not needed, as any time-bias in the denominator should be identical to (and therefore cancelled by) any time-bias in the numerator. Here, however, TWIPS2 has been forgone for a modified version of TWIPS2 which uses the output of P_-/P_+^2. In that algorithm, time-biases are no longer identical in the numerator and the denominator. As a result, TVG has now become necessary and has been introduced directly to the time history prior to post-processing. The use of a time-varying gain has been mentioned in the figure captions wherever appropriate. The ROC curves for these two scenarios have been processed by searching for the maximum value returned by either algorithm of each processed return within the region extending from 1 to 4 ms. In Figure 4.29 and Figure 4.31, the target is not in the water. In the standard sonar, bubble scattering is visible in the region from 1.00 to 3.00 ms. This has been illustrated using a plot of P_+, which has been shown to exhibit maxima at the location of bubble clouds (see section 4.2.1).

In Figure 4.29 – Figure 4.34, it is shown that the bubble scattering is mostly suppressed in the TWIPS output, as evidenced by the lack of small-scale ripples in the temporal region corresponding to their location (1 ms – 3 ms). In Figure 4.30 and Figure 4.32, the bubble

distribution has been maintained as nearly that used for Figure 4.29 and Figure 4.31, but the target has been introduced and is clearly visible within both sonars centred near 3.50 ms. This measurement in that it proves that TWIPS is useful not only when standard correlation methods fail, a result confirmed by the ROC curves shown below in Figure 4.34.

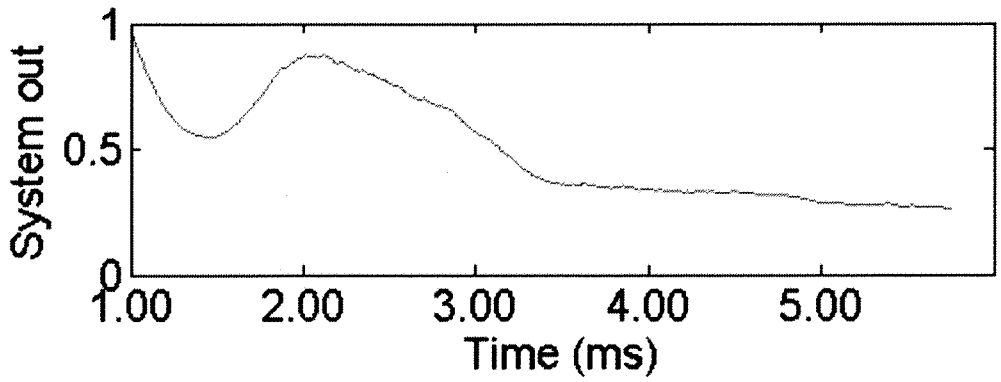

Figure 4.28 Median of P_+ for all data in Figure 4.29 - Figure 4.32. In the region before 1.50 ms, the data indicates even-harmonic nonlinear distoration in the outgoing pulse. This is result (clipping in the outgoing pulse) is not unexpected. The hydrophone was placed near to the source, where levels exceeded those which could be measured accurately using the equipment available for this experiment.

The bubble size distribution of the cloud present during TS=-10 dB measurements is shown in Figure 4.42.

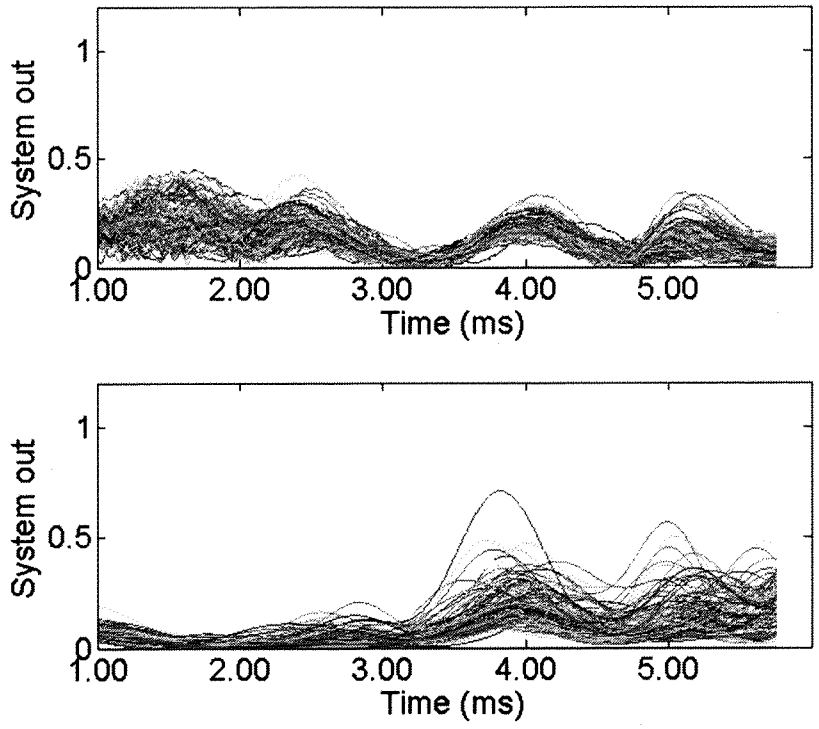

Figure 4.29 No target present; bubbles present from 1 ms to 3 ms. Top- Standard sonar; Bottom- a version of TWIPS2b (P_-/P_+^2). Time-varying gain has been applied to the time history data before processing. This plot displays 100 records captured at 1 second intervals.

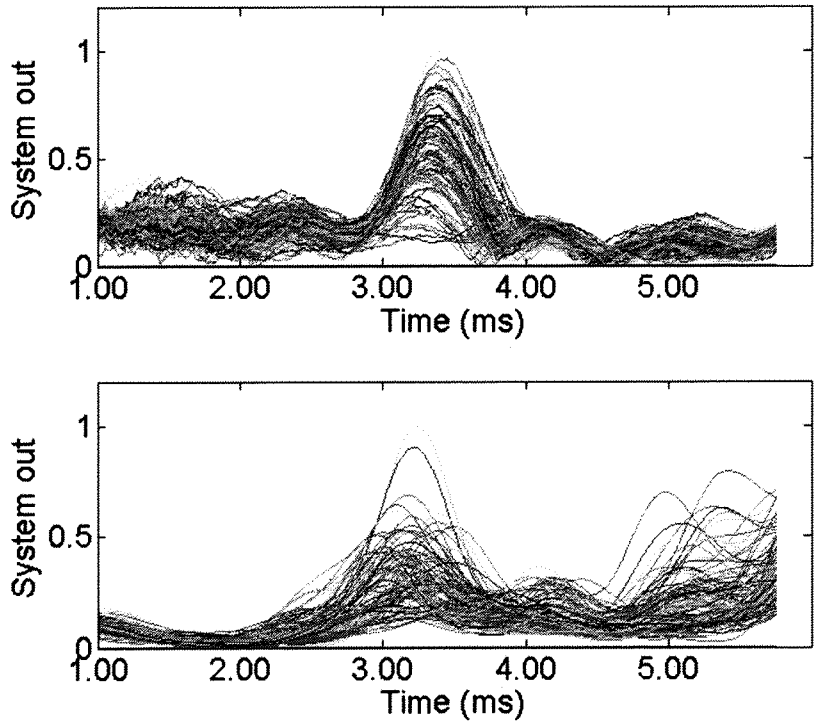

Figure 4.30 Target present between 3 and 4 ms; bubbles present from 1 ms to 3 ms. Top- Standard sonar; Bottom- a version of TWIPS2b (P_-/P_+^2). Time-varying gain has been applied to the time history data before processing. This plot displays 100 records captured at 1 second intervals.

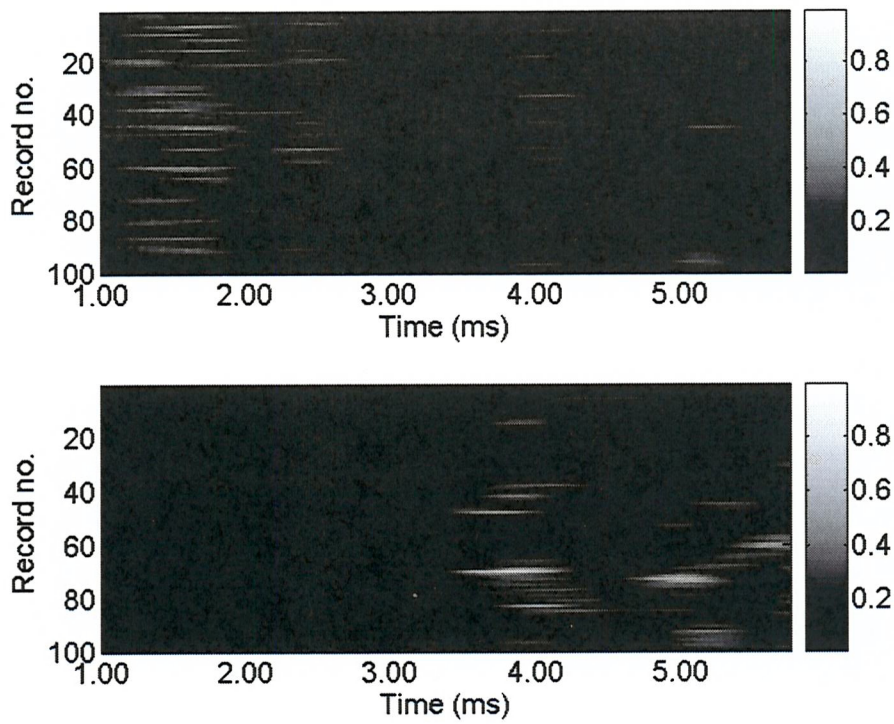

Figure 4.31 No target present; bubbles present from 1 ms to 3 ms. Top- Standard sonar; Bottom- a version of TWIPS2b ($P-/P_+^2$). (Same data as shown in Figure 4.29, but displayed as an image). Time-varying gain has been applied to the time history data before processing.

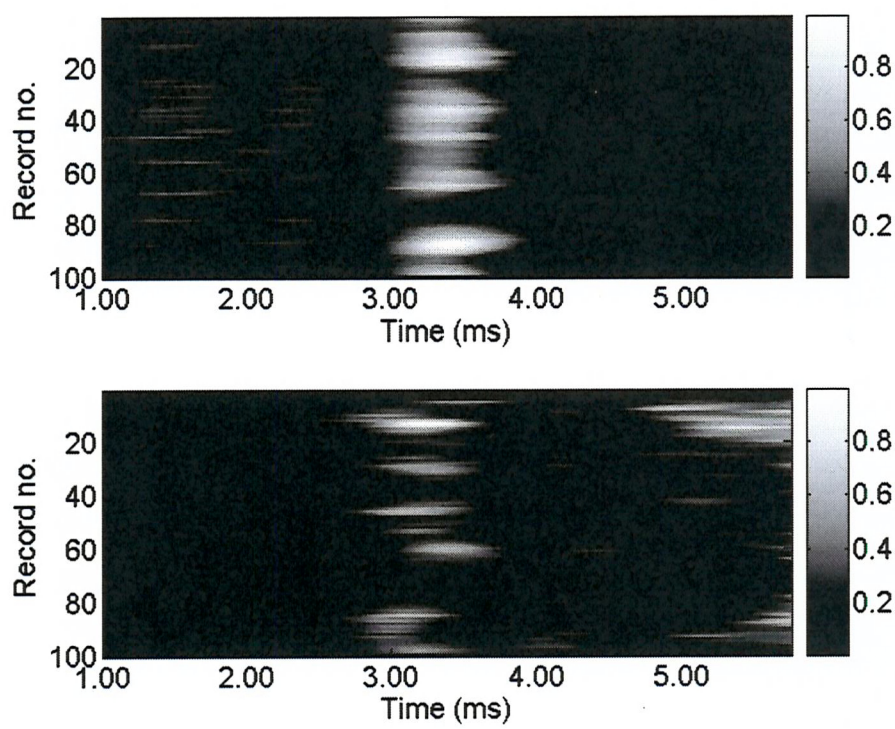

Figure 4.32 Target present between 3 and 4 ms; bubbles present from 1 ms to 3 ms. Top- Standard sonar; Bottom- a version of TWIPS2b ($P-/P_+^2$). (Same data as shown in Figure 4.30.). Time-varying gain has been applied to the time history data before processing. TS=-10 dB.

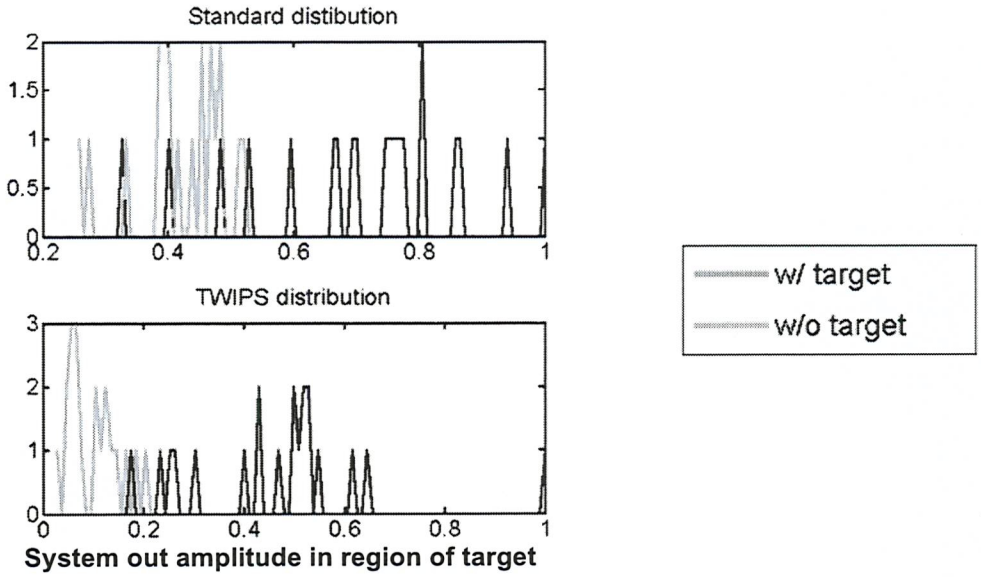

Figure 4.33 Probability distribution functions for the time window corresponding to the region containing the target (TS=-10 dB) and bubble-cloud in Figure 4.29-Figure 4.32. These are the points which have been used to construct the ROC shown in Figure 4.34.

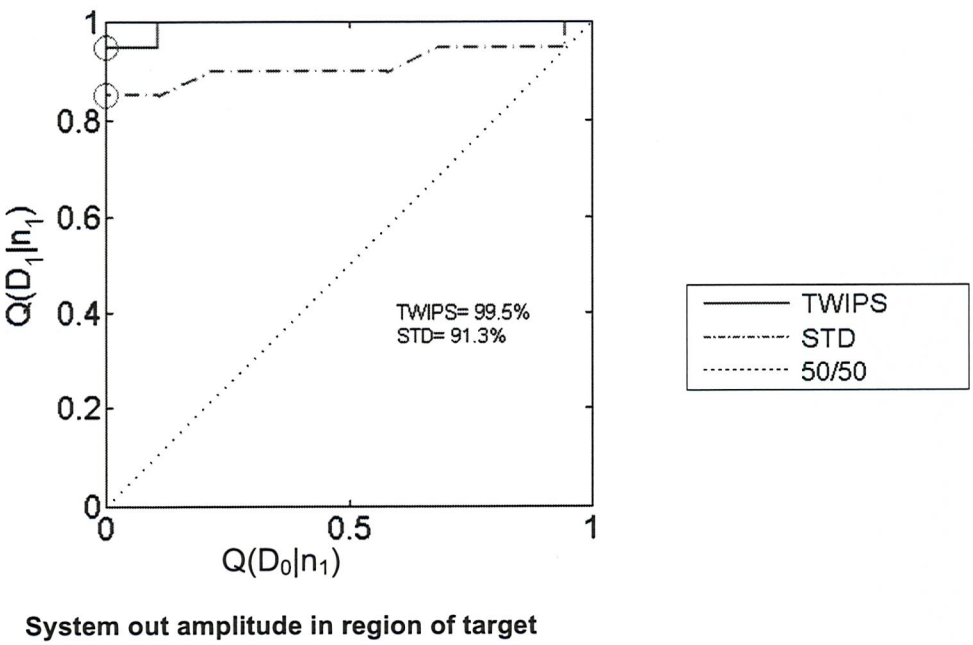

Figure 4.34 ROC for the scenario (TS=-10 dB) studied in Figure 4.29-Figure 4.32. The percent of all true positive detections which have been made by either algorithm (calculated as the area under each curve) have been shown.

The ROC curve above (Figure 4.34) shows simply that the target in this case can almost always be detected using either TWIPS or

standard sonar with very few false positives resulting; an unsurprising result given the prominent visibility of the target in Figure 4.29-Figure 4.32. However, the fact that the TWIPS statistic is vertical from 0% true detection up to ~80% true detection emphasises the following point: it is possible to operate TWIPS in a variety of conditions with a high threshold, and obtain ~50% detection without any false positives. The advantages of such a system will be discussed later in the. The next set of results presented here was obtained with the target and bubble cloud in the same location as for the above analysis (that is, for the data displayed in Figure 4.29-Figure 4.32), but the target strength was reduced by 5 dB from -10 dB to -15 dB. The two data sets, that is the TS=-10 dB and TS=-15 dB data, have each been normalised locally. Therefore, in the data presented within this chapter, a TWIPS or Standard Sonar output of "1" when TS=-10 dB is not identical in an absolute sense to the corresponding algorithm output of "1" when TS=-15 dB.

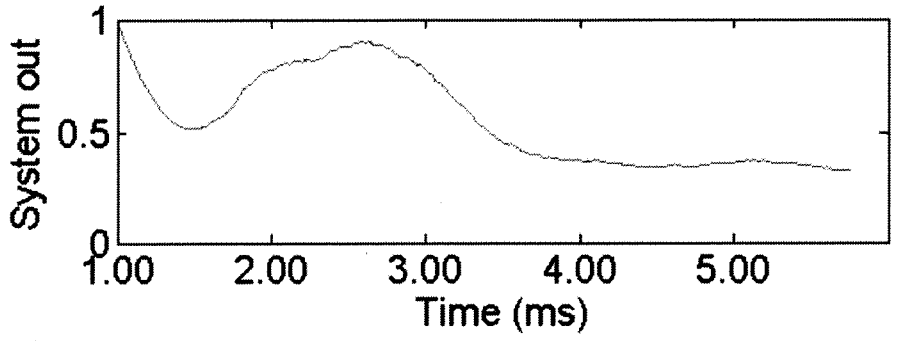

Figure 4.35 Median of P_+ for Figure 4.36-Figure 4.39 (See caption, Figure 4.28).

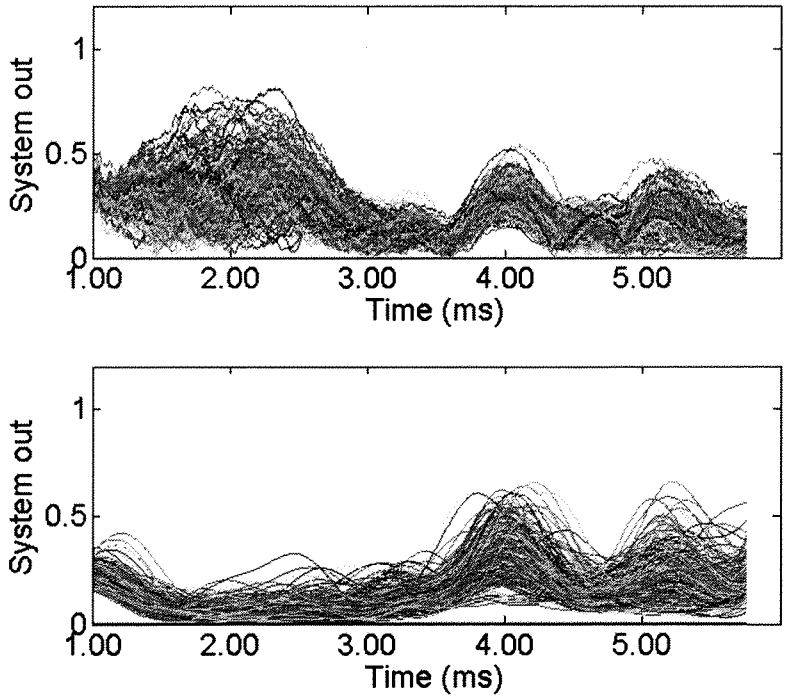

Figure 4.36 No target present; bubbles present from 1 ms to 3 ms. Top- Standard sonar; Bottom- a version of TWIPS2b (P_-/P_+^2). Time-varying gain has been applied to the time history data before processing. This plot displays 200 records captured at 1 second intervals.

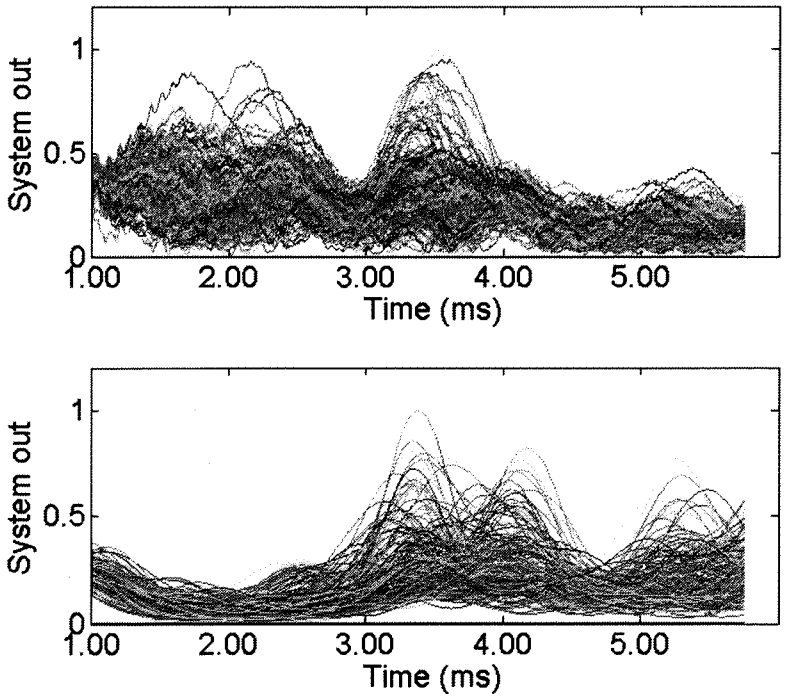

Figure 4.37 Target of TS=-15 dB present between 3 and 4 ms; bubbles present from 1 ms to 3 ms. Top- Standard sonar; Bottom- a version of TWIPS2b (P_-/P_+^2). Time-varying gain has been applied to the time history data before processing. Note the significant suppression of bubble scatter between 1 ms and 3 ms in the TWIPS output. This plot displays 200 records captured at 1 second intervals.

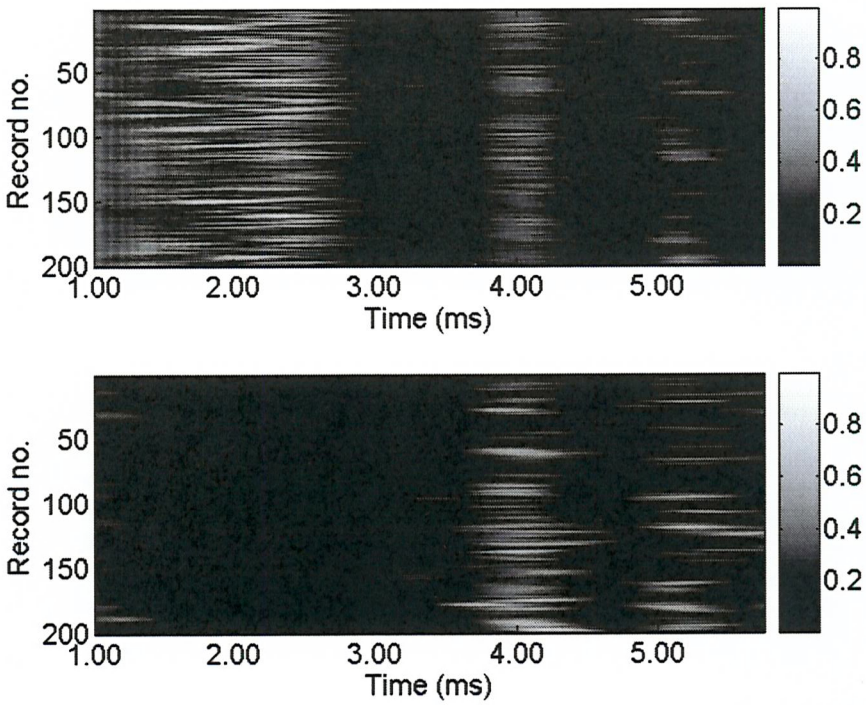

Figure 4.38 No target present; bubbles present from 1 ms to 3 ms. Top- Standard sonar; Bottom- a version of TWIPS2b ($P./P_+^2$) (Same data as shown in Figure 4.29, but displayed as an image). Time-varying gain has been applied to the time history data before processing.

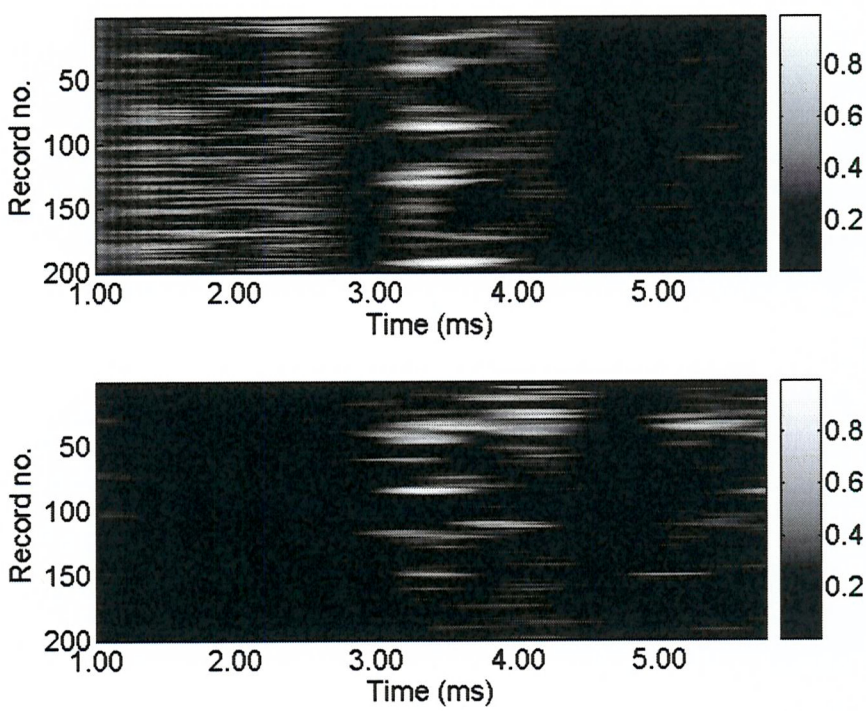

Figure 4.39 Target of TS=-15 dB present between 3 and 4 ms; bubbles present from 1 ms to 3 ms. Top- Standard sonar; Bottom- a version of TWIPS2b ($P./P_+^2$) (Same data as shown in Figure 4.30). Time-varying gain has been applied to the time history data before processing. Note the significant suppression of bubble scatter between 1 ms and 3 ms in the TWIPS output.

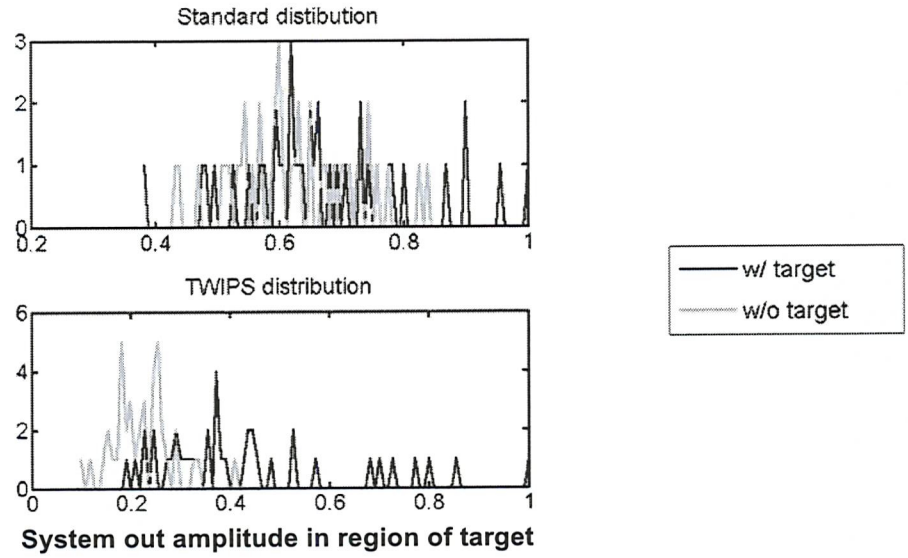

Figure 4.40 Probability distribution functions for the time window corresponding to the target location (TS=-15 dB) shown in Figure 4.25. These are the points which have been used to construct the ROC shown in Figure 4.37.

The ROC curve below (Figure 4.41) is based on the data displayed in Figure 4.36-Figure 4.39 (and summarised as probability density functions in Figure 4.40). As explained above, the tank configuration used to acquire these results is the same as that configuration used to obtain the data with the TS=-10 dB results.

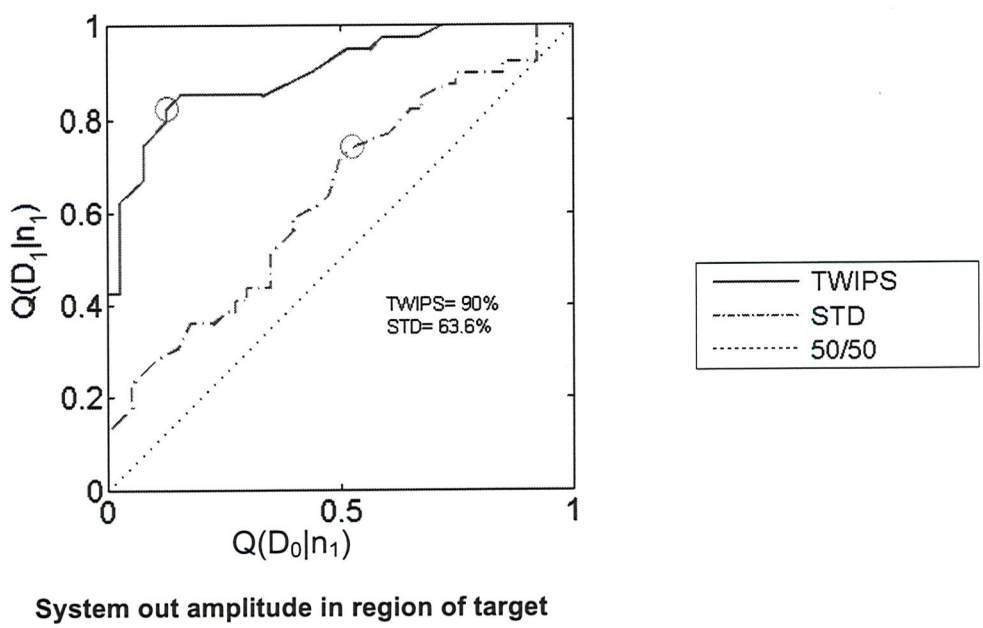

Figure 4.41 ROC for scenario studied in Figure 4.36 - Figure 4.39. TS=-15 dB.

It was stated before the presentation of the two previously shown data sets (represented by Figure 4.28 - Figure 4.41) that the only quantity varied between the two sets was target strength. As evidence of the steadiness of the bubble cloud throughout the course of these measurements (an undertaking of approximately 30 minutes), the bubble size distribution for these clouds is shown below in Figure 4.42.

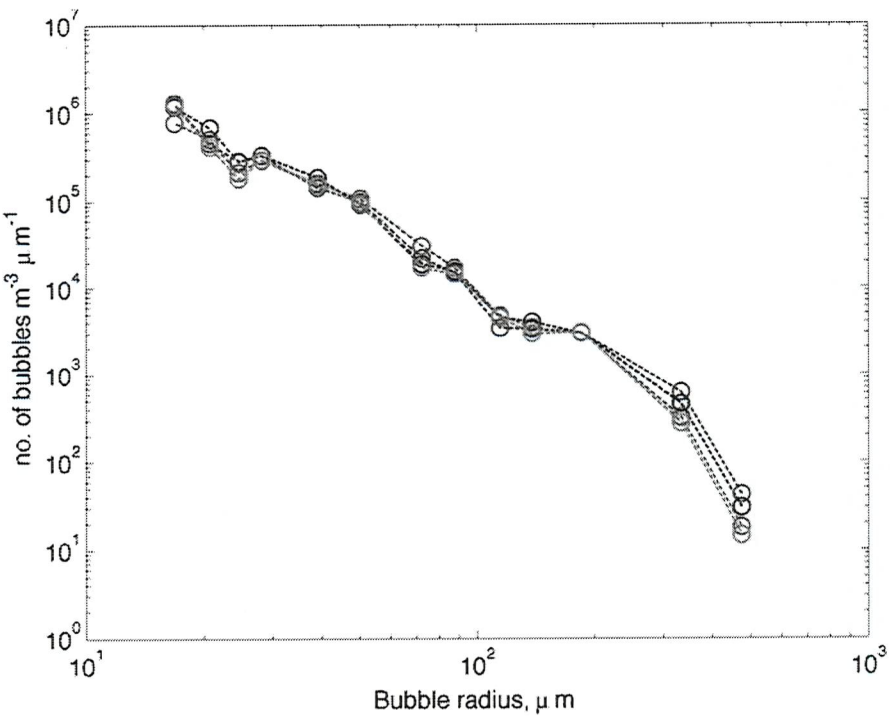

Figure 4.42 Bubble size distribution measurements for the data shown in the two previously shown data sets (Figure 4.28 - Figure 4.40)

4.2.3 Simulation reflecting experimental conditions

The simulation results which were presented in the previous chapter

were useful in that they indicated promise for the success of TWIPS. It was however not possible to recreate the conditions enforced in the simulation when operating the tank experiment. Therefore, it is informative at this point to return to the simulation and attempt to reconstruct the experiment to see if reasonable agreement between the model and the experiment can be achieved.

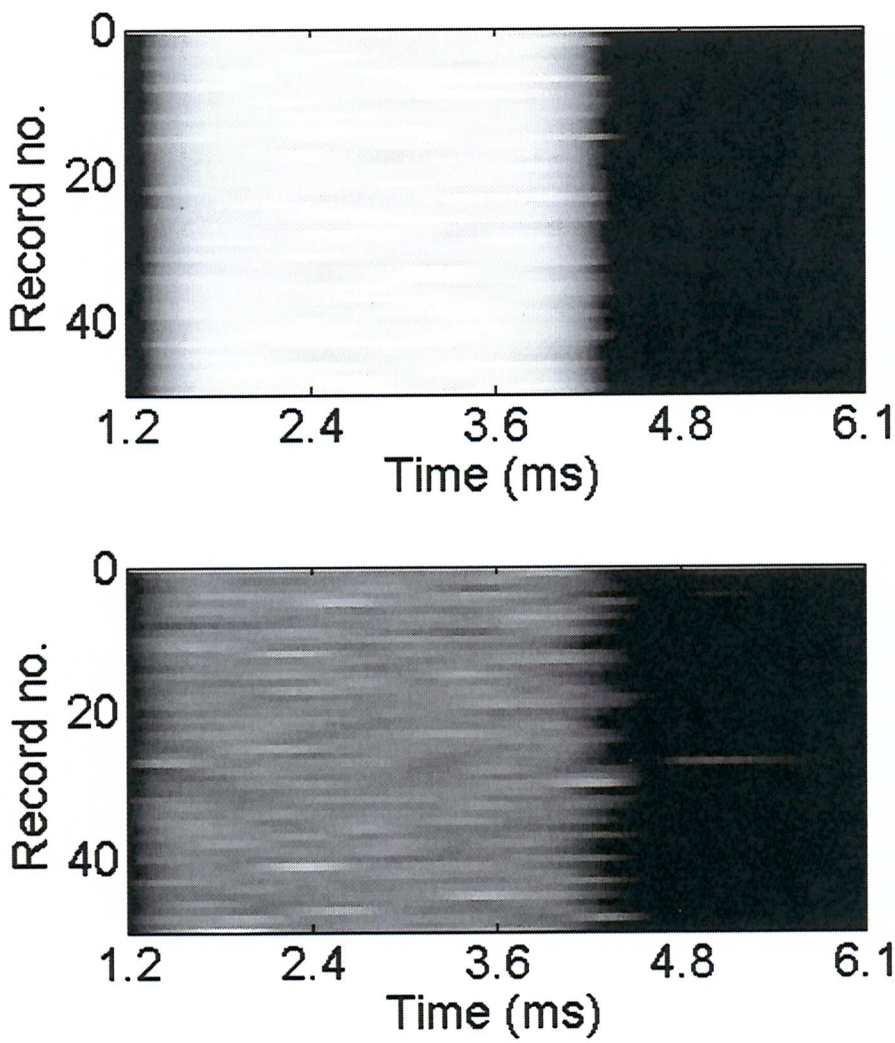

Figure 4.43 Simulated data. No target present; bubbles present from 1 ms to 3 ms. Top- Standard sonar; Bottom- a version of TWIPS2b (P_-/P_+^2). Time-varying gain has been applied to the time history data before processing.

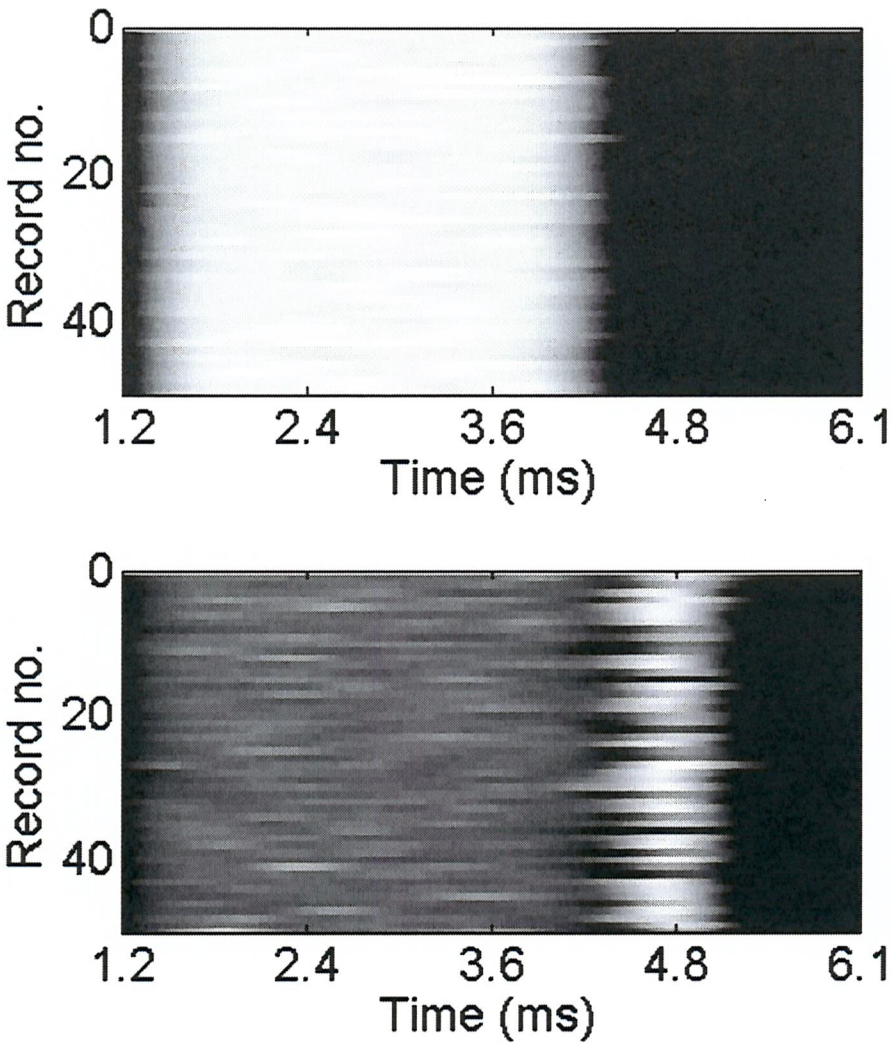

Figure 4.44 Simulated data. Target of TS=-15 dB present between 4 and 5 ms; bubbles present from 1 ms to 4 ms. Top- Standard sonar; Bottom- a version of TWIPS2b (P_-/P_+^2) Time-varying gain has been applied to the time history data before processing.

The simulated data presented here shows clear success of TWIPS over the standard sonar when detected a target located behind a bubble cloud at 6 kHz using P_-/P_+^2. The target here has a target strength of TS=-15 dB, and the input sound pressure is approximately equivalent to the sound pressure level encountered in the tank. The most substantial difference between the simulated conditions and the experimental conditions is the lack of simulated multiple-reflections. In the tank the multiple reflection pattern and its time-varying nature

caused by bubble interference is the largest source of difficulty for TWIPS. The simulation shows that a reduction in multiple reflections (as may be encountered in open-water conditions) will improve the performance of TWIPS.

4.3 Discussion

In shallow-water surveillance, false alarms can be costly. In that scenario, an alarm might require the time-consuming deployment and subsequent retrieval of assets such as divers, dolphins, or autonomous underwater vehicles (AUVs). For this reason, we seek a detection system which has the capability of performing at a very low-false alarm rate.

For the purpose of understanding the detection statistics, consider the two hypothetical detection systems described by the ROC curves shown below[20]. The overall performance of these two systems, as measured by the sum total of the area beneath each curve, is nearly identical. However, in practice, these systems will behave very differently. In the low-threshold regime, for a given number of search "pings", System A will have a higher probability of returning a true-positive detection. Nonetheless, in that same threshold regime, System A will return a significant number of false positives. If the

[20] An introduction to ROC curves appears in the appendix.

threshold is set very high, then System B will return a false positive very rarely, while System A will be virtually unusable. Therefore, given a choice between System A and B, the former is preferable the situation where the result of a false positive is some sort of expensive process, System B is more well-suited to shallow-water sonar search operations.

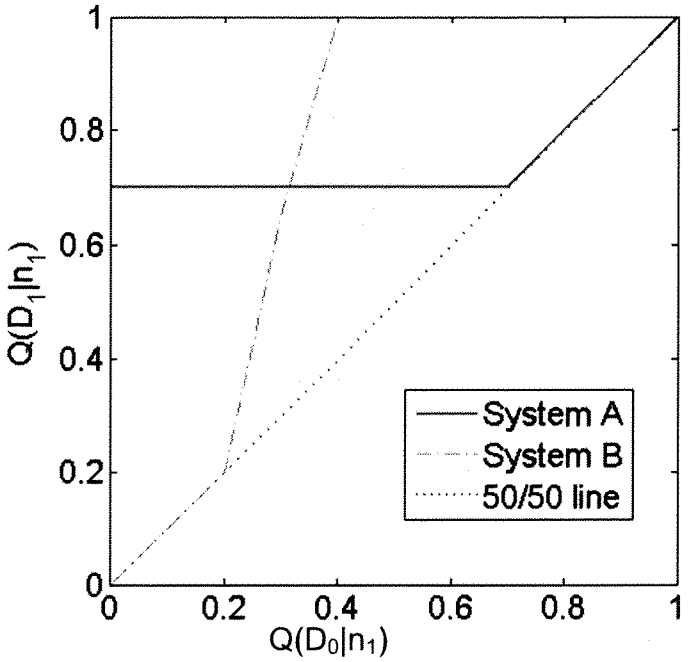

Figure 4.45 Two example ROC curves

Indeed in reviewing the TWIPS output, it is seen that the system returns spurious results, but also occasionally returns very high amplitude pulses. The results of the field studies give insight into the physical mechanism responsible for this spuriousness, and so a complete discussion of this topic is reserved for the next chapter. The result of this spuriousness, however, is that it is possible to operate TWIPS with very low false alarm rates. In the case of the ROC for the TS=-10 dB case (Figure 4.34), TWIPS achieved a 95% true-positive

rate before inaccurately reporting a false positive, while the standard sonar achieved 85%. In practical terms, the 10% difference may not indicate that TWIPS gives tremendous advantage; both systems behave in a relatively similar manner (that is, the ROCs for the two systems indicate similar trends). The tremendous advantage of TWIPS in this case is instead visible in the time histories. In that output (shown two different ways in Figure 4.30 and Figure 4.32), the amount of bubble-scatter suppression can be seen by comparing TWIPS with the standard sonar between 1 ms and 3 ms. That region shows clear scatter suppression by TWIPS, while the standard sonar shows the undesirable bubble scatter. This can be studied by looking at the medians for those data sets, as shown in Figure 4.46.

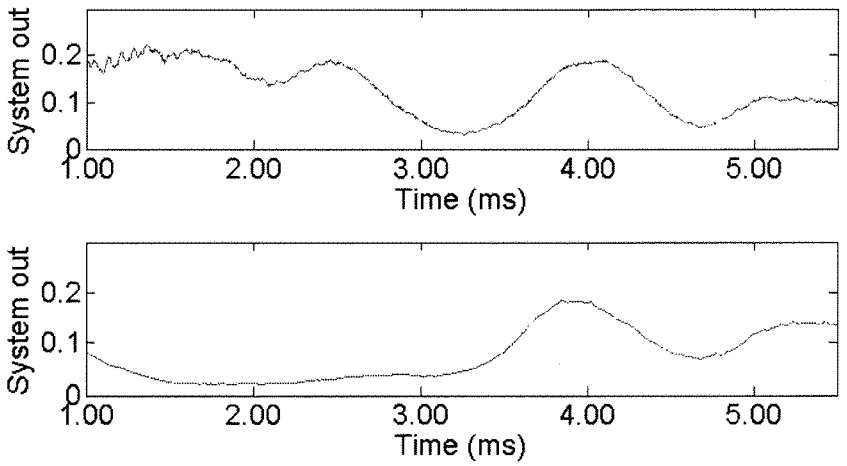

Figure 4.46 Median of all records for the TS=-10 dB data set. (*Top*) Standard sonar (*Bottom*) TWIPS.

The medians of all the TS=-10 dB data reveal the impressive bubble scatter suppression exhibited by TWIPS. In Figure 4.46, the bubble cloud is located between 1 ms and 3 ms, and the target is centred near 4 ms. By comparing the mean value in the bubbly region to the

maximum target value for the two systems, the degree to which bubble scattering has been suppressed can be quantified as shown in Table 4.1.

Table 4.1 Bubble scatter suppresion statistics based on medians of TS=-10 dB data (see Figure 4.46)

	Maximum value: target	Mean value: bubbly region	Ratio: target to bubble scatter
Standard	0.19	0.17	1.14
TWIPS	0.18	0.03	6

In Table 4.1, the ratio of the maximum system value at the target location to the mean value in the bubbly region has been calculated for TWIPS and for the standard sonar according to the medians of the TS=-10 dB data. This gives a type of signal-to-noise (SNR) ratio which can be used to evaluate the effectiveness of the bubble scatter suppression by either algorithm. In Figure 4.46, it can be seen that the standard sonar amplitude in the region of the bubble cloud is nearly the equal to the system output in the target region. This is reflected by the SNR ratio calculation in Table 4.1, which shows the target signal to be only about 14% greater than the bubble signal when the standard sonar is applied. However, TWIPS is much more effective at suppressing the bubble signal, and so the corresponding SNR is about 7.8 dB. Since on average the target signal is greater than the bubble signal for both algorithms in this operating condition, the resulting ROCs are nearly identical (see Figure 4.34). However, a closer analysis of the SNR has revealed that the standard sonar functioned in this case only because the target strength was strong

enough to allow the target signal to overcome the bubble scatter. In contrast, TWIPS has suppressed the bubble scatter considerably, and it is therefore expected that TWIPS would continue to function well in this condition even if the target strength were to be reduced. The SNR data suggests that any significant reduction of the target strength in this condition would cause the standard sonar to fail. This hypothesis can be checked by reviewing the TS=-15 dB data. In the ROC for the TS=-15 dB data (Figure 4.41) where the bubble size distribution has been kept the same as for the TS=10 dB data, it can be seen the 5 dB reduction in target strength has caused the standard sonar to fall far below the performance level of TWIPS. It should be noted that the TWIPS ROC for this case climbs to a 45% true positive detection rate before any false positives confused the algorithm. This is consistent with the above-described advantage of a system which can be operated effectively. It was seen in the TS=-10 dB analysis that TWIPS is effective at suppressing bubble scatter, making the bubble cloud almost invisible in the median statistic (Figure 4.46). The same approach has been applied here to the TS=-15 dB data, and similar results are obtained.

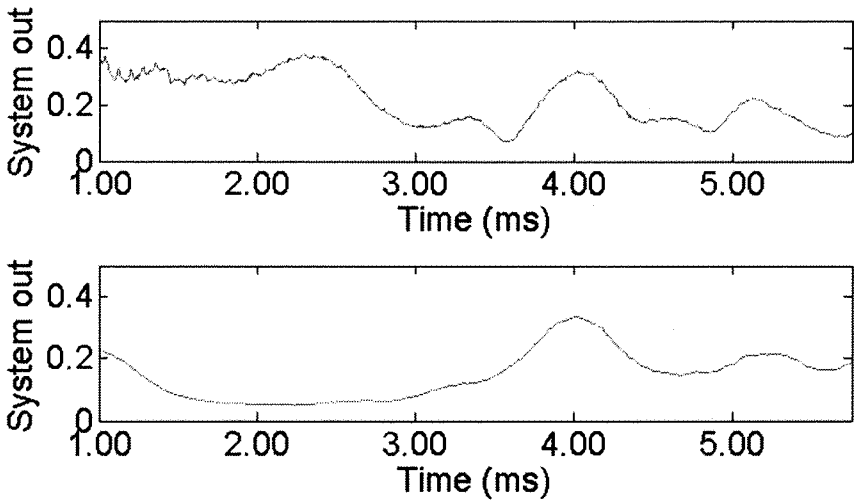

Figure 4.47 Median of all records for the TS=-15 dB data set. (*Top*) Standard sonar (*Bottom*) TWIPS.

Table 4.2 Bubble scatter suppresion statistics based on medians of TS=-15 dB data (see Figure 4.47)

	Maximum value: target	Mean value: bubbly region	Ratio: target to bubble scatter
Standard	0.32	0.29	1.10
TWIPS	0.37	0.08	4.6

Table 4.2 summarises Figure 4.47, and shows that once again, the SNR for the standard sonar makes that algorithm only just viable for this condition (that is it performs better than a 50/50 guess according to the ROC shown in Figure 4.41). In contrast, TWIPS suppresses the bubble scatter in an impressive manner, and allows the target to be clearly visible in Figure 4.47. This experiment has proven that TWIPS is capable of suppressing bubble scatter. This result will be confirmed and expanded in the next chapter, when TWIPS is tested during sea trials at Empress Dock, Southampton and in Southampton Water.

4.4 Conclusions

In this chapter, it has been shown that TWIPS is capable of

differentiating between bubble scatter and linear scatter. This method is capable of functioning when the target of interest spatially independent of the bubble cloud by which it is being obscured. In clear water, TWIPS performed as well as a simple correlating sonar, finding the target 100% of the time and returning 0% false positive. In bubbly water, TWIPS tends to exhibit sporadic detection behaviour. However, when detections are made, the algorithm returns very high amplitude signals; as was predicted in the output the computational model presented in the previous chapter. In water where standard sonar is not able to perform better than about $Q(D_1 \mid n_1):Q(D_0 \mid n_1)$ 100%:50%; these sporadic high amplitude spikes make it possible to operate TWIPS with no false alarms $Q(D_1 \mid n_1):Q(D_0 \mid n_1)$ 45%:0%. It was argued that in an environment where false alarms can be costly and inconvenient, the prospect of having a detection system with 0% false alarm rate is very attractive.

The analysis in this chapter did not reveal the source of these sporadically present, very high amplitude signals. The next chapter will use the results of a TWIPS sea trial as a platform to offer an explanation for their origin.

5 Sea trials

UNITED STATES HAS SECRET SONIC WEAPON – JAZZ

Europe falls captive as crowd riot to hear dixieland

New York Times Headline, 6 November 1956, Felix Belair Jr.

5.1 Introduction

The tank tests described in Chapter 3 suggested strongly that the TWIPS method might improve sonar performance in bubbly water. However, the limitations of bubble size distribution and tank size limit the degree to which these conclusions can be extrapolated to real-world conditions. To eliminate that uncertainty, a series of sea-trials were conducted to test the effectiveness of TWIPS in real-world conditions. These trials were conducted in two parts: dockside tests (26 February 2008), and open-water tests (27 February 2008). This section will describe the test methodologies, and will establish that the Twin Pulse methodology can substantially improve sonar performance in bubbly water.

5.2 Equipment

The same acoustic source/acquisition systems were used for the sea trials as were used for the tank tests. Shore power was used to drive the equipment during dock-side tests. During open-water tests, the output of an on-board inverter was used to drive the systems. Two mounting assemblies were used during the course of sea-trials. For

the dock-side experiment, the acoustic sources and receiver were mounted on a pontoon which has been shown in Figure 5.1 and Figure 5.2. During the open-water tests, the acoustic transducers were mounted on in a steel tow-fish frame as shown in Figure 5.2 and Figure 5.4.

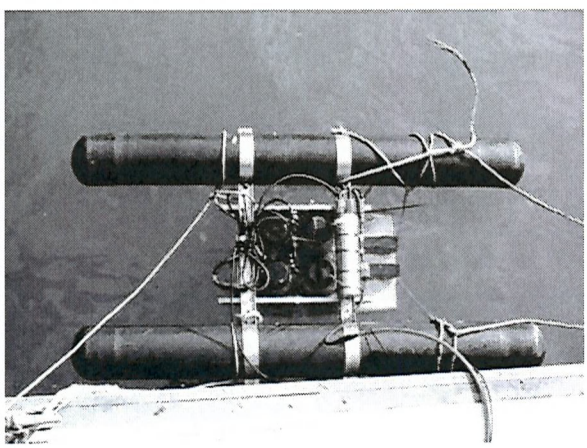

Figure 5.1 This photo shows a downward-looking view of the pontoons supporting the sources in the water. When the system is at rest, the acoustic centre of the array is located approximately 20 cm below the surface.

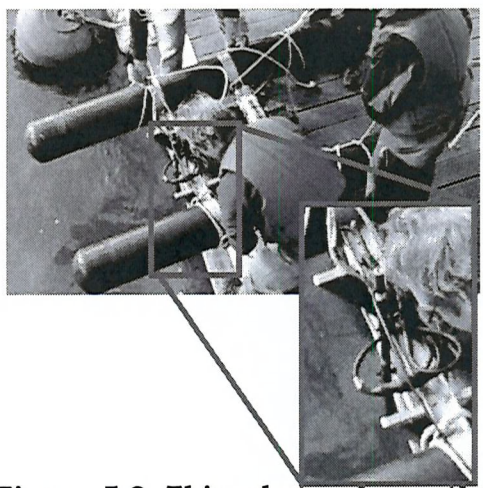

Figure 5.2 This photo shows the pontoon, but with detail on the vertically-suspended receiver. The acoustic centre of the receiver was located 5 cm laterally from the nearest edge of the steel source-support frame, with the deepest portion of the microphone located 5 cm below the acoustic centre of the source array.

During the tank experiments, the acoustic arrays were mounted in a Maltese Cross configuration. However, during the open water tests, the frames available dictated that a 2 x 2 configuration be used. The directionality pattern for this transducer system when arranged in a 2 x 2 pattern has not been measured. However, the directivity of an N x N array over all horizontal directions θ_a and all vertical directions φ_a can be calculated as $E(\theta_a, \varphi_a)$ using the result shown in (5.1) [133].

$$E(\theta_a,\phi_a) = E_e(\theta_a)\frac{sin(N\pi(s/\lambda)sin\theta_a sin\phi_a)}{Nsin((\pi s/\lambda)sin\theta_a sin\phi_a)}\frac{sin(N\pi(s/\lambda)sin\theta_a cos\phi_a)}{Nsin((\pi s/\lambda)sin\theta_a cos\phi_a)} \quad (5.1)$$

In the equation above, the horizontal directivity each element is represented as $E_e(\theta_a)$, s is the element spacing, and λ is the wavelength. The directivity of the individual elements was unknown, so uniform (monopole) directivity was assumed. Monopole directivity is a reasonable assumption where the product of the wavenumber and the primary dimension kL is much less than one [131]. In this case, however, the primary dimension and operating frequency are identical, and so $kL = 2\pi$. As a result, it can be assumed that the directivity of the individual array elements is better than was allowed for in the calculation. This means that the output of equation in (5.1) which is shown in Figure 5.3 underestimates the overall system directivity.

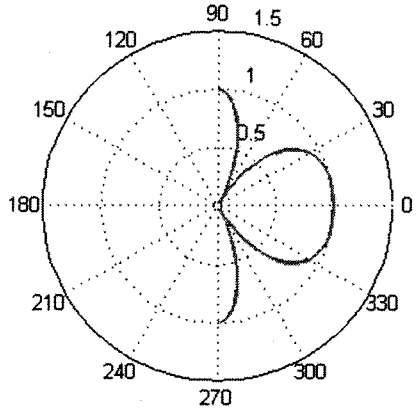

Figure 5.3 One-sided directivity pattern of a 2 x 2 array of monopole-like pistons having a spacing of 250 mm and an operating wavelength of 250 mm. In this plot, 0 deg corresponds to the direction the pistons face. Since the array is arranged in an NxN pattern, symmetry can be used to argue that directivity is independent of angular orientation about a vector normal to the plane defined by the transducer faces.

Since the array is arranged in an N x N pattern, symmetry can be

used to argue that the directivity is independent of angular orientation about a vector normal to the plane defined by the transducer faces. During the open water tests, the acoustic centre of the hydrophone was located 10 cm aft of the rear two sources, aligned with the axis formed by the tow-fish tow-line, and 5 cm below the lower plane formed by the was suspended by a carbon-fibre pole which mounted on the flow straighteners aft of the acoustic drivers on the tow-fish.

Figure 5.4 Prof T G Leighton assists in mounting the tow-fish used to carry the driver array during open-sea trials.

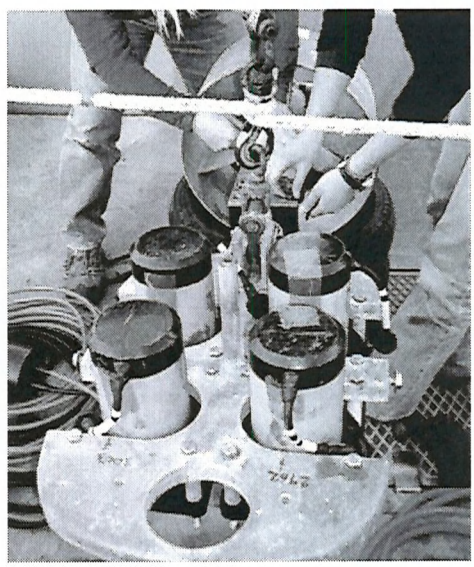

Figure 5.5 An overhead view of the tow-fish used during open sea trials.

5.3 Time-varying gain

In section 2.5.1.1, the concept of time-varying gain (TVG) was discussed. It was pointed out that many scanning systems incorporate a gain which accommodates for spreading and attenuation before data is passed to the output algorithm. Also discussed was the fact that a system designed for use in turbulent, shallow waters where acoustic bubble and sediment interactions

occur throughout the acoustic field (such as in the tank experiments), such a gain is not appropriate. However, in those cases where there are several meters of water of clear below a near-surface bubble cloud but above the sea-bottom, some benefit might be realised from the use of TVG. For the purpose of fairness in comparing the standard sonar to TWIPS, quadratic TVG has been applied to all time series before post-processing.

It should be noted that the driving source has 3 lobes: a main lobe, and two side lobes (see Figure 5.3). The source in these field trials has been arranged such that it is down-firing. As a result, in the absence of bubbles, by merit of the fact that the only significant reflective source in the water is the sea-bottom, most of the sound emitted by the main lobe which reaches the hydrophone will be sea-bottom backscatter. Further, sound emitted by the side lobes will tend to be reflected away from the receiver according to the law of reflection [11].

5.4 Experimental goals and limitations

From Figure 5.1, it can be seen that the sources were arranged in a down-firing configuration. This allowed continuous monitoring of the signal returned from the sea-bed. The goal of both the dock-side and the open-water trials was to establish whether in fact TWIPS was capable of identifying the sea-depth when standard correlation and/or

high-frequency commercial echosounders[21] failed as a result of bubble scattering. During dockside measurements, bubbles were generated by a rigid-inflatable boat (RIB) which was also tied alongside the dock. When under way during open water tests, wake bubbles were generated by three different sources in turn: the research vessel towing the array and capturing the data, a RIB dispatched locally to enhance bubble scattering, and ship traffic in Southampton Water.

One clear problem with these tests is the lack of a baseline measurement. As established in Appendix 1, the development of a ROC curve depends on the ability to measure the system with and without the target present. Clearly, it is not possible to remove the sea-bottom. An alternative to changing the shape of the sea-bottom might be to conduct the same tests in waters of different depths[22]. However, these tests were trials of opportunity. The staff producing bubbles during the dockside measurements were not available to produce bubbles at different parts of the tidal cycle. Logistical considerations made it impossible to take the research vessel out for more than one day; and the channel in which open water

[21] The echosounder was only in use during open-water trials, as this system was mounted to the tow-vessel used for those tests.

[22] This could be accomplished either by recreating test conditions in different locations, or by repeating tests in the same location, but at different stages of the tidal cycle.

measurements were performed has a generally flat bottom (especially in the region where large ships were followed).

A second limitation on the tests results from the fact that the bubble-counting equipment was not available for these measurements. The inability to capture bubble size-distribution data means that the information presented in this chapter is certainly incomplete. However, it can not be logically disputed that, when a vessel is travelling in the wake of a large ship, and the depth sounder suddenly ceases to operate, it is likely that large, dense bubble clouds are located beneath that vessel. The final chapter of this document will address the need for bubble-size distribution data taken simultaneously with in-situ TWIPS performance measurements.

5.5 Dock-side tests

Before going to the open water, the TWIPS system was assembled at Empress Dock, National Oceanography Centre, Southampton. After completing basic diagnostic tests to ensure normal operation of the sound production and acquisition systems, TWIPS measurements were made in clear water. Then, the system was exposed to a variety of different types of bubble clouds, all of which were generated by a RIB located 7.8 m upstream of the receiver. The acoustic pontoon was held in place by lines attached to the dock. The configuration for these tests is shown below in Figure 5.6 and Figure 5.7.

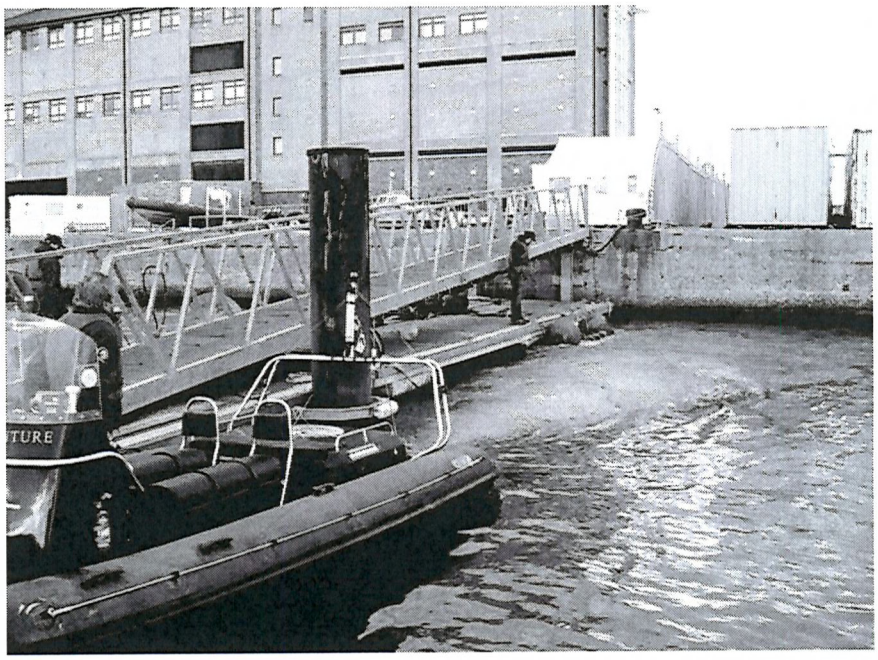

Figure 5.6 Here the RIB is shown generating bubbles to scatter the sound generated by the floating acoustic platform. The blue RIB in the foreground is being operated by member of the technical staff at the National Oceanography Centre, Southampton.

Figure 5.7 Prof T G Leighton (right) discusses the measurement method with the author (left) whilst the source platform is held in place next to the dock

Processed output was not monitored during tests, so the degree to which the bottom was obscured by bubble scattering was not known.

Observations of raw signal output suggested to the experimenters that in fact that bottom was essentially invisible when the pontoon was placed directly in the RIB engine exhaust plume, so efforts were made to reduce the directness with which the exhaust plume was aimed at the source/receiver. In fact, a review of the data shows that the cloud was insufficiently dense to suppress completely the signal from the sea-bottom in the so-called standard sonar output for more than a few seconds at a time.

5.5.1 Interpulse delay

During initial tank tests (see Chapter 3), it was noticed that tank reverberation made it impossible to obtain useful results with interpulse[23] delays less than about 50 ms. In fact, the best results were obtained using inter-pulse delays of 100 ms, so that delay was used during most tank tests. In the laboratory, the upper limit of this delay was dictated by the amount of time it took any bubble to travel more than about a 0.37 of a wavelength. This quantity was effectively a function of the rise-rate of the largest bubbles. It can be reasoned that, as a result of the fact that the bubbles studied in the dockside measurements were propeller-generated, the median bubble velocity was considerably higher than in the tank. The fact that the bubbles

---

[23] That is, the delay within any pulse pair between a ping and its phase-reversed compliment. This is not to be confused with the intra-pulse delay - the time between any set of pulse pairs.

are being propelled violently across the water column, rather than rising naturally under their own buoyancy, reduced the amount of time that it took any bubble to move more than about 0.37 of a wavelength. In practice, this means that the best results for the dockside measurements were made with an interpulse delay of 20 ms and 50 ms.

5.5.2 Results

The data from this portion of the field measurements was analysed in a variety of ways. First, the data gathered with no bubbles in the water is reviewed to determine whether the bottom is visible in output from both the standard processor and TWIPS.

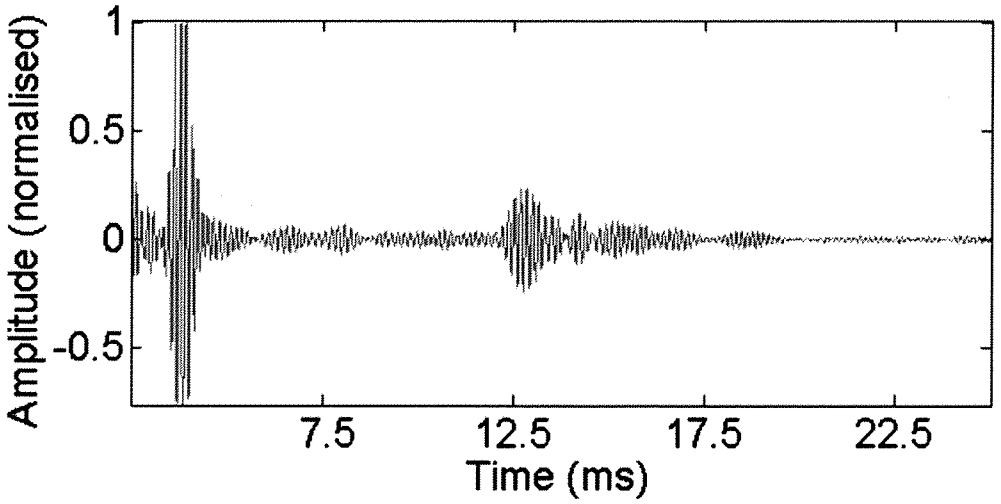

Figure 5.8 A sample ping taken dockside. The first large return (around 2 ms) is most likely a result of the proximity of either the pier structure or the sea-wall. The second largest return (near 12.5 ms) corresponds to the seabottom. There are other low amplitude features between 2 and 12.5 ms, all of which correspond to other static physical features within the acoustic environment (as is evidenced by the fact that these features appear regularly in each record)

A sample ping is shown above in Figure 5.8. In this figure, returns corresponding to several static physical features within the acoustic field are visible. The largest feature is the first reflection, visible near

2 ms. This reflection is the result of either the pier structure or the sea, the proximities of which are both visible within Figure 5.6 and Figure 5.7. While it was possible to alter the temporal structure of this peak by moving the pontoon, it was not possible to altogether eliminate its presence. This was nonetheless unimportant, as the critical feature of interest was the sea-bottom, visible near 12.5 ms. In the time period between 2.5 ms and 12.5 ms, there are a variety of small-scale reflections. These reflections were all constant in temporal location and amplitude throughout the bubble-free study, and so correspond to stationary physical features located at various places within the acoustic field. Those peaks located after 12.5 ms correspond to multipath reflections and distant reflecting objects.

The data captured in the absence of bubbles was processed using the standard sonar and TWIPS, as shown in Figure 5.9. This set of results is shown with time as the vertical axis to emphasise the fact that this data was obtained using a down-looking system. The TWIPS output in this experiment was calculated using P_-/P_+^2. It is advantageous to square the bottom, as this increased bubble scatter suppression. It should be noted that in those cases where the bubble cloud and the target are co-located (see the simulation described in the second chapter), it is not practical to employ squaring in the denominator, as even harmonic suppression can then overwhelm information carried at the fundamental frequency which is in the numerator.

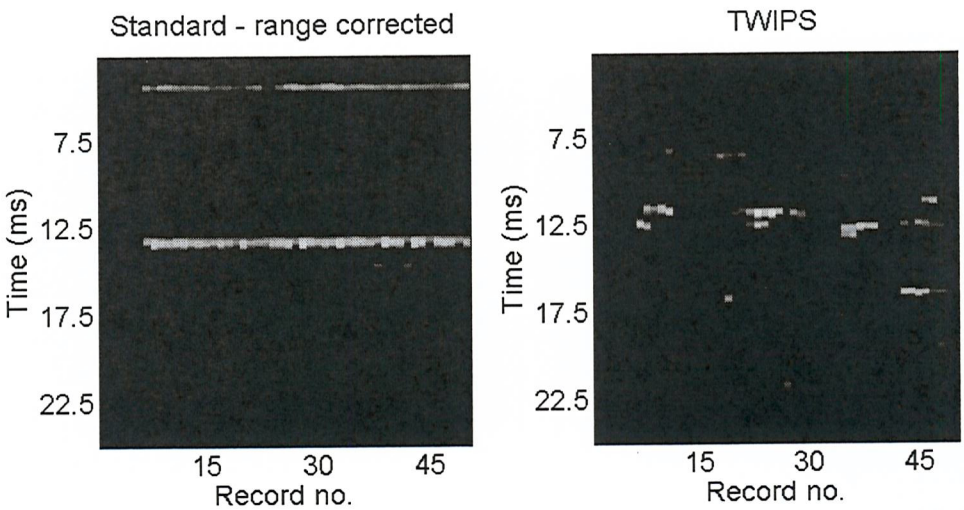

Figure 5.9 The output of the standard processor (left) and TWIPS (right) for the bubble-free dockside data. The interpulse delay applied here was 50 ms. In both images, only the top 60% of values are visible to highlight features of interest. In the standard sonar image (left), only the refelction of the sea-bottom is visible. The TWIPS timage (right) shows the reflection from sea-bottom near 12.5 ms, in addition to the remnants of other linearly scattering features from within the field (as described in the caption of Figure 5.8).

The analysis of the bubble-free data shows the standard sonar working in the expected fashion - the sea-bottom is clearly and regularly visible. Also visible in that output at around 2.5 ms is the reflection from the feature located near the pontoon, as mentioned above. The contrast between this output and the TWIPS output highlights some contrasts in algorithm behaviour. The TWIPS image shows the sea-bottom near 12.5 ms, however the amplitude of those peaks are unsteady as is characteristic for the sonar. Also clearly visible in the TWIPS output are those peaks corresponding to the other, smaller linear reflectors located between 2.5 ms and 12.5 ms as mentioned above in the discussion of Figure 5.8. Interestingly, the peak corresponding to the reflector located near the source/receiver location (visible near 2.5 ms in the standard sonar output) is not visible in the TWIPS output. This can be explained through close

examination of the time-series in Figure 5.8 in the region of 2.5 ms. Such an analysis shows that this peak is clipped as a result of the close proximity of the reflector to the source/receiver location. Clipping, represented by flat-top features on otherwise sinusoidal waves, is in fact a type of nonlinear distortion equivalent to the enhancement of odd-harmonics within the harmonic series for that signal [134]. If the clipped portion of the time series was perfectly square and symmetrical about the amplitude axis, one would expect that this energy would appear exclusively in the numerator P_-, which highlights odd harmonics. However, the signal not perfectly square, and in fact contains a significant amount of even harmonic energy, as testified to when comparing P_- to P_+ for this scenario (see Figure 5.10)

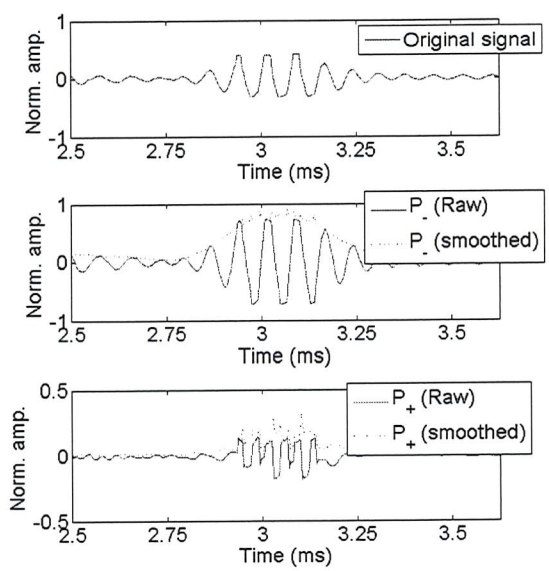

Figure 5.10 Clipping near the beginning of a sample time record used in producing the bubble-free data studied in Figure 5.8 and Figure 5.9. At top is shown the raw signal (return from the first portion of the two-part pulse). In the middle is the result for P_-, which highlights odd-numbered harmonics (including the fundamental). At bottom is the result for P_+, which highlights even-numbered harmonics. It is interesting to note the original clipped signal contains significant even harmonic energy, so that when it is processed using P_-/P_+^2, the clipped signal is suppressed significantly (see Figure 5.9).

Having established that both algorithms are capable of identifying the seabottom in the absence of bubbles, the discussion now turns to the consideration and comparison of system performance in the presence of bubbles.

With an interpulse time of 50 ms, good evidence of bubble suppression is obtained, as shown in Figure 5.11 below. In this figure, the bottom is visible between 12.5 ms and 17.5 ms when data is analysed using either the standard sonar or TWIPS. However the bubble cloud which is prevalent in the standard sonar output between 0 ms and 7.5 ms is completely suppressed by TWIPS. Note the degree to which the visibility of the seabottom is reduced from runs 200-300.

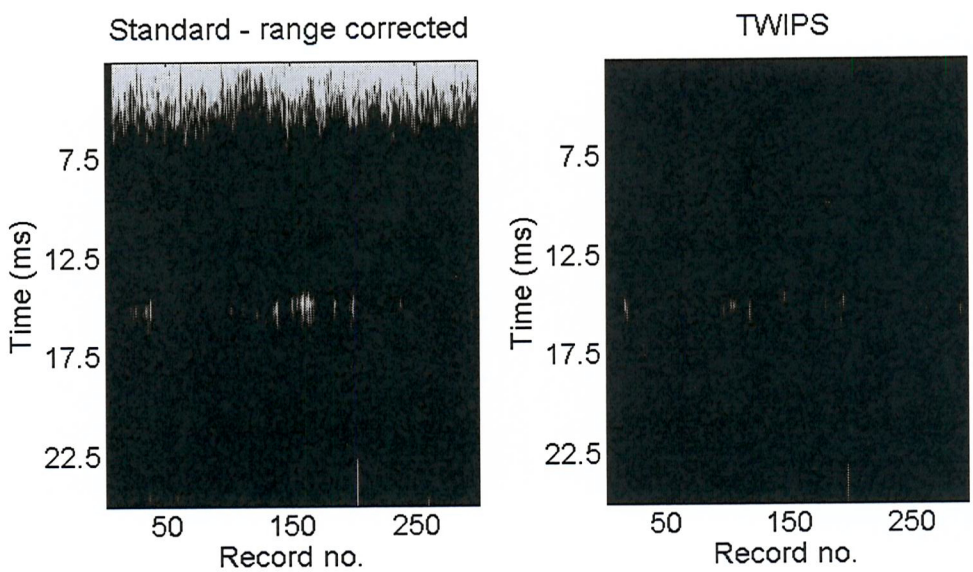

Figure 5.11 Dockside results obtained using an interpulse time of τ = 50 ms. The bottom is visible between 12.5 ms and 17.5 ms when the data is viewed using either the standard sonar or TWIPS (processed using $P./P_+^2$ with geometric averageing of each five lines in denominator). However the bubble cloud which is prevalent between 0 ms and 7.5 ms in the standard sonar is completely suppressed by TWIPS.

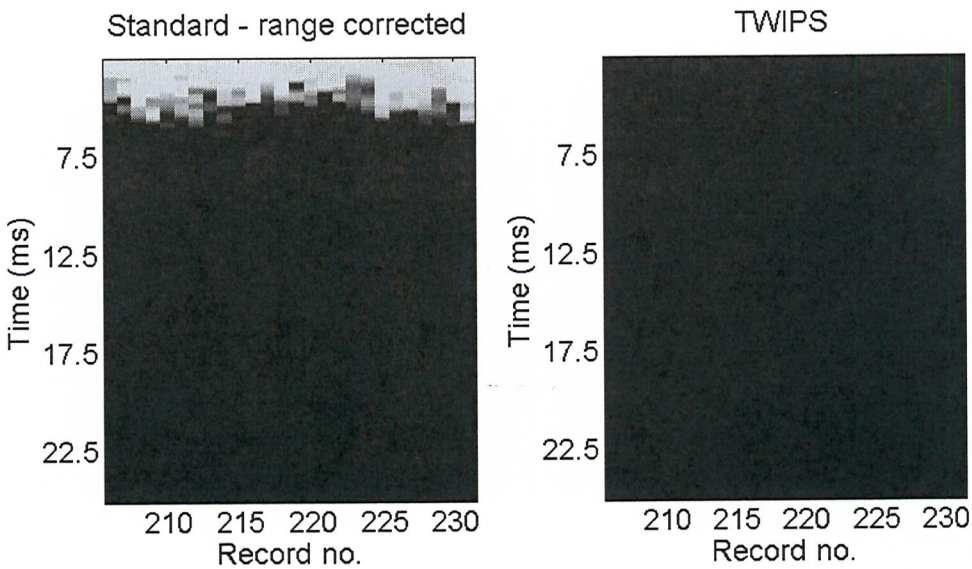

Figure 5.12 Results obtained using an interpulse time of τ = 50 ms. This figure is a detail of Figure 5.11 for record numbers 200-235. The bottom here is completely obscured by bubble scattering when the system is viewed using the output of standard sonar. TWIPS (processed using $P./P_{+}^{2}$ with geometric averageing of each five lines in denominator) allows a single glint of the bottom at record number 228.

When comparing the results shown in Figure 5.11 and Figure 5.12 (with bubbles) to those shown in Figure 5.9, it can be seen that the bottom has gone from a position corresponding to a two-way travel time of near 12.5 ms to a position corresponding to a two-way travel time of almost 15 ms. This observation is consistent with the fact that the tide was coming in during these measurements.

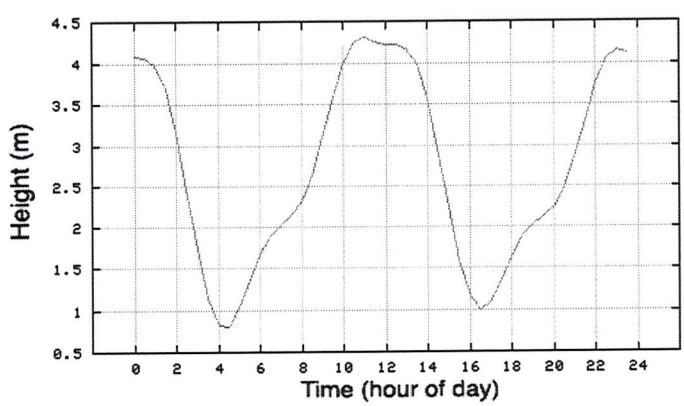

Figure 5.13 Tide chart for Southampton Harbour on the day of the dock-side measurements. Bubble free results (Figure 5.9) were taken at 14h20m, and data in presence of bubbles (Figure 5.11, Figure 5.12, Figure 5.14, Figure 5.15) was taken from 15h20m-15h40m. (Source: Service Hydrographique et Océanographique de la Marine, France)

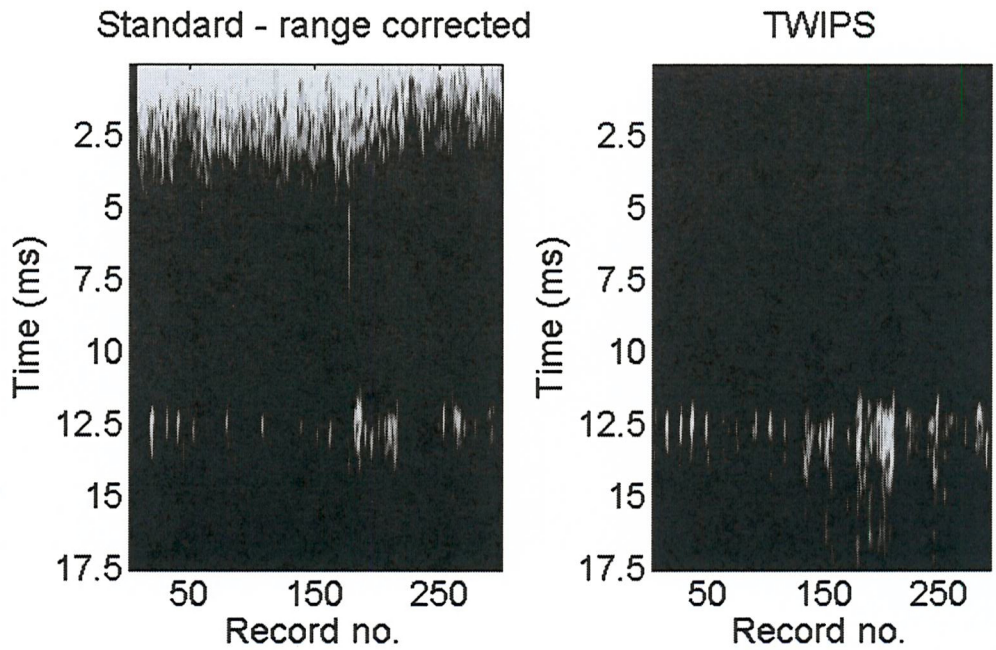

Figure 5.14 Results obtained using an interpulse time of τ = 20 ms. At left are shown the results when the data has been analysed using the standard processing. At right appears the TWIPS output (processed using P_-/P_+^2 with geometric averageing of each five lines in denominator). The sea-bottom and the bubbles are both visible within the standard sonar output. TWIPS supresses the bubble output, leaving only the response from linear scatterers at the ground location and after.

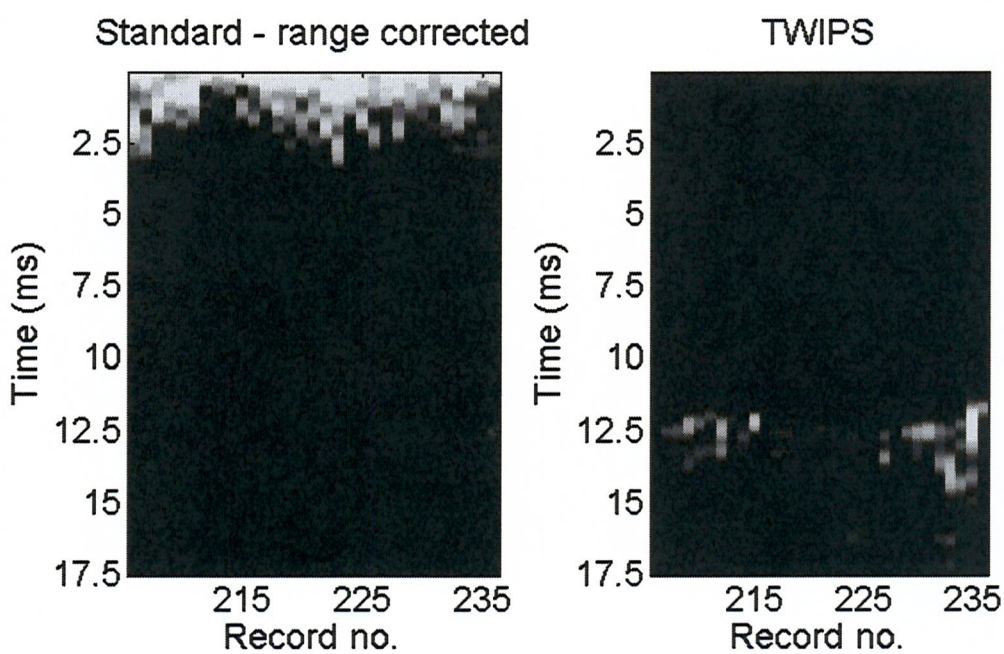

Figure 5.15 Results showing a detailed view of lines 210-235 from Figure 5.14 (obtained using an interpulse time of τ = 20 ms). Standard sonar output is at left, and TWIPS output (processed using P_-/P_+^2 with geometric averageing of each five lines in denominator) is at right. During the acquisition of the data shown in this figure, the bubbles (0 ms – 2 ms) have almost completely overwhelmed the response from the seabottom in the standard sonar (~8 ms), although some response from the bottom is visible.

5.6 Open water tests

On 27 February 2008, the TWIPS technique was tested in Southampton Water using the R/V Bill Conway to drag the acoustic source. Southampton Water is a stretch of sea leading from the Solent to Southampton, and is the route used by all ship-traffic to and from Southampton. The goal of these tests was to investigate the effectiveness of TWIPS under various conditions. As stated in the introduction to this section, two turbulence sources were used to introduce bubbles into the acoustic field

1) The vessel generated its own bubbles by slowly increasing its speed and allowing the source to drift in its wake. Tests of this type were conducted at 2,4, and 6 knots.
2) The research vessel ventured into the wakes of ships travelling through Southampton Water. The research vessel maintained a speed of approximately 4 knots whilst in the wake of passing ships. This made it possible to prolong the amount of time during which measurements could be made in the wake, but made it impossible to measure ship-wake scattering in the absence of self-generated bubbles (*e.g.* those bubble generated by the research vessel). Safety concerns made it impossible to bring the R/V Bill Conway to rest whilst in the wakes of passing ships.

5.6.1 Results from data acquired wakes

The acoustic platform was dragged in the wake of the R/V Bill

Conway, and records were taken at one second intervals. Whilst acquiring the data presented below in Figure 5.16, the Bill Conway travelled at three different speeds successively. For lines 1-100, the speed was held at 2 knots. The speed was increased to 4 knots after line 100, and that speed was maintained until line 200, at which point the speed was increased to 5 knots. Equipment considerations made it unsafe to travel above 5 knots whilst towing the acoustic pontoon.

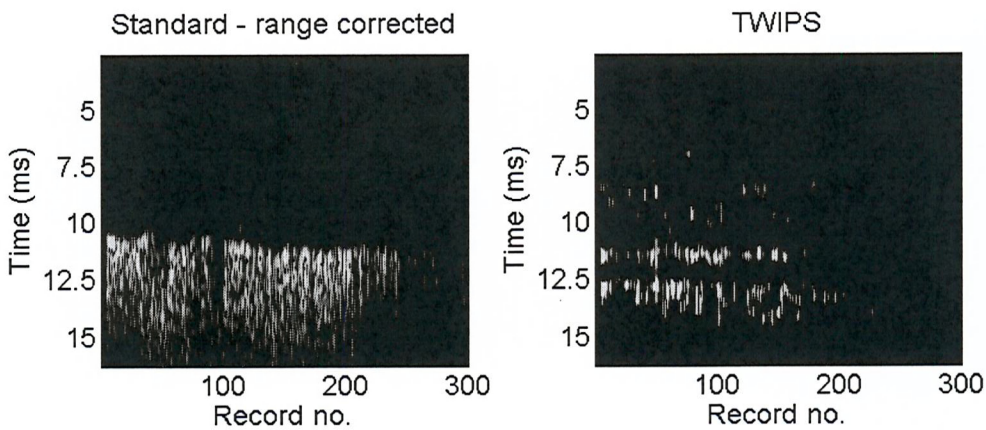

Figure 5.16 Data acquired whilst towing the acoustic platform behind the R/V Bill Conway. At left is shown the output from the standard sonar, and at right is shown the TWIPS output (interpulse time τ = 50 ms; processed using P_-/P_+^2 with geometric averageing of each five lines in denominator). Boat speed was varied every 100 records. For lines 1-100, the speed was held at 2 knots. The speed was then increased to 4 knots. After line 200, the speed was increased to 5 knots. The TWIPS figure shows the output from those values between the 95th and 99th percentile range of the entire data set.

In Figure 5.16, the visibility of the bottom reduces in both output sets as speed is increased. At record 1, the bottom appears to be somewhere near 10 ms. The main bottom contour appears in the standard sonar seems to be located just after 10 ms, and seems to be preceded by a faint, parallel contour. The fact that two reflections are returned in quick succession (the two-way time separation appears to be about 0.5 ms) near the bottom would suggest the presence of a

soft, acoustically penetrable layer of a thickness on the order of 32 cm (assuming a "slow"[24] mixed layer with a sound speed of about 1300 ms). It is interesting to note that TWIPS indicates that the bottom is about 1 ms further away from the surface than does the standard sonar. Indeed this is most likely to do with the fact that peak in the linear reflection is about 1 ms after the beginning of the return from the bottom. The change in two-way travel time to the bottom contour correlates well with increases in speed, and so may be the result of either a slope in the sea bottom, the decreased sound speed with an increase in void fraction (as a result of a thicker wake), or a combination of these two factors.

The data acquired whilst travelling at 5 knots (records 250-300 in Figure 5.16) has been shown in detail in Figure 5.17 below. The output shows shortcomings in the output of both TWIPS and the standard sonar. The output of the simple correlation process is noisy, and the TWIPS output is sporadic and makes it difficult to identify the bottom.

This data set would seem to be inconclusive. Visually, the bottom contour is easiest to identify in the standard sonar output. The lack bright region near the top of the standard sonar output seems to

---

[24] That is, a layer of reduced sound speed compared to the open water just above it.

suggest the wake in this case was not particularly strong, and so the advantages of a bubble-scatter suppression algorithm are not readily apparent.

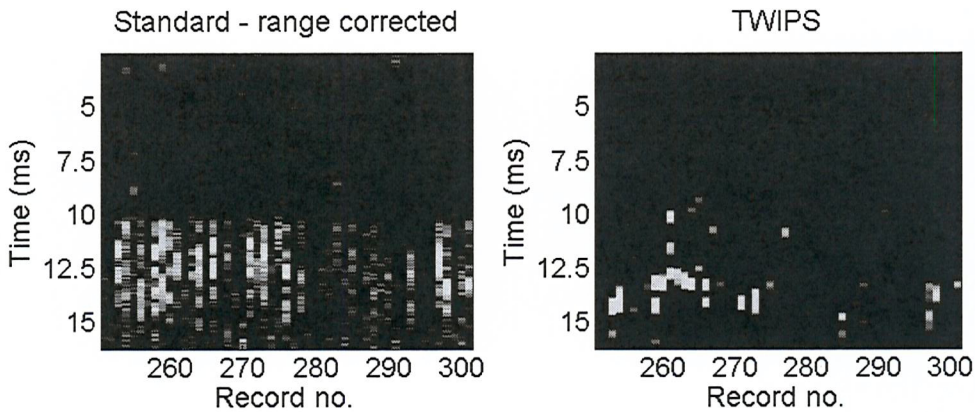

Figure 5.17 A detail of data displayed in Figure 5.16. This data was acquired whilst the Bill Conway travelled at 5 knots, and the acoustic platform was dragged behind in that vessel's wake. The TWIPS figure shows the output from those values between the 95th and 99th percentile range of the displayed data set.

The next data set presented was taken in the wake of a large freighter, and show illustrate how bubble scattering suppression can be useful while under way in the open water. After acquiring the previous data set, it was noticed that the B/V Season Trader (shown in Figure 5.18) was passing through Solent Water heading out to sea.

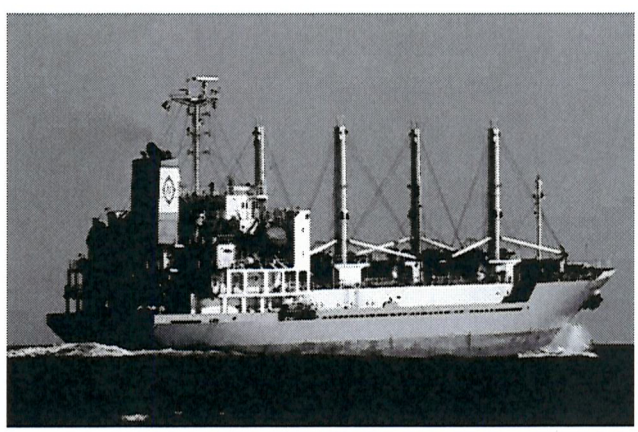

Figure 5.18 B/V Season Trader (IMO 9179402) as photographed by Kelvin Davies (image available from www.shipspotting.com)

Table 5.1 Ship data for B/V Season Trader (Source: Lloyd's Register)

Flag	Philippines
Dry weight	8995 metric tons
Draft	7.865 m
Length	139 m
Beam	20.6 m

It was decided to follow this ship, and run the sonar acquisition system whilst travelling in its wake. As the Bill Conway approached the centreline of the Season Trader wake, the depth sounder on-board the research vessel transitioned from showing the true depth (19 m), to showing "0 m". This type of problem is commonly encountered by ships travelling within wakes generated by the passage of other ships. Conventional depth sounders operate via a simple transmit/receive mechanism. The transmit transducer emits sound ultrasonic pulses downwards from the bottom of the ship hull at regular intervals. When one of these acoustic pulses reaches the bottom, a reflection is returned to the boat, and is recorded by the receive transducer (on simple echosounding systems, the send/receive operations are handled by the same transducer). The depth sounding system assumes a sound speed, and the two-way travel time is thereby converted to a depth estimate. However, when travelling in the wake of a large ship, backscattering from the bubbles within the wake can prevent normal system operation when within a few ship-lengths of the source ship [84]. This effect will tend to result in the echo-sounder returning either an error message or an unrealistic depth (such as 0 m). During this sea trial, when the on-board depth sounder stopped working, and R/V Bill Conway had been positioned

along the wake centreline travelling to the same bearing as B/V Season Trader, TWIPS data acquisition began. At that point in time, the leading vessel was approximately 30 m ahead of the trailing vessel. The Bill Conway travelled at 4 knots – the maximum speed at which acceptable data could be acquired (see Figure 5.16). The Season Trader appeared to be drawing away from the research vessel of a rate of approximately 3 knots (corresponding to a rate of 7 knots for that ship) according to the skipper on board the Bill Conway. The data acquired during this period of time is shown in the following two figures (Figure 5.19 and Figure 5.20, acquired sequentially). Note that the location of the bottom (around 24 ms) only becomes obvious as trailing vessel falls far behind the leading vessel, and the wake fades (Figure 5.20). Data acquisition ended when the Season Trader was estimated to be about 250 m in front of the Bill Conway.

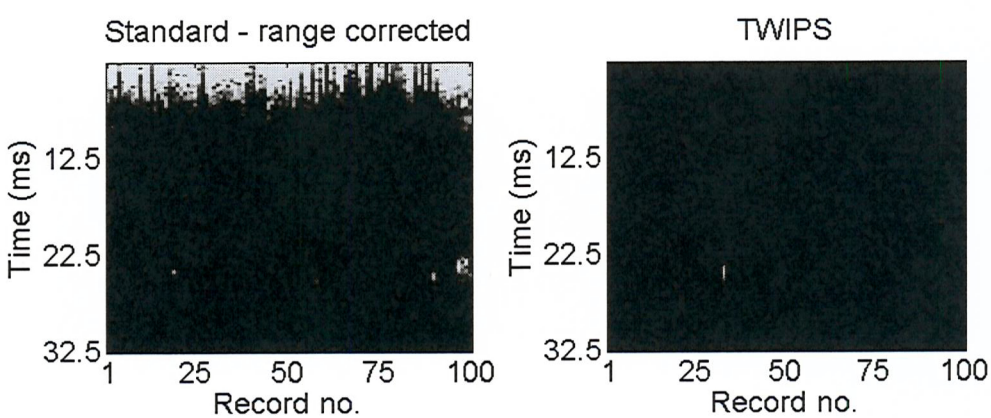

Figure 5.19 Data acquired whilst trailing B/V Season Trader (Standard sonar, right; TWIPS, left). Glints of the bottom at around 24 ms are visible in the output of the standard processor, but bubble scattering in the upper regions of the water column is the dominant feature. In the TWIPS output (values between the 95th and 99th percentile of the entire data set shown), there is a single glint in the vicinity of 24 ms corresponding to the bottom; bubble scattering has been completely suppressed in that view.

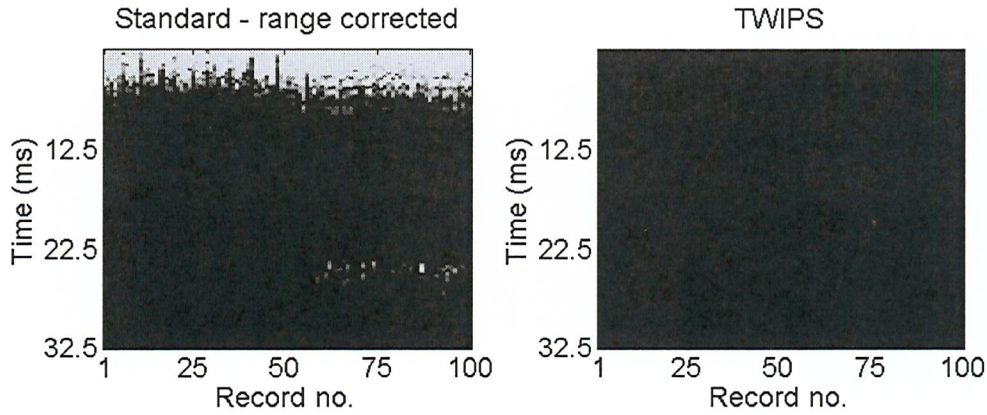

Figure 5.20 Acquisition of the data shown here began immediately after the acquisition of the data shown in that shown in Figure 5.19 ceased. In the standard sonar image, bubble scattering from the upper layer is a dominant feature. As the wake fades (as R/V Bill Conway increased its range to B/V Season Trader to 250m) near record 50, the bottom becomes visible. The bottom also becomes visible near that point in time in the TWIPS output (values between the 95th and 99th percentile of the entire data set shown), but the bottom is only visible in 4 of the final 50 records.

As soon as the acquisition of the data shown in Figure 5.19 ceased, acquisition of that data displayed in Figure 5.20 began. As explained above, the Bill Conway was travelling at just over half of the speed of the Season Trader. Record 1 of the figure corresponds to when the trailing vessel was behind the leading vessel by about 150 m, while Record 100 was taken when the separation was approximately 250 m. In Figure 5.20, the bottom is revealed in both the standard sonar and TWIPS output at around record 50. Each of the outputs has appealing visual features. A single glance at that output reveals to the viewer a highly time-variant feature near the top of the water column (the bubble cloud). At record 76, a large feature seems to present in the bottom third of the water column. The bottom is plainly visible from about record 50 onwards. The TWIPS output is less visually appealing, and less consistent, but reveals the essential features

nonetheless. The bottom is visible in 4 records (55, 60, 63, and 97) and the suspended scatterer in record 76 mentioned previously is also visible here.

5.7 Discussion

In assessing the data presented in the previous section, four chief aspects of TWIPS will be discussed here; environmental considerations (which will in fact lead to a discussion on pulse separation time), variations in processing, and overall system performance.

5.7.1 Environmental considerations: dockside versus open water

The data shown in this chapter was collected with the acoustic pontoon in two different configurations: restricted statically alongside a dock, and whilst being towed behind a boat travelling in Southampton Water, a high-traffic shipping channel. The results collected in the first configuration certainly appear to be more favourable for showing TWIPS to be useful. In Figure 5.11, the sea-bottom is visible consistently in both the output of both TWIPS and standard sonar, but the bubble cloud is a dominant feature of the standard output whilst TWIPS obscures the bubble scattering completely. In principle, it is impressive that TWIPS is capable of hiding the scatter from a ship while still revealing the location of the sea bottom. However, the fact is that the bottom is simply not hidden within the standard output makes it difficult to argue that TWIPS here offers a technological improvement. To show how TWIPS is in this case beneficial, the information shown in Figure 5.12 is reviewed.

That figure is constructed from the records 200-230 of Figure 5.11, wherein the standard sonar shows only the bubble cloud as the bottom location has been completely obscured. However, by analysing that same data using TWIPS, the bubble cloud response is not only suppressed, but the bottom location is revealed in a single record. The primary drawback here is that the bottom is only visible *once*; and while the peak describing the bottom location is clearly visible, it would nonetheless be desirable to somehow alter the TWIPS algorithm so that the bottom would become visible more often. The results shown in Figure 5.14 and Figure 5.15 seem to offer an explanation for the limitedly impressive performance of TWIPS seen in Figure 5.12. To acquire the data shown in Figure 5.11 and detailed in Figure 5.12, an interpulse time of τ = 50 ms was used.

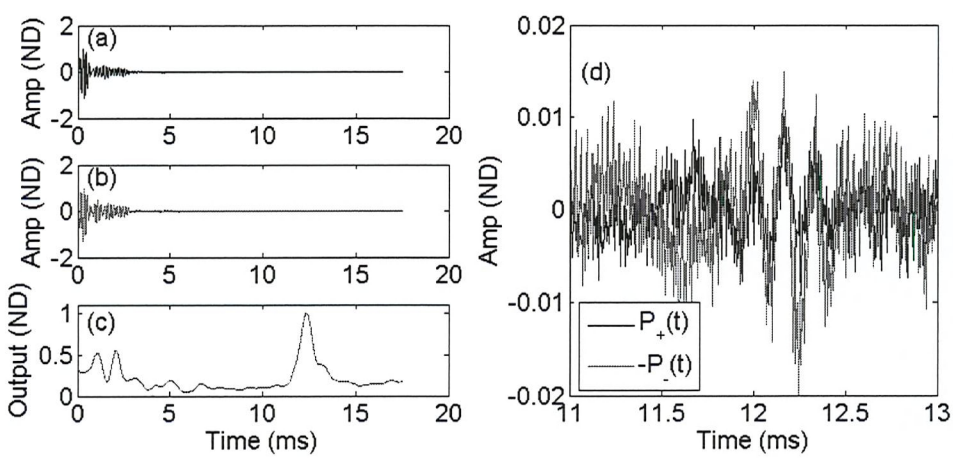

Figure 5.21 A detailed study of record number 75 from in Figure 5.14. "Amp (ND)" here stands for "Amplitude, Non-dimensional". *(a)* The positive return from that record. Bubble scattering (visible in the first few milliseconds) dominates the response. The bottom (near 12 ms) is not readily visible *(b)* The negative return from the same record exhibits the same features as the return from the positive pulse. *(c)* The TWIPS output for this record, when incorporating 5 record geometric means in the denominator. The raw TWIPS output for this record is shown below in Figure 5.22 (at bottom of figure). Note the substantial peak near 12 ms, corresponding to the sea-bottom.

Figure 5.21 above lends some insight into how minute the detail of interest is with respect to the entire time history. In this case, the time record is about 18 ms long, and the visible portion of feature of interest is only 2.5 cycles at 6 kHz (0.4 ms). While one might argue that outgoing signal is 8 cycles at 6 kHz, and so the sought feature must also be this length. However an acoustic wave which must travels through a bubbly environment will tend to be attenuated, and this reduction in level will tend to diminish the amplitude of the detectable signal. When the maximum amplitude of the diminished signal is either equal to or less than the mean acoustic level in the environment being observed, the detectable portion of the wave packet of interest will effectively be shortened.

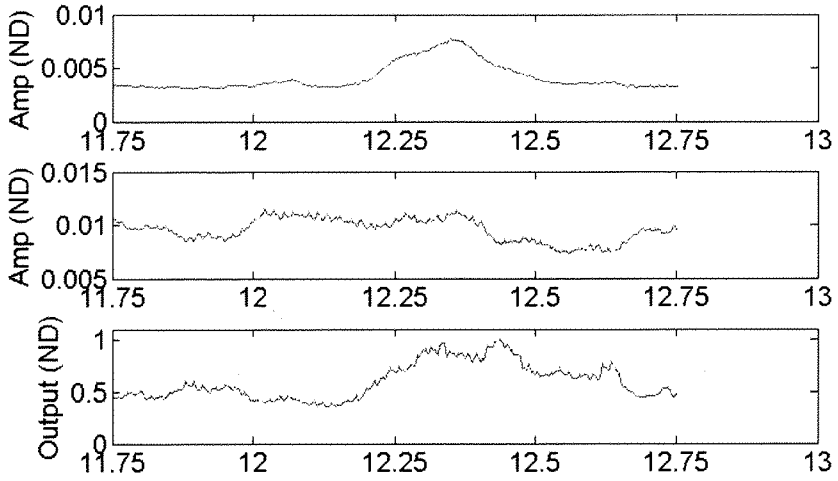

Figure 5.22 Producing the TWIPS output from the data shown in Figure 5.21, after applying rectification and 0.15 ms averaging. At top is shown the smoothed version of P_- . In the middle, the smoothed verison of P_+. At bottom, is shown the ratio P_-/P_+^2, similar to (but less smoothed than) Figure 5.21(*c*), which has had multi-line averaging applied. The non-dimensionalisation applied here is based on the maximum of the entire respective record for each quantity, the whole of which is not shown here.

In the case of the bubble cloud, studied in Figure 5.21 and Figure 5.22, the beginning and ending portions of the emitted Gaussian pulse are not visible; the remaining visible portion of the sought pulse is approximately equal in amplitude to the signal by which it is surrounded[25].

This argument illustrates the point that the backscattering and attenuation affect not only affect the outgoing pulse, but also the return pulse. The laboratory study in the previous chapter was limited to establishing a TWIPS proof-of-concept. The ROC statistics are not necessarily those that might be encountered in the field, because the highly reverberant conditions of the tank altered the degree to which field conditions could be reproduced. Strong multi-path reflections in that test environment dictated that even small changes in target and receiver placement would change the entire reverberant signature within the tank[26]. Further, even though the

---

[25] Using the scale shown above, the RMS level for the signal corresponding to the bottom-reflection is 0.104, while the RMS level for the entire signal for the period extending from after bubble scattering has ended until the end of the record is 0.107.

[26] By moving the receiver by a few centimetres, one could alter the interference pattern such that reflections which were previously invisible became visible, and vice-versa. Similarly, by changing the target orientation by only a few degrees side-to-side or up-down, the target could be made acoustically invisible.

target was the linear scatterer of interest, some of these multi-path reflections were temporally coincident with the source-cloud-receiver travel time. This means that it was never possible in that environment to measure bubble cloud scattering suppression in the absence of coincident though undesirable (and misleading) linear reflections.

However, in the sea trials, large acoustic volumes with a smaller number of reflection boundaries were ensonified than in the tank tests. The decrease in reflection surfaces results in a commensurate reduction in image-sources, which in turn reduces the probability of a boundary-reflected ray arrival at any given point in time [3]. Especially reduced when going from the tank-tests to the sea-trials was the presence of boundary reflections arrivals coincident with the back-scattering from the bubble cloud. As a result, in analysing the sea-trial data, it is possible to break the problem into the two requisite scatterer/target parts. In each figure showing the data acquired in cases where bubbles were present within the water column (Figure 5.11-Figure 5.20) bubble scattering is visible in the standard sonar output in the upper portion of the water column, and yet is not visible in the TWIPS output. It seems clear that the theoretical bubble scattering-abilities of TWIPS are functional in practice. Interestingly, TWIPS seems capable of functionally diminishing bubble scattering well regardless of whether an interpulse delay of 20 ms or 50 ms is used.

However, it seems that small changes in the bubble cloud change the target-receiver path length, and thereby interrupt target detection. The point being made here is that the interference with sonar by bubble scattering is two fold. The first difficulty presented by the presence of a bubble cloud is back-scattering. Back-scattering will tend to affect any sound passing into and/or through a bubble-cloud. It is however particularly bothersome in monostatic active sonar situations where bubbles lie between the send/receive transducer and the target of interest. In that situation, back-scattering not only interferes with the acoustic path between the source and the target, but also on the return acoustic path between the target and the source. These conclusions are summarised in the next section.

5.8 Conclusions

Based on these arguments, one could draw the following conclusions concerning TWIPS performance:

1) Bubble scatter suppression within large bubble clouds is more robust to the effects of cloud evolution than is target detection. Interpulse spacings of as large as several seconds can still give enough acoustic information to result in effective bubble scatter suppression.
2) Target scatter detection is highly sensitive to bubble cloud evolution. Detection ability degraded considerably during sea trials as the interpulse space was increased from 20 ms to 50

ms, from 50 ms to 100 ms, and finally from 100 ms to 5 s. From a detection standpoint, the results obtained with an interpulse time of 5s were unusable.

3) The variability in the performance of TWIPS is a function of bubble cloud evolution during the interpulse pause. Small changes in target-receiver path-length and sound-speed during the pause can result in the already-diminished (see Figure 5.21) signal not being properly aligned during signal summation, thus eliminating the chance of detection.

As described at the beginning of Chapter 4, the acoustic system used for tests was limited in terms of the number of pulses which could be loaded on to it. The conclusions drawn above suggest that the target identification ability of the algorithm could be improved if the inter-pulse timing could be reduced to below τ=20 ms. This option would only be viable if a system were available which allowed very short, high power bursts, or if a mid-power high-bandwidth system was available and would allow production of simultaneous, closely temporally spaced, out of phase sinusoidal frequency sweeps. The next and final chapter will question the way in which Nature deals with the problems encountered when using sonar in littoral water.

6 Cetacean acoustics in bubbly water

> *Although human subtlety may make various inventions which, by the help of various machines reaching the same end, it will never devise an invention more beautiful, nor more simple, nor more to the purpose than Nature does; because in her inventions nothing is lacking, and nothing is superfluous...*
>
> -Leonardo da Vinci[27]

Many types of cetaceans possess extraordinary biosonar abilities [30]. For example, sperm whales are capable of producing transient sounds as loud as 223 dB (peak-to-peak) re 1 μPa RMS at 1 m [135]; and bottlenose dolphins are able to distinguish between the content within various elastic shells using echolocation [136]. As was established at the beginning of Chapter 2, no commercial device exists which is able to echolocate successfully in bubbly waters. In contrast to this human limitation, some dolphins are able to compete successfully in habitats in which bubbles clouds are regularly present, such as coastal waters.

---

[27] Notebook XIV, as translated by Jean Paul Richter in 1888

The focus here is on dolphins which are capable of echolocating in the littoral zone. Shallow waters typically present two impediments to acoustic surveying: scattering by sediments, and scattering by bubbles. This chapter will address the knowledge base concerning ways in which dolphins deal with the challenges presented by sediment scattering, and use known data to draw inferences concerning methodologies dolphins might employ to overcome bubble scattering. It will be seen that some types of animals which inhabit near-shore waters echolocate using dual-pulses of the type employed for TWIPS. Analysis will show however that the amplitudes of the sounds generated by these animals are too low to facilitate the employment of TWIPS. Thus, it remains unknown what competitive advantage is gained by the use of dual pulses by these animals.

It is well-known that the abilities of dolphins to seek, tag, and track certain types of targets far exceeds the tactile abilities of many human-designed platforms. As a practical testament to this fact, the operational Marine Mammal Systems (MMS) arm of the US Navy uses dolphins to find and mark underwater objects. Moore stated that MMS are "an unusual, effective, and unique solution to current problems of mine and obstacle hunting" [137]. Helweg *et al.* [138], after the onset of war in Iraq in which MMS were used extensively [139, 140], stated that "the US Navy's mine-hunting dolphin systems have proven competence in shallow water and very shallow water mine countermeasures". Recent efforts by the Space and Naval

Warfare Systems Center, San Diego (SSC-SD) Biosonar Program Office to construct a dolphin biomimetic sonar (DBS) for use in littoral waters highlight the fact any conceptual advances in the understanding of dolphin biosonar would be well-received by practitioners in the underwater acoustics community. The USN MMS division employs the passive and active acoustic abilities of both bottlenose dolphins (*Tursiops truncatus*) and sea lions (*Zalophus californianus*) [137]. Sea lions (see Figure 6.1), which have exceptionally sensitive hearing [141, 142] and are generally not able to echolocate [143], are employed purely for their passive abilities. Whether other types of mammals are retained within the service is not known, but the potential advantages of employing other species of odontecetes, especially those with competitive advantages in the littoral zone, is an idea explored within this section.

Figure 6.1 POINT LOMA, Calif. (April 12, 2007) - Marine mammal handlers give a demonstration of the Navy Marine Mammal Program. The Navy uses sea lions to mark and retrieve objects and to locate mines. U.S Navy photo by Mass Communication Specialist Seaman Daisy Abonza. (Photo and caption courtesy US Navy NewStand; www.news.navy.mil)

The motivating question here is as follows: If man-made sonar devices are not capable of identifying solid objects in bubble clouds, how is it that some dolphins are capable of competing successfully in environments where bubbles are regularly present in large numbers? This section will proceed as follows. First, it will be argued that the majority of extant scientific knowledge concerning cetacean acoustics is based on studies of a very limited sample of species; all of which are known to compete at least partially in deep waters. It will then be shown that there are relatively under-researched acoustically-active species of odontocetes which for at least 10 million years have competed almost exclusively in littoral waters. Rare, hi-fidelity recordings of these animals will then be analysed to show that acoustic repertoire of these animals contains sounds which appear to share many characteristics with the TWIPS-type signals developed in Chapter 2. These recordings, however, are insufficient to establish with certainty the nature of the vocalisations emitted by these types of dolphins when echolocating in littoral waters. Thus, it will be argued, a that further study of littoral-based acoustically-active odontocetes may yield enormous benefit for the sonar community.

Data will be presented to show that for many cetaceans, the auditory range far exceeds the vocal range. This data will be used to bolster the argument that some cetaceans are dependent enough on nonlinear propagation and/or scattering to have justified the

evolutionary development of sensory abilities capable of taking advantage of these physics.

6.1 Naval exploitation of marine mammal acoustic abilities

The US Navy uses dolphins to locate, tag, and track underwater objects and personnel. As illustrated in Figure 6.2, these dolphins are highly trained, and can be loaded onto dry beds such that they can be redeployed in any theatre worldwide (provided that the water conditions are suitable for the dolphins). The Marine Mammal Systems arm of the US Navy is the most advanced of its type anywhere in the world. The bottlenose dolphins they use are critically important for security operations. Furthermore, as a result of the extensive training undergone by these animals, they are well-suited to the unique needs of behavioural testing. As such, US Navy dolphins have been used for a great number of the bioacoustic studies which have been published in the literature.

It is not surprising that the USN MMS choose to use bottlenose dolphins for their operations requiring advanced acoustic perception. Bottlenose dolphins have outstanding acoustic capabilities, are well-known for being behaviourally robust, and for interacting well with people. Further, in response to their charismatic personalities, many people anthropomorphise dolphins, making them desirable working companions [108]. Bottlenose dolphins are the species of cetacean

most successfully kept in captivity, largely as a result of their ability to survive and thrive in confined tanks [144].

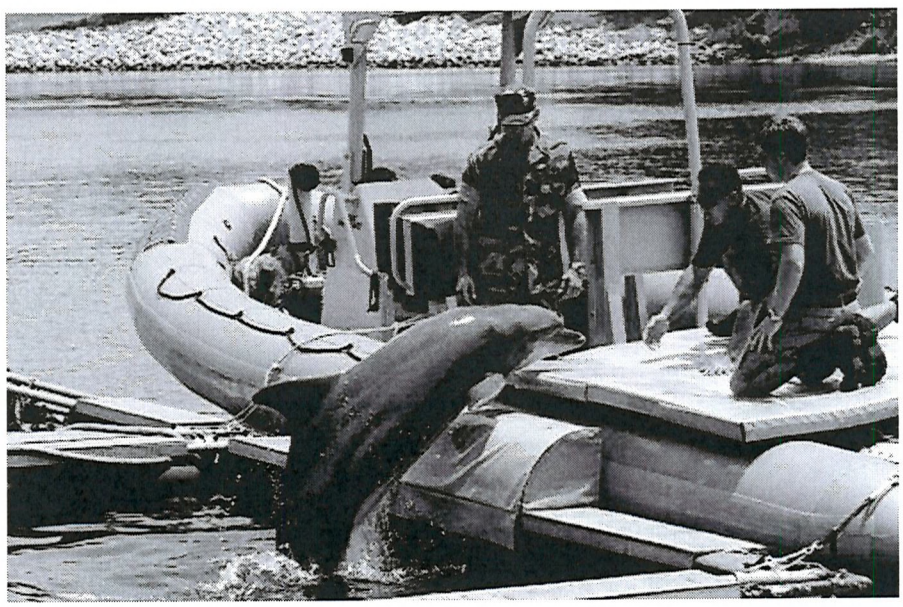

Figure 6.2 PANAMA CITY, Fla. (June 13, 2007) - Aviation Structural Mechanic 2nd Class Shaun McDonald, center, assigned to Naval Special Clearance Team One (NSCT) 1, brings "Ten," a Marine Mammal System (MMS) dolphin, aboard a rigid hull inflatable boat (RHIB) during a demonstration as part of Autonomous Underwater Vehicle (AUV) Fest 2007. Sponsored by the Office of Naval Research (ONR), AUV Fest is the largest in-water demonstration of unmanned underwater, surface, air and ground vehicles ever conducted. U.S. Navy photo by Mr. John F. Williams. (Photo and caption courtesy US Navy NewStand; www.news.navy.mil)

6.2 Biosonar studies on captive marine mammals

As a result of their accessibility and level of comfort with human interaction, captive dolphins are particularly convenient for use in biosonar studies. One would expect then a correlation between those types of cetaceans which are most often found in captivity, and those which are most well-understood. Au has pointed out that there are "very few statistical data on biosonar signals", except from the literature on Bottlenose dolphins (*Tursiops truncatus*), Beluga whales (*Delphinapterus leucas*), and False killer whales (*Pseudorca crassidens*) [145]. Indeed, those species identified as being the most statistically

well-understood are amongst those which are most often found in captivity, as shown in Table 6.1 [144].

Table 6.1 Species of cetaceans which are most commonly kept in captivity, after Mayer [144]

Common name	Species	Natural Habitat
Bottlenose dolphin	*Tursiops truncatus*	Temperate and tropical waters. Absent only from those waters 45 degrees poleward in either hemisphere where the water is too cold to support them. Appear to be two ecotypes: a coastal forma and an offshore form [146].
Orca	*Orcinus orca*	Found in all waters of the world; more abundant in cooler waters. [146].
Beluga	*Delphinapterus leucas*	Arctic/subarctic waters. Found both close to shore and in the open sea. [146].
Pacific white-sided dolphin	*Lagenorhynchus obliquidens*	Temperate waters of the North Pacific; avoids both tropical and Arctic waters [146].
Common dolphin	*Delphinus delphis*	All tropical and warm-temperate waters. Long-beaked: more common in coastal water, short-beaked: more common in offshore waters [146].
Pilot whale	*Globicephala sp*	Both northern and southern hemispheres. Tropical and temperate waters throughout the world [146].
Hawaiian spinner dolphin	*Stenella longirostris*	Hawaiian islands [146]

All of the animals listed in the table above occupy mostly open waters. From an engineering perspective, bioacoustic data gathered on these species is therefore most likely useful for open water missions. However, as stated in the opening chapter of this thesis, modern ocean acoustic research is largely focused on the solution of sonar problems encountered in the littoral zone. While all of the species listed in Table 6.1 spend some amount of their time in the littoral zone, none of them are confined to shallow water. The human ability to study biocapability in the shallow water habitat has therefore been hampered as a result of a limited accessibility to those

cetaceans which specialise in shallow water applications of biosonar. A logical conclusion might then be that the littoral sonar state-of-art could stand to improve based on in-depth studies those acoustically-active cetaceans which compete exclusively or nearly-exclusively in shallow-water habitats. Interestingly, a review of the literature reveals that several of the shallow-water based, acoustically-active cetaceans waters are also associated with the production of pulse sets which at cursory review seem quite similar to TWIPS-type pulses. The next section of this chapter will offer a discussion of what little is known about the effects of bubbles on biosonar.

6.2.1 The effect of bubbles on the echolocation abilities of captive Beluga whales

A review of the literature reveals only one case where the effect of microbubbles on the echolocation abilities of dolphins has been observed in a controlled environment; a 1992 anecdotal publication by Fasick [147]. Fasick, then an animal trainer at the National Aquarium in Baltimore, Maryland, reported that a plumbing malfunction caused large numbers of air bubbles to become entrained in the 1.2 million gallon tank at their facility for a 14-day period. No void fraction or bubble size distribution measurements were performed. The paper does however state that the bubbles were fine enough in size to not rise out under buoyancy, and sufficient enough in number to cause the water appear more opaque than usual. Prior to the plumbing malfunction, Beluga whales captive in the tank regularly performed a

blindfolded echolocation demonstration for live audiences. The demonstration is described as follows:

> Eyecups are first placed over a whale's eyes. The whale is then sent on a retrieval behavior before the first ring is thrown to the left of the center deck. The whale hears the splash of the ring and gains directional information of the ring's proximity in the pool. Echolocation may then be used to pinpoint the ring's exact location. Upon finding the first ring, the whale must then locate the second ring which is thrown to the right of the center deck, approximately thrity feet from the first ring. The whale again turns in the direction of the splash and pinpoints the exact location by echolocation. Performance criteria for this behavior is that both rings are located and brought back to the center deck ... All three beluga whales performed this behavior at criteria level prior to the [bubble] entrapment situation. However, for eleven days ... coincident with the period when air bubbles were entrapped in the water, the whale's echolocation performance was exceptionally poor. Rings were sometimes located perfectly, but more often either one or both of the rings were not located. No similar problems with this behavior have been recorded in the past and no other behaviors appeared to be affected by the air entrapment problem ... Upon the realization that the air in the water may be interfering with the whales' echolocation capabilities, the echolocation behavior was omitted from the daily presentations until the air entrapment was eliminated ... When the echolocation behavior was tested [following the reduction of air entrapment], the whales performed it to the previously established criterion level.

This interesting source proves that cetacean echolocation abilities can be affected negatively by bubbles suspended within the water column. However, it might be wondered whether the whales in question

previously had the ability to overcome bubble scattering, and lost that ability once they became accustomed to bubble-free conditions in captivity. Such a degradation in behavioural capability is not unheard of, especially for feeding-related abilities [45].

6.3 Acoustic mammals in littoral waters

The point has already been made in this chapter that most marine bioacoustic data has been collected from animals which are often found in open (non-littoral) waters. This section will study what is known of the vocal repertoire for those acoustically-active mammals which spend the majority of their lives in littoral waters.

In 2004, Leighton [24] published the hypothesis that twin inverted pulses might be used to detect solid objects in bubbly water. The computational study published by Leighton *et al.* [24] and presented at the beginning of Chapter 2 followed that approach, and showed the twin-pulse hypothesis to be a viable solution to the problem of interest [72]. Subsequent to the 2004 twin-pulse proposal by Leighton, Li *et al.* [148], showed that the Yangtze finless porpoise creates pulses of similar form to those proposed in Leighton *et al.*, as shown below in Figure 6.3.

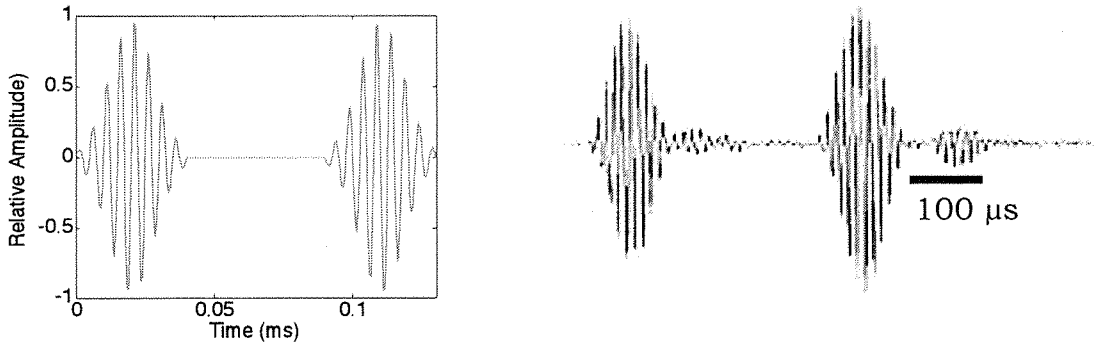

(a) *(b)*

Figure 6.3 *(a)* A pulse recommended by Leighton *et al.* [72] for the purpose of detection of solid objects in bubbly water. *(b)* A Yangtze finless porpoise echolocation pulse published by Li *et al.* [148].

The striking visual similarity between the acoustic pulse designed by our group (Figure 6.3 *(a)*), and the Finless porpoise pulse reported by Li *et al.* (Figure 6.3 *(b)*) led to the following question: *Do some* odontocetes *use TWIPS-type pulses to "see" through bubble clouds?* This section will now proceed by reviewing what is known about various odontocetes and double-pulse vocalisations. It will be seen that all species which are associated with double- and multiple-pulses[28] (listed in Table 6.2) inhabit littoral waters exclusively or nearly exclusively.

Further, it will be seen that, while some species of mammal may produce audio signals which are similar to those shown in Figure 6.3

---

[28] "Dual-pulses" and "multi-pulses" are defined within the body of the text later in this chapter. "Dual pulses" are those signals where a second, equi-amplitude, phase reversed, apparent echo follows an initial pulse. "Multi-pulses" are acoustic structures which are similar in form to dual pulses, but consist of many apparent echoes.

(b), the amplitude of these bioacoustic signals is too low to be effective in generating bubble nonlinearities. This limit in signal amplitude means that TWIPS does not appear to be a method in use by the odontocetes considered here. Listed below in Table 6.2 are all-known species which produce signals of the type (or similar to that) which is shown in Figure 6.3.

Table 6.2 Cetaceans associated with dual- and multi-pulses

Genus	Species	Primary Habitat		
Cephalorhynchus	Hector's dolphin, *Cephalorhynchus hectori*	Coastal New Zealand, often in estuaries	Dawson [34]	
	Commerson's dolphin, *Cephalorhynchus commersonii*	Coastal East Argentina, South Chile, & Indian Ocean	Goodall *et al.* [149]; Kamminga & Wiersma [150]; Evans *et al.* [151]	**I**
	Heaviside dolphin, *Cephalorhynchus heavisidii*	West coast of South Africa	Watkins *et al.* [152]	**II**
	Chilean/Black dolphin, *Cephalorhynchus eutropia*	Coastal Chile	Watkins *et al.* [153, 154], Götz *et al.* [155]	
Phocoena	Finless Porpoise, *Neophocoena phocaena*	Coastal Asia.	Li *et al.* [156]	**III**
	Dall's porpoise, *Phocoena dalli*	Coastal and non-coastal, warm temperate to sub-arctic waters of the Northern Pacific Ocean.	Evans *et al.* [151], Awbrey *et al.* [157].	**IV**

Group I: Have been recorded (single hydrophone) sustained sets of equal-amplitude pulses with constant separation times

Group II: Near-shore habitats, but the authors have found no recordings

Group III: Equal amplitude phase inverted pulses which Li *et al.* [154] call surface reflections

Group IV: Some evidence of multiple pulses but no evidence of equal amplitude

The pulse-production abilities of each of the species mentioned in Table 6.2 will now be considered in more detail.

6.3.1 The Yangtze finless porpoise (*Neophocaena phocaeniodes*)

The Yangtze finless porpoise is one of three subspecies of finless porpoise, and can only be found in the Yangtze River and shallow waters surrounding China. This mammal and its geographic distribution are depicted in Figure 6.4. There are no known reports of finless porpoise sightings in deep water in the literature. The finless porpoise is listed as endangered [158]. The scientific community has benefited greatly from the efforts of three particular scientists who have documented and studied the acoustic abilities of this rare animal: Kexiong Wang and Ding Wang, both of the Institute of Hydrobiology within the Chinese Academy of Sciences, and Tomonari Akamatsu of the National Research Institute of Fisheries in Japan [154, 156, 159-172].

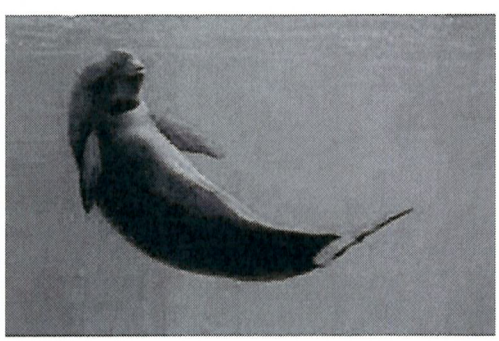

(a) *(b)*

Figure 6.4 (a) The Yangtze Finless porpoise (used with written permission from Dr Michael Noonan, University of Cansus). (b) a map showing the geographic distribution of the Yangtze Finless Porpoise. Map distributed and reproduced under the GNU Free Documentation License.

Figure 6.3 was presented because of the striking visual similarity between the sound produced by the finless porpoise (published by Li *et al.* [148]) and the TWIPS source sound designed by Leighton *et al.*

[24]. Those two pulses share many features. Each acoustic signal appears to be comprised chiefly of two 8-10 cycle tone-bursts, each of which is within a Gaussian envelope. In both cases, the pulse emissions are separated by a time period approximately equivalent to the length of two tone-bursts. In the case of the sound designed for the computer simulation (Figure 6.3. *(a)*), there is only silence between the two pulses. However, in the figure depicting the alleged acoustic emission of the finless porpoise, there are artefacts which are visually similar to the two chief pulses, but reduced in amplitude by a factor of about five.

If the pulse shown in Figure 6.3 *(b)* consisted of (1) two inverse pulses and (2) high-amplitude energy, then it is conceivable that the sound could be used to identify solid objects in bubbly water via a methodology similar to TWIPS. To address these two queries, each of the authors listed on the paper in which the pulse was printed were contacted. During correspondence with one of the authors, Songhai Li, it was established both that no reference sound had been recorded (meaning that amplitude information was not available), and that a digital version of the data was not available for analysis by our group [173].

In a publication by Li *et al.* [154] on the structure of pulse trains produced by finless porpoises, it is pointed out that finless porpoises often produce sounds containing a so-called double-pulse or multi-

pulse structure. In these cases, there appears a tone burst of length τ_{burst} followed by a rest and then a second tone burst, usually of a length which is approximately equal to τ_{burst} of the first sound. The onset of these acoustic emissions is separated temporally by a gap τ_{delay}. The quantity τ_{delay} is usually somewhere between 1 and 3 times longer than τ_{burst}. If this pulse pattern appears once (pulse, pause, pulse), it is termed a "double-pulse" structure. If the pulse pattern repeats itself many times, it is termed a "multi-pulse" structure. Examples of these types of sounds are shown in Figure 6.5. The double- and multi-pulse structures exhibit two features which are of particular interest from the perspective of this dissertation:

(1) Each successive pulse is opposite in phase to the preceding pulse within any multi-pulse set.

(2) The individual tone burst components of any given double- and multi- pulse structure are at least equal in magnitude in both of the examples given by Li *et al.* [154], and twenty of the examples shown by Li *et al.* [156]. In several of the examples, the magnitude of the second pulse *exceeds* that of the first.

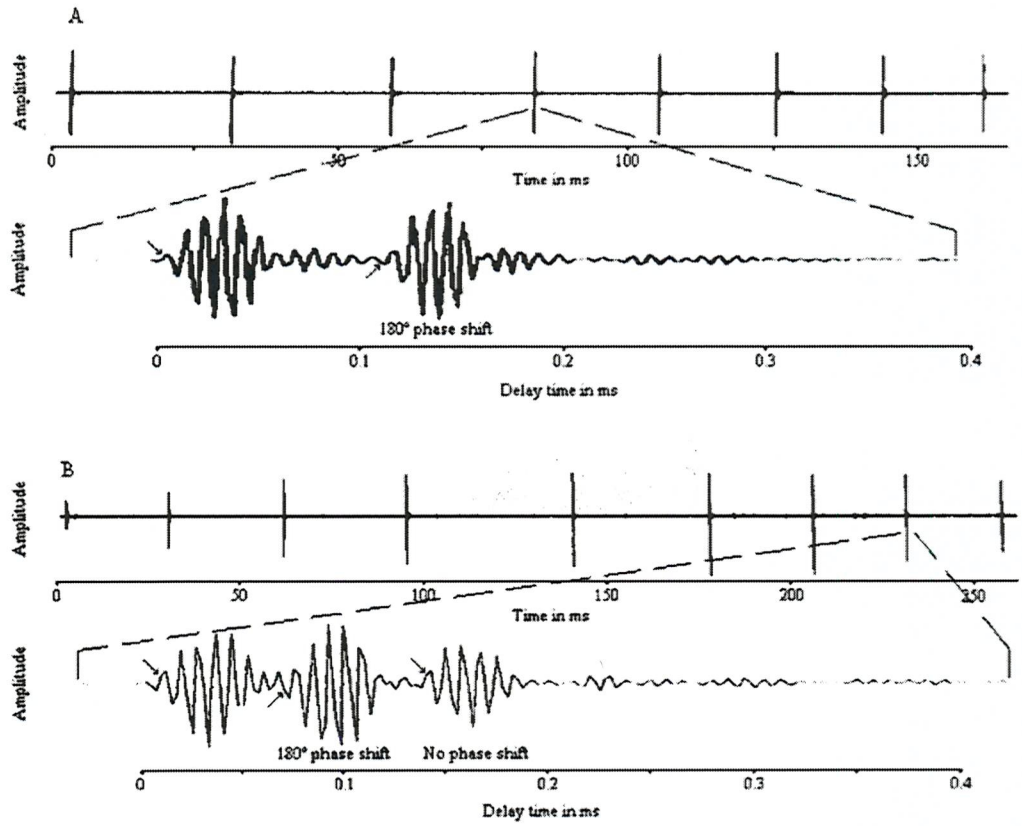

Figure 6.5 (A) Double-pulse and (B) multi-pulse structure, recorded in presence of Yangtze finless porpoise, figure from Li *et al.* [154]

After reporting the sounds emitted by the finless porpoise [156], Li *et al.* noted the inverted-phase relation between successive pulses (feature 1 above), and published a second paper [154] based on a hypothesis concerning the origin of the clicks. They observed that finless porpoises would emit echolocation pulses, which would be subsequently received by their hydrophones. They then hypothesised that later "echoes" within the multi-pulse structures are the result of reflections off the sea-air interface, where the impedance mismatch is such that water-borne incident sounds give way to water-borne phase-reversed reflections (see 4.1.3). They then calculated the delay between the initial and subsequent pulses τ_{delay} to estimate the

distance between the porpoise and the hydrophone using the method demonstrated with the vocalisations of spinner dolphins (*Stenella longirostris*) by Lammers *et al.* [174] and Aubauer *et al.* [175]. In the case of multi-pulse structures where there are three or more distinct acoustic peaks, the third peak was generally observed to be in phase with the first peak. Li *et al.* [154] suggest that these pulses are the result of bottom-reflections.

It is posited here (following the original position of Kamminga and Wiersma [150]) that these multiple pulses are not the result of surface and bottom reflections, but rather are all vocalisations generated directly by the porpoises in question. This proposition is based on amplitude considerations, as will now be explained. Feature (2) highlighted above pertained to the fact that the peak amplitude for individual pulses within a multi-pulse click may remain equal or may even increase with time. Such a feature would be highly unlikely were the multi-pulse structures to be the result of surface reflections.

It was explained in 4.1.3 using data published by Medwin [1] that reflections of water-borne sounds off the sea-air interface tend to have an amplitude which is much less than the incident sound. The calculation used there has been adapted to more closely represent the situation in question as shown in Figure 6.6.

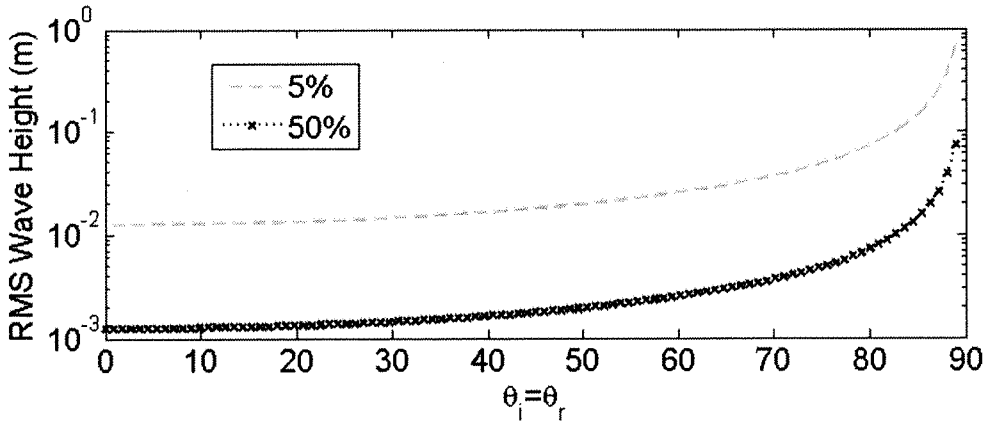

Figure 6.6 These curves describe for energy at 115 kHz and at angles of incidence from $0° \leq \theta_i \leq 89°$ the wave-height which will give perfect reflections for no more than than the specified percentage of incident rays (based on extrapolation from Medwin [1]).

This figure shows how unlikely it is to receive reflection off of a pressure-release surface of amplitude equal to the input signal. To understand how to compare the output from this analysis to the assumptions of Li *et al.* [154], it is necessary to estimate the angle at which reflections would have had to occur when vocalisations were travelling from the porpoises to the receiver. The receiver in that paper was placed in four different locations, all of which were located beyond the exterior limit of the porpoise pen. For a porpoise located halfway down into the water column, the angles of reflection (according to the approach used for Figure 6.6) would have been between 87 and 89.5 degrees. At that angle of reflection, the probability of a reflection of amplitude equal to the incoming pulse for an RMS wave height of more than a centimetre is less than 50%. However, in the 20 pulses shown in Figure 3 of Li *et al.* [163], the amplitude of the second pulse is at least equal to that of the first pulse in 100% of the examples. Even more unusual is the fact that the amplitude of the second pulse

exceeds that of the first in 90% of the examples! The authors acknowledge this problem, and introduce the negligence of geometric spreading within their model, saying:

> "If we account for the loss of transmission caused by the spherical or cylindrical spread and absorption of signals in water, it is difficult to explain the phenomenon of equal or higher amplitude of the second of third pulse than of the initial pulse in double- and multi-pulse clicks. However, considering the transmission beam pattern of echolocation signals [145], this phenomenon may have been caused by on-axis reflections and off-axis direct incidence"

In other words, Li *et al.* are suggesting that the initial arrival may have been in a side lobe, while the later arrival (which they suggest to be a reflection) emanated from the main lobe.

Aubauer *et al.* [175] pioneered the use of a single hydrophone for the estimation of source-distance estimates based on the time gap between an initial arrival and the subsequent arrival of its reflection by the surface. In that paper, the source-receiver geometry was relatively similar to that used in Li *et al.* [154], as per Table 6.3 below.

Table 6.3 A comparison of the conditions under which Aubauer *et al.* [175] and Li *et al.* [154] recording their data.

Mammal under study (Author)	Depth of transducer (measured) (m)	Depth of phonating animals (calculated) (m)	Approximate range to phonating animals (m)
Spinner dolphin (Aubauer *et al.* [175])	3	0.8-3.0	61-67 m
Finless porpoise (Li *et al.* [154])	0.7/1.4	0.5 – 2.5	~50 m

However, despite the relative similarity in geometry between the two setups, Aubauer makes no mention of reflections having amplitude anywhere near that of the incident pulse. In fact, in a published sample pulse train, the reflections are very small indeed when compared to their corresponding direct signals, as shown in Figure 6.7 below.

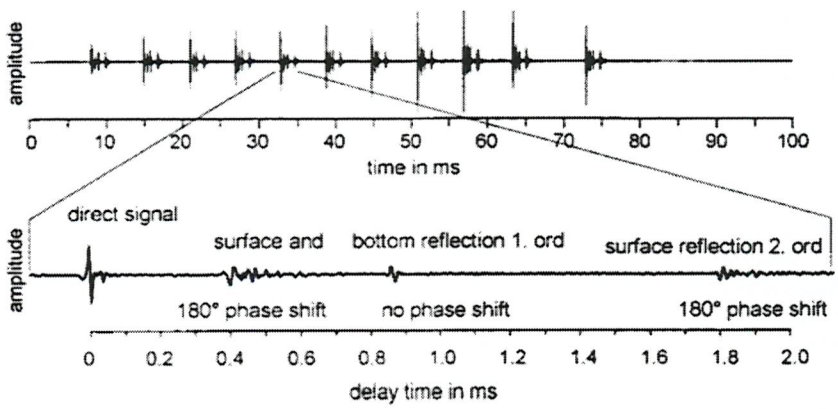

Figure 6.7 (*Top*) Spinner dolphin burst pulse signal with multipath propagation recorded in shallow waters along the Waianae Coast of Oahu. The sequence is shown in the time-domain, interclick interval 5-10 ms. (*Bottom*) Enlargement of a single burst pulse with first- and second-order multipath propagation. (Caption and figure after Aubauer *et al.* [175]).

The hypothesis of Li *et al.* [154] that in this case the double- and multi-pulse artefacts observed were the result of surface reflection may be plausible. However, the probabilistic reflection amplitude expectation calculated by Medwin [1] and the experimental result of

Aubauer *et al.* [175] can be used to inform an analysis of the results of Li *et al.* [154] (compare the equi-amplitude apparent echoes in Figure 6.5 with the reduced amplitude true echoes found in Figure 6.7). Such an analysis suggests that the results of Li *et al.* are not conclusive. Indeed Au [145] writes that "it is often difficult to discern whether multiple pulses are being emitted by the animal or are the result of surface reflections. The animal-hydrophone geometry must be known, or several consecutive signals from a moving animal must be recorded." The most straightforward way to establish without uncertainty the source of this phenomenon would be to employ multiple hydrophones [20, 176-178]. If the animals themselves were creating these reversed-phase pulse structures, it would be instructive to consider why these animals had gone to the trouble of developing the unique ability. It might be posited that the habitat in which the finless porpoise thrives has motivated the development of some acoustic solution which calls upon the use of equi-amplitude phase reversed pulses. A test for this logic would be to consider other regions in the world containing similar habitats (*e.g.* shallow, turbid waters), and to look for other animals which may have evolved similar abilities [179].

One genus of dolphins which occupy a habitat similar to that inhabited by the finless porpoise is that of *Cephalorhynchus*. It will be seen in the next section that there is reason to believe that these cetaceans also generate equi-ampltitude phase-reversed pulses.

6.3.2 Genus *Cephalorhynchus*

In 1981, Kamminga and Wiersma [150] published a paper analysing the sounds of the harbour porpoise (*Phoceona phocoena*), the beluga whale (*Delphinapterus leuca*), and Commersons dolphin (*Cephalorhynchus commersonii*). It was found that recordings made in the presence of each of these animals revealed pulse trains where, upon closer examination, it was seen that each pulse contained one or more "sub-pulses". As the 1980's progressed, the problem of dolphin by-catch in fishing nets began to receive increased attention from biologists and acousticians whom sought to reduce the tendency for dolphins to get caught in fishing nets. Members of the genus *Cephalorhynchus* seemed particularly susceptible to gill-nets; a considerable concern, as at the time *Cephalorhynchus* was not well-understood by the scientific community, but assumed to be rare (This assumption was eventually justified by abundance studies. All four species of *Cephalorhynchus* are currently recognised as being endangered [180]). To this end, a report was issued by the International Whaling Commission, entitled Biology of the genus *Cephalorhynchus* [181]. This report elucidates the sounds made by most members of this genus, and suggests that Commerson's dolphin (*Cephalorhynchus commersonii*), Hector's dolphin (*Cephalorhynchus hectori*), and the Chilean dolphin (*Cephalorhynchus eutropia*), all make double- and triple-pulses. A study on Heaviside's dolphin (*Cephalorhynchus heavisidii*) is included in the IWC report cited above, but that publication contains no information on the acoustic

emissions of that species. These double- and triple- pulses were termed "multiple pulses" by both Dawson [34] and Evans *et al.* [151].

On that basis, this document now turns to consider multiple pulses as the dolphins within this genus. *Cephalorhynchus* is comprised of four dolphins: Hectors dolphin (*Cephalorhynchus hectori*), Commerson's dolphin (*Cephalorhynchus commersonii*), the Chilean (or Black) dolphin (*Cephalorhynchus eutropia*), and Heaviside's dolphin (*Cephalorhynchus heavisidii*). These species inhabit a widespread but discontinuous distribution of habitats, all which of can be described as being "similar types of neritic environments, including estuarine river bars, surf zones, and headlands" [182]. These habitats are spread around the Southern hemisphere, as shown in Figure 6.8. Based on evidence gained during a study of mitochondrial DNA, Pichler *et al.* [182] have attempted to map the development of the genus. They hypothesise that *Cephalorhynchus* developed in West Africa, and then dispersed eastward towards New Zealand and continued east to South America. The South American population moved northwards with the glaciation of Tierra del Fuego, where the Chilean dolphin and Commerson's dolphin formed. They also propose that the population of Commerson's dolphin which exists in the Kerguelen Islands and the Cook Strait (within the Southern Ocean between Africa and Australia) arrived more recently; perhaps even within the last 10000 years).

While the vocal repertoire for some dolphins is very well-known, very little acoustic data has been collected on these dolphins. That information which has been published suggests strongly that they are capable of generating equi-amplitude phase-reversed pulses [150].

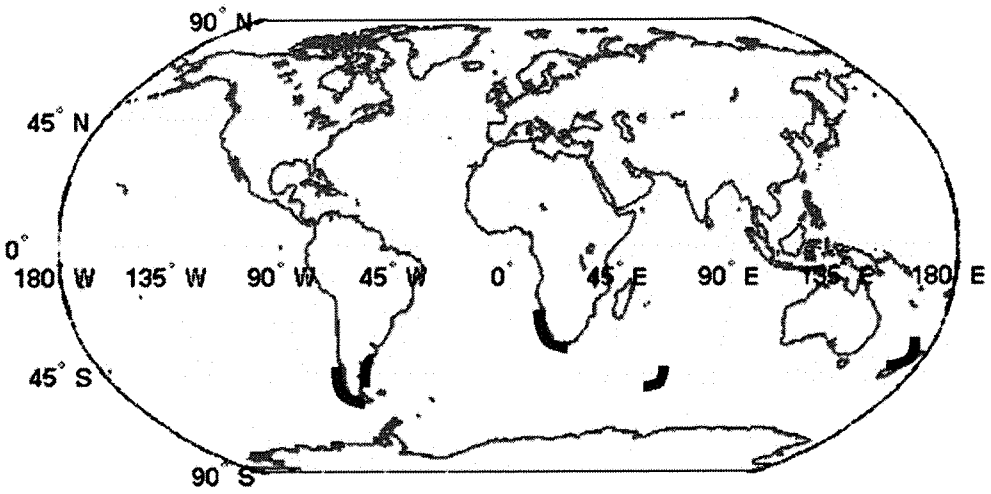

Figure 6.8 Shown as dark black are regions which are known to be inhabited by members of the genus *Cephalorhynchus* as described by Pichler *et al.* [182].

6.3.2.1 Hector's dolphin, *Cephalorhynchus hectori*

Of all the species in this genus, Hector's dolphin is the most well-documented acoustically. This endangered species is common to New Zealand waters, and is fragmented into at least three genetically distinct subpopulations [183]. Two of the subspecies inhabit the South Island, while the third inhabits the North Island. This third set is now recognised as a distinct subspecies, Maui's dolphin (*Cephalorhynchus hectori maui*). Hector's dolphins have a marked preference for inshore waters, and are rarely seen more than 4 nautical miles offshore [184]. Oliver noted in 1922 that this species is

"never seen far from the coast" [185]. This species, like others in the genera, is small, with adults measuring between 1.2 and 1.6 m and weighing only about 50 kg.

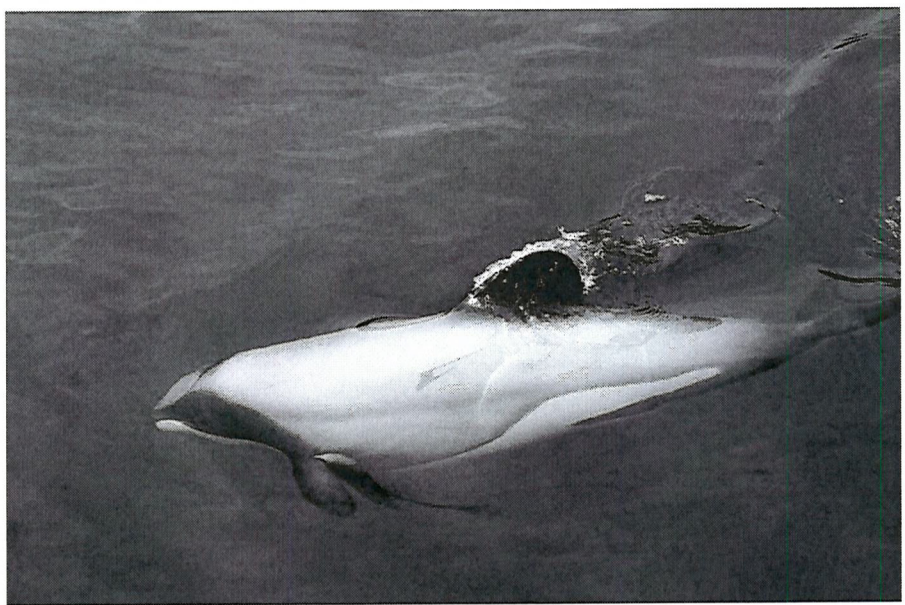

Figure 6.9 A Hector's dolphin. Note the rounded dorsal fin, a characteristic feature within this genera (Photo by James Shook and distributed under the Creative Commons license).

Digitally-captured acoustic recordings of Hector's dolphin vocalisations captured by Dr Steve Dawson[29] were sent to the author for study. The data was analysed in the interest of revealing any presence of twin inverted pulses, where the second pulse in a pair represents an inverted version of the first pulse. The data was taken on 27 and 30 January 2003 in Flea Bay on Banks Peninsula NZ in 12 m of water. Hydrophone depth was about 10 meters. The recordings were made using an analogue instrumentation recorder (Racal Store 4

---

[29] Dr Steve Dawson [steve.sawson@stonebow.otago.ac.nz], Department of Marine Science, University of Otago, Dunedin, New Zealand

DS 150 Hz – 160 kHz +/- 1 dB) and a Sonatech 8178 hydrophone (100 Hz – 160 kHz +/- 3 dB). The preamplifier used to record the hydrophone output was reported by Dr Dawson to have a flat frequency response over the frequencies contained within the vocalisations analysed here. The sounds were digitised at an effective sampling rate of 353 kHz (16 bit).

An initial visual inspection of the Hector's dolphin data revealed several possible candidates for inverted pulse pairs. A single example was chosen randomly for the discussion here.

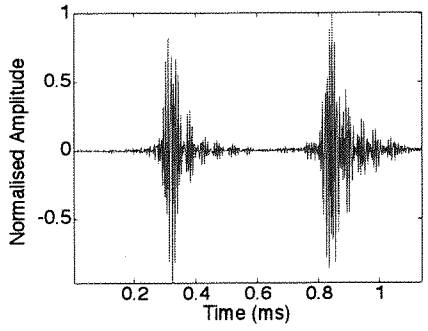

Figure 6.10 An example of a segment of a recording of vocalisations by Hector's dolphin.

The example shown in Figure 6.10 at first glance exhibits some qualities that one might expect to see in a pulse inverted pair. By breaking visually the sample into two segments (0-0.6 ms and 0.6-1.2 ms), it appears that the first segment contains a negative asymmetry with a single strong minimum near 0.35 ms, while the second segment contains a positive asymmetry with a single strong maximum just after 0.8 ms. This heuristic analysis suggests that further investigation for evidence that the second segment is an inverted

version of the first version is worthwhile.

The auto-correlation for an 10x oversampled version of the signal shown in Figure 6.10 was analysed, and shows that the second segment is very nearly the inverse of the second segment (See Appendix 2 for a definition of the inverse of a signal). A review a single 6-second recordings set by Dawson contained 214 echolocation pulses, 132 of which were identified as being double pulses. The data set analysed, though adequate for documenting basic features of sounds generated by Hector's dolphin, was not well-suited in its raw state for phase analysis. Phase-matching requires higher sampling rates than does more general analysis, because the features of interest are necessarily small scale with respect to the length of the overall echolocation waveform.

The available Hector's dolphin data was sampled at f_s = 353 kHz giving a folding frequency $f_s/2$ = of 176.5 kHz, the folding frequency being the upper limit for meaningful frequency information for the ensemble. A power spectral density of the 401-point click recording shown in Figure 6.10 was made using the Welch method with a 100 point Hamming windows and 50% overlap. Those results are shown below in Figure 6.11.

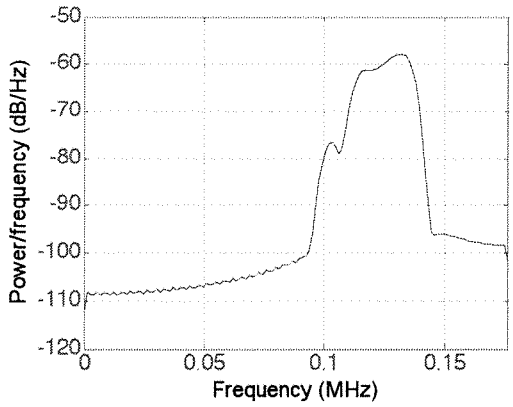

Figure 6.11 Frequency content of click shown in previous slide.

The important point to notice in Figure 6.11 is that the majority of the click energy is near the folding frequency. The main peak extends from near 100 kHz to the acquisition limit near 140 kHz. This indicates that perhaps some information relevant to the click analysed has been lost as a result of undersampling. Having presented the relevant data on Hector's dolphin, the extant data on Hector's dolphin, the next section presents the small amount of data on Commerson's dolphin which exists.

6.3.2.2 Commerson's dolphin (*Cephalorhynchus commersonii)*

Commerson's dolphin is distributed in two locations: the east coast of South America, and in the Kerguluelen Islands some 8000 km to the east of the Argentinean coastline. Although as remarked above Commerson's dolphin tends to occupy only near-shore waters, at least one vagrant dolphin of this species has been observed off the African continental subshelf some 4000 km from the nearest distribution limits [186]. Despite the fact that several Commerson's dolphins exist

within captivity [187] very little has been published concerning the acoustic vocalisations of the species. Watkins *et al.* [152] reported having made acoustical observations of this species during a cruise on the R/V Hero in December 1966 using equipment capable of recording frequencies from 60 – 10000 Hz. In that work, the authors concluded that this species was only capable of producing low-level sounds. However, in 1980, Watkins and Schevill re-studied vocalisations of *C. commersonii* [153] and recognised that in fact the sounds generated by this species contain significant energy up to "at least 100 kHz", in contrast to the conclusions of their earlier study. Kamminga and Wiersma in 1980 [150] studied captive samples of Commerson's dolphin at the Duisburg Zoo. These dolphins were in the same tanks as a small pod Belgua whales, but the authors observed that their recordings "did not appear to be disrupted by the sounds of the Beluga, because of the abundant sonar production of the Cephalorhynchus." Interestingly, although Kamminga and Wiersma went to the trouble of submerging two hydrophones (separated vertically by 15 cm) they never analysed the synchronicity of the two signals to establish whether in fact the observed multiple pulses emanated directly from the animals.

A detail of the individual components within a single pulse train recorded by Kamminga and Wiersma has been reproduced below in Figure 6.12. The energy within these signals is centred near 120 kHz, 20 kHz above the upper limit for vocalisations of *C. commersonii*

estimated by Watkins and Schevill [153].

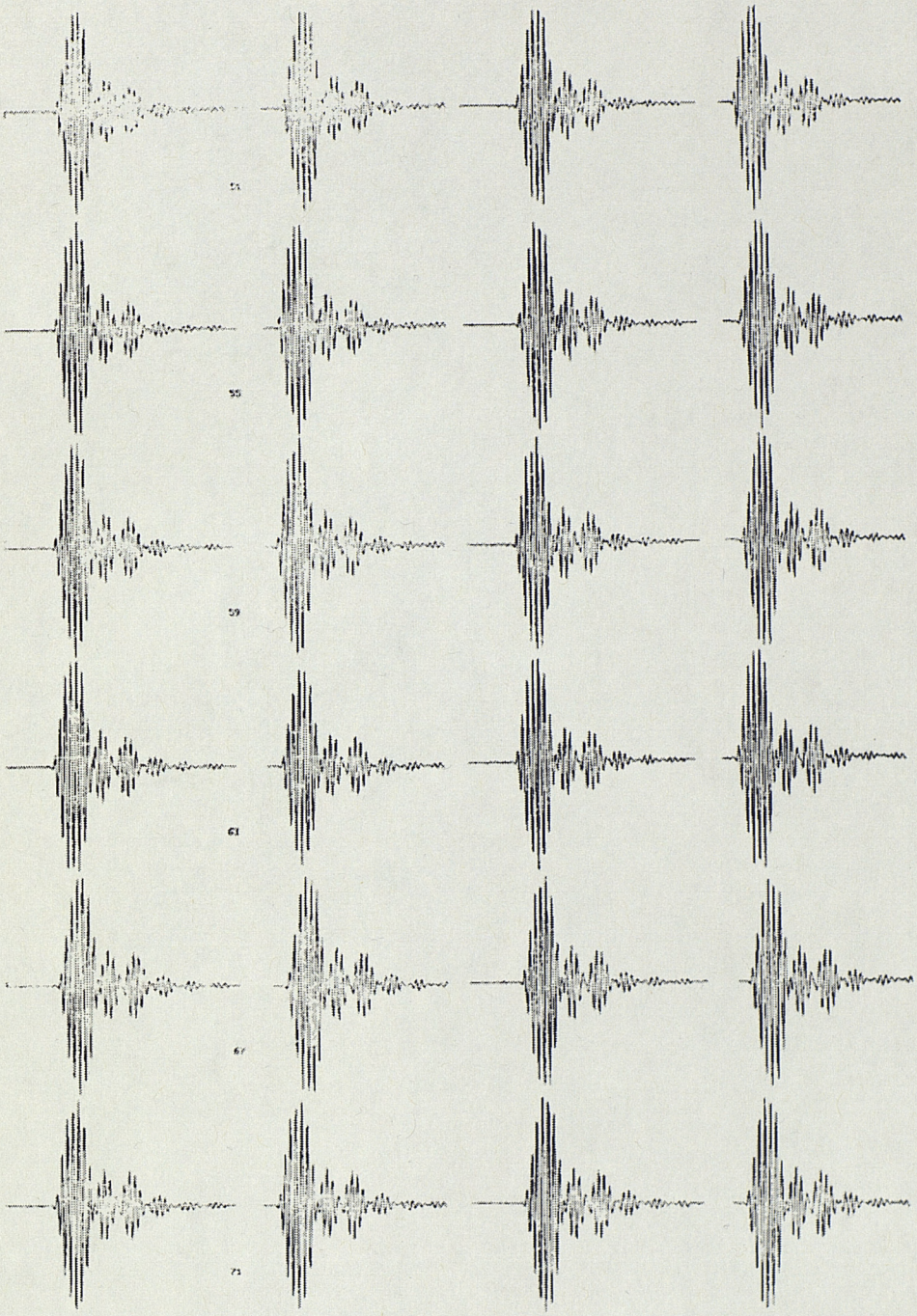

Figure 6.12 Sequence of successive pulses, taken from Kamminga and Wiersma [150]

Each multiple pulse observed in that study was observed to consist of several sequential tone packets (a tone packet here is a limited bandwidth 5-10 cycle signal with a Gaussian envelope). At first study,

a trained underwater acoustician might suggest that presence of secondary pulses is indicative of reflection-boundary interactions within the propagation path. Were this to be the case, then the first pulse to arrive would be the sound emanated by the porpoise, and the secondary pulses would be the result of reflections from either the air-sea interface or sea-bottom. Kamminga and Wiersma state that the multiple pulse structures they recorded appeared to be temporally steady for a given animal during a given pulse sequence, meaning that the inter-pulse rate did not appear to change over multiple pulses. Based on that data, the authors drew the following conclusion [150] :

> There is no doubt, in our opinion, that these reverberations are characteristic of the sound-producing mechanism and possibly its propagation path along the dolphin's head and are therefore inevitably connected to the emitted sonar pulse.

While this conclusion is indeed consistent with the concept proposed in this chapter, Kamminga and Wiersma lack evidence for this statement. If the dolphin/hydrophone geometry was static during the click-train, then the reverberation structure resulting from multi-paths exterior to the dolphin's head would be unchanging. The only conclusive way to determine the source of these clicks would have been through the use of multiple receivers – a technique which the authors did not employ. Nonetheless, it is worth noting that the cited experts feel strongly that the multiple-pulse structure shown in Figure 6.12 was generated directly by the dolphin under observation. Evans *et al.* [151] state that "Commerson's dolphins also produce double

pulses", but did not show any evidence to this effect.

Dziedzic and Bueffrenil [188] produced a publication on the study of sounds produced by the Commerson's dolphins of the Kerguelen Islands. In that study, it was attempted to measure the emissions of free-ranging dolphins in a fjord, but their vocalisations were masked by ambient noise. Two animals were then captured and secluded in a creek within a 6 x 6 x 2.6 m cage built with a 10 cm x 10 cm mesh. These specimens were kept there for 65 hours, during which time their acoustic emissions below 130 kHz were monitored continuously. The sounds reported were "similar to reports for other populations" [188], though the centre-frequency for tone packets was 116 kHz whereas Kamminga and Wiersma [150] observed a centre-frequency of 120 kHz in their South American study. Dziedzic and Bueffrenil noted a reduction in vocal activity with increasing time in activity – a behaviour the authors identified as a symptom of stress. There was no report of any production of double pulses by the animals observed in that study.

6.3.2.3 Heaviside's dolphin (*Cephalorhynchus heavisidii*)

Heaviside's dolphins are found around the tip of South Africa and along the West coast to Nambia [189]. It is similar in size to the other members of this genus, and is also generally only seen in coastal settings. Reeves *et al.* [190] state that this species generally occurs in waters less than 100 m deep, but has been seen up to 45 nautical

miles in water as deep as 180 m. Watkins *et al.* [152] made the only known acoustic field observations of this species in the 1970's, but the equipment used in those observations was unable to record signals higher than 10000 Hz.

6.3.2.4 Chilean/Black dolphin (*Cephalorhynchus eutropia*)

The Chilean dolphin was labelled in 2002 by Folkens *et al.* [190] as one of the "most poorly studied cetaceans". Consistent with this observation, very few little is known about the vocal repertoire of this species [191]. This lack of information is presumably a result of the fact that the Chilean dolphin lives only in waters which are difficult to access, and so comes into contact with humans only rarely compared to the other more visible members of the genus. According to Goodall [149]:

> [T]he Chilean dolphin inhabits two distinct areas: (1) the channels from Cape Horn to Isla Chiloé and (2) open coasts, bays and river mouths north of Chiloé, such as waters near Valdivia and Concepción. It seems to prefer areas with rapid tidal flow, tide rips, and shallow waters over banks at the entrance to fjords. The dolphins readily enter estuaries and rivers.

Watkins *et al.* [152] attempted in 1977 to record the sounds of *C. eutropia*, but heard only very low level sounds described as "a series of rapid pulses, up to 500 per second, produced in a somewhat stereotyped sequence. The sound varied in duration from 0.4-2.0 seconds." The equipment used by Watkins *et al.* however had an upper limit near 30 kHz. As Goodall *et al.* [149] point out, if the

operating frequency used by *C. eutropia* is similar to that used by of *C. commersonii* and *C. hectori* (120-150 kHz), it would be unsurprising that the low frequency recording equipment used by Watkins *et al.* [152] captured returned only low level signals.

In 2005, Götz, Antunes, and Heinrich [155] made recordings of free-ranging Chilean dolphins using a two-element vertical array. In correspondence, Antunes informed the author that he had identified "many cases of clicks that could fit in [the] double- [or] multiple-pulse category". No data was available for review by the author. As such, it continues to be unconfirmed that the Chilean dolphin is capable of generating double- or multiple- pulses

In reviewing the genus *Cephalorhynchus,* it has been shown that the available acoustic data either suggests that each species is capable of producing double pulses, or is too sparse to rule out that possibility.

6.3.3 Dall's porpoise (*Phocoena dalli*)

Some evidence exists which suggests that Dall's porpoise (*Phocoena dalli*) is capable of generating double pulses [151]. This habitat of this mammal is not restricted to the near-shore zone, unlike the other species which have been mentioned in this chapter so far. It is found over the continental shelf and in offshore waters from approximately the US – Mexico border (32 °N) and central Japan (35 °N) north to the Bering and Okhotsk seas; but not in the shallow north-eastern Bering

Sea [190]. In oceanic waters, Dall's porpoise can be found in the central North Pacific north of 41°N. In general, this animal has a preference for deep (more than 600 ft/180 m), cool (less than 63°F/17°C) waters. Some Dall's porpoises shift seasonally from north and offshore in summer to south and inshore in winter."[190]

Evan's *et al.* [151] describe the double pulses they observed from Dall's porpoise as follows:

> Each component of a double pulse is only about half as long as a single pulse and may show considerable amplitude modulation. The first component shows more spectral broadening above the dominant frequency of 139 kHz than the second component because of its more pronounced frequency modulation and higher harmonics at the beginning"

6.3.4 Summary concerning the production of twin pulses by free-ranging marine mammals

The major hindrance in determining the mammals discussed do in fact generate TWIPS-type pulses is the lack of acoustic records which were taken in a manner specifically designed to determine the relevant features of the pulses. As stated above, the sampling frequency must be sufficiently great to allow robust analysis of the phase. Multi-element acquisition systems should be used to show undoubtedly that multi-pulses emanate from the species in question, and are not the result of environmental reflections as some investigators have proposed [192].

Sound level information concerning echolocation clicks generated by the members of *Cephalorhynchus* is limited, but no sounds louder than 160 dB have been recorded. This could either indicate that indeed these dolphins are relatively quiet (as compared for instance to Bottlenose dolphins *Tursiops truncatus* which are capable of generating clicks as loud as 228 dB (peak-to-peak) re 1 μPa RMS, or that all of the calibrated recordings gathered to date have not been on-axis observations (a possibility, given the narrow beam-widths which have been reported in the literature [34, 193]).

As was stated earlier, the purpose of this chapter is not necessarily to propose that dolphins and porpoises employ TWIPS-type processing. Rather, it is proposed that some actively-echolocating marine mammals which live almost exclusively in shallow waters have evolved the unique ability to generate high-frequency phase-inverted pulse-sets. These sounds happen to be similar to those sounds used in conjunction with TWIPS, but higher in frequency by more than an order of magnitude, and lower in level by 50-60 dB [34]. The fact that no other marine mammals are known to possess this ability suggests that these sounds somehow facilitate successful echolocation in the littoral acoustic environment. A computational exercise was carried out to determine whether it is in fact a plausible proposition that any of the animals which seem to produce phase-inversed pulse pairs are capalble of employing TWIPS. This method requires nonlinear responses by a majority of bubbles within the ensonified cloud. It turns out that this hypothesis can be ruled out simply through the analysis of an idealised best-case sceneario, where all of the bubbles within the cloud are coincident with the resonant frequency of the ensonifying pulse. Hector's dolphin has been observed creating twin-inverted echolocation pulses of the type shown in Figure 6.10 with a centre frequency of around 120 kHz and an amplitude of 160 dB re 1μPa at 1 m. Here, that signal is idealised as a band-limited twin pulse of the type shown in Figure 6.3 (a), and used to ensonify a single bubble of the size which would be at resonance at 120 kHz (that is a bubble having an undisturbed radius of aroud 160 microns; see equation (2.2)). The pressure radiated to a distance of 1 meter from this ensonified bubble has been calculated and is shown in Figure 6.13.

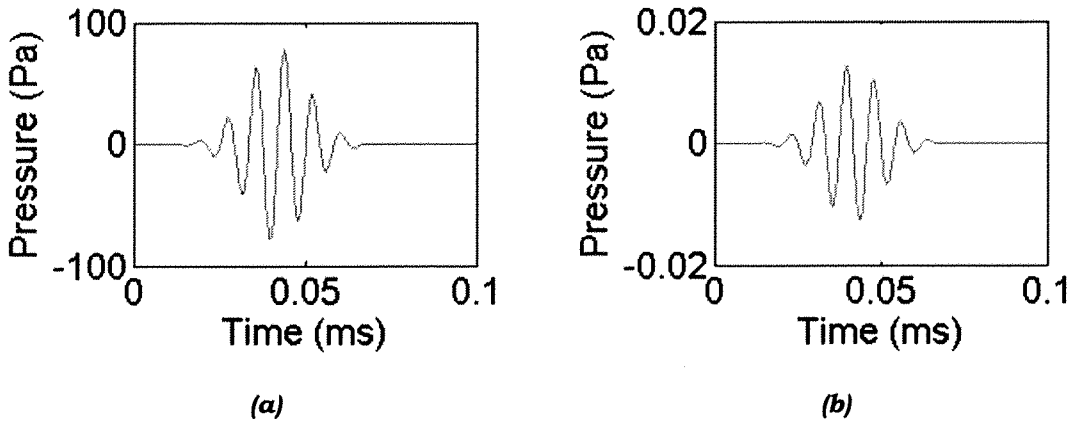

Figure 6.13 This calculation, an idealised best-case scenario test case, has been performed to evaluate whether or not any known dolphins might use TWIPS. The pulse emission by a Hector's dolphin used in the model (160 dB re1μPa at 1 m) as shown in *(a)* has been used to excite a resonant bubble which is a distance of 1 m from the acoustic centre of the mammal. The calculated pressure reradiation by that bubble to a distance of 1 m has been shown in *(b)* The lack of superharmonics in the bubble suggests that it is unlikely that members of the genus *Cephalorhynchus* employ TWIPS as a method for identifying food and assisting navigation. Bubble dynamics calculated using the Herring-Keller formulation as shown in (2.8) [46] [47].

Figure 6.13 shows that even the bubble most likely to display nonlinear behaviour, a resonant bubble near the source, has responded linearly to the input sound. This means that certainly no other bubbles within the field respond nonlinearly, which suggests that TWIPS is not being used by any of the dolphins which have been discussed here. It should be noted that marine mammal observations tend to be performed in calm conditions, where bubble populations are minimal. The lack of dense bubble clouds may dictate that these mammals do not have a need to echolocate at high levels at the time of observation.

6.4 Conclusions

Here it has been suggested that sonar studies would benefit from an increase in the number acoustic surveys which are dedicated to the

study of coastal-based marine mammals. This impetus is coincident with a parallel effort which is already underway in the conservation community. As a result of the fact that coastal habitats are often disturbed by human activities, dolphins and porpoises that thrive in those settings face serious conservation threats. Some investigators have already begun to call for an increase in abundance studies of marine mammals in coastal habitats so that the human impact on Natural life in these habitats can be understood quantitatively [194]. It would behove the scientific community at large to ensure that the researchers who are now being funded to perform abundance studies in coastal and riverine habitats are also in possession of acoustic data-acquisition equipment.

It was shown to be likely that several types of cetaceans, including the finless porpoise and all members of the genus *Cephalorhynchus*, generate dual- and multiple-pulse signals. These assertations cannot be confirmed until field-researchers acquire more data on these species. It was seen that those species that may produce dual- and multiple- pulses do not seem to generate sounds at levels very much greater than 160 dB. This information was used to inform the development of a brief computational study, the results of which led to the conclusions that those animals which might generate dual- and multiple-pulses probably do not use TWIPS.

7 Conclusions

This thesis has documented the development, from theoretical concept to sea trial, of a technology which has been shown to represent an advance in the state of the art in littoral sonar. This concluding chapter will be used to summarise the results, and to offer some insight into ways in which TWIPS research might proceed.

It was shown in Chapter 1 that conflicts are increasingly taking place in shallow waters, and that the navies of the world require significant technological advances if they are to protect successfully the littoral environment. In Chapter 2, the Twin Inverted Pulse Sonar (TWIPS) concept was introduced. The principals behind this method were developed by first reviewing basic bubble dynamics, and then studying ways in which this theory had been used by other investigators to increase bubble contrast in ultrasonic biomedical imaging. The Pulse Inversion (PI) method was modified and adapted according to the conditions predicted beneath a breaking wave to develop TWIPS. A computationally-developed TWIPS virtual proof-of-concept was then presented, and it was shown that this method could successfully detect the presence of a target TS = -25 dB within an oceanic bubble cloud containing 35 million bubbles. The results seemed to indicate that the proposed algorithm is capable of operating with a very low false-alarm rate. It was also argued in this chapter that the TWIPS

concept could find application not only in sonar applications, but also in biomedical ultrasound and technologies which are based on electromagnetic radiation, such as radar and lidar.

Based on the success of the computational study, it was decided to develop a laboratory test to evaluate the practicability of TWIPS. The transferability of these results to the ocean would be completely dependent on the degree to which the bubble cloud used in the experiment resembled the types of clouds encountered in the ocean. As a result, Chapter 3 was dedicated to a review of the literature on bubble clouds, both naturally-occurring and artificially produced. That chapter ended with the presentation and evaluation of the Bubbly Fluid Generator (BFG), a device capable of producing bubble clouds sufficiently ocean-like to facilitate the sought data transferability.

The TWIPS hypothesis was then tested on bubble clouds produced in a controlled environment. During those tests, it was seen that the target resulted in occasional high-amplitude detection spikes, while the bubbles almost never resulted in such returns – a result consistent with the predictions of the computational study. The usefulness of these results were studied using ROC charts, which were used to establish that TWIPS is capable of operating as a conservative detector. For such a system, high values can be achieved for the ratio of true positive rate to false negative rate ($Q(D_1 \mid n_1):Q$

($D_1|n_0$)). In practical terms, this means that the use of a sufficiently high threshold gave occasional positive returns, almost all of which were true positives. As a result, it was predicted that a field-implementation of TWIPS would almost certainly require high numbers of acoustic returns (on the order of tens) in order to facilitate correct decisions.

After the development of a laboratory-based proof-of-concept for TWIPS, a field trial was developed to test the system in real-world conditions as described in Chapter 5. The trial was conducted in two stages: the first stage was conducted with a down-firing static acoustic source/receiver system mounted alongside a marina dock. The second stage was conducted with the same acoustic source/receiver system dragged behind R/V Bill Conway which navigated through a shipping channel. In the first set of tests, bubbles were generated using a nearby RIB. In the second set of experiments, bubbles were generated using either the same RIB, the R/V Bill Conway, or passing ships. The dockside results showed that TWIPS enabled the detection of the sea-bottom when that feature was either not visible or highly obscured within the standard sonar output. The results of the open-water tests showed a lower percentage of bottom-detections than did the dock-side results; a result which was argued to be a function of the long path-length associated with the deeper water encountered in the shipping channel. In both the dockside and open-water results, the most striking difference between

the standard sonar output and that of TWIPS occurred in the top two meters of the water column. In that region, where the bubbles were located, back-scattering dominated the standard sonar output, while the TWIPS algorithm concealed this undesirable feature almost entirely. Such bubble-scattering suppression is an important and useful feature of this new technology. As argued in the body of the text, a useful system for detecting the presence of objects in bubbly water.

In Chapter 6, it was shown that inverted pulse sets of the type developed for use with TWIPS have also been detected by biological researchers during field studies on some types of marine mammals. Particular attention was paid to the sounds of the finless porpoise, and all of the members of the genus *Cephalorhynchus* (including Hector's dolphin, Heaviside's dolphin, the Chilean dolphin, and Commerson's dolphin); all of which inhabit littoral waters almost exclusively. The limited information available on vocalisations of the members of *Cephalorhynchus* suggests that these animals may be able to generate controlled pulse sets wherein each successive pulse is 180° out of phase with the last. Similarly, it was suggested that the Finless porpoise may have such a capability. It was shown that surprisingly little acoustic data exists for acoustically-active marine mammals which inhabit only littoral waters.

Given the current strategic importance of the littoral zone, and the

deficit in knowledge concerning acoustic know-how in that environment, it seems prudent for researchers to develop the knowledge base on acoustically active inhabitants of littoral waters. It stands to reason that those animals which have competed in that environment for the last several tens of millions of years may have evolved acoustic solutions which have so far eluded the sonar community.

8 References

[1] H. Medwin, "Specular scattering of underwater sound from a wind-drive surface," *Journal of the Acoustical Society of America,* vol. 41, p. 1485, 1967.

[2] C. S. Clay and H. Medwin, *Acoustical Oceanography: Principals and Applications.* New York, 1977.

[3] A. D. Pierce, *Acoustics : an introduction to its physical principles and applications.* New York: McGraw-Hill Book Co., 1981.

[4] T. G. Leighton, "Guest editorial," *Applied Acoustics special issue on 'The detection of buried marine targets',* vol. 69, pp. 385-386, 2008.

[5] R. D. Kaplan, "How we would fight China," in *The Atlantic Monthly.* vol. 295, 2005.

[6] S. E. Johnson, "'Silent Hammer' will test SSGN as clandenstine base," in *Sea Power,* 2004.

[7] M. Yaalon, "Ethical dilemmas in counterterroism," *Azure,* pp. 55-63, Autumn 2007.

[8] J. C. Preisig and G. B. Deane, "Surface wave focusing and acoustic communications in the surf zone," *Journal of the Acoustical Society of America,* vol. 116, pp. 2067-2080, Oct 2004.

[9] P. D. Thorne, P. J. Hardcastle, and R. L. Soulsby, "Analysis of acoustic measurements of suspended sediments," *Journal of Geophysical Research-Oceans,* vol. 98, pp. 899-910, Jan 15 1993.

[10] D. C. Finfer, T. G. Leighton, and P. R. White, "Issues relating to the use of 61.5 dB conversion factor when comparing airborne and underwater anthropogenic noise levels," *Applied Acoustics,* vol. 69, pp. 464-471, 2008.

[11] T. G. Leighton, *The Acoustic Bubble.* London: Academic Press, 1994.

[12] J. X. Zhou and X. Z. Zhang, "Shallow-water reverberation level: Measurement technique and initial reference values," *IEEE Journal of Oceanic Engineering,* vol. 30, pp. 832-842, Oct 2005.

[13] Cheif, Naval Operations, "The United States Navy in "Desert Shield"/"Desert Storm": Summary Report," Navy Historical Centre, 1991.

[14] O. Kreisher, "Service experts eye 'leap ahead' in mine warfare capabilities," in *Sea Power,* 2004.

[15] A. G. Davies and P. D. Thorne, "Advances in the study of moving sediments and evolving seabeds," *Surveys in Geophysics,* vol. 29, pp. 1-36, 2008.

[16] "China's military might: The long march to be a superpower," in *The Economist* London, 2007.

[17] R. O'Rourke, "China modernization: Implications for U.S. Navy capabilities - background and issues for Congress," Congress Research Service, Order Code: RL33153, 2007.

[18] R. O'Rourke, "China Modernization: Implications for U.S. Navy Capabilities - Background and Issues for Congress," Congressional Research Service, Order Code: RL33153, 2007.

[19] "Navy acquisitions improved littoral war-fighting capabilities needed : report to the Chairman and ranking minority member Subcommittee on Military Research and Development Committee on Armed Services House of Representatives," in *GAO-01-493*: US GAO, 2001.

[20] J. L. Spiesberger, "Hyperbolic location errors due to insufficient numbers of receivers," *Journal of the Acoustical Society of America,* vol. 109, pp. 3076-79, 2001.

[21] R. J. Urick, *Principles of underwater sound,* 3rd ed. New York: McGraw-Hill, 1983.

[22] M. V. Trevorrow, S. Vagle, and D. M. Farmer, "Acoustical Measurements of Microbubbles within Ship Wakes," *Journal of the Acoustical Society of America,* vol. 95, pp. 1922-1930, Apr 1994.

[23] S. A. Thorpe, "On the clouds of bubbles formed by breaking wind-waves in

deep water, and their role in air-sea gas transfer," *Philosophical Transactions of the Royal Society of London A (Mathematical and Physical Sciences),* vol. 304, pp. 155-210, 1982.

[24] T. G. Leighton, "From seas to surgeries, from babbling brooks to baby scans: The acoustics of gas bubbles in liquids," *International Journal of Modern Physics B,* vol. 18, pp. 3267-3314, Oct 20 2004.

[25] T. G. Leighton, "What is ultrasound?," *Progress in Biophysics and Molecular Biology,* vol. 93, pp. 3-83, 2007.

[26] F. A. Duck, *Physical properties of tissue : a comprehensive reference book.* London ; San Diego: Academic Press, 1990.

[27] F. M. White, *Fluid Mechanics,* 3rd ed. St. Louis: McGraw-Hill Inc., 1994.

[28] D. H. Simpson and P. N. Burns, "Pulse inversion Doppler: a new method for detecting nonlinear echoes from microbubble contrast agents," in *1997 IEEE Ultrasonics symposium,* 1997, pp. 1597-1600.

[29] C. C. Shen and P. C. Li, "Pulse-inversion-based fundamental imaging for contrast detection," *IEEE Transactions on Ultrasonics Ferroelectrics and Frequency Control,* vol. 50, pp. 1124-1133, Sep 2003.

[30] H. L. Roitblat, W. W. L. Au, P. E. Nachtigall, R. Shizumura, and G. Moons, "Sonar recognition of targets embedded in sediment," *Neural Netw.,* vol. 8, pp. 1263-1273, 1995.

[31] R. L. Brownell, Jr. and G. P. Donovan, "Biology of the genus *Cephalorhynchus,*" in *Reports of the International Whaling Commission - Sepcial Issue 9* Cambridge, 1988.

[32] T. G. Leighton, P. R. White, D. C. Finfer, and S. D. Richards, "Cetacean acoustics in bubbly water," in *Proceedings of the International Conference "Underwater Acoustic Measurements: Technologies & Results",* Heraklion, Crete, 2005.

[33] T. G. Leighton, D. C. Finfer, and P. R. White, "Bubble acoustics: What can we learn from cetaceans about contrast enhancement?," in *IEEE International Ultrasonics Symposium,* Rotterdam, 2005, pp. 964-73.

[34] S. M. Dawson, "The high-frequency sounds of Hector's dolphins *Cephalorhynchus hectori,*" *Rep. Int. Whal. Commn. Spec. Issue,* vol. 9, pp. 339-344, 1988.

[35] S. D. Richards, A. D. Heathershaw, and P. D. Thorne, "The effect of suspended particulate matter on sound attenuation in seawater," *Journal of the Acoustical Society of America,* vol. 100, pp. 1447-1450, Sep 1996.

[36] A. Tesei, A. Maguer, W. L. J. Fox, R. Lim, and H. Schmidt, "Measurements and modeling of acoustic scattering from partially and completely buried spherical shells," *Journal of the Acoustical Society of America,* vol. 112, pp. 1817-1830, November 2002.

[37] R. Lim, J. L. Lopes, R. H. Hackman, and D. G. Todoroff, "Scattering by objects buried in underwater sediments: Theory and experiment," *Journal of the Acoustical Society of America,* vol. 93, pp. 1762-1783, April 1993.

[38] N. Lalor, "Fundamentals of vibration," in *Fundamentals of Noise and Vibration,* F. J. Fahy and J. G. Walker, Eds. New York: E&FN Spon, 1998.

[39] R. J. Pinnington, "Fundamental principles of measurement and analysis techniques," in *Fundamentals of Noise and Vibration,* F. J. Fahy and J. G. Walker, Eds. London: E&FN Spon, 1998.

[40] A. V. Oppenheim and R. W. Schafer, *Discrete-time signal processing,* 2nd ed. London: Prentice-Hall, 1989.

[41] M. H. Safar, "The exploitation of the subharmonic pressure waves from pulsating gas bubbles in an acoustic field in liquids," *J. Phys. D: Appl. Phys,* vol. 3, pp. 635-636, 1970.

[42] L. Rayleigh, "On the pressure developed in a liquid during the collapse of a spherical cavity," 1917.

[43] M. S. Plesset, "The dynamics of cavitation bubbles," *American Society of Mechanical Engineers - Journal of Applied Mechanics,* vol. 16, pp. 228-231, 1949.

[44] C. E. Brennen, *Cavitation and Bubble Dynamics.* Oxford: Oxford University

Press, 1995.
[45] D. C. Finfer, "Biological sources of acoustic transients in the English Channel and adjacent waters," in *Institute of Sound and Vibration Research.* vol. MSc Southampton: University of Southampton, MSc Thesis, 2005, p. 139.
[46] J. B. Keller and M. Miksis, "Bubble oscillations of large amplitude," *Journal of the Acoustical Society of America,* vol. 68, pp. 628-633.
[47] C. Herring, "Theory of the pulsations of the gas bubble produced by an underwater explosion," *OSRD Report 236.*
[48] T. Sheljaskow, "Bi-layer PZT/polymer composite 1D 2.5 MHz Phased Array," in *IEEE Ultrasonics Symposium,* 2000.
[49] R. Gramiak and P. M. Shah, "Echocardiography of the aortic root," *Investigative Radiology,* vol. 3, pp. 356-366, 1968.
[50] N. d. Jong, P. Frinking, F. t. Cate, and P. v. d. Wouw, "Characteristics of Contrast Agents and 2D Imaging," in *1996 IEEE Ultrasonics Symposium,* 1996, pp. 1449-1458.
[51] R. Y. Nishi, "Ultrasonic detection of bubbles with Doppler flow transducers," *Ultrasonics,* vol. 10, pp. 173-179, 1972.
[52] D. H. Simpson, C. T. Chin, and P. N. Burns, "Pulse inversion Doppler: A new method for detecting nonlinear echoes from microbubble contrast agents," *IEEE Transactions on Ultrasonics Ferroelectrics and Frequency Control,* vol. 46, pp. 372-382, 1999.
[53] W. M. Fairbank and M. O. Scully, "A new noninvasive technique for cardiac pressure measurement: resonant scattering of ultrasound from bubbles," *IEEE Transactions on Biomedical Engineering,* vol. BME-24, pp. 107-114, 1977.
[54] D. L. Miller, "Ultrasonic detection of resonant cavitation bubbles in a flow tube by their second harmonic emissions," *Ultrasonics,* vol. 19, pp. 217-224, 1981.
[55] M. Vacher, G. Gimenez, and R. Goutte, "Nonlinear behavior of microbubbles: application to their ultrasonic detection," *Acustica,* vol. 54, pp. 274-283, March 1984.
[56] R. S. Meltzer, E. G. Tickner, T. P. Sahines, and R. L. Popp, "The source of ultrasound contrast effect," *Journal of Clinical Ultrasound,* vol. 8, pp. 121-127, 1980.
[57] J. E. Powers, P. N. Burns, and J. Souquet, "Imaging instrumentation for ultrasound contrast agents," in *Advances in echo imaging using contrast enhancement* Norwell, MA: Kluwer, 1997, pp. 139-170.
[58] V. L. Newhouse and P. M. Shankar, "Bubble size measurements using the nonlinear mixing of two frequencies," *Journal of the Acoustical Society of America,* vol. 75, pp. 1473-1477, 1984.
[59] P. M. Shankar, J. Y. Chapelon, and V. L. Newhouse, "Fluid pressure measurement using bubbles insonified by two frequencies," *Ultrasonics,* vol. 24, pp. 333-336, 1986.
[60] V. A. Akulichev, V. A. Bulanov, and V. A. Klenin, "Acoustic sensing of gas bubbles in the ocean medium," *Soviet Physics - Acoustics,* vol. 32, pp. 177-180, 1986.
[61] D. Koller, Y. Li, P. M. Shankar, and V. L. Newhouse, "High-speed bubble sizing using the double frequency technique for oceanographic applications," *IEEE Journal of Oceanic Engineering,* vol. 17, July 1992.
[62] A. D. Phelps and T. G. Leighton, "High-resolution bubble sizing through detection of the subharmonic response with a two-frequency excitation technique," *Journal of the Acoustical Society of America,* vol. 99, pp. 1985-1992, 1996.
[63] A. M. Sutin, S. W. Yoon, E. J. Kim, and I. N. Didenkulov, "Nonlinear acoustic method for bubble density measurements in water," *Journal of the Acoustical Society of America,* vol. 105, pp. 2377-2384, 1998.
[64] L. A. Ostrovsky and A. M. Sutin, "Nonlinear acoustic diagnostics of discrete inhomogeneities in liquids and solids," *Proceedings of the 11th International Congress on Acousitcs,* vol. 2, pp. 137-140, 1983.
[65] L. A. Ostrovsky and A. M. Sutin, "Nonlinear sound scattering from sub-surface

bubble layer," in *Natural physical sources of underwater sound*, B. R. Kerman, Ed. Dordrecht: Kluwer academic, 1993, pp. 363-370.

[66] T. G. Leighton, D. C. Finfer, and P. R. White, "Experimental evidence for enhanced target detection by sonar in bubbly water," *Hydroacoustics*, vol. 11, pp. 181-202, 2008.

[67] M. Minnaert, "On musical air-bubbles and sounds of running water," *Philisophical Magazine*, vol. 16, pp. 235-248, 1933.

[68] C. M. Close and D. K. Fredrerick, *Modeling and Analysis of Dynamic Systems*. New York: John Wiley & Sons, Inc (published previously by Houghton Mifflin Company), 1995.

[69] W. H. Munk and F. Zachariasen, "Refraction of Sound by Islands and Seamounts," *Journal of Atmospheric and Oceanic Technology*, vol. 8, pp. 554-574, Aug 1991.

[70] T. G. Leighton, P. R. White, and D. C. Finfer, "Detection of Objects in Bubbly Water," United Kingdom, 2005.

[71] T. G. Leighton, "Nonlinear bubble dynamics and the effects on propagation through near-surface bubble layers," *High Frequency Ocean Acoustics*, vol. 728, pp. 180-193, 2004.

[72] T. G. Leighton, P. R. White, and D. C. Finfer, "Possible applications of bubble acoustics in nature," *Proceedings of the 28th Scandinavian Symposium on Physical Acoustics, Ustaoset, Norway*, 2005.

[73] T. G. Leighton, D. C. Finfer, and P. R. White, "Cavitation and cetacean," *Revista de Acustica*, vol. 38, pp. 37-81, 2007.

[74] T. G. Leighton, D. C. Finfer, and P. R. White, "Cavitation and Cetacean," in *Proceedings of the 19th International Congress on Acoustics* Madrid, Spain, 2007, pp. 1-31.

[75] T. G. Leighton, D. C. Finfer, and P. R. White, "Sonar which penetrates bubble clouds (Invited Paper)," in *Proceedings of the Second International Conference on Underwater Acoustic Measurements, Technologies and Results*, Crete, Greece, 2007, pp. 555-562.

[76] T. G. Leighton, P. R. White, and D. C. Finfer, "Bubble acoustics in shallow water: Possible applications in nature," in *International Conference on Boundary Influences in High Frequency, Shallow Water Acoustics*, Bath, UK, 2005, pp. 433-40.

[77] T. G. Leighton, P. R. White, D. C. Finfer, and S. D. Richards, "Cetacean acoustics in bubbly water (Invited Paper)," in *Proceedings of the International Conference on Underwater Acoustic Measurements, Technologies and Results*, Heraklion, Crete, 2005, pp. 891-8.

[78] T. G. Leighton, D. C. Finfer, and P. R. White, "Hypotheses on the exploitation of bubble acoustics by cetaceans (Abstract-only)," *Journal of the Acoustical Society of America*, vol. 121, p. 3039, 2007.

[79] T. G. Leighton, P. R. White, and D. C. Finfer, "Hypotheses regarding exploitation of bubble acoustics by cetaceans," in *Proceedings of the 9th European Conference on Underwater Acoustics*, Paris, France, 2008, pp. 77-82.

[80] S. Kumar and C. E. Brennen, "Nonlinear effects in the dynamics of clouds of bubbles," *Journal of the Acoustical Society of America*, vol. 89, pp. 707-714, Feb 1991.

[81] D. Chu and L. C. Hufnagle, "Time varying gain (TVG) measurements of a multibeam echo sounder," in *IEEE Oceans 2006*, Boston, MA, 2006, pp. 1-6.

[82] A. D. Phelps and T. G. Leighton, "Measurement of bubble populations near the sea surface using combination frequencies: adaptation and calibration of device between two sea trials," in *Natural physical processes associated with sea surface sound*, Southampton, England, 1997, pp. 198-210.

[83] S. Vagle and H. Burch, "Acoustic measurements of the sound-speed profile in the bubbly wake formed by a small motor boat," *Journal of the Acoustical Society of America*, vol. 117, pp. 153-163, Jan 2005.

[84] M. Trevorrow, "High-frequency acoustic scattering and absorption effects within ship wakes," in *Boundary Influences in High Frequency, Shallow Water*

Acoustics, University of Bath, UK, 2005, pp. 439-446.

[85] A. D. Phelps and T. G. Leighton, "Oceanic bubble population measurements using a buoy-deployed combination frequency technique," *IEEE Journal of Oceanic Engineering*, vol. 23, pp. 400-410, October 1998.

[86] M. Buckingham and M. Richardson, "On tone-burst measurements of sound speed and attenuation in sandy marine sediments," *IEEE Journal of Oceanic Engineering*, vol. 27, pp. 429-453, July 2002.

[87] T. G. Leighton, S. D. Meers, and P. R. White, "Propagation through nonlinear time-dependent bubble clouds and the estimation of bubble populations from measured acoustic characteristics," *Proceedings of the Royal Society of London, Series A (Mathematical, Physical and Engineering Sciences)*, vol. 460, pp. 2521-50, 2004.

[88] C. C. Coussios and R. A. Roy, "Applications of acoustics and cavitation to noninvasive therapy and drug delivery," *Annual Review of Fluid Mechanics*, vol. 40, pp. 395-420, 2008.

[89] T. M. Allen and P. R. Cullis, "Drug delivery systems: Entering the mainstream," *Science*, vol. 303, pp. 1818-1822, Mar 19 2004.

[90] R. G. Holt, R. A. Roy, C. R. Thomas, C. Farny, T. M. Wu, X. M. Yang, and P. Edson, "Therapeutic bubbles: Basic principles of cavitation in therapeutic ultrasound," *Therapeutic Ultrasound*, vol. 829, pp. 13-17, 2006.

[91] F. Fedele, A. J. Coleman, T. G. Leighton, P. R. White, V. F. Humphrey, S. Ryves, A. M. Hurrell, and D. C. Finfer, "An ultrasound based passive monitoring system for extracorporeal shock wave lithotripsy (ESWL)," *Proceedings of the Institute of Acoustics*, pp. 770-3, 2006.

[92] W. S. Chen, C. Lafon, T. J. Matula, S. Vaezy, and L. A. Crum, "Mechanisms of lesion formation in high intensity focused ultrasound therapy," *2002 IEEE Ultrasonics Symposium Proceedings, Vols 1 and 2*, pp. 1443-1446, 2002.

[93] C. C. Coussios, C. H. Farny, G. Ter Haar, and R. A. Roy, "Role of acoustic cavitation in the delivery and monitoring of cancer treatment by high-intensity focused ultrasound (HIFU) (vol 23, pg 105, 2007)," *International Journal of Hyperthermia*, vol. 23, pp. 327-327, May 2007.

[94] X. M. Yang, R. A. Roy, and R. G. Holt, "Bubble dynamics and size distributions during focused ultrasound insonation," *Journal of the Acoustical Society of America*, vol. 116, pp. 3423-3431, Dec 2004.

[95] I. Pastirk, X. Zhu, R. M. Martin, and M. Dantus, "Remote characterization and dispersion compensation of amplified shaped femtosecond pulses using MIIPS," *Optics Express*, vol. 14, pp. 8885-8889, Sep 18 2006.

[96] J. Kasparian and J. P. Wolf, "Physics and applications of atmospheric nonlinear optics and filamentation," *Optics Express*, vol. 16, pp. 466-493, Jan 7 2008.

[97] G. Mejean, J. Kasparian, J. Yu, S. Frey, E. Salmon, and J. P. Wolf, "Remote detection and identification of biological aerosols using a femtosecond terawatt lidar system," *Applied Physics B-Lasers and Optics*, vol. 78, pp. 535-537, Mar 2004.

[98] J. Kasparian, M. Rodriguez, G. Mejean, J. Yu, E. Salmon, H. Wille, R. Bourayou, S. Frey, Y. B. Andre, A. Mysyrowicz, R. Sauerbrey, J. P. Wolf, and L. Woste, "White-light filaments for atmospheric analysis," *Science*, vol. 301, pp. 61-64, Jul 4 2003.

[99] T. H. Jeys, W. D. Herzog, J. D. Hybl, R. N. Czerwinski, and A. Sanchez, "Advanced trigger development," *Lincoln Laboratory Journal*, vol. 17, pp. 29-62, 2007.

[100] P. O. Ho, W. S. Wilkinson, and A. C. Tseung, "The suppression of intermodulation product generation in materials and structures used in radio communications," in *IEEE Colloquium on Passive Intermodulation Products in Antennas and Related Structures*, 1989, pp. 5/1-5/5.

[101] W. H. Higa, "Spurious signals generated by electron tunneling on large reflector antennas," *Proceedings of the IEEE*, vol. 63, pp. 306-313, 1975.

[102] R. F. Elsner, "'Rusty bolt' demonstrator," *IEEE Transactions on Electromagnetic Compatibility*, vol. EMC-24, pp. 420-421, 1982.

[103] P. L. Lui and A. D. Rawlins, "Passive non-linearities in antenna systems," in *Passive Intermodulation Products in Antennas and Related Structures, IEE Colloquium on*, 1989, pp. 6/1-6/7.

[104] R. Johannessen and S. J. Gale, "Potentional interference sources to GPS and solutions appropriate for applications to civil aviation," *IEEE AES Magazine*, pp. 3-9, January 1990.

[105] "Report to the chairman and ranking minority member, subcommittee on military research and development, committee on armed services, House of Representatives: Improved littoral war-fighting capabilites needed," U. S. G.A.O., Ed., 2001.

[106] H. Medwin and C. S. Clay, *Fundamentals of acoustical oceanography*. Boston: Academic Press, 1998.

[107] H. Medwin, "*In-situ* acoustic measurements of bubble populations in coastal ocean waters," *Journal of Geophysical Research*, vol. 75, pp. 599-611, 1970.

[108] E. Meyer and E. Skudrzyk, "On the Acoustical Properties of Gas Bubble Screens in Water (Ueber die Akustischen Eigenschaften von Gasblasenschleiern in Wasser)," *Acustica*, 1953.

[109] E. L. Carstensen and L. L. Foldy, "Propagation of sound through a liquid containing bubbles," *Journal of the Acoustical Society of America*, vol. 19, pp. 481-501, May 1947.

[110] L. E. Kinsler, A. R. Frey, A. B. Copppens, and J. V. Sanders, *Fundamentals of acoustics*, Fourth ed. New York: Wiley, 1962.

[111] T. G. Leighton, D. C. Finfer, E. J. Grover, and P. R. White, "Spiral bubble nets of humpback whales: An acoustic mechanism," in *Underwater Acoustics and Measurements: Technologies & Results; 2nd International Conference & Exhibition*, Heraklion, Crete, 2007, pp. 583-588.

[112] T. G. Leighton, D. C. Finfer, E. J. Grover, and P. R. White, "An acoustical hypothesis for the spiral nets of humpback whales and the implications for whale feeding," *Acoustic Bulletin*, vol. 22, pp. 17-21, 2007.

[113] F. E. Fox, S. R. Curley, and G. S. Larson, "Phase velocity and absorption measurements in water containing air bubbles," *Journal of the Acoustical Society of America*, vol. 27, pp. 534-539, May 1955.

[114] W. R. Turner, "Microbubble persistence in fresh water," *Journal of the Acoustical Society of America*, vol. 33, pp. 1223-1233, September 1961.

[115] N. D. Breitz and H. Mediwn, "Instrumentation for *in-situ* acoustical measurements of bubble spectra under breaking waves," *Journal of the Acoustical Society of America*, vol. 86, pp. 739-743, 1989.

[116] D. M. Farmer and S. Vagle, "Waveguide propagation of ambient sound in the ocean-surface bubble layer," *Journal of the Acoustical Society of America*, vol. 86, pp. 1897-908, 1989.

[117] D. M. Farmer and S. Vagle, "Bubble measurements using a resonator system," in *Natural physical processes associated with sea surface sound*, University of Southampton, 1997, pp. 155-162.

[118] G. B. Deane, "Sound generation and air entrainment by breaking waves in the surf zone," *Journal of the Acoustical Society of America*, vol. 102, pp. 2671-2689, 1997.

[119] T. G. Leighton and G. B. N. Robb, "Preliminary mapping of void fractions and sound speeds in gassy marine sediments from subbottom profiles," *JASA Express Letters*, vol. 124, Noveber 2008.

[120] C. Gunay, D. Dondurur, and M. Ergun, "Sonar and high resolution seismic studies in the Eastern Black Sea," *Turkish Journal of Earth Sciences*, vol. 11, pp. 61-81, 2002 2002.

[121] J. M. Bull, M. Gutowski, J. K. Dix, T. J. Henstock, P. Hogarth, T. G. Leighton, and P. R. White, "3D Chirp sub-bottom imaging system: Design and first 3D volume," in *Underwater Acoustic Measurements: Technologies & Results*, Heraklion, Crete, 2005.

[122] O. M. Griffin, R. D. Peltzer, A. M. Reed, and R. F. Beck, "Ship wakes and their radar images," *Annual review of Fluid Mechanics*, vol. 34, pp. 469-502, 2002.

[123] R. L. Stefan and A. J. Szeri, "Surfactant scavenging and surface deposition by

rising bubbles," *Journal of Colloid and Interface Science,* vol. 212, pp. 1-13, 1998.
[124] T. G. Leighton: Stated in lecture during MSc course on underwater acoustics, 2005.
[125] F. P. Incropera and D. P. DeWitt, *Fundamentals of heat and mass transfer,* 5th ed. New York: Wiley, 2002.
[126] D. G. H. Coles and T. G. Leighton, "Autonomous spar-buoy measurements of bubble populations under breaing waves in the Sea of the Hebrides," in *Second International Conference on Underwater Acoustic Measurements; Technologies and Results,* Heraklion, Crete, 2007, pp. 543-548.
[127] P. Doust, "transducer experiement," T. G. Leighton, Ed., 2005.
[128] M. Gutowski, J. Bull, T. Henstock, J. Dix, P. Hogarth, T. Leighton, and P. White, "Chirp sub-bottom profiler source signature design and field testing," *Marine Geophysical Researches,* vol. 23, pp. 481-492, 2002.
[129] J. M. Bull, M. Gutowski, J. K. Dix, T. J. Henstock, P. Hogarth, T. G. Leighton, and P. R. White, "Design of a 3D Chirp sub-bottom imaging system," *Marine Geophysical Researches,* vol. 26, pp. 157-169, Jun 2005.
[130] R. Clift, J. R. Grace, and M. E. Weber, *Bubbles, Drops, and Particles.* San Diego: Academic Press, 1978.
[131] D. A. Bies and C. H. Hansen, *Engineering noise control: theory and practice,* 2nd ed. London New York: E & FN Spon, 1996.
[132] Millenium Research Group, "Outlook good for nuclear medicine and other imaging markets," *Journal of Nuclear Medicine,* vol. 48, p. 16N and 38N, June 2007.
[133] H. E. King and J. L. Wong, "Directivity of a uniformly excited N X N array of directive elements," *Ieee Transactions on Antennas and Propagation,* vol. Ap23, pp. 401-404, 1975.
[134] E. Kreyszig, *Advanced engineering mathematics.* New York: Wiley, 1967.
[135] B. Møhl, M. Wahlberg, P. T. Madsen, L. A. Miller, and A. Surlykke, "Sperm whale clicks: Directionality and source level revisited," *Journal of the Acoustical Society of America,* vol. 107, pp. 638-648, January 2000.
[136] G. C. Gaunaurd, D. Brill, H. Huang, P. W. B. Moore, and H. C. Strifors, "Signal processing of the echo signatures returned by submerged shells insonified by dolphin "clicks:" Active classification," *Journal of the Acoustical Society of America,* vol. 103, pp. 1547-1557, 1998.
[137] P. W. Moore, "Mine-hunting dolphins of the Navy," in *Detection and Remediation Technologies for Mines and Minelike Targets II,* Orlando, FL, USA, 1997, pp. 2-6.
[138] D. A. Helweg, P. W. Moore, S. W. Martin, and L. A. Dankiewicz, "Using a binaural biomimetic array to identify bottom objects ensonified by echolocating dolphins," *Bioinspiration & Biomimetics,* vol. 1, pp. 41-51, 23 May 2006.
[139] T. Butcher, "Dolphins called in to search for harbour mines," in *The Daily Telegraph* London, 2003.
[140] A. Kirby, "Dolphins clear mines the natural way," BBC news, 2003.
[141] P. W. B. Moore and W. W. L. Au, "Underwater localization of pulsed pure-tones by California Sea Lion (Zalophus-Californianus)," *Journal of the Acoustical Society of America,* vol. 58, pp. 721-727, 1975.
[142] P. W. B. Moore, "Underwater localization of click and pulsed pure-tone signals by California Sea Lion (Zalophus-Californianus)," *Journal of the Acoustical Society of America,* vol. 57, pp. 406-410, 1975.
[143] C. W. Turl, "The Ability of the California Sea Lion, Zalophus-Californianus, to Bistatically Detect and Localize Echoes from Underwater Targets," *Journal of the Acoustical Society of America,* vol. 82, pp. 381-383, Jul 1987.
[144] S. Mayer, "A review of the scientific justifications for maintaining cetaceans in captivity," Whale and Dolphin Conservation Society, Bath1998.
[145] W. W. L. Au, *The Sonar of Dolphins.* New York: Springer-Verlag, 1993.
[146] T. G. Leighton, "Personal communication: Hearing by some cetaceans extends to higher frequencies than do acoustic emissions by those same animals,"

Dolphin hearing allows for nonlinear processing ed, 2007.

[147] J. I. Fasick, "Echolocation interference in the presence of air bubbles," in *Soundings: Newsletter of the International Marine Animal Trainers Association.* vol. 17, 1992, pp. 12-14.

[148] S. Li, K. Wang, D. Wang, and A. T., "Echolocation signals of the free-ranging Yangtze finless porpoise (*Neophocaena phocaenoides asiaeorientialis*)," *Journal of the Acoustical Society of America,* vol. 117, pp. 3288-96, 2005.

[149] R. N. P. Goodall, K. S. Norris, A. R. Galeazzi, J. A. Oporto, and I. S. Cameron, "On the Chilean dolphin, *Cephalorhynchus eutropia* (Gray, 1846)," *Rep. Int. Whal. Commn. Spec. Issue,* pp. 197-257, 1988.

[150] C. Kamminga and H. Wiersma, "Investigations on cetacean sonar II. Acoustical similarities and differences in odontocete sonar signals," *Aquatic Mammals,* vol. 8, pp. 41-62, 1981.

[151] W. E. Evans, F. T. Awbrey, and H. Hackbarth, "High frequency pulses produced by free-ranging Commerson's dolphin (*Cephalorhynchus commersonii*) compared to those of Phocoenids," International Whale Commision, Cambridge1988.

[152] W. Watkins, W. E. Shevill, and P. B. Best, "Underwater sounds of *Cephalorhynchus heavisidii* (Mammalia: Cetacea)," *Journal of Mammalogy,* vol. 58, pp. 316-320, 1977.

[153] W. A. Watkins and W. E. Schevill, "Characteristic features of the underwater sounds of *Cephaorhynchus commersonii,*" *Journal of Mammalogy,* vol. 41, pp. 738-739, 1980.

[154] S. H. Li, K. X. Wang, D. Wang, and T. Akamatsu, "Origin of the double- and multi-pulse structure of echolocation signals in Yangtze finless porpoise (Neophocaena phocaenoides asiaeorientialis)," *Journal of the Acoustical Society of America,* vol. 118, pp. 3934-3940, Dec 2005.

[155] T. Götz, R. Antunes, and S. Heinrich, "Echolocation clicks of free-ranging Chilean dolphins," in *16th Biennial Conference on the Biology of Marine Mammals,* San Diego, CA, 2005, p. 111.

[156] S. H. Li, K. X. Wang, D. Wang, and T. Akamatsu, "Echolocation signals of the free-ranging Yangtze finless porpoise (Neophocaena phocaenoides asiaeorientialis)," *Journal of the Acoustical Society of America,* vol. 117, pp. 3288-3296, May 2005.

[157] F. T. Awbrey, J. C. Norris, A. B. Hubbard, and W. E. Evans, *The bioacoustics of the Dall's porpoise salmon drift net interaction.* San Diego, 1979.

[158] Cetacean specialist group 1996, "Neophocaena phocaenoides ssp, asiaorientalis," in *2007 IUCN red list of threatened species*: IUCN, 2007.

[159] T. Akamatsu, D. Wang, K. X. Wang, and Y. Naito, "Biosonar behaviour of free-ranging porpoises," *Proceedings of the Royal Society B-Biological Sciences,* vol. 272, pp. 797-801, Apr 22 2005.

[160] T. Akamatsu, D. Wang, K. X. Wang, and Z. Wei, "Comparison between visual and passive acoustic detection of finless porpoises in the Yangtze river, China," *Journal of the Acoustical Society of America,* vol. 109, pp. 1723-1727, Apr 2001.

[161] T. Akamatsu, J. Teilmann, L. A. Miller, J. Tougaard, R. Dietz, D. Wang, K. X. Wang, U. Siebert, and Y. Naito, "Comparison of echolocation behaviour between coastal and riverine porpoises," *Deep-Sea Research Part Ii-Topical Studies in Oceanography,* vol. 54, pp. 290-297, 2007.

[162] T. Akamatsu, D. Wang, K. X. Wang, Z. Wei, Q. Z. Zhao, and Y. Naito, "Diving behaviour of freshwater finless porpoises (Neophocaena phocaenoides) in an oxbow of the Yangtze River, China," *Ices Journal of Marine Science,* vol. 59, pp. 438-443, Apr 2002.

[163] S. H. Li, D. Wang, K. X. Wang, T. Akamatsu, Z. Q. Ma, and J. B. Han, "Echolocation click sounds from wild inshore finless porpoise (Neophocaena phocaenoides sunameri) with comparisons to the sonar of riverine N. p. asiaeorientalis," *Journal of the Acoustical Society of America,* vol. 121, pp. 3938-3946, Jun 2007.

[164] T. Akamatsu, D. Wang, K. Nakamura, and K. Wang, "Echolocation range of

captive and free-ranging baiji (Lipotes vexillifer), finless porpoise (Neophocaena phocaenoides), and bottlenose dolphin (Tursiops truncatus)," *Journal of the Acoustical Society of America,* vol. 104, pp. 2511-2516, Oct 1998.

[165] T. Akamatsu, D. Wang, K. Wang, S. Li, S. Dong, X. Zhao, J. Barlow, B. S. Stewart, and M. Richlen, "Estimation of the detection probability for Yangtze finless porpoises (Neophocaena phocaenoides asiaeorientalis) with a passive acoustic method," *Journal of the Acoustical Society of America,* vol. 123, pp. 4403-4411, Jun 2008.

[166] T. Akamatsu, D. Wang, K. X. Wang, and Y. Naito, "A method for individual identification of echolocation signals in free-ranging finless porpoises carrying data loggers," *Journal of the Acoustical Society of America,* vol. 108, pp. 1353-1356, Sep 2000.

[167] T. Akamatsu, A. Matsuda, S. Suzuki, D. Wang, K. X. Wang, M. Suzuki, H. Muramoto, N. Sugiyama, and K. Oota, "New stereo acoustic data logger for free-ranging dolphins and porpoises," *Marine Technology Society Journal,* vol. 39, pp. 3-9, Sum 2005.

[168] T. Akamatsu, D. Wang, and K. X. Wang, "Off-axis sonar beam pattern of free-ranging finless porpoises measured by a stereo pulse event data logger," *Journal of the Acoustical Society of America,* vol. 117, pp. 3325-3330, May 2005.

[169] S. G. Li, D. Wang, K. X. Wang, J. Q. Xiao, and T. Akamatsu, "The ontogeny of echolocation in a Yangtze finless porpoise (Neophocaena phocaenoides asiaeorientalis)," *Journal of the Acoustical Society of America,* vol. 122, pp. 715-718, Aug 2007.

[170] W. Kexiong, W. Ding, T. Akamatsu, L. Songhai, and X. Jianqiang, "A passive acoustic monitoring method applied to observation and group size estimation of finless porpoises," *Journal of the Acoustical Society of America,* vol. 118, pp. 1180-5, 2005.

[171] S. H. Li, K. X. Wang, D. Wang, S. Y. Dong, and T. Akamatsu, "Simultaneous production of low- and high-frequency sounds by neonatal finless porpoises," *Journal of the Acoustical Society of America,* vol. 124, pp. 716-718, Aug 2008.

[172] S. H. Li, D. Wang, K. X. Wang, and T. Akamatsu, "Sonar gain control in echolocating finless porpoises (Neophocaena phocaenoides) in an open water (L)," *Journal of the Acoustical Society of America,* vol. 120, pp. 1803-1806, Oct 2006.

[173] L. Songhai, W. Kexiong, W. Ding, and T. Akamatsu, "Echolocation signals of the free-ranging Yangtze finless porpoise (neophocaena phocaenoides asiaeorientialis)," *Journal of the Acoustical Society of America,* vol. 117, pp. 3288-96, 2005.

[174] M. Lammers, W. W. L. Au, R. Aubauer, and P. E. Nachtigall, "A comparitave analysis of the pulsed emissions of free-ranging Hawaiian spinner dolphins," in *Echolocation in Bats and Dolphins,* J. Thomas, C. F. Moss, and M. Vater, Eds. Chicago: University of Chicago, 2004, pp. 414-419.

[175] R. Aubauer, M. Lammers, and W. W. L. Au, "One-hydrophone method of estimating distance and depth of phonating dolphins in shallow water," *Journal of the Acoustical Society of America,* vol. 107, pp. 2511-2516, 2000.

[176] P. R. White, D. C. Finfer, T. G. Leighton, C. Powles, and O. N. Baumann, "The localisation of whales using acoustics," *Proceedings of the Institute of Acoustics,* vol. 28, pp. 48-59, 2008.

[177] P. R. White, T. G. Leighton, D. C. Finfer, C. Powles, and O. N. Baumann, "Localisation of sperm whales using bottom mounted sensors," *Applied Acoustics,* vol. 67, pp. 1074-1090, 2006.

[178] J. L. Spiesberger and M. Wahlberg, "Probability density functions for hyperbolic and isodiachronic locations," *Journal of the Acoustical Society of America,* vol. 112, pp. 3046-3052, 2002.

[179] C. Darwin, *The orgin of species by means of natural selection.* London: D. Appleton & Co., 1889.

[180] "The IUCN Red List of threatened species," International Union for

Conservation of Nature and Natural Resources, Cambridge, England 2006.
[181] "Biology of the genus *Cephalorhynchus*," International Whaling Commission, Cambridge1988.
[182] F. B. Pichler, D. Robineau, R. N. P. Goodall, M. A. Meyer, C. Olivarria, and C. S. Baker, "Origin and radiation of Southern Hemisphere coastal dolphins (genus *Cephalorhynchus*)," *Molecular Ecology,* vol. 10, pp. 2215-2223, 2001.
[183] E. Slooten and B. L. Taylor, "Cephalorhynchus hectori," in *2007 IUCN red list of threatened species*: IUCN, 2000.
[184] F. B. Pichler, S. M. Dawson, E. Slooten, and C. S. Baker, "Geographic isolation of Hector's dolphin populations described by mitochondrial DNA sequences," *Conservation Biology,* vol. 12, pp. 676-682, Jun 1998.
[185] W. R. B. Oliver, "Review of the cetacea of the New Zealand Seas," *Proceedings of the Zoological Society of London,* vol. 43, pp. 627-639, 1922.
[186] P. de Bruyn, G. Hofmeyr, and M. de Villiers, "First record of a vagrant Commerson's dolphin, *Cephalorhyncus commersonii,* at the southern African continental shelf," *African Zoology,* vol. 41, pp. 131-133, 2006.
[187] B. E. Joseph, J. E. Antrim, and L. H. Cornell, "Commerson's dolphin (*Cephalorhynchus commersonii*): A discussion of the first live birth within a marine zoological park," *Zoo Biology,* vol. 6, pp. 69-77, 1986.
[188] A. Dziedzic and V. d. Bueffrenil, "Acoustic signals of the Commerson's dolphin, *Cephalorhynchus Commersonii,* in the Kerguelen Islands," *Journal of Mammalogy,* vol. 70, pp. 449-452, 1989.
[189] P. B. Best and R. B. Abernethy, "Heaviside's dolphin (*Cephalorhynchus heavisidii*)." in *Handbook of Marine Mammals*, S. H. Ridgway and R. Harrison, Eds.: Academic Press, 1994.
[190] P. A. Folkens, R. R. Reeves, B. S. Stewart, P. J. Clapham, and J. A. Powell, *Guide to marine mammals of the world,* 1st ed. New York: A.A. Knopf : Distributed by Random House, 2002.
[191] S. Heinrich, "Ecology of Chilean dolphins and Peale's dolphins at Isla Chiloé, southern Chile," in *School of Biology.* vol. PhD: University of St Andrews, 2006, p. 239.
[192] S. Li, K. Wang, D. Wang, and T. Akamatsu, "Echolocation signals of the free-ranging Yangtze finless porpoise (*Neophocaena phocaenoides asiaeorientialis*)," *Journal of the Acoustical Society of America,* vol. 117, pp. 3288-3296, 2005.
[193] B. Mohl and S. Andersen, "Echolocation: high-frequency component in the click of the Harbour Porpoise (*Phocoena ph. L.*)," *Journal of the Acoustical Society of America,* vol. 54, pp. 1368-1372, 1973.
[194] S. Dawson, P. Wade, E. Slooten, and J. Barlow, "Design and field methods for sighting surveys of cetaceans in coastal and riverine habitats," *Mammal review,* vol. 38, pp. 19-49, 2008.
[195] R. N. McDonough and A. D. Whalen, *Detection of Signals in Noise,* 2nd ed. London: Academic Press, 1995.
[196] T. Fawcett, "ROC Graphs: Notes and practical considerations for researchers," HP Laboratories, Palo Alto, CA2004.
[197] P. Flach and S. Wu, "Reparing concavities in ROC curves," *Proceedings of the 2003 workshop on computational intelligence,* pp. 38-44, 2003.

Appendices

1 Receiver operating characteristic (ROC) curves

1.1 Overview

Detection algorithms are used in a variety of disciplines: wi-fi networks, medicine, airport security, sonar/radar, hi-energy physics, the search for extra-terrestrial life, *etc.* In each of these applications, the goal of the detection algorithm is to attempt to determine whether or not a target is present. In order for ROC analysis to be appropriate, the detection system must be a discrete classifier; *i.e.* it can only return one of two responses: positive or negative. In general, the decision whether to return a positive or a negative result is based on the outcome of a comparison between an observed quantity and some threshold. That is, the data available to the algorithm is searched for conspicuous factors. If those conspicuous factors are numerous enough or high enough in amplitude (*e.g.* they are higher than allowed for by some threshold), then the system returns a positive result. Since such systems are not infallible, an observer evaluating the algorithm output must allow for the following possible outcomes, as outlined in Table 1.1 below.

Table 1.1 Rubric of possible outcomes (known as the 'confusion matrix') for a detection system. For the symbolic representations included in this table, Q is the probability of a given outcome, D is the true decision class (1: target present, 0: target absent), and n is the hypothesised class (where 1 and 0 are as before).

		Hypothesised class	
		Positive	*Negative*
True class	*Yes*	True positive $Q(D_1\|n_1)$	False positive $Q(D_0\|n_1)$
	No	False negative $Q(D_1\|n_0)$	True negative $Q(D_0\|n_0)$

The probability of a true positive is known as the *true positive rate* $Q_1(v)$, while the *false positive rate* is then $Q_0(v)$. By plotting the true positive rate against the false negative rate for a given system under a particular condition, one can create a receiver operating characteristic (ROC) curve which can be used to summarise system performance. The goal of this dissertation is the development of a sonar system which will advance the start-of-the-art with respect to target detection in bubbly water. In order to qualify the new technology as a better performer than the state-of-the-art technology, it is necessary to quantify the system performance of both systems under the same conditions, and compare the results. ROC curves are used in Chapters 4 to facilitate this comparison. Excellent summaries of concepts related to ROC graphs are given by McDonough and Whalen [195] and Fawcett [196].

1.1.1 Detection analysis

As stated above, to develop a ROC curve, it is first necessary to

establish the distribution of the signal being used to make the detection decision. Where the system output is a value v, a binary decision system can be characterised based on two probability density functions: one for the system output in presence of a target $q_1(v)$, and the other for the output of that same system in absence of a target $q_0(v)$, as illustrated in Figure 1.1.

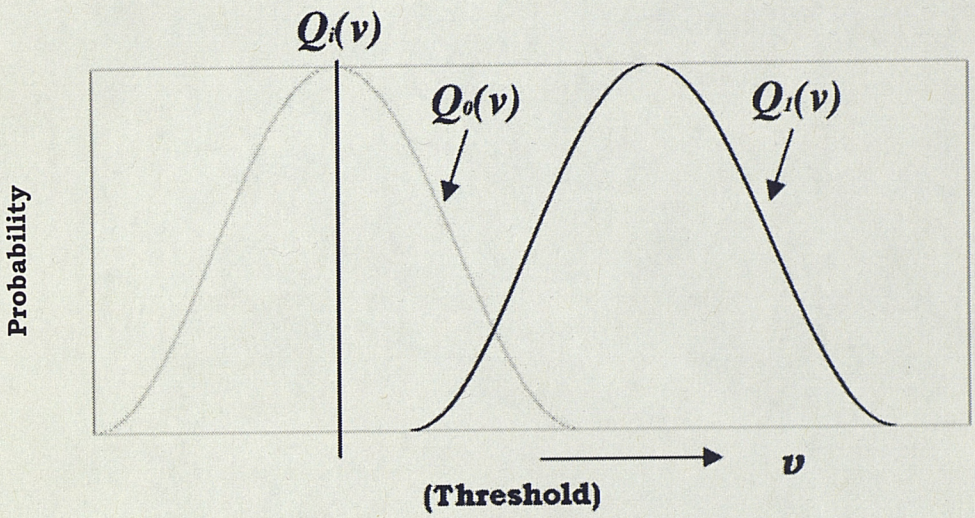

Figure 1.1 Hypothetical distribution for a decision system. The space of all probabilities for all values of the threshold v can be used to yield a ROC curve. The probability distribution on the left represents the distribution of responses in the absence of a target, $Q_0(v)$. The function to the right (in bold) represents the distribution of responses in the presence of a target, $Q_1(v)$. ROC space is then defined according to the set of all points for all thresholds ($Q_0(v)$, $Q_1(v)$). To understand ROC space, it is instructive to first consider a few important individual points per the explanations given in

Table 1.2.

Table 1.2 Some points of interest in ROC space

Point	Explanation
(0,0)	A strategy whereby no positive classifications are ever issued. This classifier will never make a mistake, but will also never give any positive information.
(1,1)	The classifier indiscriminately returns positive decisions, regardless of the input. This strategy is logically the opposite of that represented by (0, 0).
(0,1)	A perfect classifier. The system is always capable of telling whether a positive or negative decision is appropriate.

A system which when classified according to $\in(Q_0(v), Q_1(v))$ tends towards the left side of the graph (see Figure 1.2, 'System A') may be thought of as a conservative system [196]. A conservative system is one where positive classifications are only made with strong evidence and so give few false positives; but such systems often have low-true positive rates. This can be compared against systems which tend towards the upper right-hand side of a ROC graph (see Figure 1.2, 'System B'). Such classifiers may be termed liberal, in that they will make positive classifications based on weak evidence. This will result in the correct classification of nearly all positives, but often at the expensive of high-false positive rates [196].

The line labelled in Figure 1.2 as the '50/50 line', $Q(D_1|n_1) = Q(D_0|n_0)$ is

equivalent to a random guess. A random guess can be mapped as follows: if the output of the system is a positive classification 50% of the time, then it would be expected that ½ of all positive inputs and ½ of all negative inputs will have been correctly classified. This would give the point (0.5, 0.5) in ROC space. If the rate of positive classification is increased to 95%, then both the true positive and false positive rates will rise accordingly, giving the point (0.95, 0.95).

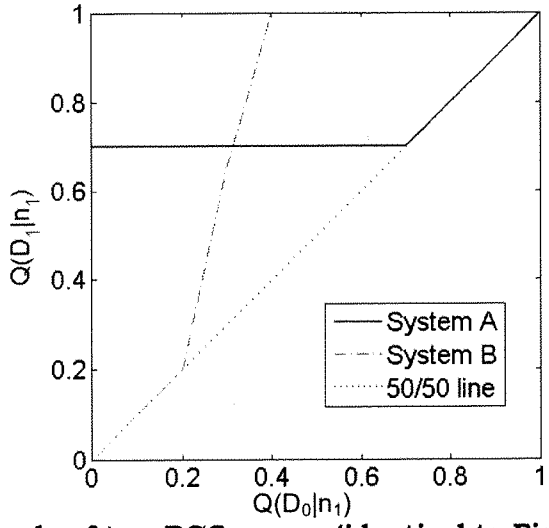

Figure 1.2 An example of two ROC curves (identical to Figure 4.45).

Any classifier that results in a ROC curve extending below the 50/50 line performs worse than a random guess; thus this region of the plot is generally empty. If a system produced, for instance, a point in ROC space (0.4, 0), then the logical presumption is that decisions corresponding to that threshold should be reversed, resulting in the point (0, 0.4). It is therefore reasonable to say that a classifier which is characterised by a point below the 50/50 diagonal has useful information – but that information has been applied incorrectly [197].

The area below a ROC curve is an indicator of the usefulness of the decision classifier. Since random guesses result in the diagonal line that goes from (0, 0) to (1, 1) as explained above, it is unrealistic for any classifier to have an area under the curve (AUC) of less than 0.5. The upper bound for this quantity is 1. According to Fawcett, [196], "the AUC of a classifer is equivalent to the probability that the classifier will rank a randomly chosen positive instance higher than a randomly chosen negative instance." The point on the ROC curve which is furthest from the 50/50 line will correspond to the threshold which results in the highest ratio of $Q_1(v)/Q_0(v)$ for that classifier.

2 Definition of an inverse signal

The simplest way in which to establish whether one pulse is the inverse of another is to auto-correlate the signal containing both pulses and analyse the polarity of the peaks. Consider the simple click train illustrated graphically in Figure 2.1 *(a)* and *(c)*.

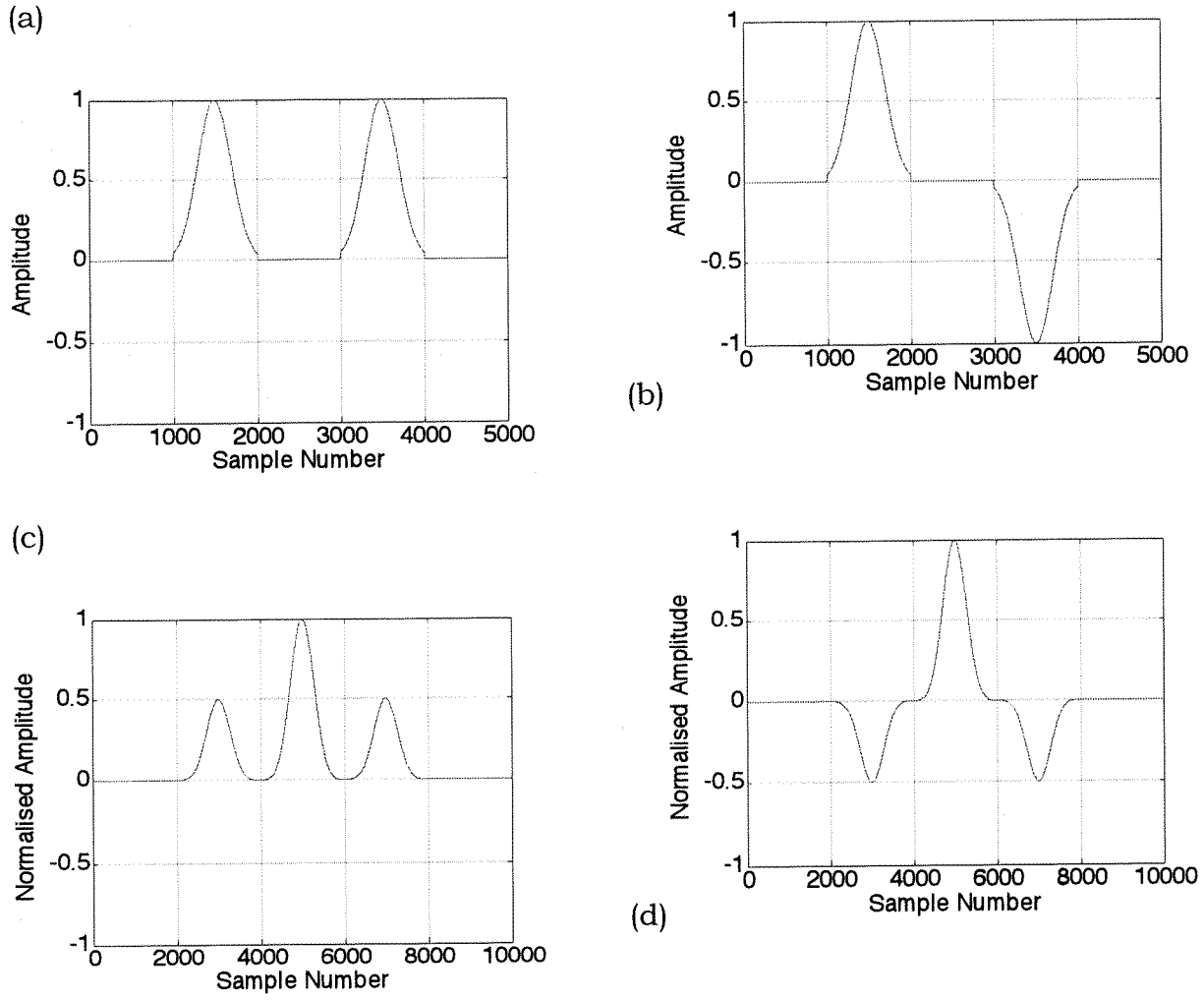

Figure 2.1 *(a)* A simple click train. *(b)* A simple click train in which the first segment (before 2000 samples) is the polarity-switched version of the second segment (after 3000 samples). *(c)* and *(d)* represent the auto-correlation function for figures *(a)* and *(b)* respectively.

The fact that the auto-correlation function for the positive-positive

clicktrain (Figure 2.1 *(a)* and *(c)*) contains only positive "sidelobes", whereas the positive-negative clicktrain (Figure 2.1 *(b)* and *(d)*) contains negative sidelobes is indicative of a feature which can be exploited to search data sets for inverted pairs.

3 Publications by the author

Given here is a complete chronological list of all publications which D C Finfer authored or co-authored during his PhD studies.

[i] T. G. Leighton, D. C. Finfer, and P. R. White, "Bubble acoustics: What can we learn from cetaceans about contrast enhancement?," in IEEE International Ultrasonics Symposium, Rotterdam, 2005, pp. 964-73.

[ii] T. G. Leighton, P. R. White, and D. C. Finfer, "Target detection in bubbly water," PCT/GB2006/002335 2005.

[iii] T. G. Leighton, P. R. White, and D. C. Finfer, "Bubble acoustics in shallow water: Possible applications in nature," in International conference on boundary influences in high frequency, shallow water acoustics, Bath, UK, 2005, pp. 433-40.

[iv] T. G. Leighton, P. R. White, and D. C. Finfer, "Possible applications of bubble acoustics in nature," Proceedings of the 28th Scandinavian Symposium on Physical Acoustics, Ustaoset, Norway, 2005.

[v] T. G. Leighton, P. R. White, and D. C. Finfer, "Detection of Objects in Bubbly Water," GB 0513031.5 2005.

[vi] T. G. Leighton, P. R. White, D. C. Finfer, and S. D. Richards, "Cetacean acoustics in bubbly water (Invited Paper)," in Proceedings of the International Conference on Underwater Acoustic Measurements, Technologies and Results, Heraklion, Crete, 2005, pp. 891-8.

[vii] T. G. Leighton, P. R. White, D. C. Finfer, and S. D. Richards, "Cetacean Acoustics in Bubbly Water," in Proceedings of the International Conference "Underwater Acoustic Measurements: Technologies & Results", Heraklion, Crete, 2005.

[viii] F. Fedele, A. J. Coleman, T. G. Leighton, P. R. White, V. F. Humphrey, S. Ryves, A. M. Hurrell, and D. C. Finfer, "An ultrasound based passive monitoring system for extracorporeal shock wave lithotripsy (ESWL)," Proceedings of the Institute of Acoustics, pp. 770-3, 2006.

[ix] D. C. Finfer, T. G. Leighton, and P. R. White, "Marine mammals, noise, and sonar in shallow, coastal, bubbly waters," in Proceedings of the Institute of Acosutics, Southampton, 2006, pp. 69-74.

[x] T. G. Leighton, D. C. Finfer, and P. R. White, "Not Sonar," in The Independent on Sunday London, 2006.

[xi] P. R. White, T. G. Leighton, D. C. Finfer, C. Powles, and O. N. Baumann, "Localisation of sperm whales using bottom mounted sensors," Applied Acoustics, vol. 67, pp. 1074-1090, 2006.

[xii] D. C. Finfer, P. R. White, and T. G. Leighton, "Biological sources of ambient noise in the North East Atlantic Ocean," in Underwater Acoustic Measurements: Technologies & Results, Crete, 2007, pp. 1223-1228.

[xiii] D. C. Finfer, P. R. White, T. G. Leighton, M. Hadley, and E. J. Harland, "On clicking sound in UK waters and a preliminary study of their possible biological origin," in Fourth International Conference on Bio-Acoustics, Loughborough, 2007, pp. 209-216.

[xiv] T. G. Leighton, D. C. Finfer, E. J. Grover, and P. R. White, "An acoustical hypothesis for the spiral nets of humpback whales and the implications for whale feeding," Acoustic Bulletin, vol. 22, pp. 17-21, 2007.

[xv] T. G. Leighton, D. C. Finfer, E. J. Grover, and P. R. White, "Spiral bubble nets of humpback whales: An acoustic mechanism," in Underwater Acoustics and Measurements: Technologies & Results; 2nd International Conference & Exhibition, Heraklion, Crete, 2007, pp. 583-588.

[xvi] T. G. Leighton, D. C. Finfer, and P. R. White, "Ocean acoustic circumpropagation in the ice seas of Europa." vol. 319: ISVR Technical Report, University of Southampton, 2007, p. 31.

[xvii] T. G. Leighton, D. C. Finfer, and P. R. White, "Hypotheses on the exploitation of bubble acoustics by cetaceans (Abstract-only)," The Journal of the Acoustical Society of America, vol. 121, p. 3039, 2007.

[xviii] T. G. Leighton, D. C. Finfer, and P. R. White, "Sonar which penetrates bubble clouds (Invited Paper)," in Proceedings of the Second International Conference on Underwater Acoustic Measurements, Technologies and Results, Crete, Greece, 2007, pp. 555-562.

[xix] T. G. Leighton, D. C. Finfer, and P. R. White, "Cavitation and Cetacean," in Proceedings of the 19th International Congress on Acoustics Madrid, Spain, 2007, pp. 1-31.

[xx] T. G. Leighton, D. C. Finfer, and P. R. White, "Cavitation and cetacean," Revista de Acustica, vol. 38, pp. 37-81, 2007.

[xxi] D. C. Finfer, T. G. Leighton, and P. R. White, "Issues relating to the use of 61.5 dB conversion factor when comparing airborne and underwater anthropogenic noise levels," Applied Acoustics, vol. 69, pp. 464-471, 2008.

[xxii] T. G. Leighton, D. C. Finfer, and P. R. White, "The problems with acoustics on a small planet," Icarus, vol. 193, pp. 649-652, 2008.

[xxiii] T. G. Leighton, D. C. Finfer, and P. R. White, "Experimental evidence for enhanced target detection by sonar in bubbly water," Hydroacoustics, vol. 11, pp. 181-202, 2008.

[xxiv] P. R. White, D. C. Finfer, T. G. Leighton, C. Powles, and O. N. Baumann, "The localisation of whales using acoustics," Proceedings of the Institute of Acoustics, vol. 28, pp. 48-59, 2008.